T.R.
GEBZE TECHNICAL UNIVERSITY
GRADUATE SCHOOL OF NATURAL AND APPLIED SCIENCES

DESIGN OF SILOS AS MULTI-TIERED STEEL BRACED FRAME

YASEMİN EZGİ AKYILDIZ
A THESIS SUBMITTED FOR THE DEGREE OF
MASTER OF SCIENCE
DEPARMENT OF CIVIL ENGINEERING
EARTHQUAKE AND STRUCTURAL ENGINEERING PROGRAM

GEBZE
2021

T.R.

GEBZE TECHNICAL UNIVERSITY

GRADUATE SCHOOL OF NATURAL AND APPLIED SCIENCES

DESIGN OF SILOS AS MULTI-TIERED STEEL BRACED FRAME

YASEMİN EZGİ AKYILDIZ

A THESIS SUBMITTED FOR THE DEGREE OF

MASTER OF SCIENCE

DEPARTMENT OF CIVIL ENGINEERING

EARTHQUAKE AND STRUCTURAL ENGINEERING PROGRAM

THESIS SUPERVISOR

PROF. DR. BÜLENT AKBAŞ

GEBZE

2021

T.C.
GEBZE TEKNİK ÜNİVERSİTESİ
FEN BİLİMLERİ ENSTİTÜSÜ

SİLOLARIN ÇOK KATMANLI ÇELİK ÇAPRAZLI ÇERÇEVE OLARAK TASARIMI

YASEMİN EZGİ AKYILDIZ
YÜKSEK LİSANS TEZİ
İNŞAAT MÜHENDİSLİĞİ ANABİLİM DALI
DEPREM VE YAPI MÜHENDİSLİĞİ PROGRAMI

DANIŞMANI
PROF. DR. BÜLENT AKBAŞ

GEBZE
2021

GEBZE TEKNİK ÜNİVERSİTESİ	**YÜKSEK LİSANS JÜRİ ONAY FORMU**

GTÜ Fen Bilimleri Enstitüsü Yönetim Kurulu'nun 01/07/2021 tarih ve 2021/30 sayılı kararıyla oluşturulan jüri tarafından 14/07/2021 tarihinde tez savunma sınavı yapılan Yasemin Ezgi AKYILDIZ'ın tez çalışması İnşaat Mühendisliği Anabilim Dalı Deprem ve Yapı Mühendisliği Programında YÜKSEK LİSANS tezi olarak kabul edilmiştir.

JÜRİ

ÜYE (TEZ DANIŞMANI)	: PROF. DR. BÜLENT AKBAŞ
ÜYE	: PROF. DR. BİLGE DORAN
ÜYE	: DR. ÖĞR. ÜYESİ ONUR ŞEKER

ONAY

Gebze Teknik Üniversitesi Fen Bilimleri Enstitüsü Yönetim Kurulu'nun ……/……/…… tarih ve ……/…….. sayılı kararı.

SUMMARY

The focus of this study is on investigating the seismic performance of Multi-Tiered Concentrically Steel Braced Frames. Multi-Tiered Concentrically Steel Braced Frames are created when a tall single-story bay is divided into multiple bracing panels over the height, without diaphragms or out-of-plane column supports between the base and roof. Multi-Tiered Concentrically Steel Braced Frames are widely used as a lateral force-resisting system in tall single-story buildings such as industrial warehouses, airplane hangars, stadiums, and performing arts and convention centers.

In this research, three silos, which store wheat as a material, with three different brace configurations, sitting on the same foundation, are modeled with the design principle of 'Multi-Tiered Ordinary Concentrically Steel Braced Frames'. The brace configurations for these three silos are X-Bracing, 2-Tier X-Bracing and Chevron Bracing, respectively. In this study, steel element calculations are performed and brace, beam and column elements are designed. Besides, the seismic performance of silos during an earthquake is investigated by linear and nonlinear analysis. In order to reach more accurate and precise results, Time History Analysis is used. According to linear and nonlinear analysis results, three silos with different brace configurations are compared.

As a result of these studies, it is understood that the seismic performance of X-Bracing and 2-Tier X-Bracing are similar while Chevron Bracing behaves totally different from the others.

Keywords: Multi-Tiered Ordinary Concentrically Steel Braced Frames, Silo, Linear Analysis, Nonlinear Analysis.

ÖZET

Bu çalışmanın odak noktası Çok Katmanlı Merkezi Çelik Çaprazlı Çerçevelerin sismik performansını araştırmaktır. Çok Katmanlı Merkezi Çelik Çaprazlı Çerçeveler, yüksek tek katlı bir bölme, taban ile çatı arasında diyafram ve düzlem dışı kolon desteği olmadan, yükseklik boyunca birden fazla destek paneline bölündüğünde oluşturulur. Çok Katmanlı Merkezi Çelik Çaprazlı Çerçeveler, endüstriyel depolar, uçak hangarları, stadyumlar, gösteri sanatları ve kongre merkezleri gibi yüksek tek katlı binalarda yanal kuvvetlere karşı dayanıklı sistem olarak yaygın bir biçimde kullanılmaktadır.

Bu araştırmada aynı temel üzerine oturan içlerinde malzeme olarak buğday bulunan ve üç farklı çapraz konfigürasyonuna sahip üç adet silo 'Çok Katmanlı Sınırlı Merkezi Çelik Çaprazlı Çerçeveler' tasarım ilkesi ile çözülmüştür. Belirlenen çapraz konfigürasyonları sırasıyla X-Çapraz, 2-Katmanlı X-Çapraz ve Ters V Çaprazdır. Bu çalışmada, çelik eleman hesaplamaları yapılarak çapraz, kiriş ve kolon elemanları tasarlanmış olup siloların deprem anındaki sismik performansları doğrusal ve doğrusal olmayan analizler ile incelenmiştir. Daha doğru ve kesin sonuçlara ulaşmak için Zaman Tanım Alanında Analiz yapılmıştır. Doğrusal ve doğrusal olmayan analizlerin sonuçlarına göre farklı çapraz konfigürasyonlarına sahip üç silo karşılaştırılmıştır.

Yapılan bu çalışmalar sonucunda X-Çapraz ve 2-Katmanlı X-Çapraz konfigürasyonlarının sismik performanslarının benzer olduğu, Ters-V Çapraz konfigürasyonun diğerlerinden tamamen farklı davrandığı anlaşılmıştır.

Anahtar Kelimeler: Çok Katmanlı Sınırlı Merkezi Çelik Çaprazlı Çerçeveler, Silo, Doğrusal Analiz, Doğrusal Olmayan Analiz.

TEŞEKKÜR

Başta, yüksek lisans eğitimimde ve akademik hayatımda desteğini ve yardımlarını hiçbir zaman esirgemeyip bilgisi ile bu çalışmanın oluşmasının yolunu açan danışmanım Prof. Dr. Bülent AKBAŞ'a,

ve göstermiş oldukları desteklerinden dolayı sevgili aileme ve arkadaşlarıma en içten teşekkürlerimi sunarım.

TABLE OF CONTENTS

LIST OF SYMBOLS and ABBREVIATIONS

Symbols and Abbreviations		Descriptions
R	:	Response Modification Coefficient
E	:	Modulus of Elasticity (MPa)
$(V_s)_{30}$	:	Average Shear Wave Velocity at the Top 30 meter Depth (m/s)
S_S	:	Mapped MCE_R Spectral Response Acceleration Parameter at Short Periods
S_1	:	Mapped MCE_R Spectral Response Acceleration Parameter at a Period of 1 second
F_S	:	Short Period Site Coefficient
F_1	:	Long Period Site Coefficient
S_{DS}	:	The Design Spectral Response Acceleration Parameter at Short Periods
S_{D1}	:	The Design Spectral Response Acceleration Parameter at a Period of 1 second
T_L	:	Long-Period Transition Period (s)
T_A	:	Horizontal Elastic Design Spectrum Corner Period (s)
T_B	:	Horizontal Elastic Design Spectrum Corner Period (s)
$S_{ae}(T)$	:	Horizontal Elastic Design Spectral Acceleration (g)
Ω_0	:	Overstrength Factor
F_y	:	Minimum Yield Stress (MPa)
F_u	:	Minimum Tensile Stress (MPa)
F_{ye}	:	Expected Yield Stress(MPa)
F_{ue}	:	Expected Tensile Stress (MPa)
γ	:	Weight per Unit Volume (kN/m^3 or t/m^3)
D	:	Dead Load
L	:	Live Load
Q_E	:	Earthquake Effect
ρ	:	Redundancy Factor
$Q_E^{(H)}$	:	Horizontal Earthquake Effect

$Q_E^{(X)}$	:	X-Direction Horizontal Earthquake Effect
$Q_E^{(Y)}$	:	Y-Direction Horizontal Earthquake Effect
$Q_E^{(Z)}$	:	Vertical Earthquake Effect
V	:	Volume (m^3)
W	:	Weight (t)
A_g	:	Gross Cross-Sectional Area of Member (mm^2)
L_c	:	Effective Length of the Member (mm)
r	:	Radius of Gyration (mm)
F_e	:	Elastic Buckling Stress (MPa)
F_{cr}	:	Critical Stress (MPa)
P_n	:	Nominal Compressive Strength (N)
$\phi_c P_n$	:	Design Compressive Strength (N)
P_r	:	Demand of the Member (N)
D	:	Diameter of the Member (mm)
t	:	Thickness of the Member (mm)
λ_{md}	:	Width-to-Thickness Ratio for Moderately Ductile Members
R_y	:	Ratio of the Expected Yield Stress to F_y
P_y	:	Axial Yielding Load (N)
P_{cr}	:	Critical Buckling Load (N)
k	:	Stiffness of the Member (N/mm)
δ_y	:	Axial Yielding Displacement (mm)
δ_{cr}	:	Critical Buckling Displacement (mm)
Δ_i	:	Top Displacement (cm)
V_{base}	:	Base Shear Force (kN)
AFAD	:	Disaster and Emergency Management Presidency
ANSI/AISC 341 – 16	:	Seismic Provisions for Structural Steel Buildings
ANSI/AISC 360 – 16	:	Specification for Structural Steel Buildings
ASCE7 – 16	:	Minimum Design Loads and Associated Criteria for Buildings and Other Structures
BRBFs	:	Buckling-Restrained Braced Frames
CBFs	:	Concentrically Braced Frames

CQC	:	Complete Quadratic Combination
ÇYTHYDE – 2016	:	Code on Design, Calculation and Construction Principles of Steel Structures
DD-2	:	Earthquake Ground Motion Level with 10% Probability of Exceedance in 50 years (Return Period of 475 years)
EBFs	:	Eccentrically Braced Frames
IDA	:	Incremental Dynamic Analysis
MT-BFs	:	Multi-Tiered Braced Frames
MT-BRBFs	:	Multi-Tiered Buckling-Restrained Braced Frames
MT-OCBFs	:	Multi-Tiered Ordinary Concentrically Braced Frames
MT-SCBFs	:	Multi-Tiered Special Concentrically Braced Frames
NLRH	:	Nonlinear Response History
OCBFs	:	Ordinary Concentrically Braced Frames
SCBFs	:	Special Concentrically Braced Frames
SRSS	:	Square Root of Summation of Square
TBDY – 2018	:	Turkish Building Seismic Code – 2018

LIST OF FIGURES

LIST OF TABLES

1. INTRODUCTION

1.1. Scope, Objectives and Contribution of Study

Silos are special structure types designed for storage of materials with various grain sizes for being used when necessary. In order to keep dry/granular materials such as wheat, cement, water, mud, silos are widely used in industrial buildings. The structure of a silo is normally a vertical steel tank supported by a braced steel frame seated on concrete foundation.

These structures generally have a high center of gravity, making the structure extremely sensible to ground shaking as a result of raised bending moments and axial loads. If a silo collapses, it may lead to waste of material, cleaning up the polluted material, substitution costs, and most vital one is potential injury or deaths of people. As a result of seepage of hazardous chemicals, loss of functionality, fires or environmental contaminations can happened if the earthquake damage industrial liquid storage tanks. Some common damages to ground supported tanks in past earthquakes include cracking at the bottom plate, elastic or elasto-plastic buckling of the tank wall, failure of the ground anchorage systems, sloshing damage around the roof and failure of the piping system. Thus, in order to be able to avoid the local failure, silos are designed in a way to distribute the forces within the structure again.

In order to be able to supply lateral resistance for tall single-story buildings such as commercial, performing arts, sports, and industrial structures, Multi-Tiered Braced Frames (MT-BFs) are mostly selected. MT-BFs include two or more bracing panels that are stacked in a vertical way in a single story building. For too tall stories, MT-BFs are usually used. Conventional braces that extend the full story height no longer consider as an economical or practical option. Since the brace slenderness and cross-sectional width-to-thickness limits associated with ductile braced frame requirements can be more easily fulfilled with shorter braces, MT-BFs represent an effective solution in seismic applications.

In this thesis, three silos by considering wheat as the material, sitting on the same foundation, is modeled. The purpose of this study is to examine brace, beam and column designs for Multi-Tiered Ordinary Concentrically Steel Braced Frames.

Besides, the seismic performance of the silos in the earthquake based on site observations is investigated and dynamic analysis is performed.

In the scope of the study, silos are modeled with SAP2000 Finite Element Program and linear and dynamic analysis are occurred. For the analysis calculation of three silos, 2019 Draft Pipeline Systems Code and New Zealand Society for Earthquake Engineering 2009 (Seismic Design of Storage Tanks) is used. For steel element calculations in the infrastructure, Turkish Building Earthquake Code (TBDY 2018), Minimum Design Loads and Associated Criteria for Buildings and Other Structures (ASCE7-16), Code on Design, Calculation and Construction Principles of Steel Structures (ÇYTHYDE 2016) are considered as regulation.

The effects found as a result of the tank calculations is transferred to the infrastructure through finite element model. The design of the infrastructure is carried out using the transferred loads. In the steel system, calculations are performed according to the principles of capacity design in accordance with Seismic Provisions for Structural Steel Buildings (ANSI/AISC 341-16) Section F1.4c “Multi-Tiered Braced Frames”.

Multi-Tiered Braced Frames are more effective in compressions and they use shorter braces that satisfy the slenderness limits more easily. Therefore, MT-BFs are more economical and practical than conventional braces that extend over the height of story. Besides, regarding seismic design regulations, beams and columns of Concentrically Braced Frames (CBFs) need to be designed in accordance with the forces that is created during brace yielding and buckling. Since reduced bracing member sizes in MT-BFs normally result in smaller beam and columns in addition to lower connection loads, the total cost of the structure can dramatically decrease.

Owing to Multi-Tiered Braced Frame method, the columns are supported laterally by braces at each tier level. Short braces, which are used at each tier level, instead of braces that extend the full height of story reduce dimensions of members and thus tonnage of steel. In other words, this framing configuration prevents column instability and limits the drifts to prevent braces from collapsing.

1.2. Literature Survey

1.2.1. General Information

As the construction industry moves forward with technology and innovation, designers are motivated to improve structures that perform more efficiently. Before the introduction of systems such as Multi-Tiered Braced Frames (MT-BFs), buildings with wide open spaces and high ceiling heights may seem impractical, especially in areas exposed to high seismic activity. However, specific requirements for designing these MT-BF systems are introduced in the Seismic Provisions for Structural Steel Buildings, ANSI/AISC 341-16, referred to as the 2016 AISC Seismic Provisions. This can be helpful for supporting both for these structures and for the seismic design industry.

In Multi-Tiered Braced Frame system, in a single story building, two or more panels of bracing are stacked vertical. Commonly used configurations for multi-tiered bracing are X-, Chevron and V-bracing, as shown in Figure 1.1 [1]. At intermediate levels between floors, horizontal struts extend between each panel and result in a transfer of the axial loads between the braces. Various shapes can be used for braces and struts, such as angles, pipes, tubes, or I-shapes. However, columns are typically I-shaped members and are oriented in a way that the out-of-plane buckling of the frame is about the major axis of the column, as shown in Figure 1.2 [1]. Thus, the column can tolerate out-of-plane buckling over the full height of the building. In order to decrease the minor axis unbraced lengths, the columns are braced in the plane of the frame by the struts. Instead of using braces that extend over the full height of the frame, MT-BFs use shorter braces which are more efficient in compression and more easily fulfill the limits of slenderness. Therefore, MT-BFs provide an economical and practical solution for such buildings. This framing systems are commonly used in a variety of industrial steel structures, stadiums and other sports facilities, convention halls, performing arts centers, warehouses and airplane hangars. Besides, MT-BFs are used for legs of conveyors in industrial plants, which are non-building structures. MT-BFs are also used for crane runway girders when intermediate lateral bracing is required along the column height in industrial buildings. Figure 1.3 shows the example of Multi-Tiered Braced Frames [2].

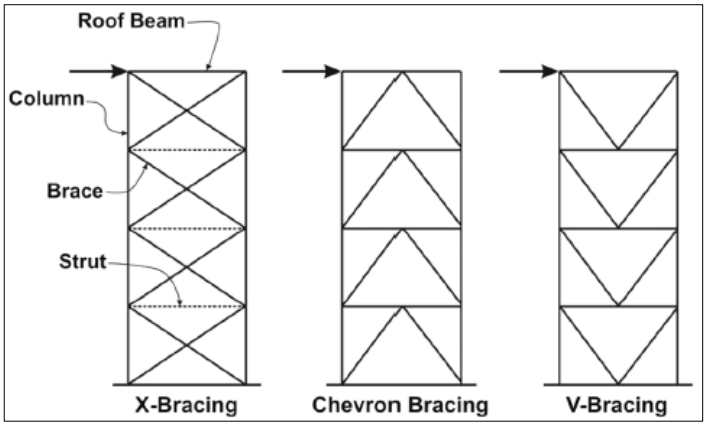

Figure 1.1: MT-BF bracing configurations.

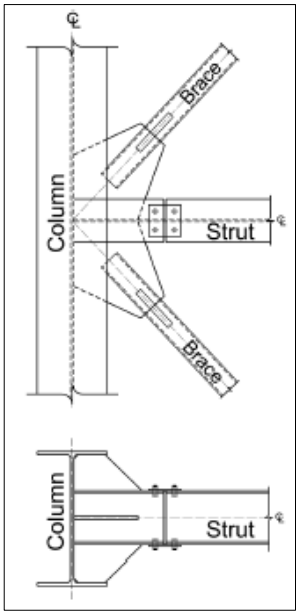

Figure 1.2: Orientation of columns and struts.

Figure 1.3: MT-BFs.

Braced frame systems are designed to tolerate seismic loads and dissipate energy from an earthquake by yielding at predetermined locations, in an effective way. Nevertheless, in taller story height structures, structuring single brace from floor to floor may not be considered as a practical way to withstand the lateral loads efficiently. For taller story heights, longer braces that is positioned at a right angle to the horizontal force are used. In this situation, it is necessary to use larger member sizes to satisfy the increased brace slenderness and resist to axial loads. Furthermore, in this case, the number of shapes of steel that ensure the seismic ductility condition is reduced. Also, increasing the angle between the floor and the brace cannot behave as efficiently as the more horizontally positioned braces against the horizontal loading. Instead of Conventional Braced Frame, using MT-BF system removes these issues and improves the desired ductile building performance for tall-single story structures.

A Conventional Braced Frame and a Multi-Tiered Braced Frame examples are shown respectively in Figure 1.4 and Figure 1.5 [3], [4].

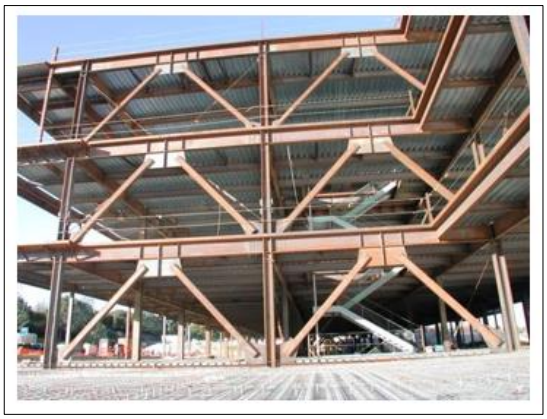

Figure 1.4: Conventional Braced Frame.

Figure 1.5: Multi-Tiered Braced Frame.

During large earthquakes, MT-BFs is modeled on the yielding of the determined elements in the frame, like other seismic systems. The ductile behavior of the elements by yielding indicates that a big portion of energy released from the earthquake can be able to absorb. This seismic energy is also dispersed by the elongation, shortening, buckling, yielding or bending behaviors that occur in the steel elements. In MT-BF systems, columns and struts are designed to be protected from damage, while braces are designed to experience deformation.

According to the differences in brace sizes and tier heights, buckling usually happens in the weakest tier. If these factors are designed in a similar way, defects in geometry and material determine the first tier of buckling and diffuse into the other tiers until all the compression braces in the frame are buckled. At this point, the struts, which has an important effect, form the load path by using tension braces. The struts and braces act as the truss system between the lateral supports and the tension braces load lateral force on the columns.

Prior to 2016 AISC Seismic Provisions, MT-BF systems were considered as K-Bracing and therefore it was restrained from use in practice. In a configuration of K-Bracing as shown in Figure 1.6, two or more braces are connected to the column at the point where there is no lateral support [5]. Therefore, unbalanced forces transmitted from the braces result in large bending forces in the columns. Without the compression struts, which are necessary to remove this undesired lateral load, the system is unstable. For this reason, this type of configuration is prohibited in seismic design. [6]

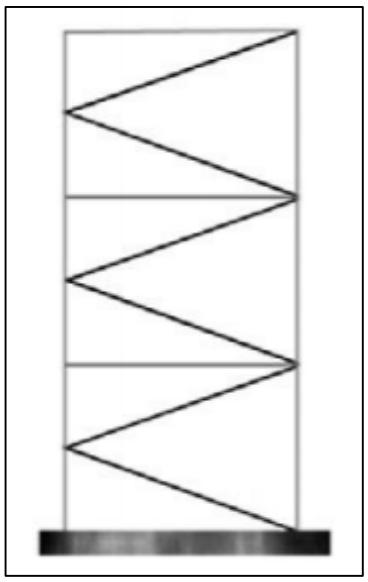

Figure 1.6: K-Braced Frame.

MT-BF system are published in the 2016 AISC Seismic Provisions regulation. Unlike K-Bracing, the use of struts prevent the transfer of bending forces to the columns. Sections of the MT-BFs as Ordinary Concentrically Braced Frames (OCBF), Special Concentrically Braced Frames (SCBF) and Buckling-Restrained Braced Frames (BRBF) can be reached Section F1.4c, F2.4e, and F4.4d, respectively. Eccentrically Braced Frames (EBF) are taken out from them. The reason of this consideration is that these frame are considered to be unable to fulfill the bracing requirements in interconnection without a diaphragm or link beam.

Multi-Tiered Braced Frame systems need a lot of ductility in order to absorb earthquake energy in areas where earthquake risk is very high. Multi-Tiered Special Concentrically Braced Frames (MT-SBCFs) are used to minimize buckling of brace at each tier and their effects on struts, columns and connections. For each direction of loading, after the compression brace buckles, it is desirable that the tensile brace has the necessary tensile strength to resist earthquake loads. Figure 1.7 shows the representation of tension and compression brace pairs at each tier for configuration of Chevron Bracing.

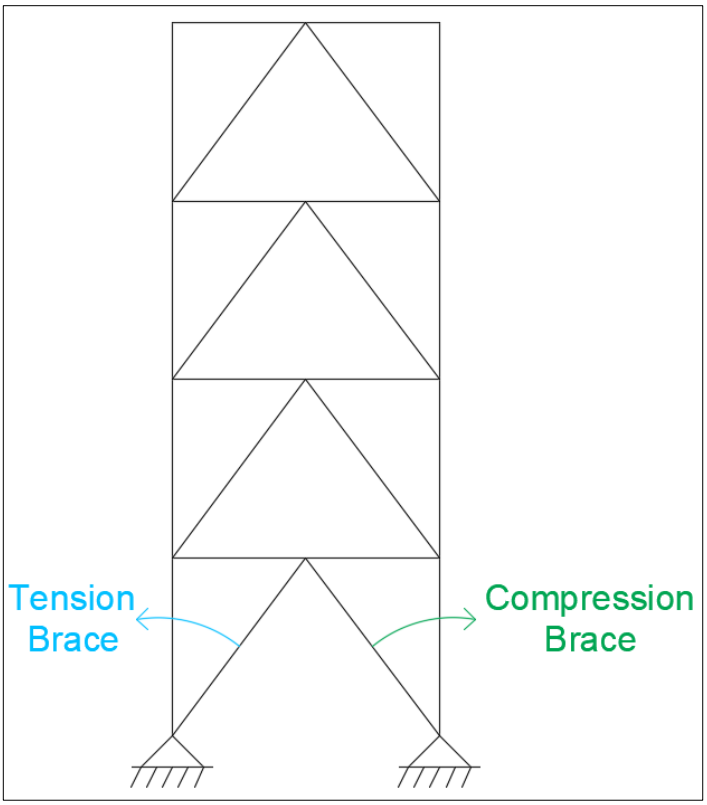

Figure 1.7: Representation of tension and compression brace pairs at each tier for Chevron Bracing.

Although there are struts that resolve the unbalanced lateral load between tiers, some bending is induced in the columns since not all of the compression braces in a single MT-BFs are buckled at the same time. The buckling of braces that experience greater horizontal drift and the buckling of braces that are not experienced drift are at different times. This unequal drift in each tiers causes bending forces in the columns. In ductile designed braces, displacements must be limited in order to prevent collapsing due to tensile and compression forces of the braces during earthquakes. The column stiffness limits the tier drifts to a significant amount. Out-of-plane behavior that may contribute to column instability should not be ignored. In general, braced frame systems give priority to behavior of the braces, while Multi-Tiered Specially Concentrically Braced Frame columns must be enough in stiffness and bending. Columns in MT-SCBF systems are expected to sufficiently stiffening the frame, while in other frames the brace behavior takes precedence. Figure 1.8 presents the progression of brace buckling and yielding in MT-SCBF [6].

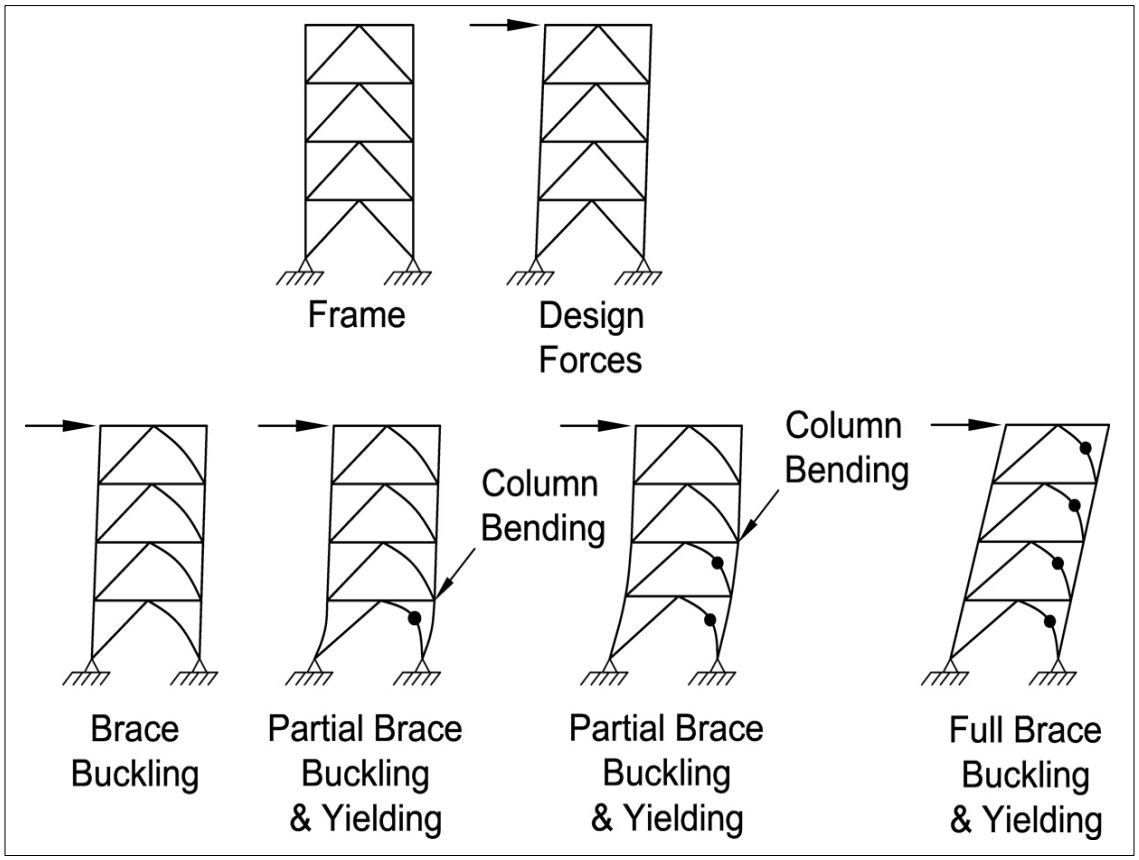

Figure 1.8: Progression of brace buckling and yielding in MT-SCBF.

Multi-Tiered Ordinary Concentrically Braced Frames (MT-OCBF) is applied in buildings in areas with low earthquake hazard. Some of the MT-BF configurations are allowed to be used in MT-OCBF. The first rule is that the braces at the same tier must be positioned in opposite directions. The second rule is that struts must divide each tier and support the columns. Since the earthquake energy is less in low seismic zones, ductility is not required for the frame system. Therefore, compared to MT-SCBF systems, the design requirements are loosened.

The design forces of each element are determined. The braces are dimensioned according to the determined axial loads. Columns, struts and connections are then sized by multiplying the results with an overstrength factor of 2 and an additional factor of 1.5. With these multiplications, it is targeted to guarantee that the inelastic behavior occurs in the braces and to ensure the stability of the frame by keeping other elements elastic. Increasing the forces by factors is also an effective way so that the columns can resist in-plane bending, which is occurred due to the forces at the braces and the drifts.

As long as additional provisions are satisfied, the requirements of lower ductility also permit structures to be supported by only tension bracing. In this system, when the braces are loaded in tension, they are only assumed effective in resisting seismic forces and any contribution from compression brace is ignored. In tension-only bracing systems, the slenderness limit for steel elements is specified as 200. Since the buckling of these braces does not affect the other steel members much, there is no need to increase the design forces of braces by a factor of 1.5. If lateral support is not provided at intermediate tiers, the frames are allowed to yield and some of unbalanced lateral loading is transferred to the columns as a bending force. The AISC Seismic Regulations specify that this unbalanced lateral force at any tier level shall not be less than 5% of the larger horizontal brace component resisted by the braces below and above the tier level.

Multi-Tiered Buckling-Restrained Braced Frames (MT-BRBF) are designed so that the compression braces retain their full strength during the major earthquakes. In SCBF systems, buckled compression braces obtain less resistance than tension braces, while in BRBF systems, compression braces can reach a value close to tensile yield strength. On account of this situation, increasing buckling behavior between tiers, is avoided. For this reason, MT-BRBF system is considered more stable than other MT-BF systems and there is no need to be placed opposing pair at tier levels.

Both tension and compression braces present ductile behavior on the principle of yielding of the steel. But, in BRBF systems, there is a load imbalance between tiers as a compression strength adjustment factor is used for all compression braces. Even though all properties such as dimension and material grade, etc. are introduced correctly, the compression strength adjustment factor creates a lateral load when the compression and tension braces come to a single node. Besides, even though two identical braces are directed in the same direction, the 2016 AISC Seismic Provisions require that a minimum notional load equal to 0.5% times the adjusted braced strength frame shear of the higher strength adjacent tier. The aim of these minimum lateral loading is to take into account unbalanced loads, the conditions caused by tolerances steel cross-sections, and varying brace strains.

The consideration of absolute and notional loads in the BRBF is visualized in Figure 1.9 [6]. Absolute loading due to two different BRBF core is represented by “ABS”. At rest of the tiers, the braces are shown with “NOT” because they do not cause load imbalances. Thereafter, columns are designed to analyze these loads in bending at every tier level.

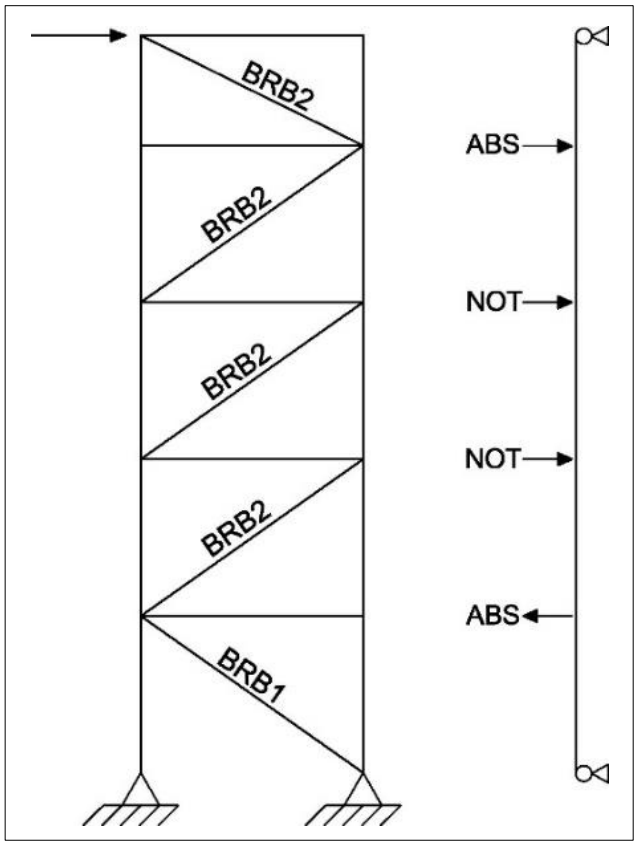

Figure 1.9: MT-BRBF column design loads.

With the introduction of Multi-Tiered Braced Frame systems into the AISC Seismic Regulation, the scope of buildings that can resist seismic forces is expanded and engineers have sufficient knowledge to design MT-BFs. Although the magnitude and location of the earthquake that will occur are not known, MT-BF systems have the necessary strength and reliability as long as they are designed in accordance with the regulation.

1.2.2. Previous Studies

Silvestri et al. (2012) proposed the first theory with two assumptions excluding the assumption of horizontal shear among sequencial grains. These two assumptions are based on the friction forces of Janssen and Koenen (1895) and the basic assumptions of Eurocode 8 (EN 1998-4 2006). This theory is concerned with studying the seismic behavior of squat silos filled with grain-like materials.

This article presents ideas for improvement to the original theory, which is put forward by Silvestri et al. More consistent results are obtained on the static and dynamic movements in the silo walls and the distribution of the vertical normal pressure. In order to check the theoretical model in static conditions, a comparison with the Janssen and Koenen (1895) theory for silo design is performed as well.

For the evaluation of seismic effects on the walls of flat-bottom silos containing grain-like materials, this study advances the general analytical formulation suggested by Silvestri et al. (2012) [7].

Uckan, Akbas, Shen, Wen, Turandar and Erdik (2014) investigated the seismic performance of silos after the Van earthquake. In order to keep dry/granular materials such as wheat, cement, water, mud, silos are widely used in industrial buildings. Tanks, which are usually in an elevated position for unloading purposes, are seated on a foundation and supported by a braced steel frame. Overturning moments at the base make the structure sensitive to axial loads in columns.

In this study, the seismic performances of the silos in the Van earthquake according to the field observations and the seismic behavior of the two steel-elevated silos in the earthquake zone are investigated, respectively. While one of the silos is not damaged, the other silo is experienced minor harms as a result of the buckling and falling of the concrete support. In order to examine the seismic behavior of two silos,

Nonlinear Dynamic Time History Analyses are carried out. Several suggestions are made so as to develop the seismic performance of new silos, lastly.

Model details of Silo-1 and Silo-2 are shown in Figure 1.10 [8].

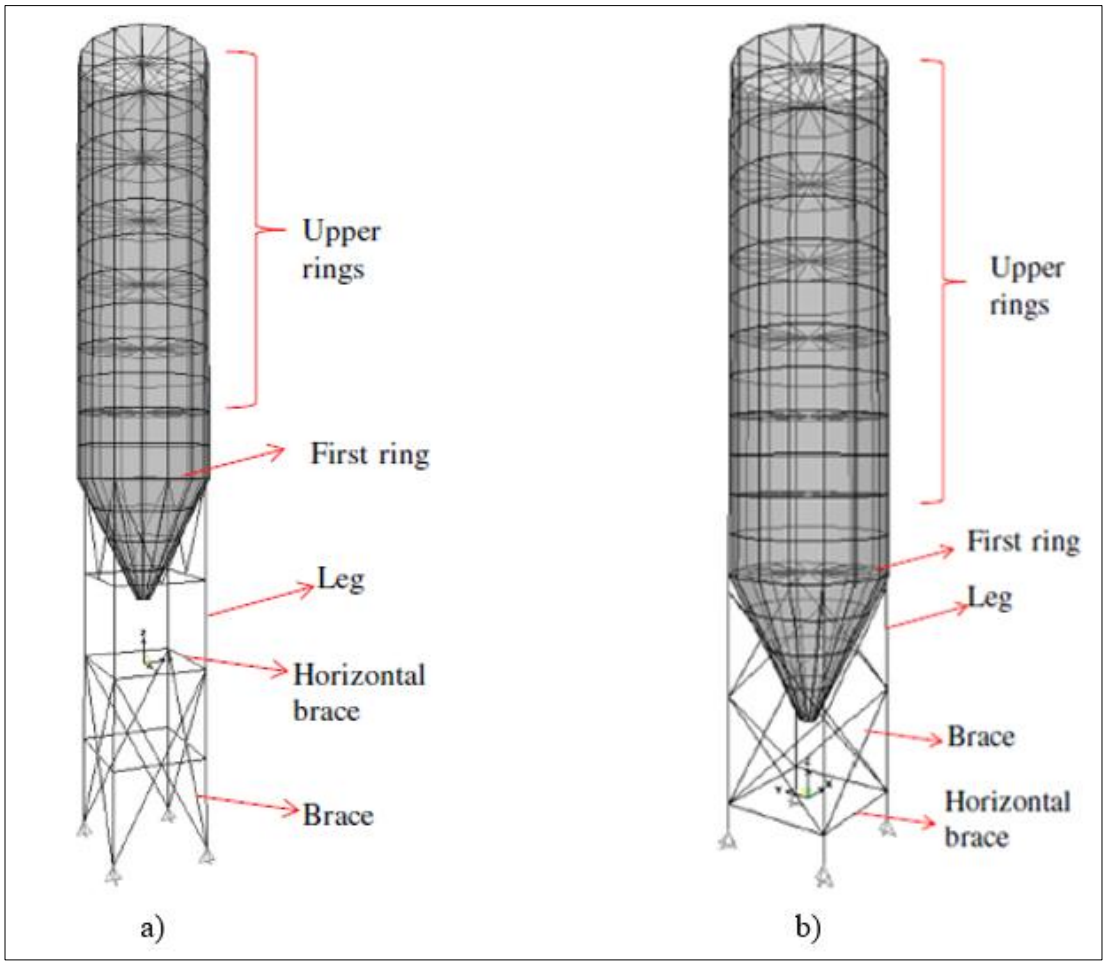

Figure 1.10: Model details of a) Silo-1, b) Silo-2.

In compliance with the interpretations of writers, most uninsured silos are either damaged or completely collapsed, during the earthquake. Legal problems also occur between silo owners and silo providers, as the movement or collapse of equipment in these silos causes market loss, business interruptions and stock damages. The predicted overall economic loss in the earthquake is 1-2 billion USD. All these experiences are a sign that the existing fragile and weak structures should be strengthened and new safe and stronger building and non-building structures should be built [8].

Imanpour and Tremblay (2014) studied the seismic performances moderately ductile 3- and 5-Tiered Concentrically Steel X-Braced Frames in accordance with present Canadian code regulations for steel structures. Nonlinear seismic behavior of

the braced frames is investigated through nonlinear dynamic analyses to study the influence of the design parameters including the number of bracing panels and the use of out-of-plane notional load in design. The focus is on the in-plane seismic demand imposed on the columns when buckling and yielding of the bracing members occur. Out-of-plane stability of columns is also investigated.

Figure 1.11 illustrates the geometry of 3- and 5-Tiered X-Braced Frames [9].

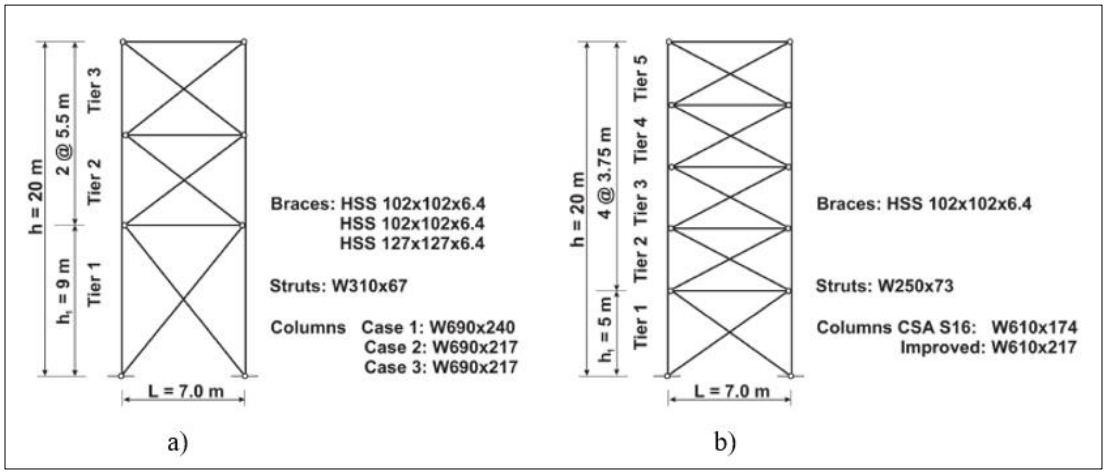

Figure 1.11: Geometry of a) 3-Tiered, b) 5-Tiered Braced Frames.

This paper shows a complementary study applied to research the limit on the number of tiers for MT-BFs designed as moderately ductile with R_d = 3.0 and specifically examines the effect of the number of tiers and the out-of-plane notional load on the seismic performance of MT-BFs. In the design of the 3-Tiered X-Braced Frame, three different amplitudes of the out-of-plane notional loads are considered due to examine the possibility of using a smaller out-of-plane load for design of MT-BFs. A 5-Tiered Braced Frame with the same height and characteristics as the 3-Tiered Braced Frame is selected to study the influence of number of bracing panels on the seismic performance of MT-BFs.

Roof drifts, drift demands in the critical tier and in-plane and out-of-plane flexural moment demands on the columns are obtained through nonlinear dynamic analysis in each case. Then, each case examines and compares to assess the design assumptions. The results of numerical studies show that the out-of-plane bending demand on the columns of MT-BFs is smaller than the value resulting from the

notional transverse load and in-plane bending demand increase with the number of tiers [9].

Imanpour, Tremblay, Fahnestock and Stoakes (2016) examined a seismic design strategy that is based on single-story Steel Concentrically Braced Frames, which are separated into two tiers. In this seismic design strategy, the columns are designed to withstand axial loads acting along with the in-plane bending demand along the frame height. This method focuses on controlling tier drifts for keeping safe the braces from inelastic behavior that can cause them to fracture.

This research discusses avoiding column instability and restraining tier drift demands to defend braces from fracture. This approach is improved for a 2-Tiered Braced Frame, which is a prototype, positioned in high seismic zone and expose to in-plane seismic demand.

The frame geometry is illustrated in Figure 1.12 [1].

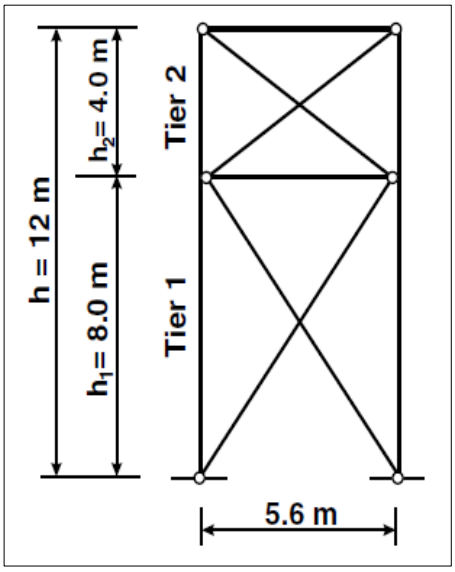

Figure 1.12: Frame geometry of a prototype 2-Tiered Steel Braced Frame.

The current seismic design regulations for Special Concentrically Braced Frames are performed to the prototype frame and its seismic behavior is investigated through nonlinear static and dynamic analyses. During these analyses, primarily the vertical distribution of the brace inelastic deformations and the effect of this distribution on the column behavior are examined, and then additional seismic analyses are carried out to evaluate the expected bending demand on the columns. Design provisions are suggested so that the column can withstand the combined axial

and bending demands. Besides, this approach focuses on controlling drifts of tiers to avoid extreme inelastic demand on the braces.

According to the research, the analyses show that the produced MT-BFs perform the targeted behavior and avoid undesirable limit states. This method should be validated for more different 2-Tier Braced Frames by developing similar design requirements. Future studies should examine the stability of columns exposed to out-of-plane bending demands, instead of columns exposed to in-plane seismic demands only [1].

Figure 1.13 illustrates the Multi-Tiered Concentrically Steel Braced Frame [1].

Figure 1.13: Multi-Tiered Concentrically Steel Braced Frame.

Imanpour, Tremblay, Davaran, Stoakes and Fahnestock (2016) evaluated the seismic performance of Multi-Tiered Steel Concentrically Braced Frames designed in compliance with the 2010 AISC Seismic Provisions. Various commercial, performing arts, sports and industrial facilities are designed as single-story steel structures. Concentrically Braced Frames (CBFs) are used to provide lateral resistance to these structures. Single brace members that extend from the foundation level to the roof level do not give practical and economical results in buildings with tall open areas. Therefore, Multi-Tiered Braced Frames configuration should be used.

In this research, the seismic performance of seven two to six tiers Special Concentrically Braced Frames (SCBFs) with a height of 9 to 30 m, located in a high seismic region are investigated according to the 2010 AISC Seismic Provisions. 3D finite element models are created with shell elements to examine the seismic

performance of buckling response of the 2- and 4-Tiered Frames by considering the buckling response of the columns. Then, for the analysis of column stability and seismic frame response, 3D finite element models with fiber-based beam-column elements are used for all frames. According to current Multi-Story CBF method, it is shown to develop drift concentration in a single tier and high in-plane column bending demand by designing Multi-Tiered CBFs. Alternative designs are investigated as a solution to the bending stretch and column instability problems that occur in some cases.

The geometry of MT-BFs with different heights and number of tiers are shown in Figure 1.14 [2].

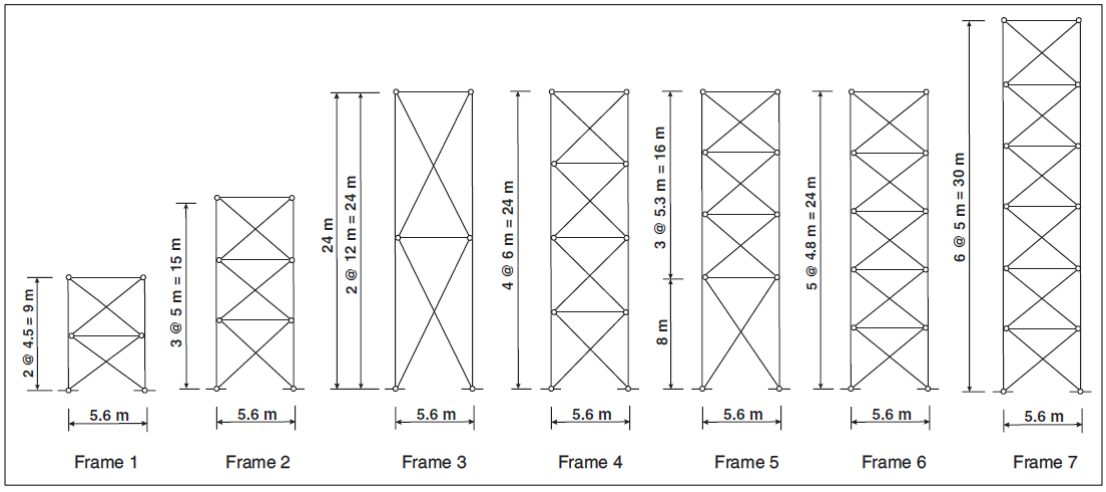

Figure 1.14: Geometry of MT-BFs studied.

According to this paper, in MT-BF designs, drift is more significant when the height of the critical tier is small compared to height of the story. This drift creates an in-plane bending request in the columns and this demand combines with the axial compressive capacity and causes the column to buckling. Tier drift leads to excessive inelastic demand on the connections and members. Hence, additional design provisions are required to consider limit states. For alternative MT-BF designs, using higher design seismic loads do not have important effects on the bending demand and the column buckling failure. It is concluded that there is more tier drift demand and lower column flexural moments in frame systems using buckling-restrained bracing compared to Conventional Braced Frames. The fixed bases have higher in-plane stiffness relative to pinned base, which helps to decrease drifts in the bottom tier.

The braced frames in this paper are limited. The accuracy of the results of the investigations should be compared with other MT-BF systems. By performing 3D finite element analysis, flexural-torsional buckling should also be examined [2].

Imanpour and Tremblay (2016) investigated the seismic response of Steel Multi-Tiered Concentrically Braced Frames in diaphragm systems. The seismic behavior of prototype 3-Tiered moderately ductile and prototype 5-Tiered limited ductile braced frames are examined in accordance with the provisions of CSA S16-14. Due to evaluate the in-plane bending demand on columns, analysis methods are suggested. The seismic behavior of the braced frames are observed using Nonlinear Response History Analysis.

Figure 1.15 shows the geometry of 3- and 5-Tiered Concentrically Braced Frames [10].

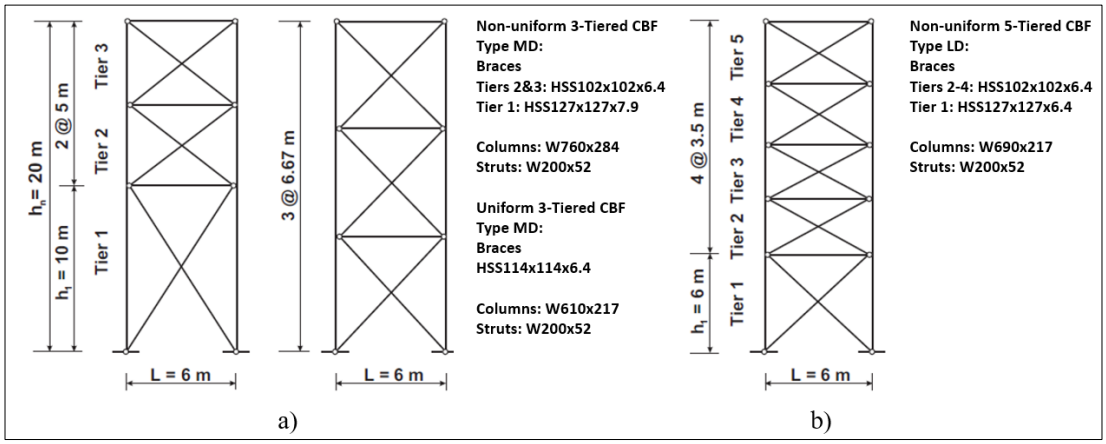

Figure 1.15: Geometry of a) 3-Tiered, b) 5-Tiered Concentrically Braced Frames.

In this article, three different prototypes, Multi-Tiered X-Braced Frames, are discussed and investigated according to the seismic design regulations of CSA S16. A structural analysis software is used to obtain column design forces and tier drifts. In order to study the seismic behavior of these three prototypes, Nonlinear Response History (NLRH) analysis is applied.

From this research, it is concluded that situations result in different tier drift and force demands, may improve in MT-BFs and should be taken into account. This study only considers in-plane behavior. Future studies should also examine out-of-plane behavior and combined in-plane and out-of-plane bending behaviors [10].

Imanpour and Tremblay (2016) studied a tall structure, which is 4-Tiered moderately ductile Concentrically Steel Braced Frame. This frame is built for an airplane hangar and is located in the seismicity zone of Canada. This system is evaluated with two loading cases as shown in Figure 1.16. The first scenario represents the braces under tension reach its expected strength in tension and the other braces under compression just buckle and reach its expected buckling strength. The second scenario represents the braces under tension remain at their expected strength and yield a little bit and the braces under compression buckle and reach their post buckling strength.

Brace loading scenario for both Multi-Storey Braced Frames and Multi-Tiered Braced Frames are shown in Figure 1.16 [11].

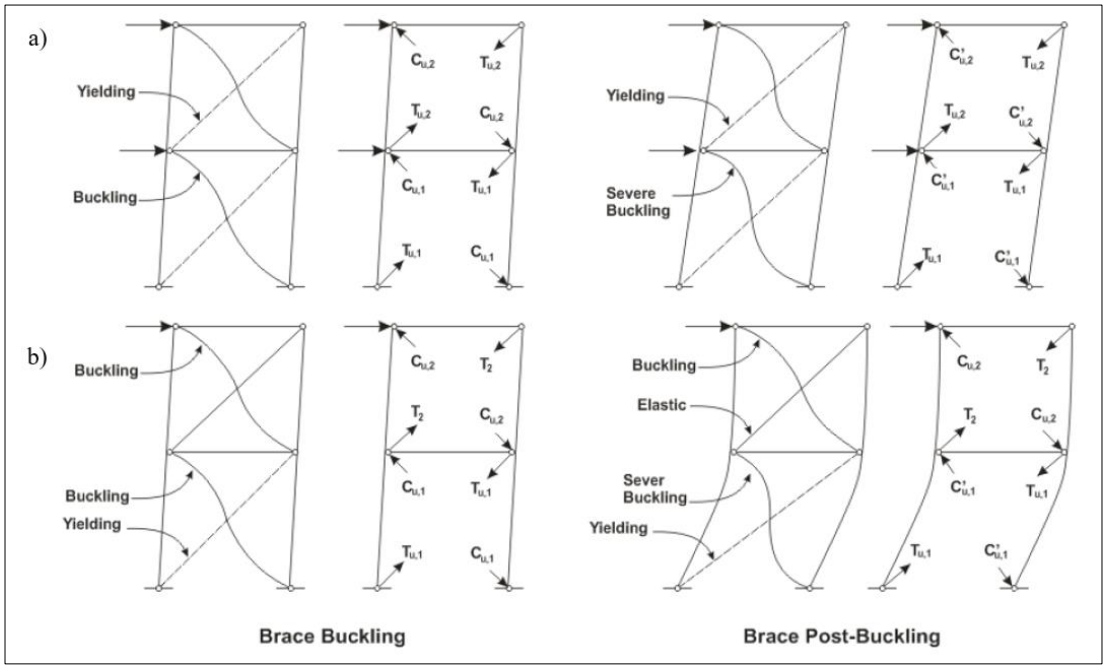

Figure 1.16: Brace loading scenario for a) Multi-Storey Braced Frames, b) Multi-Tiered Braced Frames.

The building is 24 m height and is located on a site class E in Vancouver, BC. The height and width of the airplane hangar have sufficient space for necessary maintenance activities. The airplane hangar system is created in the OpenSees and its seismic performance is examined with Nonlinear Response History (NLRH) analysis. Bracing members and struts are designed in respectively. Then, columns are designed by two design approaches: (1) excluding CSA S16 Special Requirements and (2) following CSA S16 Special Requirements.

The configuration of the 4-Tiered Concentrically Steel Braced Frame is shown in Figure 1.17 [11].

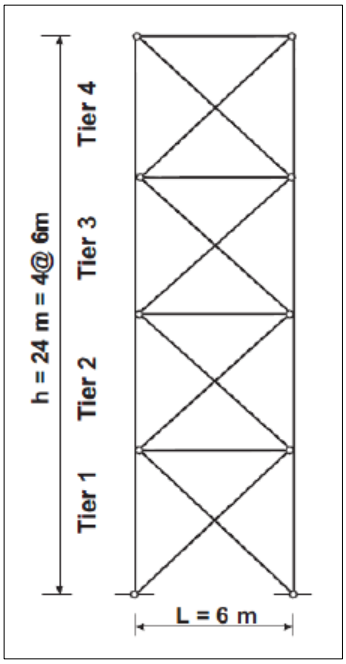

Figure 1.17: 4-Tiered Concentrically Steel Braced Frame.

In the first approach, where only axial load is considered, inelastic deformations in the braces occur in the critical tier. In this case, in-plane bending is observed in the columns and this bending causes the column buckling. In the second approach, in which the combined effect of axial load and bending moments is considered, inelastic brace deformation occur in the bottom two tiers.

This response is consistent with the brace yielding and it is concluded that there is no buckling in the columns for this frame system [11].

Agarwal and Fahnestock (2018) researched the seismic behavior of Multi-Tiered Ordinary Concentrically Braced Frames (MT-OCBFs). The expected behavior from this framework is that it provides limited inelastic deformation capacity. The interaction effects of axial force, in-plane and out-of-plane moments are comprehensively evaluated in this paper.

The results from Nonlinear Pushover and Dynamic Response History Analyses from a subset of prototype MT-OCBFs with X-Bracing proportioned per the baseline (AISC 2010a) and new (AISC 2016) versions of the AISC Seismic Provisions are evaluated and compared. The frames are used as lateral force-resisting systems in a single-story industrial steel building assumed to be located in coastal California. MT-

BFs are used along the perimeter of the building in each of the two orthogonal directions and designed as OCBFs. A 3D numerical model is created using the OpenSees simulation platform.

Frame geometries and brace configurations studied are shown in Figure 1.18 [12].

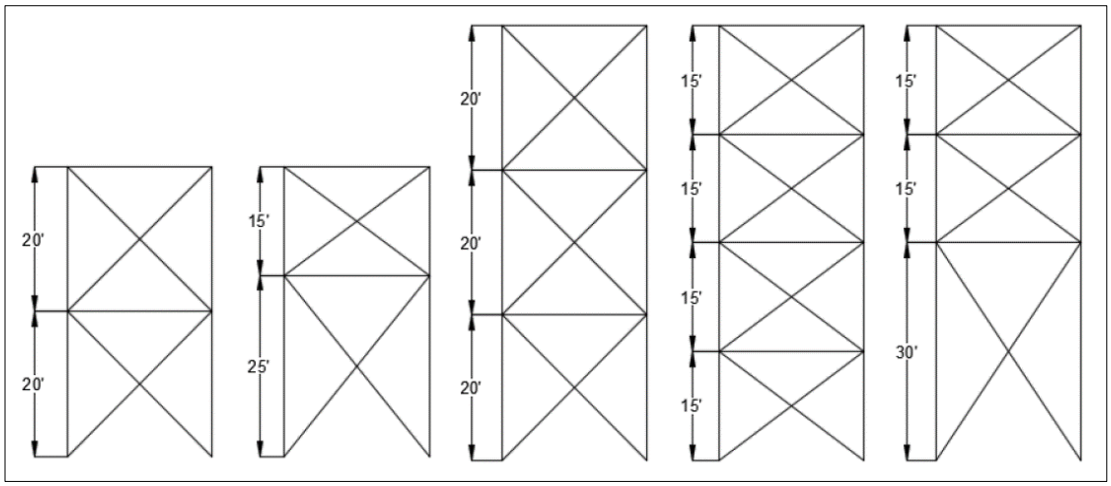

Figure 1.18: Frame geometry and brace configuration of MT-OCBFs.

In this study, the seismic performance of steel MT-OCBFs, with X-Bracing is evaluated. A set of five frames with two aspect ratios and varying number of tiers and tier height ratios are designed in accordance with the 2010 AISC Seismic Provisions (AISC 341-10), and the new 2016 AISC Seismic Provisions (AISC 341-16). AISC 341-10 does not contain guidelines for the design of MT-BFs and employ a simple axial force amplification to determine the minimum required column strength. AISC 341-16, on the other hand, contains specific guidelines for MT-BFs. In particular, the results from extensive research is used to define the minimum strength and stiffness requirements for Multi-Tiered Special Concentrically Braced Frames to achieve satisfactory seismic performance. In contrast, the research on Multi-Tiered Ordinary Concentrically Braced Frames is limited. This study assess the effectiveness of enhanced column in improving the seismic performance of MT-OCBFs.

The results of the nonlinear static (pushover) analyses show that column buckling occurs in all frames designed in accordance with AISC 341-10. All frames exhibit an initial linear elastic response until brace buckling and tension yielding occur in the braces. A series of nonlinear response history (dynamic) analysis is also conducted. The overall dynamic analysis results are in good agreement with the

pushover analysis results. Future work on MT-OCBFs should evaluate minimum stiffness requirement to address inelastic drift concentration. An ongoing study is also aimed at assessing the influence of brace configuration on the seismic performance of MT-OCBFs. Analysis techniques that both reasonably assess the imposed flexural demands on the columns and maintain the relatively simple design procedure for OCBFs are required [12].

Considering the previous studies, it can be understood that the seismic performance of steel-elevated silos located in earthquake region is comprehensively studied. Multi-Tiered Steel Concentrically Braced Frames are mostly investigated for prototype frames. In one of the sources studied, Multi-Tiered Steel Concentrically Braced Frames are evaluated as airplane hangar located on a site class E rather than prototype frames. However, solved Multi-Tiered Concentrically Braced Frames for silos is not found. Although there is a lot of research for Multi-Tiered Special Concentrically Braced Frames, it is limited for Multi-Tiered Ordinary Concentrically Braced Frames. The seismic analysis and design of silos as Multi-Tiered Ordinary Concentrically Braced Frames examine in this thesis widely in accordance with Section F1.4c in AISC 341-16.

2. METHODOLOGY

2.1. Introduction

When a structure is designed, that structure will subject to some kind of excitations such as an earthquake. An earthquake is caused by a sudden slip on a fault. The tectonic plates always move slowly, but due to friction they get stuck at their edges. When the stress on the edge overcomes the friction, an earthquake happens by releasing energy in a form of waves that travel through the earth's crust and cause the shaking that we feel [13]. Once the structure is exposed to the earthquake, it shows a response. In most cases, joints experience displacements with respect to each other cause internal forces. That means some types of the internal forces will be created within the structure. The purpose of earthquake resistant construction design is to limit the possible damages caused by these internal forces.

The main principle of the design of earthquake resistant buildings according to codes is:

- No damage to the structural and non-structural system elements in buildings, in weak earthquakes,
- The damage that may occur in structural and non-structural elements, in moderate earthquakes, remains limited and repairable,
- Limiting the occurrence of permanent structural damage to ensure life safety, in high intensity earthquakes.

The standard design earthquake ground motion for designing buildings is considered as DD-2 Earthquake Ground Motion in which the probability of exceedance of spectral magnitudes in 50 years is 10% and corresponding return period is 475 years [14].

Table 2.1: Earthquake Ground Motion Levels.

Earthquake Ground Motion Level	Probability of Exceedance	Return Period
DD-1	2% / 50 years	2475 years
DD-2	10% / 50 years	475 years
DD-3	50% / 50 years	72 years
DD-4	68% / 50 years	43 years

For designing, Mode Superposition Method is used as linear and Time History Analysis is used as nonlinear dynamic analysis methods. Mode Superposition Method is a powerful technique to reduce the computation time, when performing dynamic response analyses of linear structures. The dynamic response of a structure can be approximated by a superposition of small number of its eigenmodes, using Mode Superposition Method. Nonlinear Time History Analysis is used for simulating a structure behavior under severe earthquake which is considered more proper than Mode Superposition Method. In order to be able to perform Time History Analysis, huge amount of calculations and at least 11 earthquake ground motion sets are required.

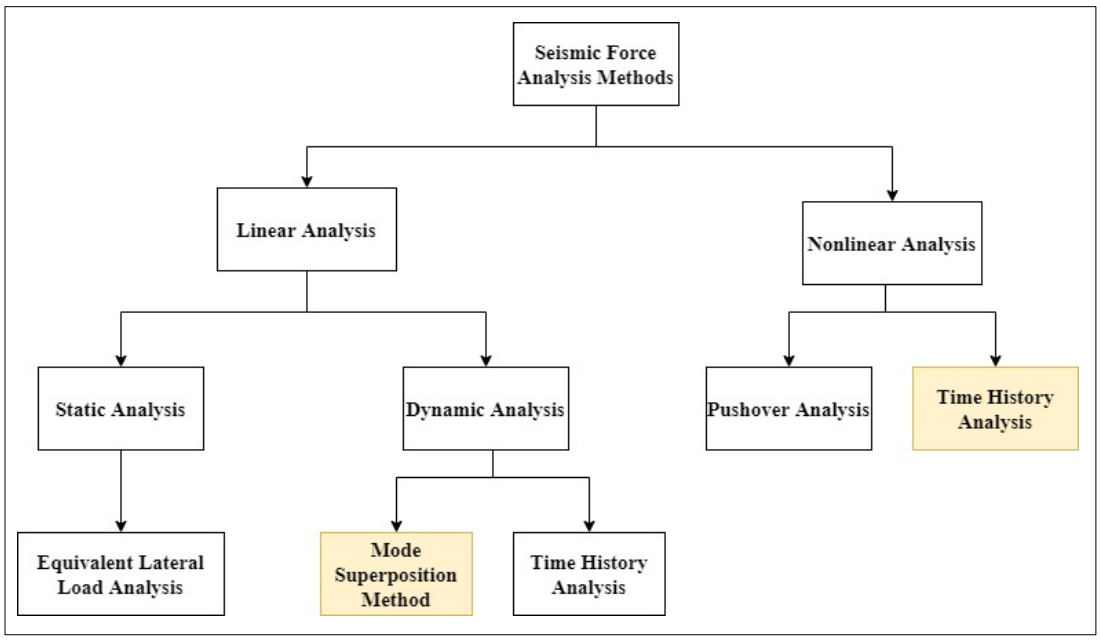

Figure 2.1: Seismic force analysis methods.

2.2. Mode Superposition Method

Mode Superposition Method is an efficient tool for evaluating of the response of linear systems subjected to dynamic agencies. It is a method of using the natural frequencies and mode shapes from the modal analysis for characterizing the dynamic response of a structure to transient, or steady harmonic excitations.

When making earthquake calculations with Mode Superposition Method, the horizontal elastic design spectrum is used in the direction of a given earthquake and in each considered vibration mode, the maximum values of the response magnitudes are calculated by the Modal Superposition Method. The largest non-synchronous modal behavior magnitudes calculated for enough vibration modes are then combined statistically to obtain approximate values of the largest behavior magnitudes.

For each considered vibration mode, the largest modal behavior magnitudes, which are displacements, story drifts, internal forces and stresses are found. These largest modal behavior magnitudes are combined using Complete Quadratic Combination (CQC) or Square Root of Summation of Square (SRSS) rules. This analysis does not provide information about when the behavior magnitude occurs and its correlation with other loadings. The values found as a result of the combination reveal the largest possible positive (absolute) value for a single modal behavior magnitude. For this reason, the concept of direction is lost in the earthquake calculation made with the Modal Superposition Method.

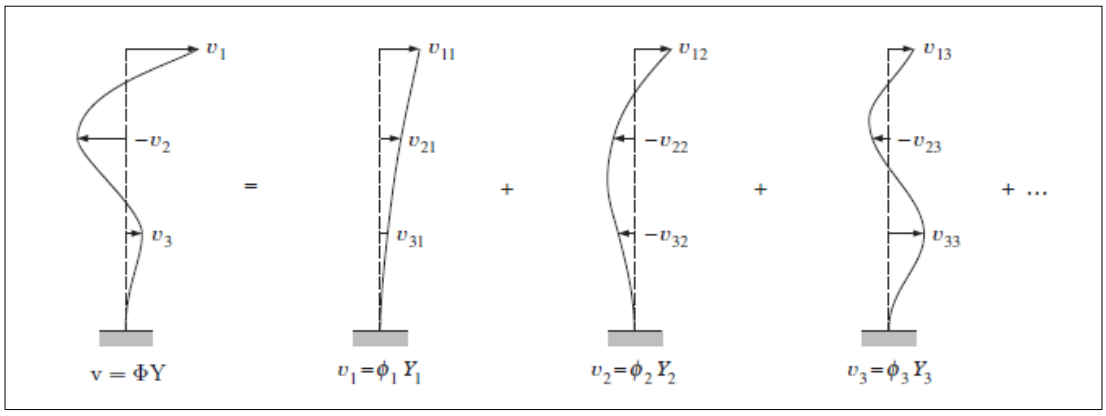

Figure 2.2: Mode Superposition Method.

2.3. Time History Analysis

Time History Analysis is a step-by-step analysis of a structure's dynamic response to a specific loading that may change with time. In order to determine the seismic response of a structure under dynamic loading of representative earthquake, Time History Analysis is used. Time History Analysis provides linear or nonlinear evaluation of dynamic structural response under loading that may change with respect to specified time function.

The purpose of Nonlinear Time History Analysis is to integrate the equation of system's motion step-by-step by considering the nonlinear behavior in the load-bearing system.

Nonlinear Time History Analysis refers to the step-by-step direct integration by time increments of the differential equation set, which expresses the equations of motion of the load-bearing system under the influence of earthquake ground motion. During this process, reason of the nonlinear behavior and change of the system stiffness matrix over time are considered.

Dynamic analysis in Time History is a kind of analysis in which the building behavior is modeled in the most accurate way, due to the fact that earthquake loads are realized by directly affecting the building.

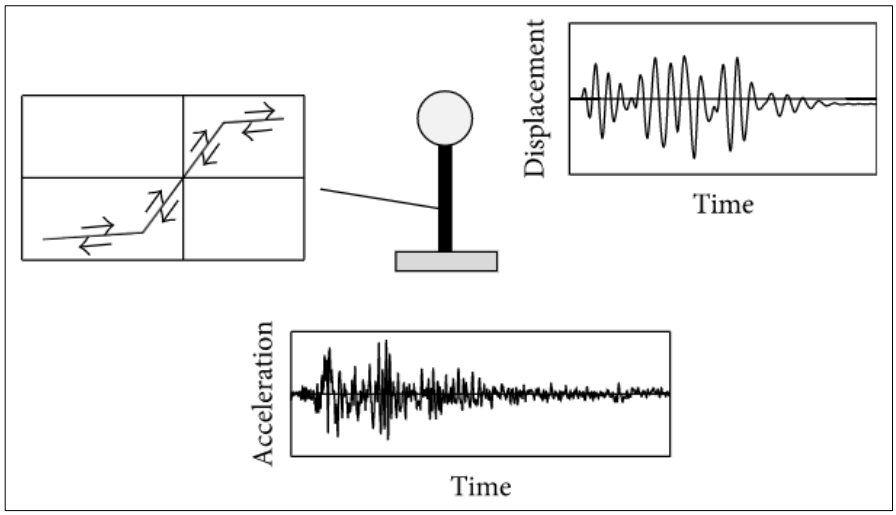

Figure 2.3: Schematic description of Nonlinear Time History Analysis.

3. MODELING OF NON-BUILDING STRUCTURE

3.1. Description of Non-Building Structures

Turkey is a highly seismically active country which is located among the Eurasian plate, Arabian plate and African plate. Besides, it is confined in an earthquake zone consists of the North Anatolian Fault Line, East Anatolian Fault Line and West Anatolian Fault Line. While the East Anatolian and North Anatolian Fault Lines occur with strike-slip faults, the West Anatolian Fault Line occurs with normal faults, causing the expansion of the Aegean. Bitlis-Zagros Fault Line, which is located on Iran-Iraq border and is one of the main parts of the African plate, applies the repulsive force to the east of Turkey causing the subduction which results in a few millimeters rising in Eastern Anatolian Region in each year.

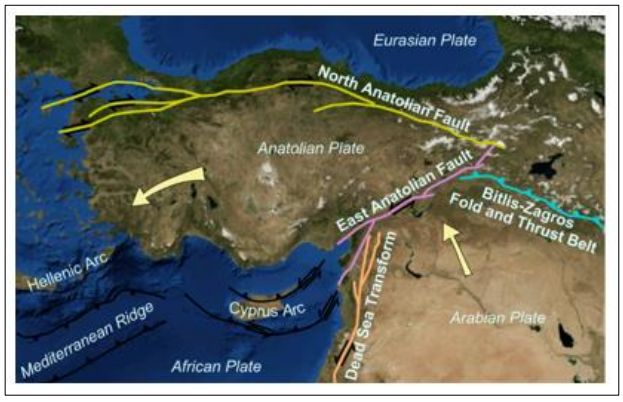

Figure 3.1: Anatolian plate.

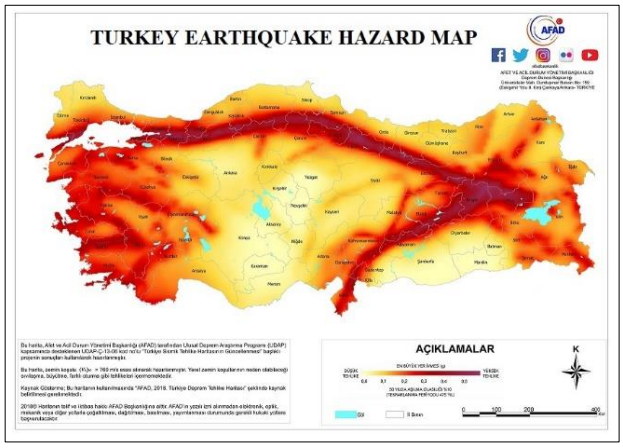

Figure 3.2: Turkey earthquake hazard map.

Cities established on alluvial grounds, which are connected to the sea and defined as loose ground, are more at risk. One of the most risky region in Izmir is the region which covers Karşıyaka-Çiğli and Menemen line. Since this region consists of alluvial ground brought by the Gediz River, Çiğli district, which is established on the current alluvium connected to Izmir's coast, is at risk. In order to examine the seismic performance of these three silos, sitting on the same foundation during an earthquake, Çiğli district of Izmir, which is an industrial area with high earthquake risk, is chosen as the location.

Figure 3.3: Active fault lines in Izmir.

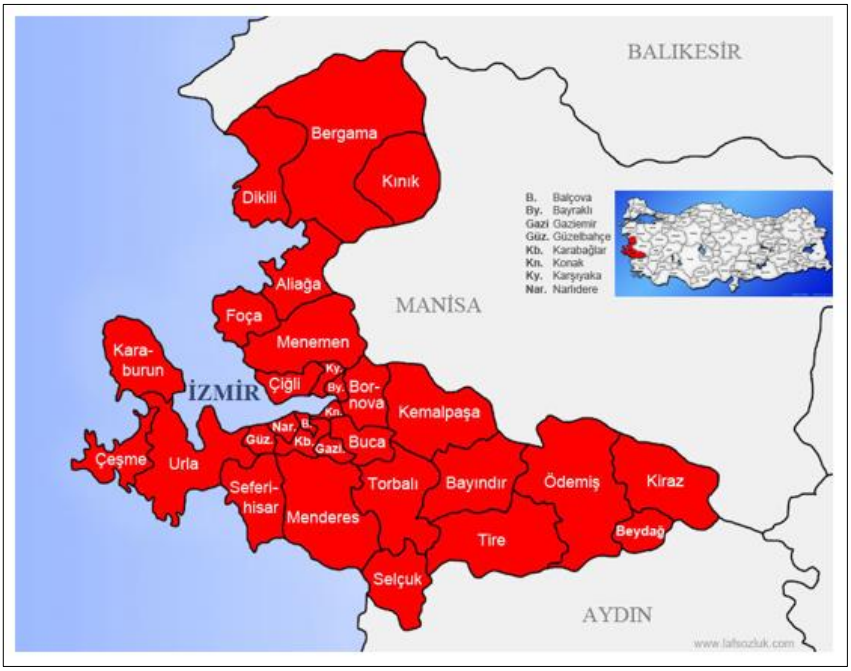

Figure 3.4: Districts in Izmir.

In order to investigate the seismic performance of three silos containing wheat, sitting on the same foundation during an earthquake, three models are selected in this study. All models are analyzed by SAP2000 Structural Analysis Software. In accordance with ASCE7-16, by selecting Response Modification Coefficient, *R* as 3.25 for non-building structures, models are designed as Multi-Tiered Ordinary Concentrically Braced Frames (MT-OCBFs) with different types of bracing configurations at 12^{m} height. Structures are modeled as a hexagon with a width of 2^{m}. Silos have four tier levels located at 2^{m}, 4^{m}, 6^{m} and 8^{m} except for the second silo, which has two tier levels located at 4^{m} and 8^{m}. Structural framing of the silos consist of columns, struts, braces, silo body, and rings inside the silo body. The columns, struts, braces, rings are modeled as steel frame elements. Modulus of Elasticity, *E* for steel materials is taken as 200000 MPa. S355JR quality steel material is used for columns and S235JR quality material is used for struts, braces and rings. Silo members are modeled as thin plate shell with 5^{mm} membrane and S235JR quality steel. The rings inside silos are located at the levels of 8.0^{m}, 10.0^{m} and 12.0^{m}. Moment releases are assigned on both ends of struts and braces. The silos are assumed to be simply supported to the ground. Cross-sectional properties are given in Table 3.1.

Table 3.1: Cross-Sectional Properties.

Component	**Silo-1**	**Silo-2**	**Silo-3**
Columns	HSS114.3X9.5	HSS127X9.5	HSS114.3X9.5
Struts	HSS76.2X6.4	HSS88.9X6.4	HSS76.2X3.2
Braces	HSS60.3X4.8	HSS88.9X6.4	HSS63.5X4.8
First ring	UPN120	UPN120	UPN120
Upper rings	UPN80	UPN80	UPN80
Body of silo	5^{mm} thin plate	5^{mm} thin plate	5^{mm} thin plate

The silos are assumed to be fully loaded with dry material, wheat. The masses are connected to the rings with infinitely rigid, weightless, and mass-less fictitious frame members.

In the modeling process, X-Bracing is used for Silo-1, 2-Tier X-Bracing is used for Silo-2 and Chevron Bracing is used for Silo-3. Steel braces are positioned in each bay and every tier level for all the silos. The configurations for Silo-1, Silo-2 and Silo-3 are shown in Figure 3.5.

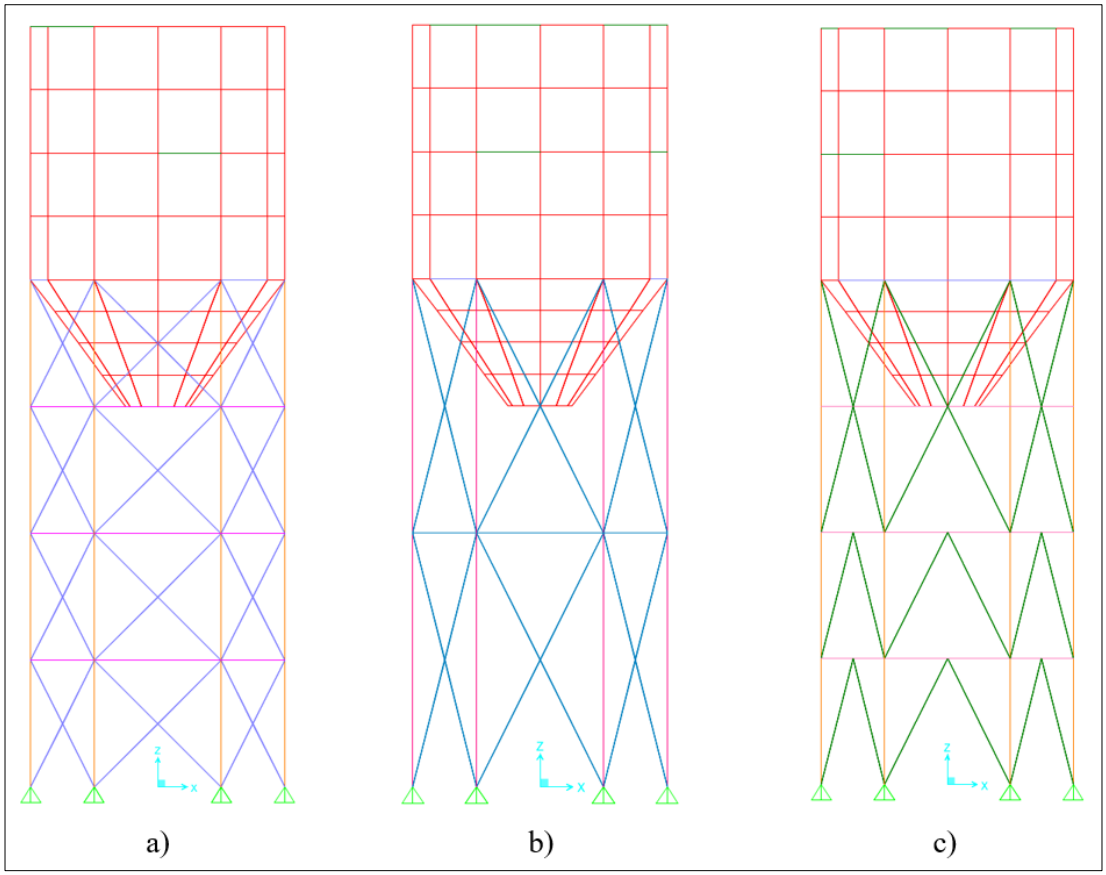

Figure 3.5: Configuration of a) Silo-1, b) Silo-2, c) Silo-3.

3.2. Seismic and Structural Design Parameters

For soil type of Çiğli, 'Turkish Accelerometric Database and Analysis System' website is selected as reference [15]. Since no data could be found for Çiğli station, Karşıyaka district, which is the closest to Çiğli, is selected with $(V_s)_{30}$ = 171 m/s as shown in Figure 3.6. By considering the value of Average Shear Wave Velocity at the Top 30^m Depth, $(V_s)_{30}$ as 171 m/s, the soil type is categorized as ZE, as shown in Table 3.2.

Ağ	İstasyon Kodu	İl	İlçe	Boylam	Enlem	Litoloji Sınıfı	Vs30 [m/s]
TK	3515	İzmir	Karşıyaka	27.094	38.4649	Ayrılmamış Kuvaterner	171

Figure 3.6: $(V_s)_{30}$ for district Karşıyaka.

Table 3.2: Local Soil Classes.

Local Soil Class	Kind of Soil	Average at the top 30 meters		
		$(V_s)_{30}$ [m/s]	$(N_{60})_{30}$ [impact/30cm]	$(c_u)_{30}$ [kPa]
ZA	Sound, stiff rocks	>1500	-	-
ZB	Slightly weathered, moderately sound rocks	760-1500	-	-
ZC	Very dense sand, gravel and claypan or weathered, very cracked weak rocks	360-760	>50	>250
ZD	Moderately dense - dense sand, gravel or very stiff clay layer	180-360	15-50	70-250
ZE	Loose sand, gravel or soft - stiff clay layer or profiles containing a soft clay layer with a total thickness of more than 3 meters that meet PI >20 and w>40% conditions	<180	<15	<70
ZF	Soil that require site-specific research and evaluation: 1) Soils with the risk of collapse and potential failure under the effect of earthquakes (liquefiable soils, highly sensitive clays, collapsible weak cemented soils, etc.), 2) Peat with a total thickness of more than 3 meters and/or clays with high organic content, 3) High plasticity (PI>50) clays with a total thickness of more than 8 meters, 4) Very thick (>35 m) soft or moderately stiff clays.			

The seismic design parameters for the non-building industrial structure located in Çiğli/Izmir are selected as follows:

- Earthquake Ground Motion Level = DD2 [13]
- Site Soil Classification = ZE [13]

Other necessary parameters are selected from Table 3.3.

Table 3.3: Site Specific Information.

Parameter	Site Specific Value	Reference
Mapped MCE_R spectral response acceleration parameter at short periods (S_S)	1.029	AFAD[1]
Mapped MCE_R spectral response acceleration parameter at a period of 1 second (S_1)	0.250	AFAD
Short period site coefficient (F_S)	1.077	AFAD
Long period site coefficient (F_1)	3.050	AFAD
The design spectral response acceleration parameter at short periods (S_{DS})	1.108	AFAD
The design spectral response acceleration parameter at a period of 1 sec (S_{D1})	0.762	AFAD
Long-period transition period (T_L)	6.000	AFAD

1. Afet ve Acil Durum Yönetim Başkanlığı – Disaster and Emergency Management Presidency [21]

The horizontal elastic design response spectrum periods (T_A, T_B, T_L) are calculated as below:

$$T_A = 0.2\frac{S_{D1}}{S_{DS}} = 0.2 \times \frac{0.762}{1.108} = 0.138\ sec.$$

$$T_B = \frac{S_{D1}}{S_{DS}} = \frac{0.762}{1.108} = 0.688\ sec.$$

$$T_L = 6.000\ sec.$$

The diagram of Design Response Spectrum is shown in Figure 3.7.

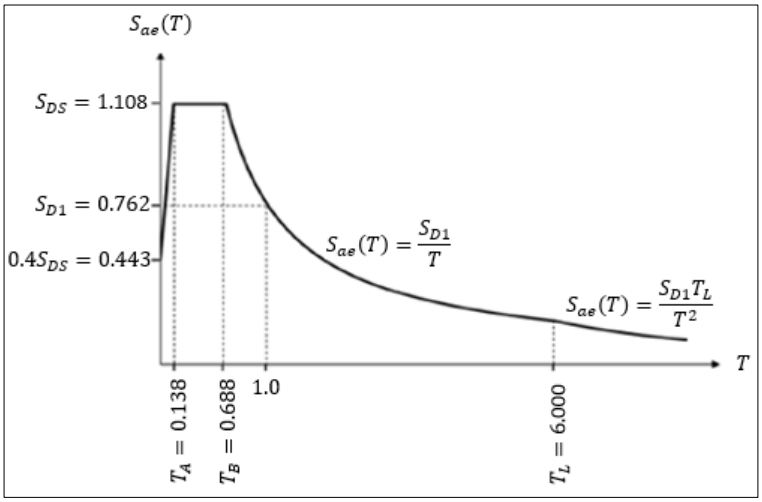

Figure 3.7: Design Response Spectrum.

The structural design parameters are given as follows:

According to ASCE7-16 Table 15.4-1, for silos which are considered as non-building industrial structures, Response Modification Coefficient, *R* and Overstrength Factor, Ω_0 are taken as 3.25 and 2, respectively.

Table 3.4: Structural Design Parameters.

Parameter	**Coefficient**
Seismic Force Resisting System	Moderately Ductile MT-OCBF
Purpose of Usage	Non-Building Industrial Structure
Building Height, h_n (m)	12
Response Modification Coefficient, *R*	3.25
Overstength Factor, Ω_0	2

3.3. Material Properties

Structural Steel (S235JR):

- Minimum Yield Stress, $F_y=235\ MPa$
- Minimum Tensile Stress, $F_u=360\ MPa$
- Expected Yield Stress, $F_{ye}=R_yF_y=329\ MPa$
- Expected Tensile Stress, $F_{ue}=R_tF_u=396\ MPa$
- Modulus of Elasticity, $E=200000\ MPa$
- Weight per Unit Volume, $\gamma=76.97\ kN/m^3$

Structural Steel (S355JR):

- Minimum Yield Stress, $F_y=355\ MPa$
- Minimum Tensile Stress, $F_u=510\ MPa$
- Expected Yield Stress, $F_{ye}=R_yF_y=443.75\ MPa$
- Expected Tensile Stress, $F_{ue}=R_tF_u=561\ MPa$
- Modulus of Elasticity, $E=200000\ MPa$
- Weight per Unit Volume, $\gamma=76.97\ kN/m^3$

3.4. Load Combinations

In accordance with Minimum Design Loads and Associated Criteria for Buildings and Other Structures (ASCE7-16) load combinations to be considered in design, according to LRFD method, are as follows:

- 1.4D
- 1.2D + 1.6L
- 1.2D + 1.0L
- $(1.2 + 0.2S_{DS})D + \rho Q_E + 0.5L$
- $(0.9 – 0.2S_{DS})D + \rho Q_E$
- $(1.2 + 0.2S_{DS})D + \Omega_0 Q_E + 0.5L$

- $(0.9 – 0.2S_{DS})D + \Omega_0 Q_E$

According to ASCE7-16 Section 12.5.3.1.a., in load combinations including earthquake effects, horizontal and vertical earthquake effects should be combined as shown in Equation 3.1, 3.2 and 3.3:

$$Q_E = \mp 1.0Q_E^{(X)} \mp 0.3Q_E^{(Y)} \mp 0.3Q_E^{(Z)} \quad (3.1)$$

$$Q_E = \mp 0.3Q_E^{(X)} \mp 1.0Q_E^{(Y)} \mp 0.3Q_E^{(Z)} \quad (3.2)$$

$$Q_E = \mp 0.3Q_E^{(X)} \mp 0.3Q_E^{(Y)} \mp 1.0Q_E^{(Z)} \quad (3.3)$$

According to ASCE7-16 Section 12.3.4.1, redundancy factor, ρ for designing non-building structures that are not similar to building is permitted to equal 1.0.

3.5. Loads Acting on Structures

The principle of silo loading is to introduce the weight of silo as empty and full to program. The weight of the structure is considered as dead load, while materials in the silos are considered as live load. Since the masses would not be concentrated at certain points in the silo, practically, live loads should be defined in the middle of the silo at 2^m intervals.

Since the weight is effective in an earthquake, all silos must be considered full in load combinations. Hence, since the effects of earthquake on Multi-Tiered Steel Concentrically Braced Frames are investigated in this study, all silos are assumed to be fully loaded.

3.5.1. Gravity Loads

The weights of all steel structural and non-structural members in the calculation model are calculated automatically by the SAP2000 Structural Analysis Software as shown in Figure 3.8.

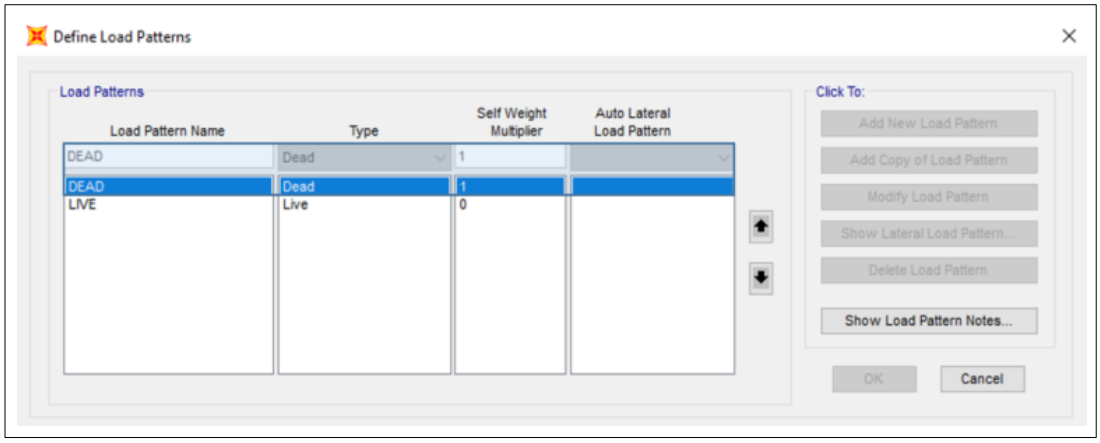

Figure 3.8: Dead load loading in Structural Analysis Software.

In order to apply live loads, three silos are idealized and loads that come from materials are calculated as follows:

- Idealization of silos:

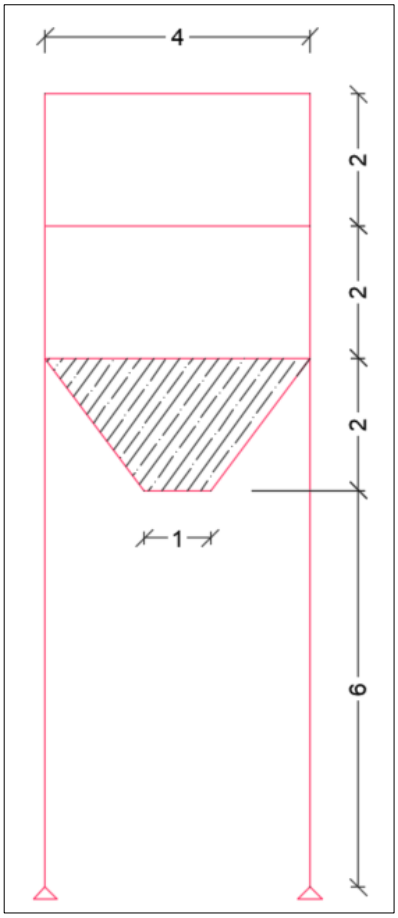

Figure 3.9: Geometry of Silo-1, Silo-2 and Silo-3.

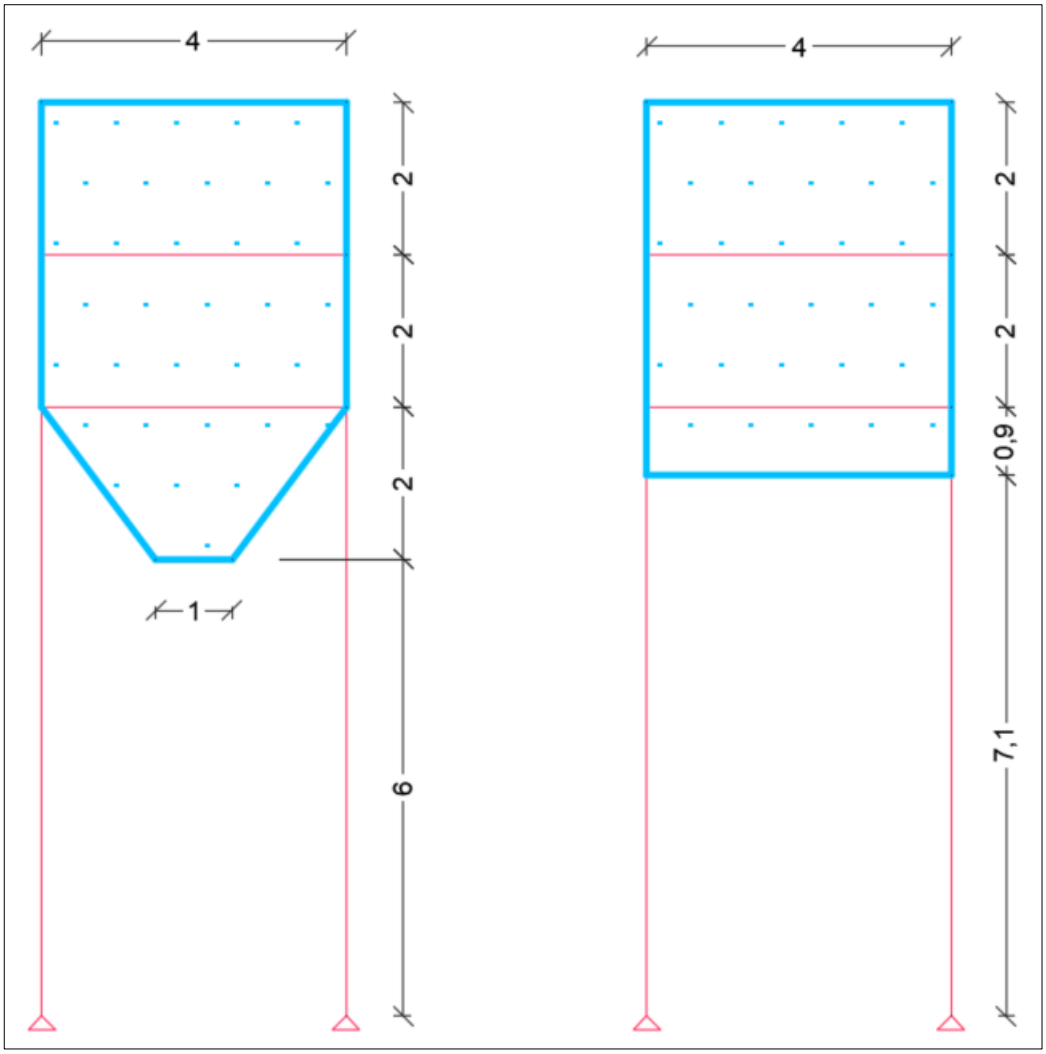

Figure 3.10: Idealized silos.

The volume of the conical system with a height of 2 m is calculated as follows:

$$V_{cone} = \frac{\pi h(R^2 + r^2 + R \times r)}{3} = \frac{\pi \times 2(2^2 + 0.5^2 + 2 \times 0.5)}{3} = 11\ m^3$$

Calculation of volume for h' cylinder is as follows:

$$V_{cylinder} = \pi R^2 h' = \pi \times 2^2 \times h' = 11\ m^3 \rightarrow h' = 0.9\ m$$

The calculations are done by taking the total silo height as 4.9 m.

- Idealized silos and live load calculation:

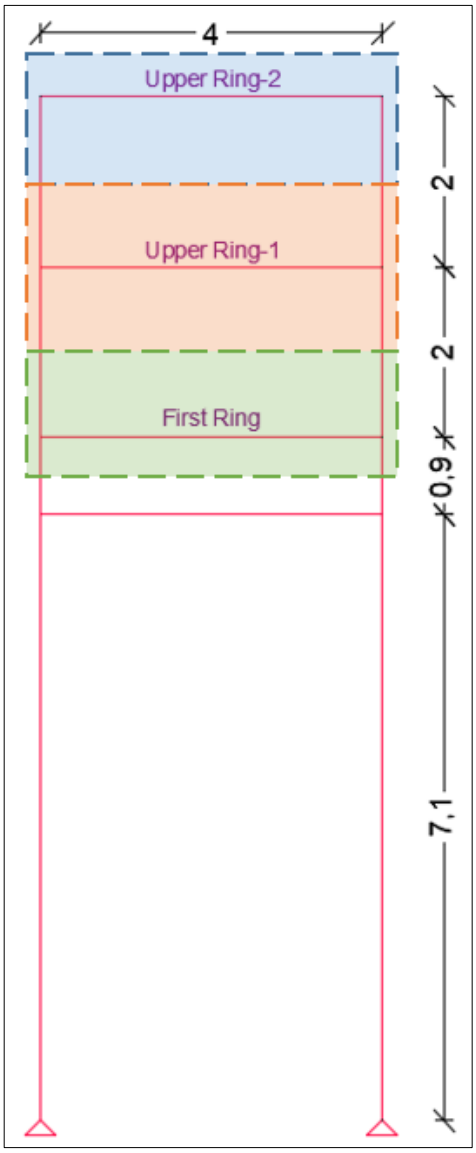

Figure 3.11: Live load distribution.

$Weight\ per\ unit\ volume\ of\ wheat, \gamma_{wheat} = 0.769\ t/m^3$

$V_{upper\ ring-2} = \pi R^2 h = \pi \times 2^2 \times 1 = 12.6\ m^3$

$W_{upper\ ring-2} = \gamma V = 0.769^{t/m^3} \times 12.6^{m^3} = 9.7\ t \cong 10.0\ t$

$V_{upper\ ring-1} = \pi R^2 h = \pi \times 2^2 \times (1+1) = 25.1\ m^3$

$W_{upper\ ring-1} = \gamma V = 0.769^{t/m^3} \times 25.1^{m^3} = 19.3\ t \cong 19.0\ t$

$V_{first\ ring} = \pi R^2 h = \pi \times 2^2 \times (1+0.45) = 18.2\ m^3$

$W_{first\ ring} = \gamma V = 0.769^{t/m^3} \times 18.2^{m^3} \cong 14.0\ t$

3.5.2. Joint Masses

Since the earthquake loads must act on the center of gravity of the total loads, the mass is assigned to the center of gravity of each ring level as shown below:

- Joint Masses for Silos:

$$Translation\ X, Y_{upper\ ring-2} = \frac{10.0^t}{9.81^{m/s^2}} = 1.02\ ts^2/m$$

$$Translation\ X, Y_{upper\ ring-1} = \frac{19.0^t}{9.81^{m/s^2}} = 1.94\ ts^2/m$$

$$Translation\ X, Y_{first\ ring} = \frac{14.0^t}{9.81^{m/s^2}} = 1.43\ ts^2/m$$

3.5.3. Earthquake Effect

The response spectrum of Çiğli district of Izmir with ZE soil type, is defined and the earthquake effects of X, Y and Z directions are calculated automatically by the SAP2000 Structural Analysis Software as shown in Figure 3.14, 3.15 and 3.16, respectively.

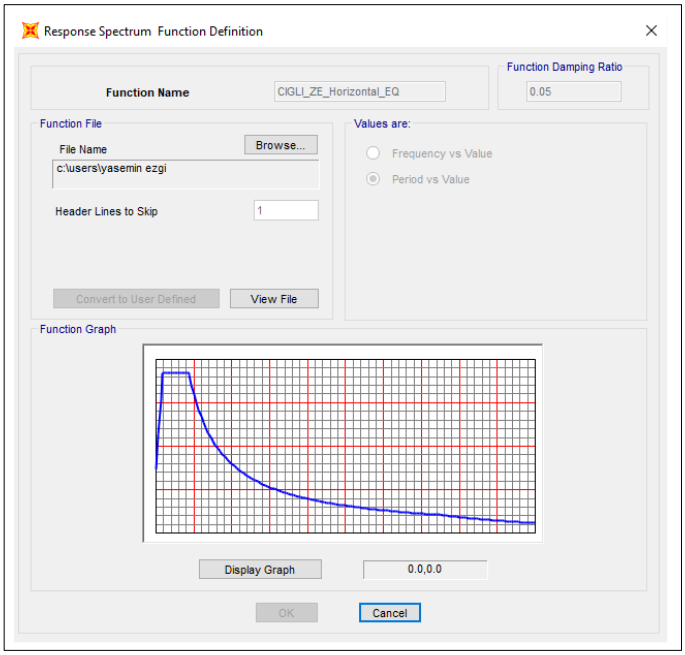

Figure 3.12: Horizontal Response Spectrum of Çiğli.

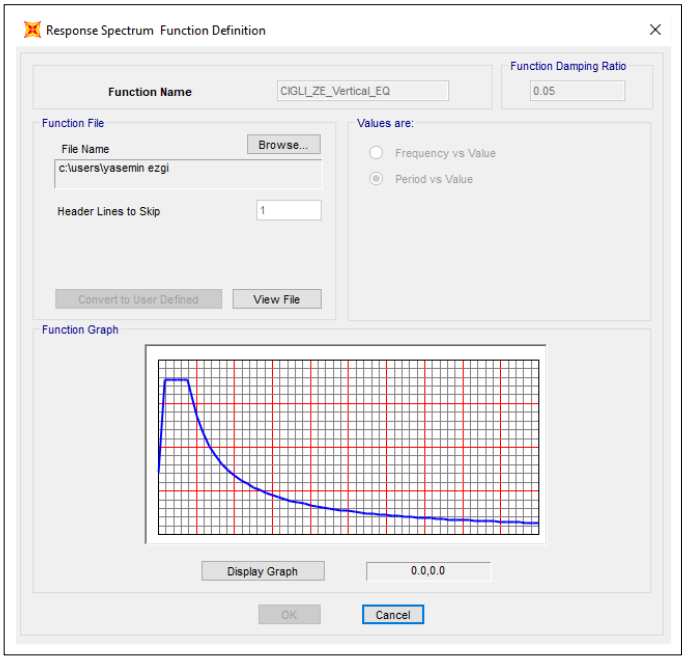

Figure 3.13: Vertical Response Spectrum of Çiğli.

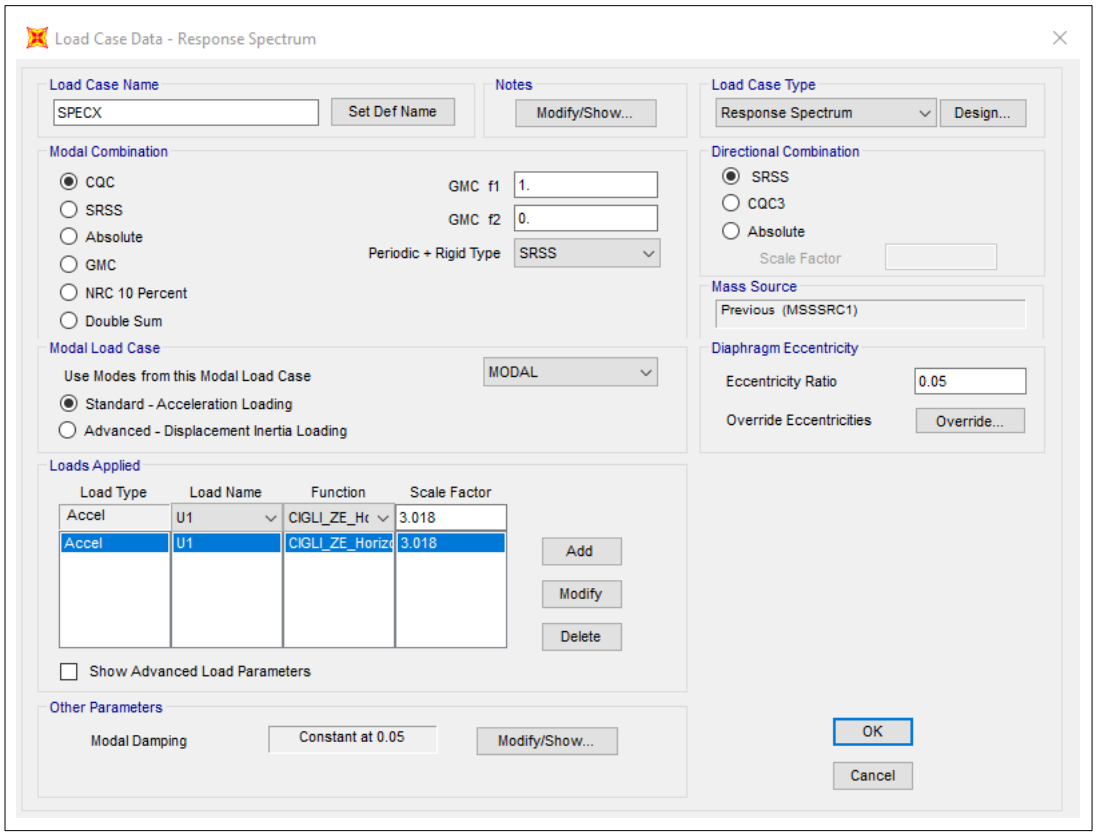

Figure 3.14: X-direction (horizontal) spectrum loading (R=3.25).

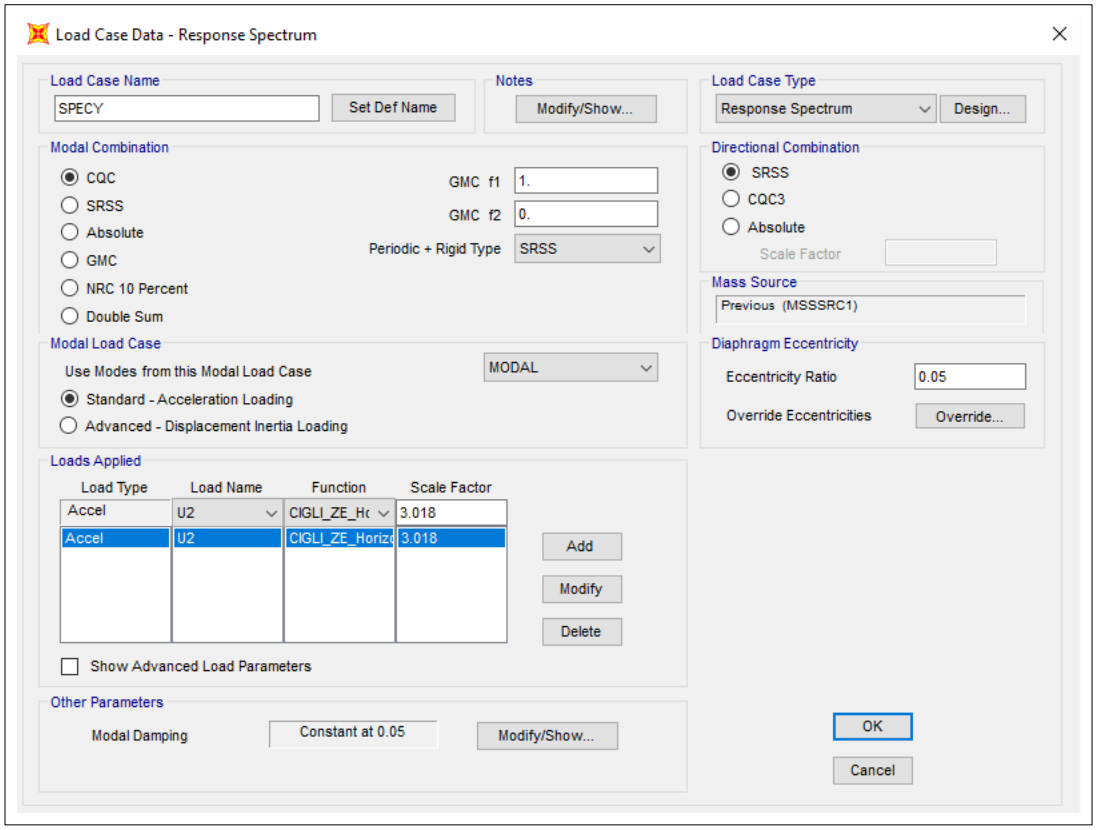

Figure 3.15: Y-direction (horizontal) spectrum loading (R=3.25).

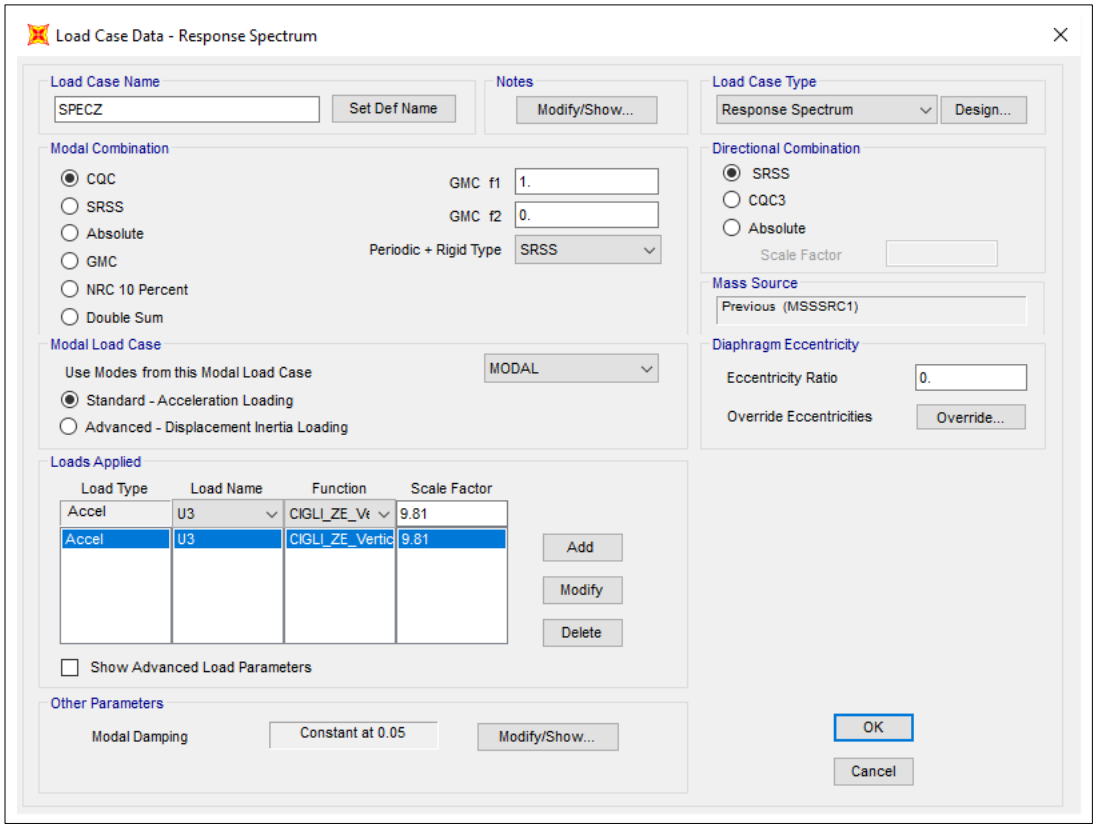

Figure 3.16: Z-direction (vertical) spectrum loading (R=1).

3.5.4. Area Loads

An approximate load is taken for the joint elements and stiffness plates around the silo perimeter. It is 98.0665 N/m^2 for all silos as shown in Figure 3.17.

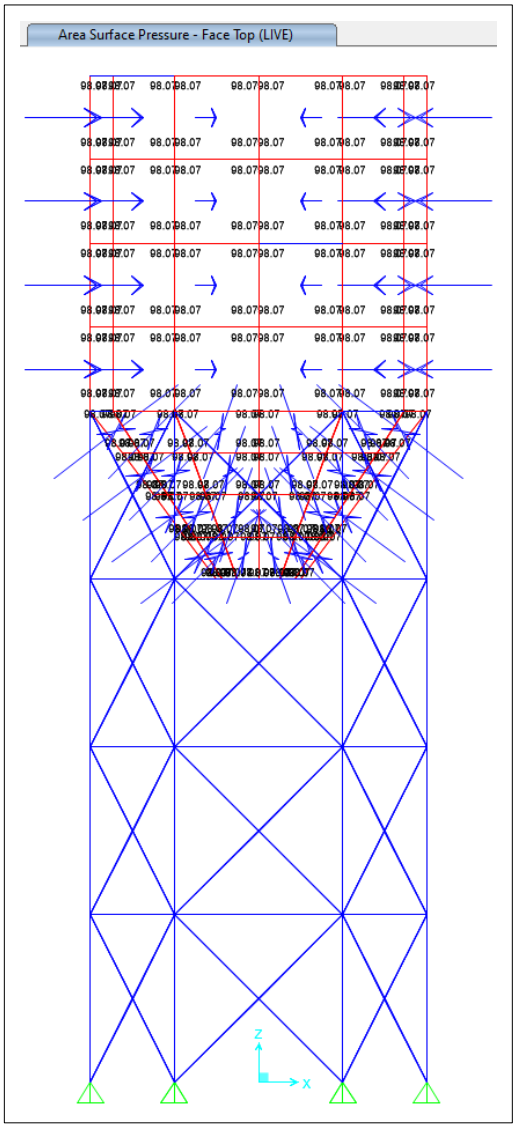

Figure 3.17: Area load on silos.

3.5.5. Foundation Calculation

Since there is no information about soil-structure interaction of the Multi-Tiered Braced Frame system could be obtained in the seismic provisions, it is not considered. However, since the ground effect is taken into account in the spectrum during the design, all silos are considered as hingedly-connected to the ground.

4. NUMERICAL LINEAR ANALYSIS

4.1. Defining Analysis Models

Models are designed as Multi-Tiered Ordinary Concentrically Braced Frames (MT-OCBFs) with three different types of bracing configurations at same height. MT-OCBF of three silos are modeled and analyzed in SAP2000 Structural Analysis Software. In this section, section properties, release conditions, joint loads and joint masses are shown.

4.1.1. Section Properties

The section properties of all silos are shown in Table 4.1 and Figure 4.1.

Table 4.1: Section Properties.

Component	Silo-1	Silo-2	Silo-3
Columns	HSS114.3X9.5	HSS127X9.5	HSS114.3X9.5
Struts	HSS76.2X6.4	HSS88.9X6.4	HSS76.2X3.2
Braces	HSS60.3X4.8	HSS88.9X6.4	HSS63.5X4.8

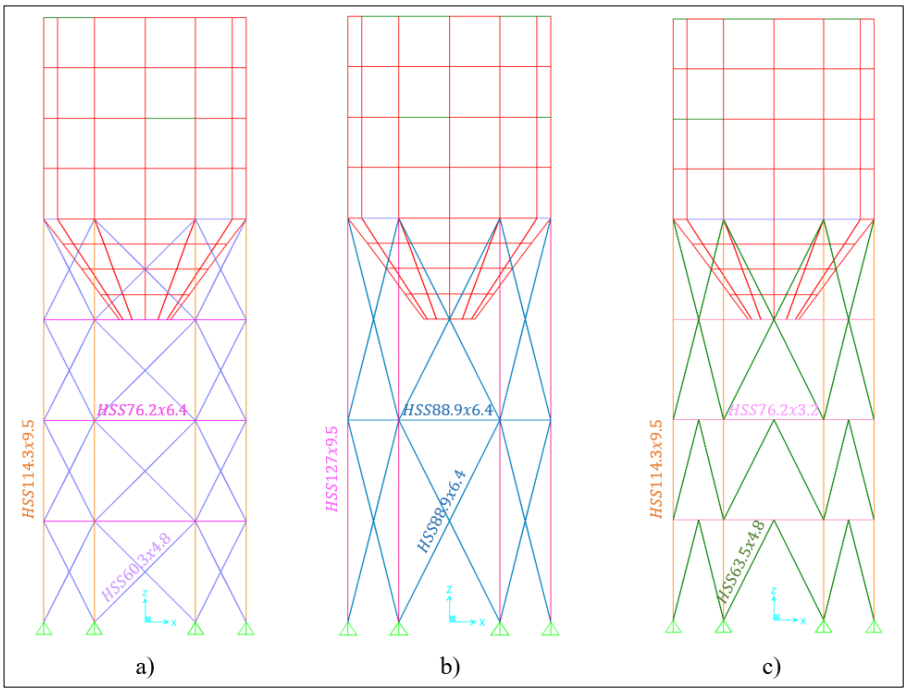

Figure 4.1: Cross-section properties for a) Silo-1, b) Silo-2, c) Silo-3.

4.1.2. Release Conditions

Except columns, all the steel members, which are struts and braces are released for all silos as shown in Figure 4.2.

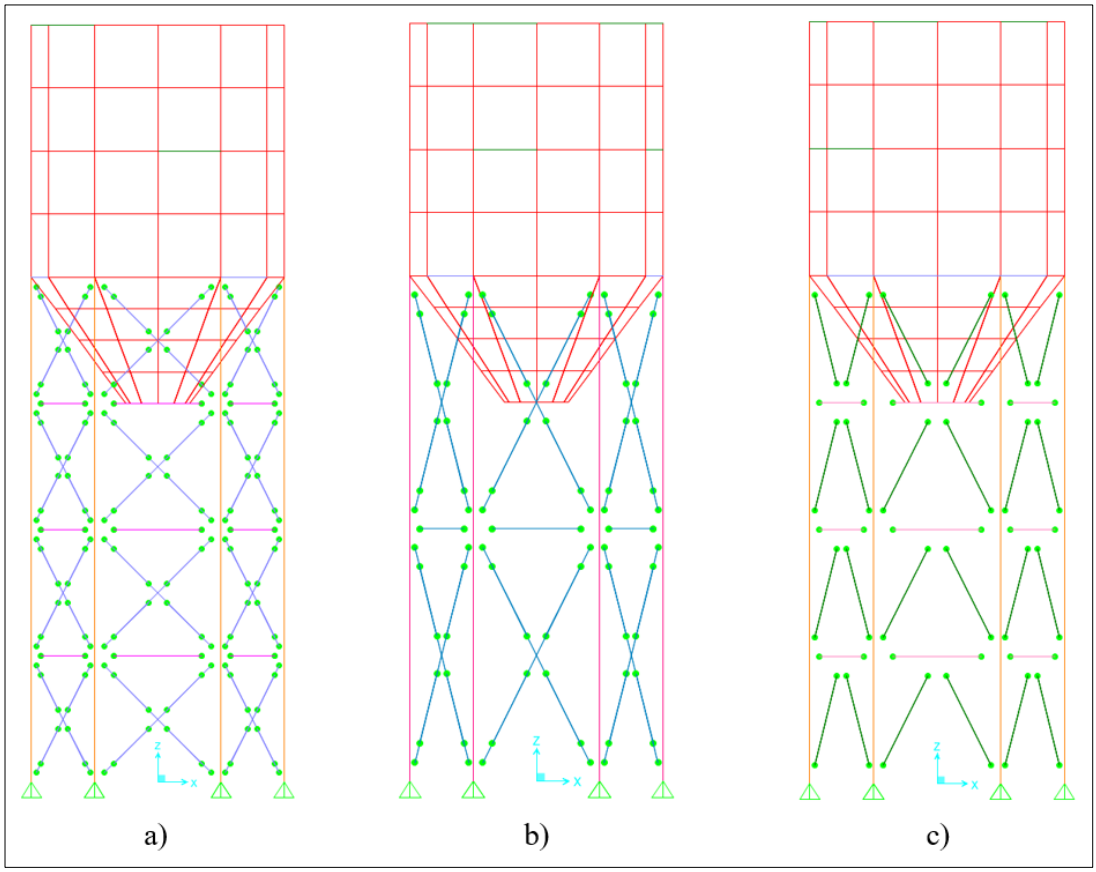

Figure 4.2: Moment releases for a) Silo-1, b) Silo-2, c) Silo-3.

4.1.3. Joint Loads and Masses

Joint loads and masses for silos are shown in Table 4.2. Besides, live loads and masses for silos are illustrated in Figure 4.3 and Figure 4.4, respectively.

Table 4.2: Joint Loads and Masses for Silos.

Component	**Loads**	**Masses**
	(ton)	(tons^2/m)
Upper ring-2	10.0	1.02
Upper ring-1	19.0	1.94
First ring	14.0	1.43

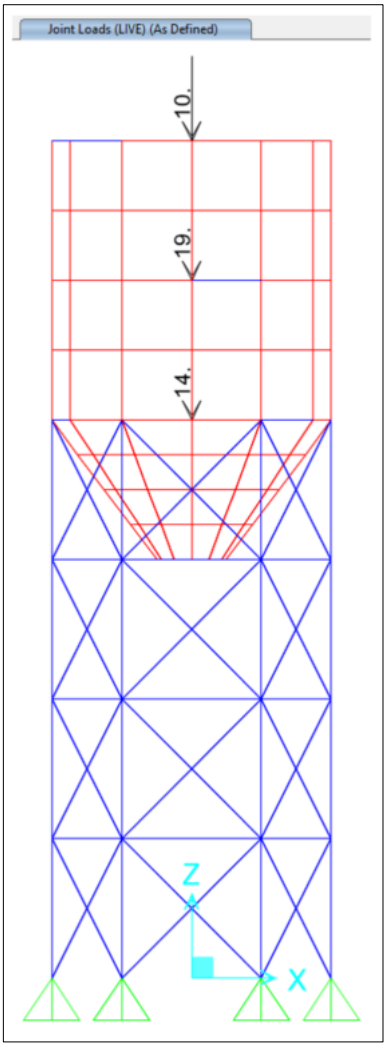

Figure 4.3: Joint live loads of silos.

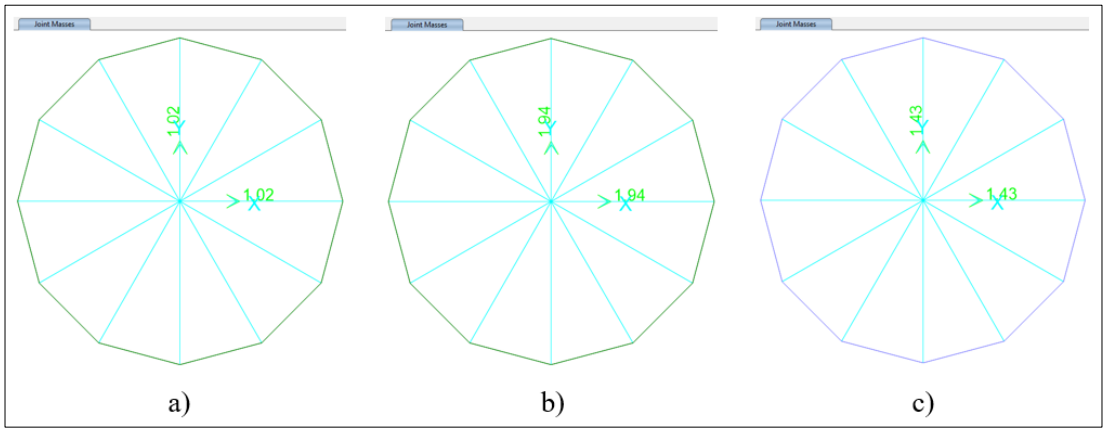

Figure 4.4: a) Upper ring-2 joint mass, b) Upper ring-1 joint mass, c) First ring joint mass.

4.2. Linear Analysis Results

Linear steel systems are performed based on TBDY-2018, ÇYTHYDE-2016, AISC 360-16 and AISC 341-16. In accordance with AISC 341-16, the conditions presented under the Section F1.4c named as "Multi-Tiered Braced Frame" of AISC 341-16 are applied in the design of silos whose all bays are braced.

In accordance with ANSI/AISC 360-16, Section E3, the critical stress, F_{cr}, is determined as follows:

- $When\ \frac{L_c}{r} \leq 4.71\sqrt{\frac{E}{F_y}} \quad or \quad \frac{F_y}{F_e} \leq 2.25 \quad ; \quad F_{cr} = \left(0.658^{\frac{F_y}{F_e}}\right)F_y \quad (E3-2)$
- $When\ \frac{L_c}{r} > 4.71\sqrt{\frac{E}{F_y}} \quad or \quad \frac{F_y}{F_e} > 2.25 \quad ; \quad F_{cr} = 0.877F_e \quad (E3-3)$

According to ANSI/AISC 341-16, Table D1.1, width to thickness ratio for moderately ductile HSS members, λ_{md} is determined as follows:

- $Walls\ of\ round\ HSS: \frac{D}{t} \leq 0.062\frac{E}{R_yF_y}$
- $If\ the\ limiting\ diameter-to-thickness\ ratio\ of\ round\ HSS\ members\ used\ as\ beams\ or\ columns\ shall\ not\ exceed: 0.077\frac{E}{R_yF_y}$

4.2.1. Brace Design

In the design of the braces, the loading that gives the most unfavorable result by using earthquake effect combinations in accordance with AISC 341-16 and AISC 360-16 should be considered. As a result of the analysis, the maximum compression forces on the braces are determined and compared with the brace capacities.

The material used for braces in all silos is S235. HSS60.3X4.8, HSS88.9X6.4 and HSS63.5X4.8 pipe profiles are used for Silo-1, Silo-2 and Silo-3, respectively.

Silo-1:

Brace Section (HSS60.3X4.8):

$A_g = 774.00\ mm^2$

Slenderness Limitation:

$L_c = 2828.43\ mm$

$r = 19.90\ mm$

$L_c/r = 2828.43^{mm}/19.90^{mm} = 142.13 < 200$ √

The Capacity of Brace Section:

$$F_e = \frac{\pi^2 E}{\left(\frac{L_c}{r}\right)^2} = \frac{\pi^2 \times 200000^{N/mm^2}}{142.13^2} = 97.71^{N/mm^2}$$

$$L_c/r = 142.13 > 4.71\sqrt{E/F_y} = 4.71\sqrt{200000/235} = 137.40;$$

$F_{cr} = 0.877F_e = 0.877 \times 97.71 = 85.69^{N/mm^2}$

$P_n = F_{cr} \times A_g = 85.69^{N/mm^2} \times 774.00^{mm^2} \times 10^{-3} = 66.63^{kN}$

$\phi_c = 0.9\ (LRFD)$

$\phi_c P_n = 0.9 \times 66.63^{kN} = \mathbf{59.69^{kN}}$

The Demand of Brace Section (Obtained from SAP2000 Structural Analysis Software):

$P_r = \mathbf{-49.26^{kN}}\ (Compression)$

Demand – Capacity Ratio:

$$\frac{P_r}{P_c} = \frac{49.26^{kN}}{59.69^{kN}} = 0.83 < 1$$ √

Limiting Width-to-Thickness Ratio (Moderately Ductile Member):

$$\frac{D}{t} = 13.6 \leq 0.062\frac{E}{R_y F_y} = 0.062\frac{200000^{N/mm^2}}{1.4 \times 235^{N/mm^2}} = 37.69 \surd$$

Silo-2:

Brace Section (HSS88.9X6.4):

$$A_g = 1540.00\ mm^2$$

Slenderness Limitation:

$$L_c = 4472.14\ mm$$
$$r = 29.50\ mm$$
$$L_c/r = 4472.14^{mm}/29.50^{mm} = 151.60 < 200 \surd$$

The Capacity of Brace Section:

$$F_e = \frac{\pi^2 E}{\left(\frac{L_c}{r}\right)^2} = \frac{\pi^2 \times 200000^{N/mm^2}}{151.60^2} = 85.89^{N/mm^2}$$

$$L_c/r = 151.60 > 4.71\sqrt{E/F_y} = 4.71\sqrt{200000/235} = 137.40;$$

$$F_{cr} = 0.877F_e = 0.877 \times 85.89 = 75.33^{N/mm^2}$$
$$P_n = F_{cr} \times A_g = 75.33^{N/mm^2} \times 1540.00^{mm^2} \times 10^{-3} = 116.00^{kN}$$
$$\phi_c = 0.9\ (LRFD)$$
$$\phi_c P_n = 0.9 \times 116.00^{kN} = \mathbf{104.40^{kN}}$$

The Demand of Brace Section (Obtained from SAP2000 Structural Analysis Software):

$$P_r = \mathbf{-89.10^{kN}}\ (Compression)$$

Demand – Capacity Ratio:

$$\frac{P_r}{P_c} = \frac{89.10^{kN}}{104.40^{kN}} = 0.85 < 1\surd$$

Limiting Width-to-Thickness Ratio (Moderately Ductile Member):

$$\frac{D}{t} = 15.1 \leq 0.062\frac{E}{R_y F_y} = 0.062\frac{200000^{N/mm^2}}{1.4 \times 235^{N/mm^2}} = 37.69\ \surd$$

Silo-3:

Brace Section (HSS63.5X4.8):

$$A_g = 819.00\ mm^2$$

Slenderness Limitation:

$$L_c = 2236.05\ mm$$
$$r = 21.00\ mm$$
$$L_c/r = 2236.05^{mm}/21.00^{mm} = 106.48 < 4\sqrt{E/F_y} = 4\sqrt{200000/235} = 117\ \surd$$

The Capacity of Brace Section:

$$F_e = \frac{\pi^2 E}{\left(\frac{L_c}{r}\right)^2} = \frac{\pi^2 \times 200000^{N/mm^2}}{106.48^2} = 174.10^{N/mm^2}$$

$$L_c/r = 106.48 \leq 4.71\sqrt{E/F_y} = 4.71\sqrt{200000/235} = 137.40;$$

$$F_{cr} = \left(0.658^{F_y/F_e}\right)F_y = \left(0.658^{235/174.10}\right) \times 235 = 133.57^{N/mm^2}$$

$$P_n = F_{cr} \times A_g = 133.57^{N/mm^2} \times 819.00^{mm^2} \times 10^{-3} = 109.39^{kN}$$

$$\phi_c = 0.9\ (LRFD)$$

$$\phi_c P_n = 0.9 \times 109.39^{kN} = \mathbf{98.46^{kN}}$$

The Demand of Brace Section (Obtained from SAP2000 Structural Analysis Software):

$$P_r = -\mathbf{72.93}^{\boldsymbol{kN}}\ (Compression)$$

Demand – Capacity Ratio:

$$\frac{P_r}{P_c} = \frac{72.93^{kN}}{98.46^{kN}} = 0.74 < 1 \surd$$

Limiting Width-to-Thickness Ratio (Moderately Ductile Member):

$$\frac{D}{t} = 14.3 \leq 0.062\frac{E}{R_y F_y} = 0.062\frac{200000^{N/mm^2}}{1.4 \times 235^{N/mm^2}} = 37.69 \surd$$

4.2.2. Strut Design

In the design of the struts, the loading that gives the most unfavorable result by using earthquake effect combinations in accordance with AISC 341-16 and AISC 360-16 should be considered. Besides, in accordance with AISC 341-16 Section F1.4c "Multi-Tiered Braced Frames", it is recommended to multiply the horizontal earthquake effects by 1.5 in combinations with overstrength. As a result of the analysis, the maximum compression forces on the struts are determined and compared with the strut capacities.

The material used for struts in all silos is S235. HSS76.2X6.4, HSS88.9X6.4 and HSS76.2X3.2 pipe profiles are used for Silo-1, Silo-2 and Silo-3, respectively.

According to ANSI/AISC 341-16, Section F1.4c.(e), the required axial strength of the struts shall be determined from the load combinations of the applicable building code, including the overstrength seismic load, with the horizontal seismic load effect, E, multiplied by a factor of 1.5. In tension-compression X-Bracing, these forces shall be determined in the absence of compression braces.

Silo-1:

Strut Section (HSS76.2X6.4):

$A_g = 1310.00\ mm^2$

Slenderness Limitation:

$L_c = 2000\ mm$

$r = 24.90\ mm$

$L_c/r = 2000^{mm}/24.90^{mm} = 80.32 < 200$ √

The Capacity of Strut Section:

$$F_e = \frac{\pi^2 E}{\left(\frac{L_c}{r}\right)^2} = \frac{\pi^2 \times 200000^{N/mm^2}}{80.32^2} = 305.96^{N/mm^2}$$

$$L_c/r = 80.32 \leq 4.71\sqrt{E/F_y} = 4.71\sqrt{200000/235} = 137.40;$$

$$F_{cr} = \left(0.658^{F_y/F_e}\right)F_y = \left(0.658^{235/305.96}\right) \times 235 = 170.39^{N/mm^2}$$

$$P_n = F_{cr} \times A_g = 170.39^{N/mm^2} \times 1310.00^{mm^2} \times 10^{-3} = 223.22^{kN}$$

$$\phi_c = 0.9\ (LRFD)$$

$$\phi_c P_n = 0.9 \times 223.22^{kN} = \mathbf{200.89^{kN}}$$

The Demand of Strut Section (Obtained from SAP2000 Structural Analysis Software):

$P_r = \mathbf{-164.02^{kN}}\ (Compression)$

Demand – Capacity Ratio:

$$\frac{P_r}{P_c} = \frac{164.02^{kN}}{200.89^{kN}} = 0.82 < 1$$ √

Limiting Width-to-Thickness Ratio (Moderately Ductile Member):

$$\frac{D}{t} = 12.9 \leq 0.077\frac{E}{R_y F_y} = 0.077\frac{200000^{N/mm^2}}{1.4 \times 235^{N/mm^2}} = 46.81 \surd$$

Silo-2:

Strut Section (HSS88.9X6.4):

$$A_g = 1540.00\ mm^2$$

Slenderness Limitation:

$$L_c = 2000\ mm$$
$$r = 29.50\ mm$$
$$L_c/r = 2000^{mm}/29.50^{mm} = 67.80 < 200 \surd$$

The Capacity of Strut Section:

$$F_e = \frac{\pi^2 E}{\left(\frac{L_c}{r}\right)^2} = \frac{\pi^2 \times 200000^{N/mm^2}}{67.80^2} = 429.45^{N/mm^2}$$

$$L_c/r = 67.80 \leq 4.71\sqrt{E/F_y} = 4.71\sqrt{200000/235} = 137.40;$$

$$F_{cr} = \left(0.658^{F_y/F_e}\right)F_y = \left(0.658^{235/429.45}\right) \times 235 = 186.90^{N/mm^2}$$

$$P_n = F_{cr} \times A_g = 186.90^{N/mm^2} \times 1540.00^{mm^2} \times 10^{-3} = 287.82^{kN}$$

$$\phi_c = 0.9\ (LRFD)$$

$$\phi_c P_n = 0.9 \times 287.82^{kN} = \mathbf{259.04^{kN}}$$

The Demand of Strut Section (Obtained from SAP2000 Structural Analysis Software):

$$P_r = \mathbf{-163.06^{kN}}\ (Compression)$$

Demand – Capacity Ratio:

$$\frac{P_r}{P_c} = \frac{163.06^{kN}}{259.04^{kN}} = 0.63 < 1 \surd$$

Limiting Width-to-Thickness Ratio (Moderately Ductile Member):

$$\frac{D}{t} = 15.1 \leq 0.077\frac{E}{R_y F_y} = 0.077\frac{200000^{N/mm^2}}{1.4 \times 235^{N/mm^2}} = 46.81 \surd$$

Silo-3:

Strut Section (HSS76.2X3.2):

$$A_g = 677.00\ mm^2$$

Slenderness Limitation:

$$L_c = 2000\ mm$$
$$r = 25.90\ mm$$
$$L_c/r = 2000^{mm}/25.90^{mm} = 77.22 < 200 \surd$$

The Capacity of Strut Section:

$$F_e = \frac{\pi^2 E}{\left(\frac{L_c}{r}\right)^2} = \frac{\pi^2 \times 200000^{N/mm^2}}{77.22^2} = 331.03^{N/mm^2}$$

$$L_c/r = 77.22 \leq 4.71\sqrt{E/F_y} = 4.71\sqrt{200000/235} = 137.40;$$

$$F_{cr} = \left(0.658^{F_y/F_e}\right)F_y = \left(0.658^{235/331.03}\right) \times 235 = 174.59^{N/mm^2}$$

$$P_n = F_{cr} \times A_g = 174.59^{N/mm^2} \times 677.00^{mm^2} \times 10^{-3} = 118.20^{kN}$$

$$\phi_c = 0.9\ (LRFD)$$

$$\phi_c P_n = 0.9 \times 118.20^{kN} = \mathbf{106.38^{kN}}$$

The Demand of Strut Section (Obtained from SAP2000 Structural Analysis Software):

$$P_r = -\mathbf{85.66^{kN}}\ (Compression)$$

Demand – Capacity Ratio:

$$\frac{P_r}{P_c} = \frac{85.66^{kN}}{106.38^{kN}} = 0.81 < 1 \surd$$

Limiting Width-to-Thickness Ratio (Moderately Ductile Member):

$$\frac{D}{t} = 25.8 \leq 0.077\frac{E}{R_y F_y} = 0.077\frac{200000^{N/mm^2}}{1.4 \times 235^{N/mm^2}} = 46.81\ \surd$$

4.2.3. Column Design

In the design of the columns, the loading that gives the most unfavorable result by using earthquake effect combinations in accordance with AISC 341-16 and AISC 360-16 should be considered. Besides, in accordance with AISC 341-16 Section F1.4c "Multi-Tiered Braced Frames", it is recommended to multiply the horizontal earthquake effects by 1.5 in combinations with overstrength. As a result of the analysis, the maximum compression forces on the columns are determined and compared with the column capacities.

The material used for columns in all silos is S355. HSS114.3X9.5, HSS127X9.5 and HSS114.3X9.5 pipe profiles are used for Silo-1, Silo-2 and Silo-3 respectively.

According to ANSI/AISC 341-16, Section F1.4c.(f), the required axial strength of the columns shall be determined from the load combinations of the applicable building code, including the overstrength seismic load, with the horizontal seismic load effect, E, multiplied by a factor of 1.5.

Silo-1:

Column Section (HSS114.3X9.5):

$A_g = 2940.00\ mm^2$

Slenderness Limitation:

$L_c = 2000\ mm$

$r = 37.40\ mm$

$L_c/r = 2000^{mm}/37.40^{mm} = 53.48 < 200$ √

The Capacity of Column Section:

$$F_e = \frac{\pi^2 E}{\left(\frac{L_c}{r}\right)^2} = \frac{\pi^2 \times 200000^{N/mm^2}}{53.48^2} = 690.26^{N/mm^2}$$

$$L_c/r = 53.48 \leq 4.71\sqrt{E/F_y} = 4.71\sqrt{200000/355} = 111.79;$$

$$F_{cr} = \left(0.658^{F_y/F_e}\right)F_y = \left(0.658^{355/690.26}\right) \times 355 = 286.25^{N/mm^2}$$

$$P_n = F_{cr} \times A_g = 286.25^{N/mm^2} \times 2940.00^{mm^2} \times 10^{-3} = 841.57^{kN}$$

$\phi_c = 0.9\ (LRFD)$

$\phi_c P_n = 0.9 \times 841.57^{kN} = \mathbf{757.41^{kN}}$

The Demand of Column Section (Obtained from SAP2000 Structural Analysis Software):

$P_r = \mathbf{-696.19^{kN}}\ (Compression)$

Demand – Capacity Ratio:

$$\frac{P_r}{P_c} = \frac{696.19^{kN}}{757.41^{kN}} = 0.92 < 1$$ √

Limiting Width-to-Thickness Ratio (Moderately Ductile Member):

$$\frac{D}{t} = 12.9 \leq 0.077\frac{E}{R_y F_y} = 0.077\frac{200000^{N/mm^2}}{1.25 \times 355^{N/mm^2}} = 34.70$$ √

Silo-2:

Column Section (HSS127X9.5):

$A_g = 3290.00\ mm^2$

Slenderness Limitation:

$L_c = 4000\ mm$

$r = 42.00\ mm$

$L_c/r = 4000^{mm}/42.00^{mm} = 95.24 < 200$ √

The Capacity of Column Section:

$$F_e = \frac{\pi^2 E}{\left(\frac{L_c}{r}\right)^2} = \frac{\pi^2 \times 200000^{N/mm^2}}{95.24^2} = 217.62^{N/mm^2}$$

$$L_c/r = 95.24 \leq 4.71\sqrt{E/F_y} = 4.71\sqrt{200000/355} = 111.79;$$

$$F_{cr} = \left(0.658^{F_y/F_e}\right)F_y = \left(0.658^{355/217.62}\right) \times 355 = 179.35^{N/mm^2}$$

$$P_n = F_{cr} \times A_g = 179.35^{N/mm^2} \times 3290.00^{mm^2} \times 10^{-3} = 590.07^{kN}$$

$$\phi_c = 0.9\ (LRFD)$$

$$\phi_c P_n = 0.9 \times 590.07^{kN} = \mathbf{531.07^{kN}}$$

The Demand of Column Section (Obtained from SAP2000 Structural Analysis Software):

$P_r = \mathbf{-474.99^{kN}}\ (Compression)$

Demand – Capacity Ratio:

$$\frac{P_r}{P_c} = \frac{474.99^{kN}}{531.07^{kN}} = 0.89 < 1$$ √

Limiting Width-to-Thickness Ratio (Moderately Ductile Member):

$$\frac{D}{t} = 14.3 \leq 0.077\frac{E}{R_y F_y} = 0.077\frac{200000^{N/mm^2}}{1.25 \times 355^{N/mm^2}} = 34.70 \surd$$

Silo-3:

Column Section (HSS114.3X9.5):

$$A_g = 2940.00\ mm^2$$

Slenderness Limitation:

$$L_c = 2000\ mm$$
$$r = 37.40\ mm$$
$$L_c/r = 2000^{mm}/37.40^{mm} = 53.48 < 200 \surd$$

The Capacity of Column Section:

$$F_e = \frac{\pi^2 E}{\left(\frac{L_c}{r}\right)^2} = \frac{\pi^2 \times 200000^{N/mm^2}}{53.48^2} = 690.26^{N/mm^2}$$

$$L_c/r = 53.48 \leq 4.71\sqrt{E/F_y} = 4.71\sqrt{200000/355} = 111.79;$$

$$F_{cr} = \left(0.658^{F_y/F_e}\right)F_y = \left(0.658^{355/690.26}\right) \times 355 = 286.25^{N/mm^2}$$

$$P_n = F_{cr} \times A_g = 286.25^{N/mm^2} \times 2940.00^{mm^2} \times 10^{-3} = 841.57^{kN}$$

$$\phi_c = 0.9\ (LRFD)$$

$$\phi_c P_n = 0.9 \times 841.57^{kN} = \mathbf{757.41^{kN}}$$

The Demand of Column Section (Obtained from SAP2000 Structural Analysis Software):

$$P_r = \mathbf{-697.66^{kN}}\ (Compression)$$

Demand – Capacity Ratio:

$$\frac{P_r}{P_c} = \frac{697.66^{kN}}{757.41^{kN}} = 0.92 < 1 \surd$$

Limiting Width-to-Thickness Ratio (Moderately Ductile Member):

$$\frac{D}{t} = 12.9 \leq 0.077 \frac{E}{R_y F_y} = 0.077 \frac{200000^{N/mm^2}}{1.25 \times 355^{N/mm^2}} = 34.70 \surd$$

5. NUMERICAL NONLINEAR ANALYSIS

5.1. Determination of Earthquakes

At the beginning of the Nonlinear Analysis, seven earthquakes with Average Shear Wave Velocities between 150 m/s – 350 m/s are selected. Then, these selected earthquakes are scaled separately according to the periods of three silos by considering the scale factor value 1 to 5. Consequently, the compatibility of the earthquakes with the design spectrum is checked.

Four earthquakes are shown in this study since the results are similar as the scaling is applied by considering the first mode period. Earthquake name, date, time, station code, location, component, record time, magnitude, average shear wave velocity, distance and biggest acceleration for the earthquakes are shown in Table 5.1.

Table 5.1: Earthquakes.

NO	EARTHQUAKE NAME	DATE	TIME	STATION CODE	EARTHQAUKE LOCATION	COMPONENT	RECORD TIME (s)	MW	V_{s30} (m/s)	DISTANCE (REPI) (km)	BIGGEST ACCELERATION (cm/s^2)
1	Aegean Sea, Seferihisar (İzmir)	30.10.2020	11:51:23	Bayraklı-3513	Aegean Sea	NS	105.00	6.6	196	72.00	106.281
2	Aegean Sea, Seferihisar (İzmir)	30.10.2020	11:51:23	Bornova-3522	Aegean Sea	NS	98.41	6.6	249	71.18	73.72
3	Iwate Japan	13.06.2008	23:43:45 (UTC)	Iwate-5774	Iwate	NS	60.00	6.9	276.3	29.38	194.10
4	Kobe Japan	16.01.1995	20:46:53 (UTC)	Kobe-1121	Kobe	NS	89.03	6.9	256	27.77	154.64

First mode is the dominant period with 0.95, 0.96 and 0.97 modal participating mass ratios in three silos, respectively. Therefore, the scaling of earthquakes is applied by considering the dominant first mode period. Scale factors of earthquakes are considered between 1 and 5 for each silos as shown in Table 5.2 and the graphs, which the scaled earthquakes for the three silos are drawn, are shown in Figure 5.1, 5.2, 5.3 and 5.4 together with the design spectrum.

Table 5.2: Scale Factors.

Earthquake	Silo-1	Silo-2	Silo-3
Bayraklı-3513	4.76	3.69	3.95
Bornova-3522	3.93	4.33	4.65
Iwate-5774	1.86	2.41	2.07
Kobe-1121	2.50	3.17	2.35

5.1.1. Bayraklı-3513 Earthquake

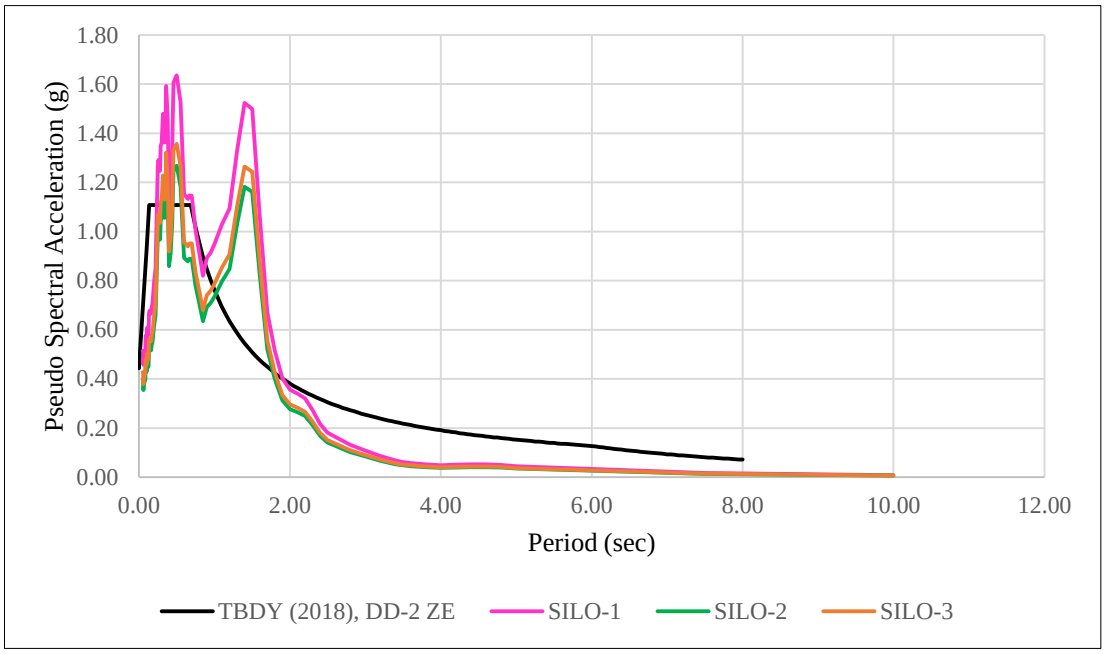

Figure 5.1: Linear elastic design spectrum and scaled response spectrums for Bayraklı-3513 Earthquake.

5.1.2. Bornova-3522 Earthquake

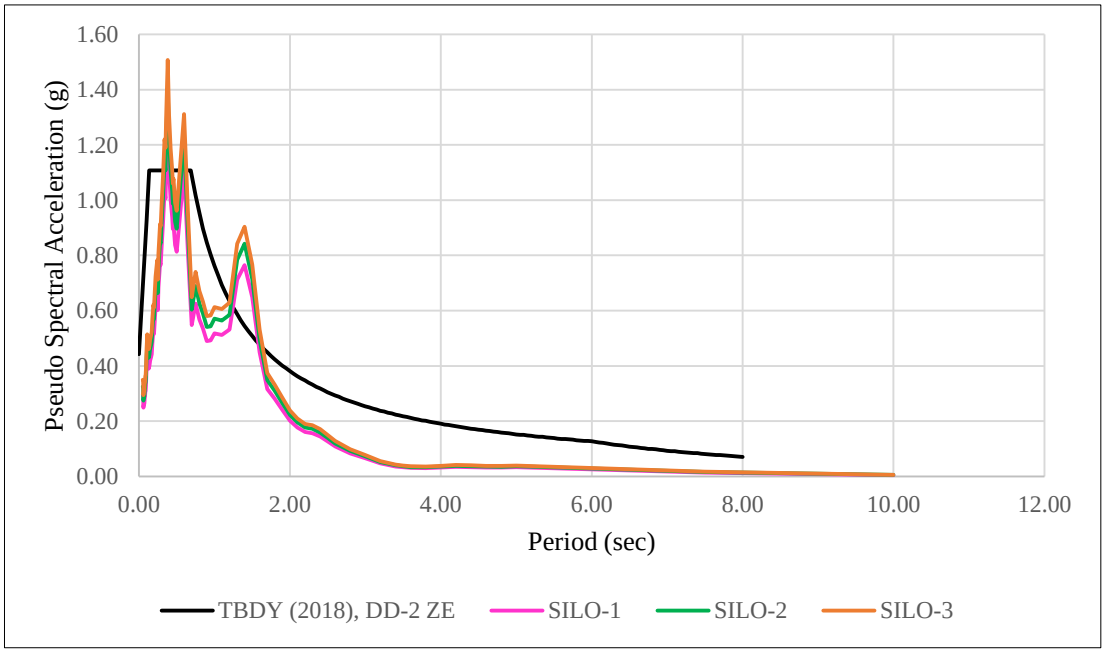

Figure 5.2: Linear elastic design spectrum and scaled response spectrums for Bornova-3522 Earthquake.

5.1.3. Iwate-5774 Earthquake

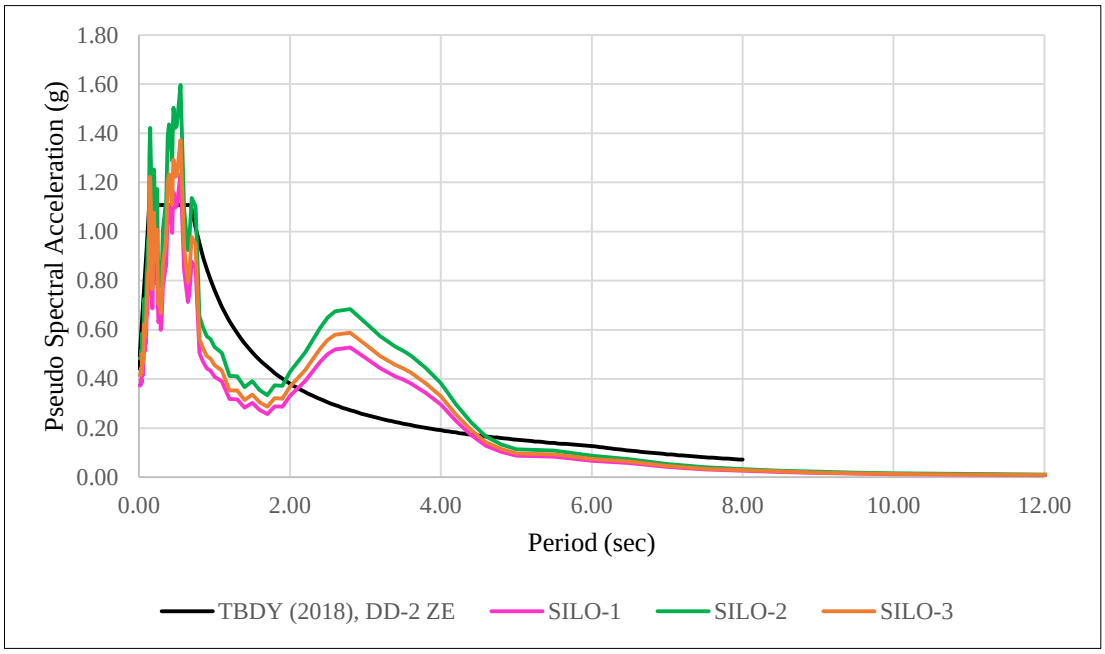

Figure 5.3: Linear elastic design spectrum and scaled response spectrums for Iwate-5774 Earthquake.

5.1.4. Kobe-1121 Earthquake

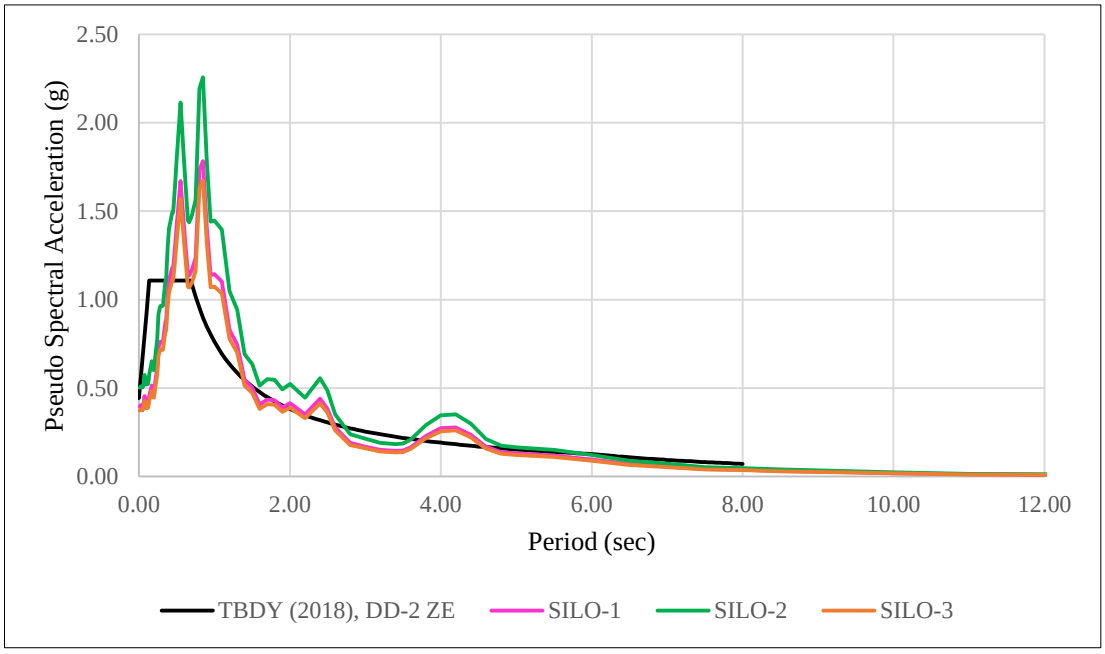

Figure 5.4: Linear elastic design spectrum and scaled response spectrums for Kobe-1121 Earthquake.

5.2. Defining Hinges

The behavior of brace shown in Figure 5.5 is defined in the frame hinge properties section in SAP2000 Structural Analysis Software. Yield and buckling force and displacement values are calculated for three brace sections and applied to the frame hinge property data for brace sections in SAP2000 Structural Analysis Software.

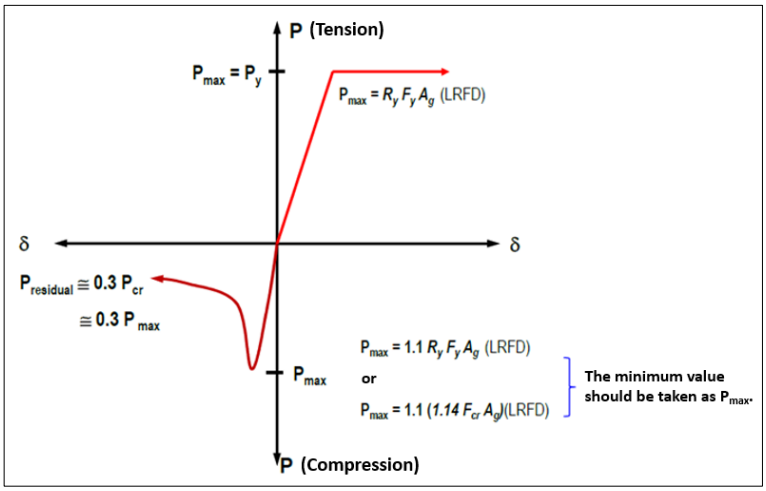

Figure 5.5: The hysteretic behavior of brace.

5.2.1. Brace of Silo-1

Brace Section (HSS60.3X4.8):

$A_g = 774.00\ mm^2$

$r = 19.90\ mm$

Material (S235):

$F_y = 235\ MPa$

$R_y = 1.4$

Yield Force:

$$P_{max} = P_y = R_y F_y A_g = 1.4 \times 235^{N/mm^2} \times 774.00^{mm^2} \times 10^{-3} \cong 255^{kN}$$

$$P_{max} = P_{cr} = min\{1.1R_yF_yA_g; 1.1(1.14F_{cr}A_g)\}$$

$$\frac{L_c}{r} = \frac{2828.427}{19.90} = 142.13 > 4.71\sqrt{\frac{E}{F_y}} = 4.71\sqrt{\frac{200000}{235}} = 137.40$$

$$F_e = \frac{\pi^2 E}{\left(\frac{L_c}{r}\right)^2} = \frac{\pi^2 \times 200000^{N/mm^2}}{142.13^2} = 97.71^{N/mm^2}$$

$$F_{cr} = 0.877F_e = 0.877 \times 97.71 = 85.69^{N/mm^2}$$

$$P_{cr} = \min\{(1.1 \times 1.4 \times 235 \times 774.00 \times 10^{-3}); (1.1 \times 1.14 \times 85.69 \times 774.00 \times 10^{-3})\} = \min\{280^{kN}; 83^{kN}\} = 83^{kN}$$

Yield Displacement:

$$k_{brace} = \frac{EA}{L_b} = \frac{200000 \times 774}{0.85 \times 2828.427} \times 10^{-3} = 64\ kN/mm$$

$$\delta_y = \frac{P_y}{k_{br}} = \frac{255}{64} = 4.0^{mm}$$

$$\delta_{cr} = \frac{P_{cr}}{k_{br}} = \frac{83}{64} = 1.3^{mm}$$

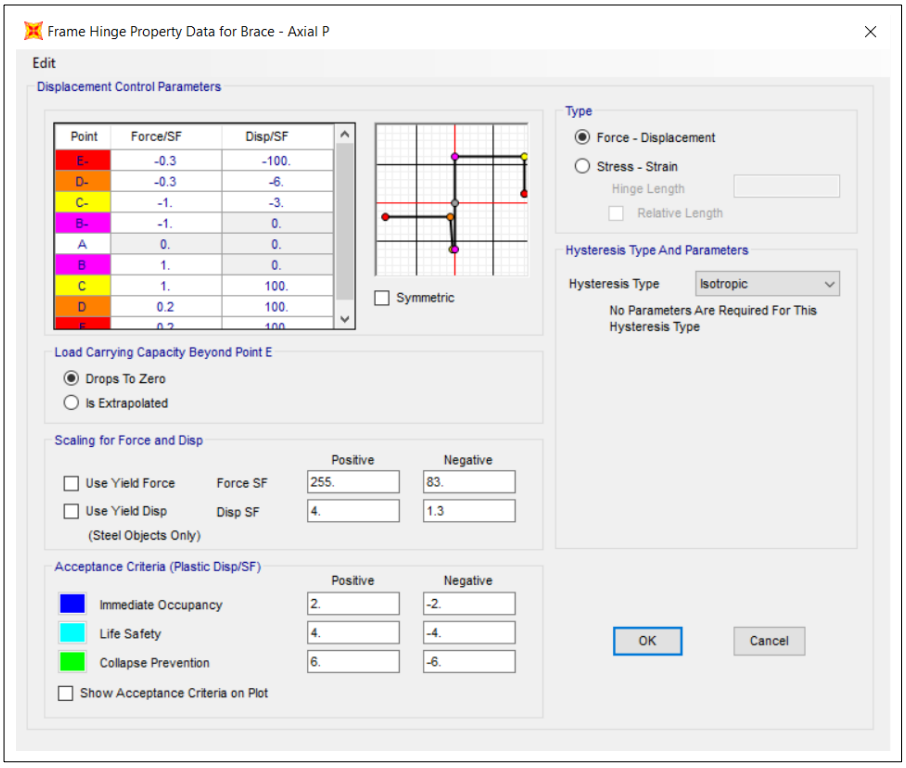

Figure 5.6: Hinge properties for brace of Silo-1 (SAP2000).

5.2.2. Brace of Silo-2

Brace Section (HSS88.9X6.4):

$A_g = 1540.00\ mm^2$

$r = 29.50\ mm$

Material (S235):

$F_y = 235\ MPa$

$R_y = 1.4$

Yield Force:

$P_{max} = P_y = R_y F_y A_g = 1.4 \times 235^{N/mm^2} \times 1540.00^{mm^2} \times 10^{-3} \cong 507^{kN}$

$P_{max} = P_{cr} = min\{1.1R_y F_y A_g; 1.1(1.14F_{cr}A_g)\}$

$\frac{L_c}{r} = \frac{4472.14}{29.50} = 151.60 > 4.71\sqrt{\frac{E}{F_y}} = 4.71\sqrt{\frac{200000}{235}} = 137.40$

$F_e = \frac{\pi^2 E}{\left(\frac{L_c}{r}\right)^2} = \frac{\pi^2 \times 200000^{N/mm^2}}{151.60^2} = 85.89^{N/mm^2}$

$F_{cr} = 0.877F_e = 0.877 \times 85.89 = 75.33^{N/mm^2}$

$P_{cr} = \min\{(1.1 \times 1.4 \times 235 \times 1540.00 \times 10^{-3}); (1.1 \times 1.14 \times 75.33 \times 1540.00 \times 10^{-3})\} = \min\{557^{kN}; 145^{kN}\} = 145^{kN}$

Yield Displacement:

$k_{brace} = \frac{EA}{L_b} = \frac{200000 \times 1540}{0.85 \times 4472.14} \times 10^{-3} = 81\ kN/mm$

$\delta_y = \frac{P_y}{k_{br}} = \frac{507}{81} = 6.3^{mm}$

$\delta_{cr} = \frac{P_{cr}}{k_{br}} = \frac{145}{81} = 1.8^{mm}$

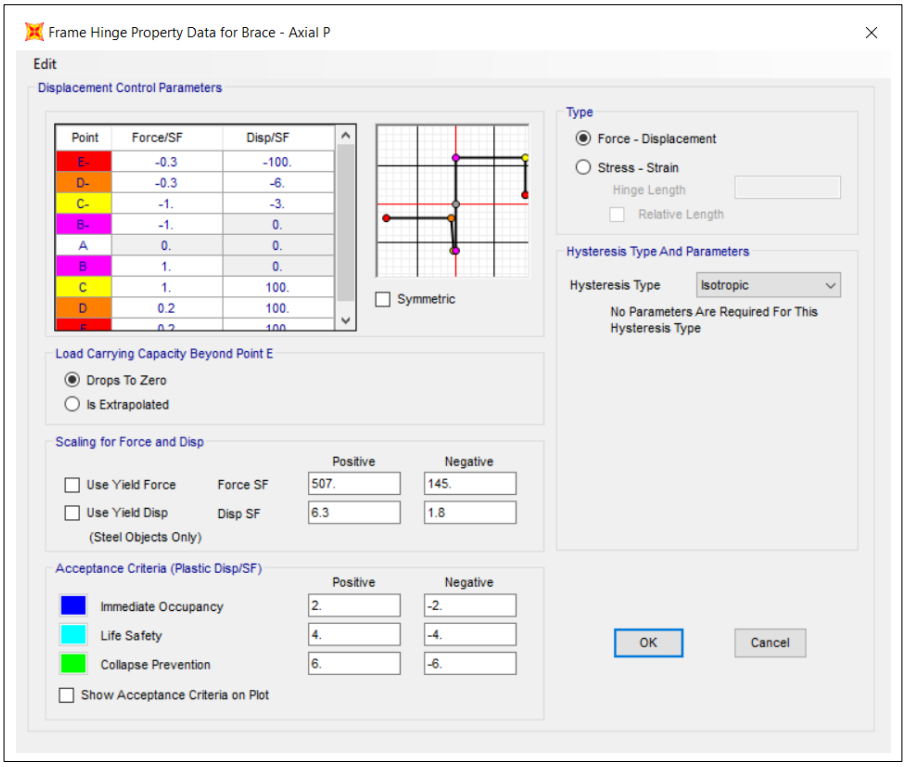

Figure 5.7: Hinge properties for brace of Silo-2 (SAP2000).

5.2.3. Brace of Silo-3

Brace Section (HSS63.5X4.8):

$A_g = 819.00\ mm^2$

$r = 21.00\ mm$

Material (S235):

$F_y = 235\ MPa$

$R_y = 1.4$

Yield Force:

$$P_{max} = P_y = R_y F_y A_g = 1.4 \times 235^{N/mm^2} \times 819.00^{mm^2} \times 10^{-3} \cong 269^{kN}$$

$$P_{max} = P_{cr} = min\{1.1 R_y F_y A_g; 1.1(1.14 F_{cr} A_g)\}$$

$$\frac{L_c}{r} = \frac{2236.05}{21.00} = 106.48 \leq 4.71\sqrt{\frac{E}{F_y}} = 4.71\sqrt{\frac{200000}{235}} = 137.40$$

$$F_e = \frac{\pi^2 E}{\left(\frac{L_c}{r}\right)^2} = \frac{\pi^2 \times 200000^{N/mm^2}}{106.48^2} = 174.10^{N/mm^2}$$

$$F_{cr} = \left(0.658^{F_y/F_e}\right)F_y = \left(0.658^{235/174.10}\right) \times 235 = 133.57^{N/mm^2}$$

$$P_{cr} = \min\{(1.1 \times 1.4 \times 235 \times 819.00 \times 10^{-3}); (1.1 \times 1.14 \times 133.57 \times 819.00 \times 10^{-3})\} = \min\{296^{kN}; 137^{kN}\} = 137^{kN}$$

Yield Displacement:

$$k_{brace} = \frac{EA}{L_b} = \frac{200000 \times 819}{0.85 \times 2236.05} \times 10^{-3} = 86\ kN/mm$$

$$\delta_y = \frac{P_y}{k_{br}} = \frac{269}{86} = 3.1^{mm}$$

$$\delta_{cr} = \frac{P_{cr}}{k_{br}} = \frac{137}{86} = 1.6^{mm}$$

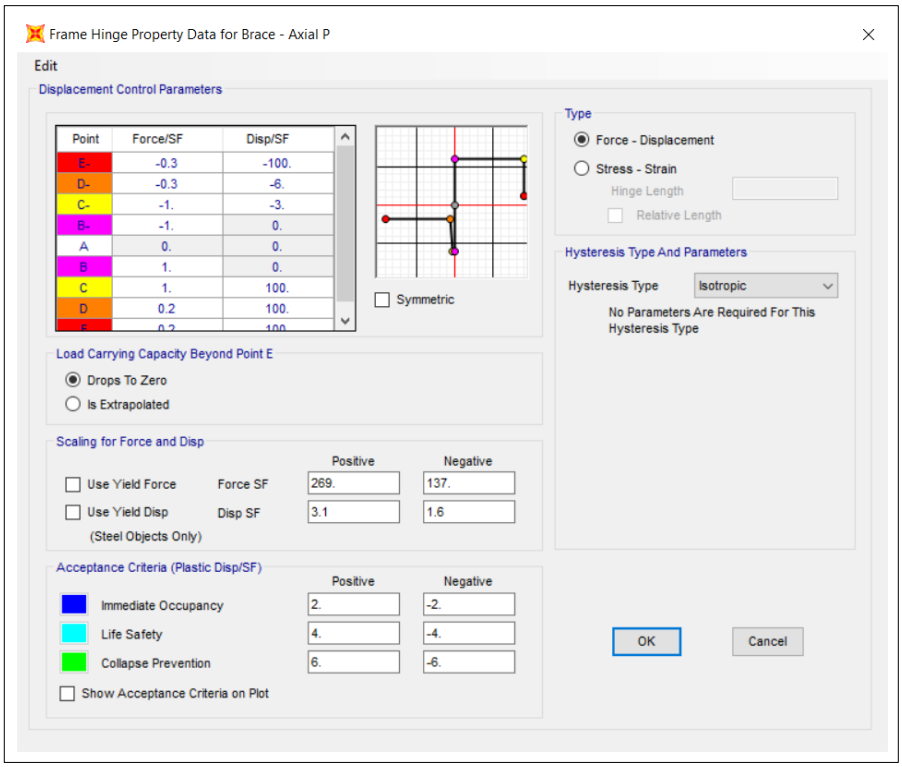

Figure 5.8: Hinge properties for brace of Silo-3 (SAP2000).

The yield and buckling forces and displacements, which are applied on SAP2000 Structural Analysis Software, are shown in Table 5.3.

Table 5.3: Yield and Buckling Forces and Displacements.

Silo Number	Brace Section	P_y (kN)	P_{cr} (kN)	δ_y (mm)	δ_{cr} (mm)
1	HSS60.3X4.8	255	83	4.0	1.3
2	HSS88.9X6.4	507	145	6.3	1.8
3	HSS63.5X4.8	269	137	3.1	1.6

5.3. Nonlinear Analysis Results

Incremental Dynamic Analysis (IDA) is an analysis method used for calculations of earthquake and structural engineering. This method evaluates the performance of structures under seismic loads, comprehensively. It relies on the results of probabilistic seismic hazard analysis to predict the seismic risk faced by a structure. IDA performs Nonlinear Incremental Dynamic Analyses of a structure under earthquake records, each scaled to various seismic intensity levels. The scaling levels are chosen to force the structure through its entire behavior range from elastic to plastic and finally to dynamic instability where it experiences collapse [16].

Incremental Dynamic Analysis is applied to three silos for the four determined earthquakes by considering the acceleration values for IDA between 0.40 g and 2.00 g. The limit value is accepted as 2.00 g which is two times more than the acceleration corresponding to the silo periods in the design spectrum. Scale factors are determined for three silos in the range of 0.40 g – 2.00 g and applied to the SAP2000 Structural Analysis Software in order to obtain the results. As a result of the Time History Analysis, deformed shapes, maximum value of axial elongation/shortening, top displacements and base shear forces are reached during the earthquake period for each earthquake and acceleration values.

5.3.1. Hinge Results for Bayraklı-3513

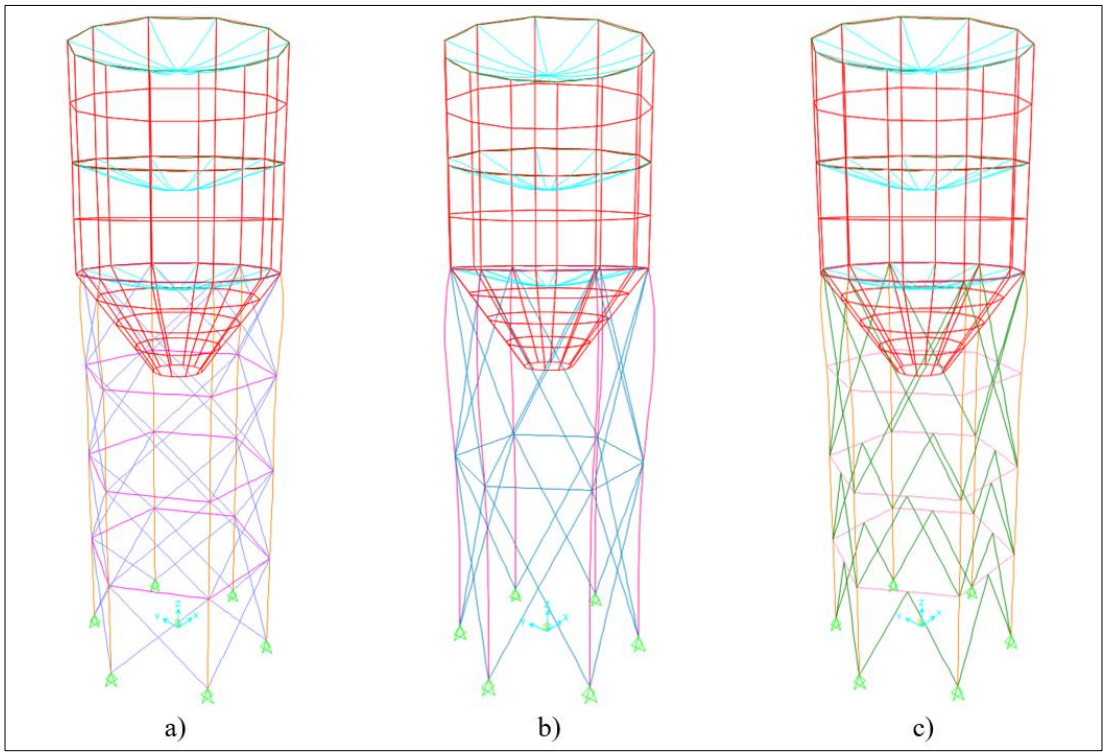

Figure 5.9: Deformed shapes of a) Silo-1, b) Silo-2, c) Silo-3 at 0.40 g (Bayraklı).

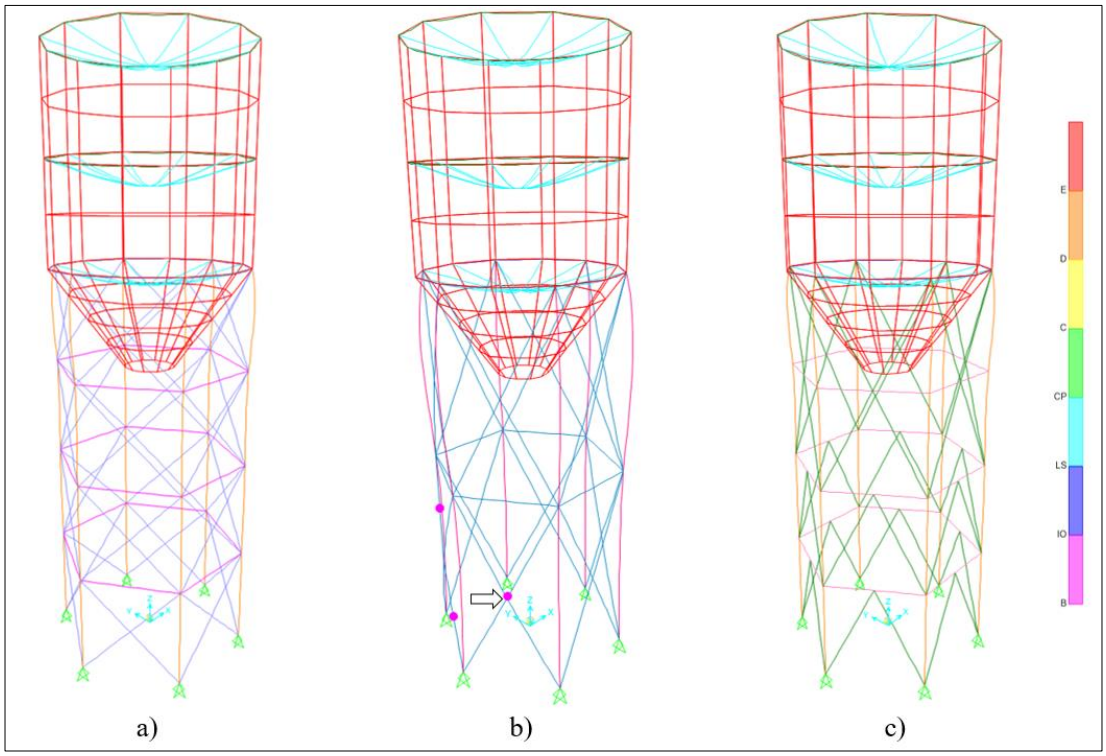

Figure 5.10: Deformed shapes of a) Silo-1, b) Silo-2, c) Silo-3 at 0.60 g (Bayraklı).

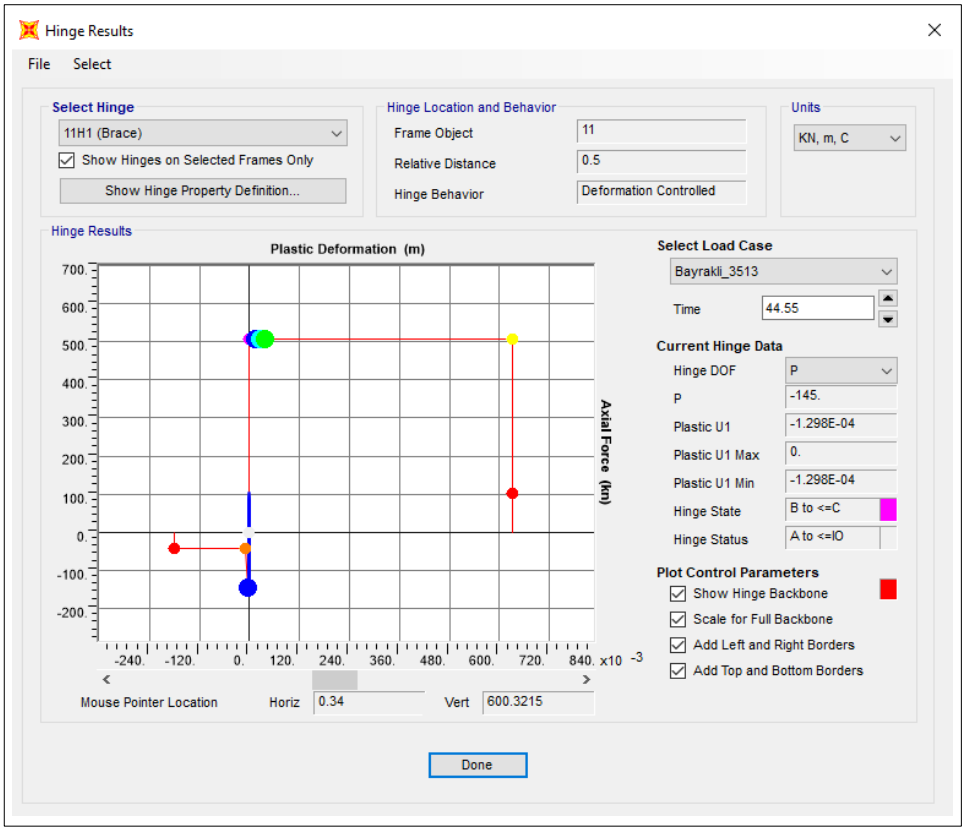

Figure 5.11: Hinge results of Silo-2 at 0.60 g (Bayraklı).

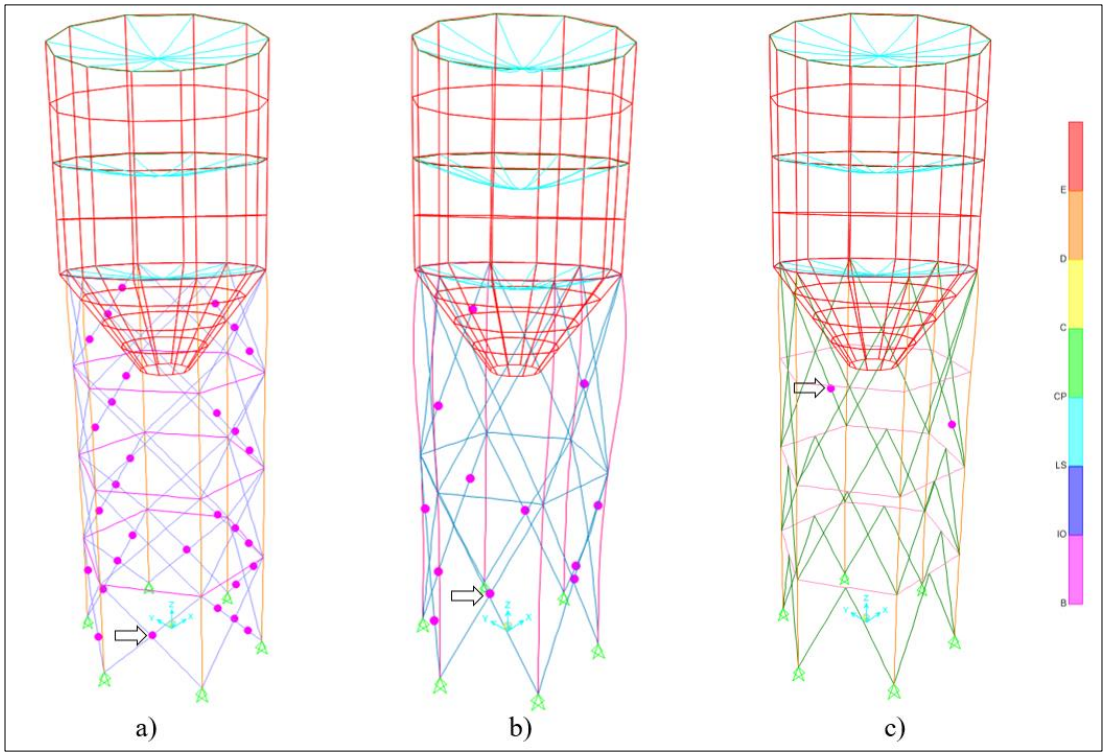

Figure 5.12: Deformed shapes of a) Silo-1, b) Silo-2, c) Silo-3 at 0.80 g (Bayraklı).

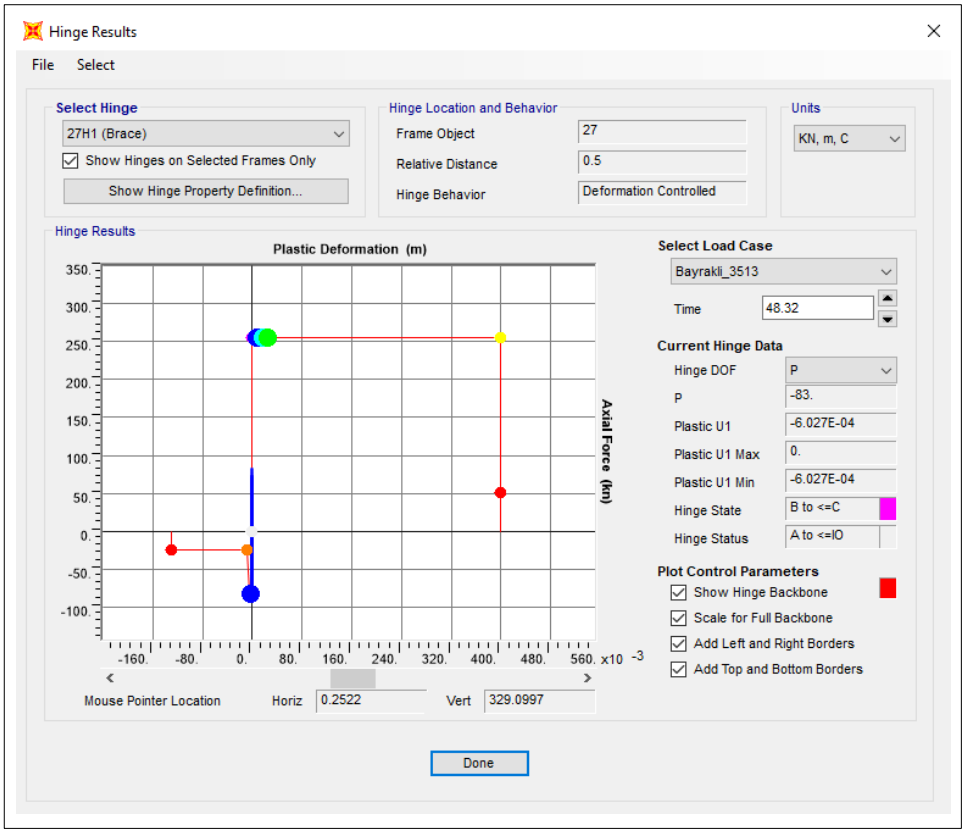

Figure 5.13: Hinge results of Silo-1 at 0.80 g (Bayraklı).

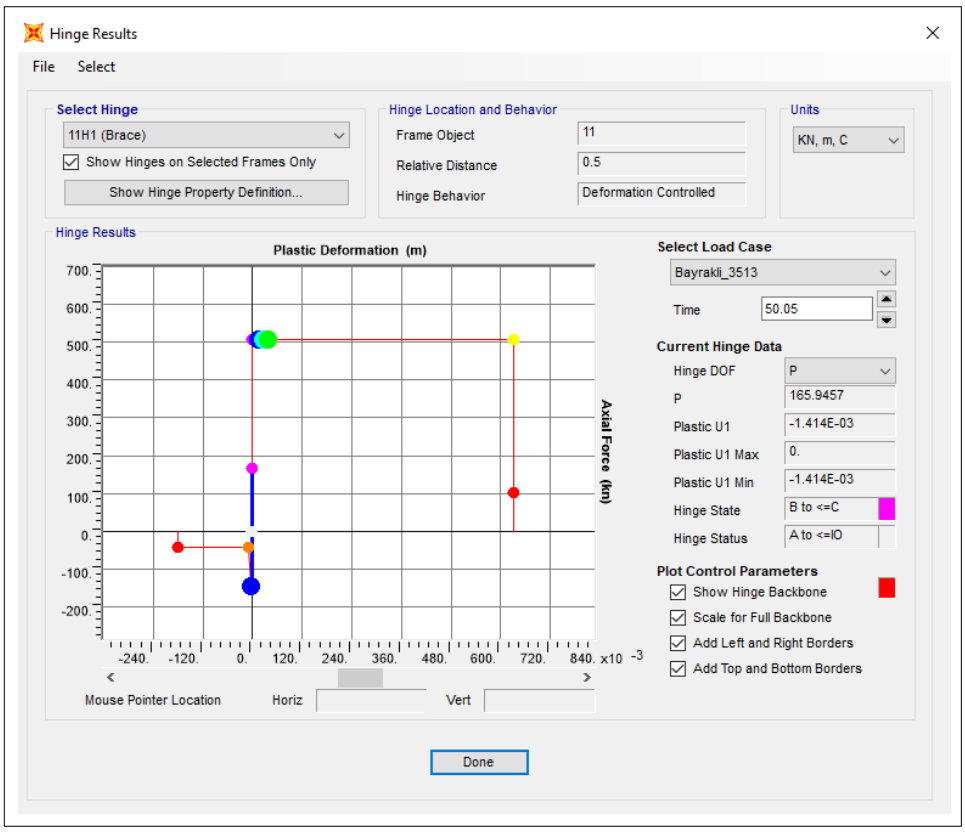

Figure 5.14: Hinge results of Silo-2 at 0.80 g (Bayraklı).

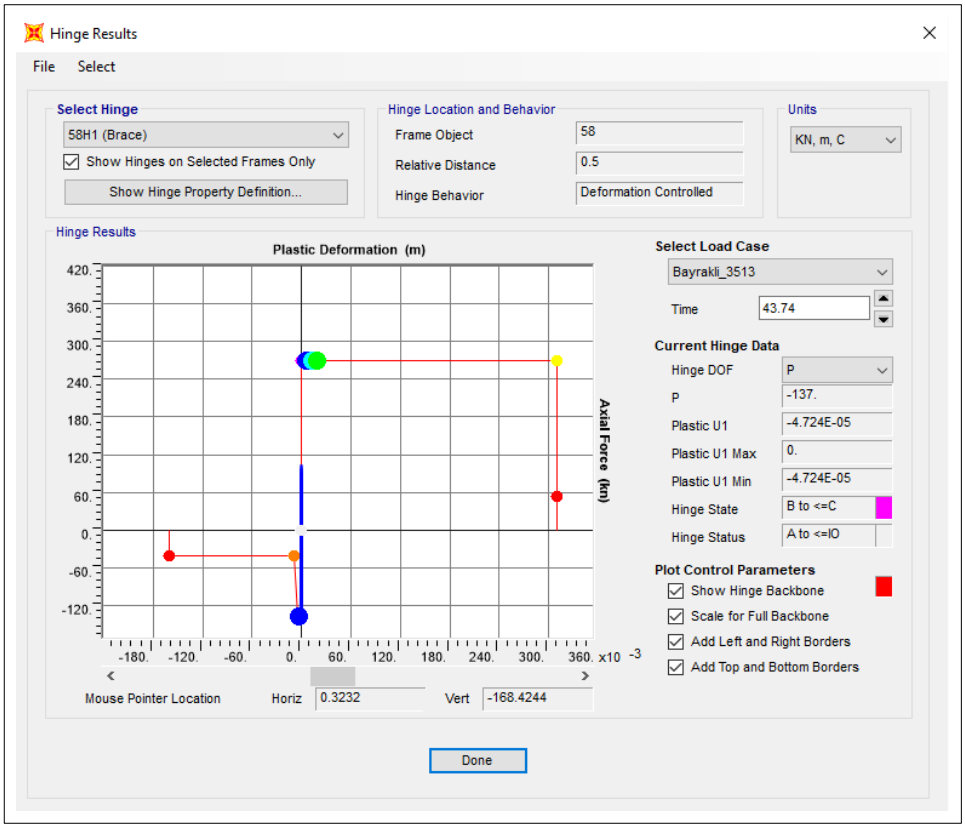

Figure 5.15: Hinge results of Silo-3 at 0.80 g (Bayraklı).

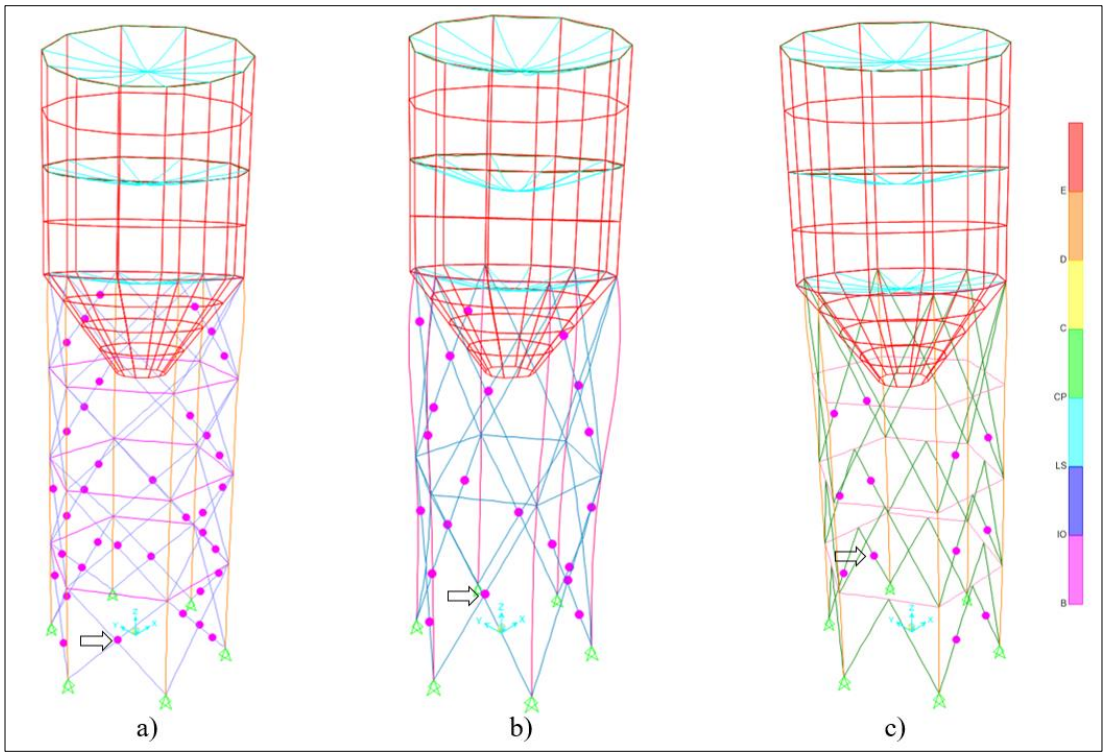

Figure 5.16: Deformed shapes of a) Silo-1, b) Silo-2, c) Silo-3 at 1.00 g (Bayraklı).

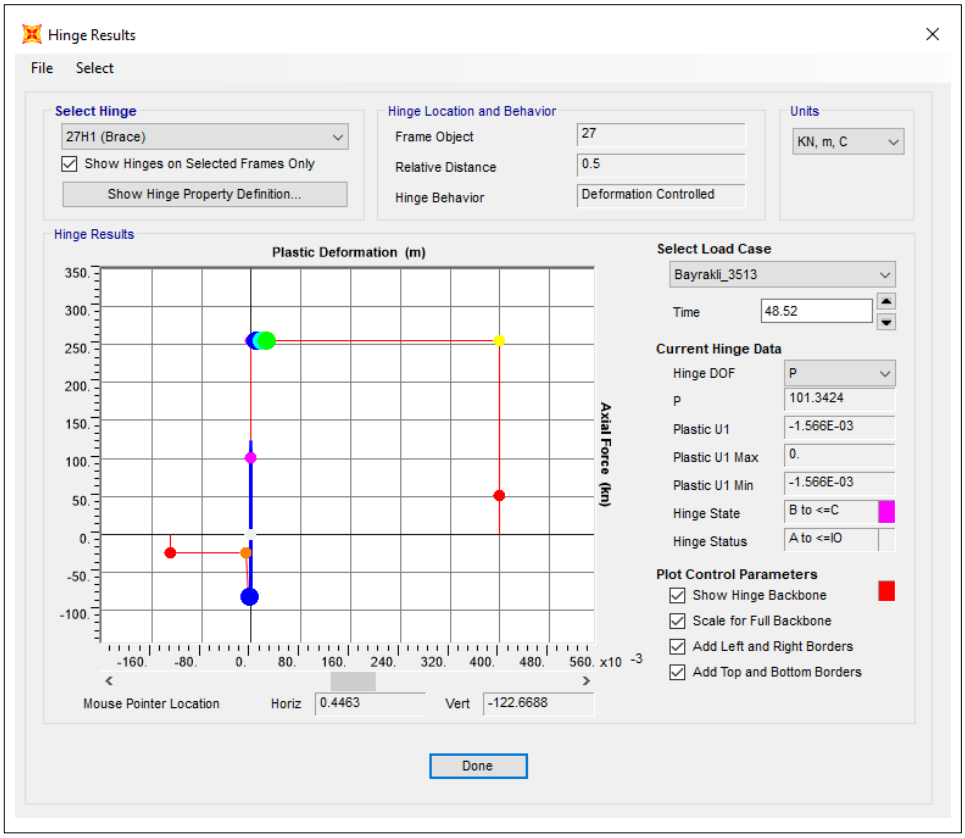

Figure 5.17: Hinge results of Silo-1 at 1.00 g (Bayraklı).

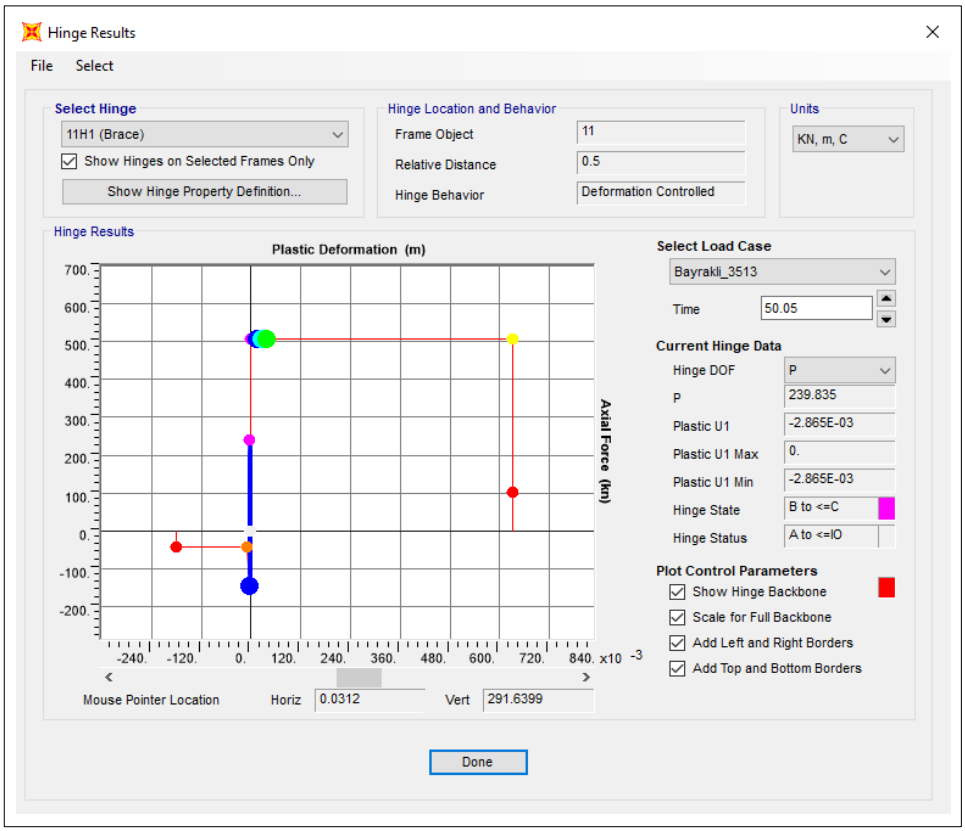

Figure 5.18: Hinge results of Silo-2 at 1.00 g (Bayraklı).

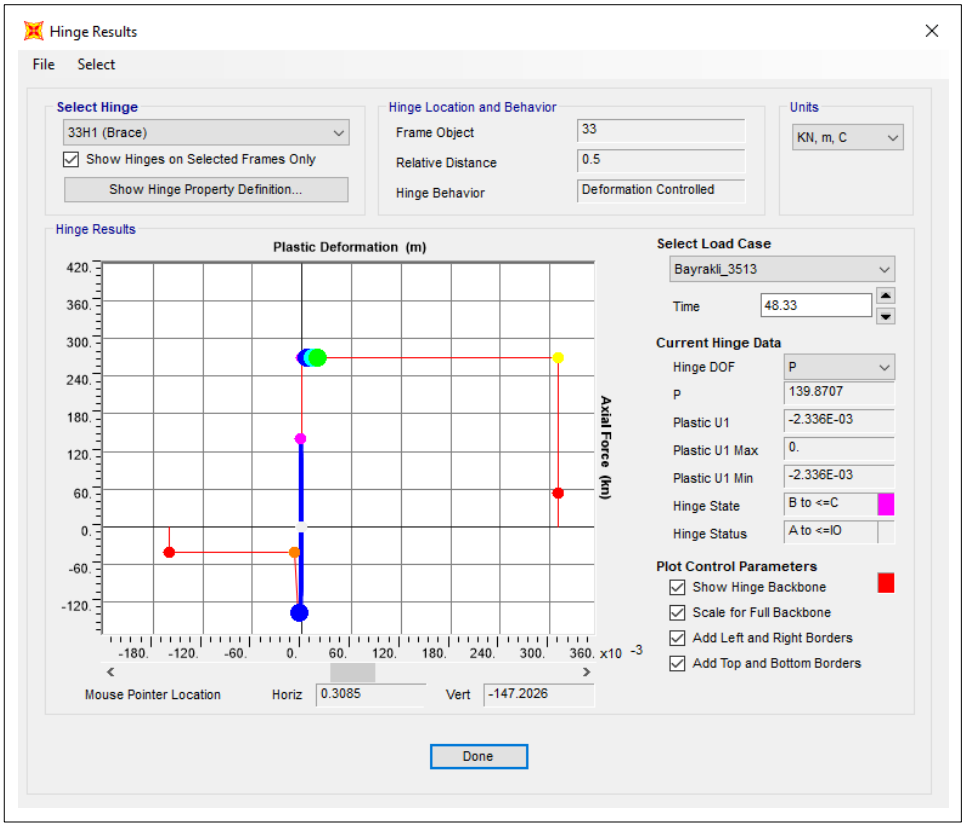

Figure 5.19: Hinge results of Silo-3 at 1.00 g (Bayraklı).

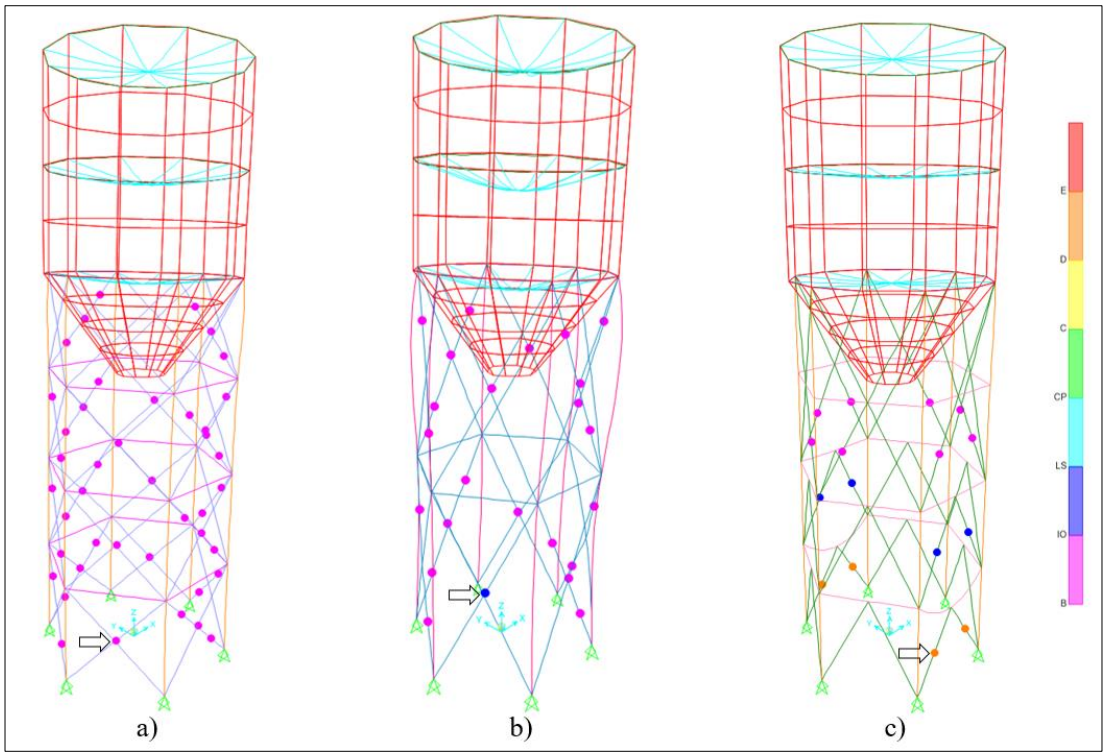

Figure 5.20: Deformed shapes of a) Silo-1, b) Silo-2, c) Silo-3 at 1.20 g (Bayraklı).

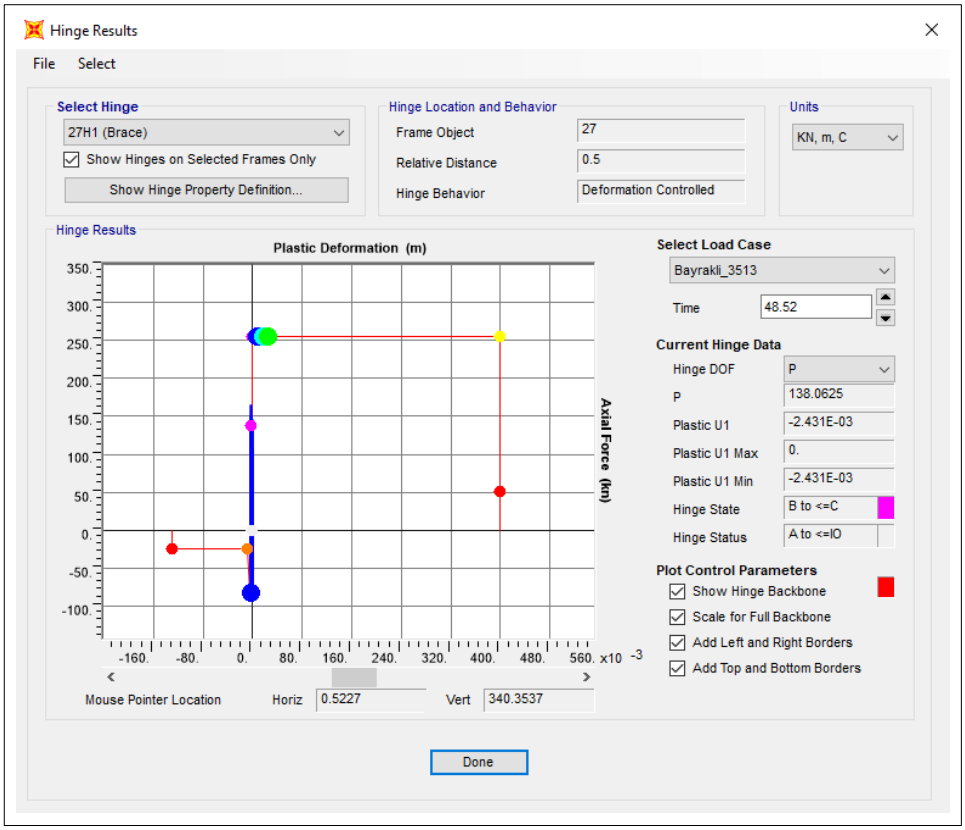

Figure 5.21: Hinge results of Silo-1 at 1.20 g (Bayraklı).

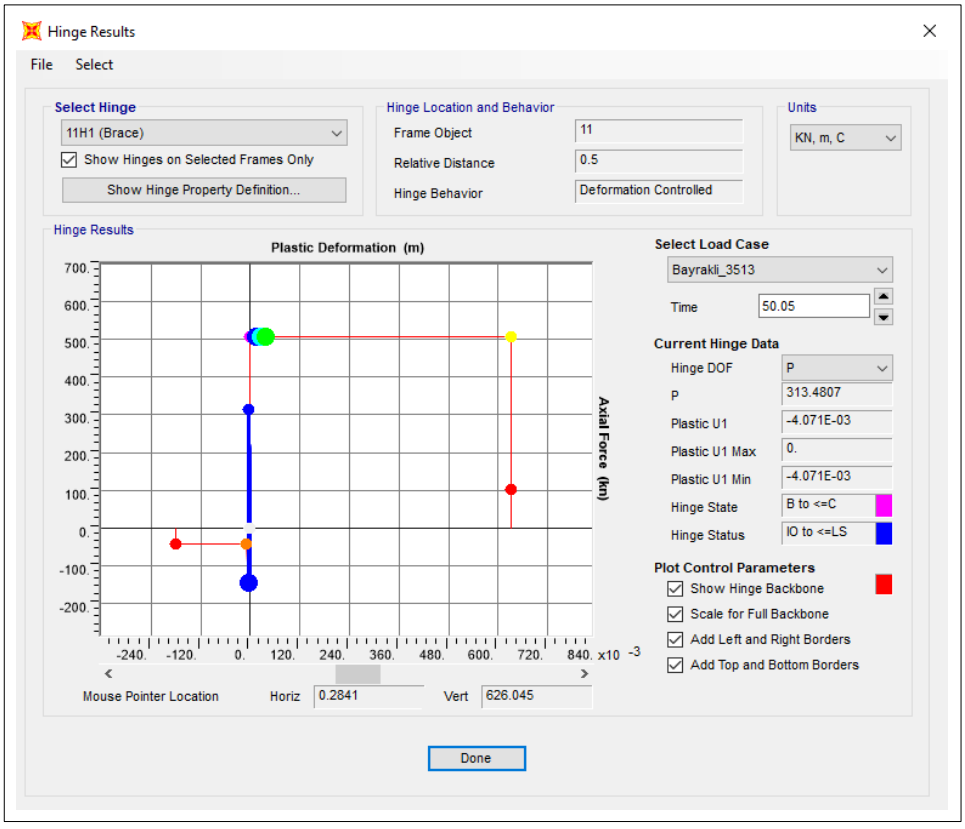

Figure 5.22: Hinge results of Silo-2 at 1.20 g (Bayraklı).

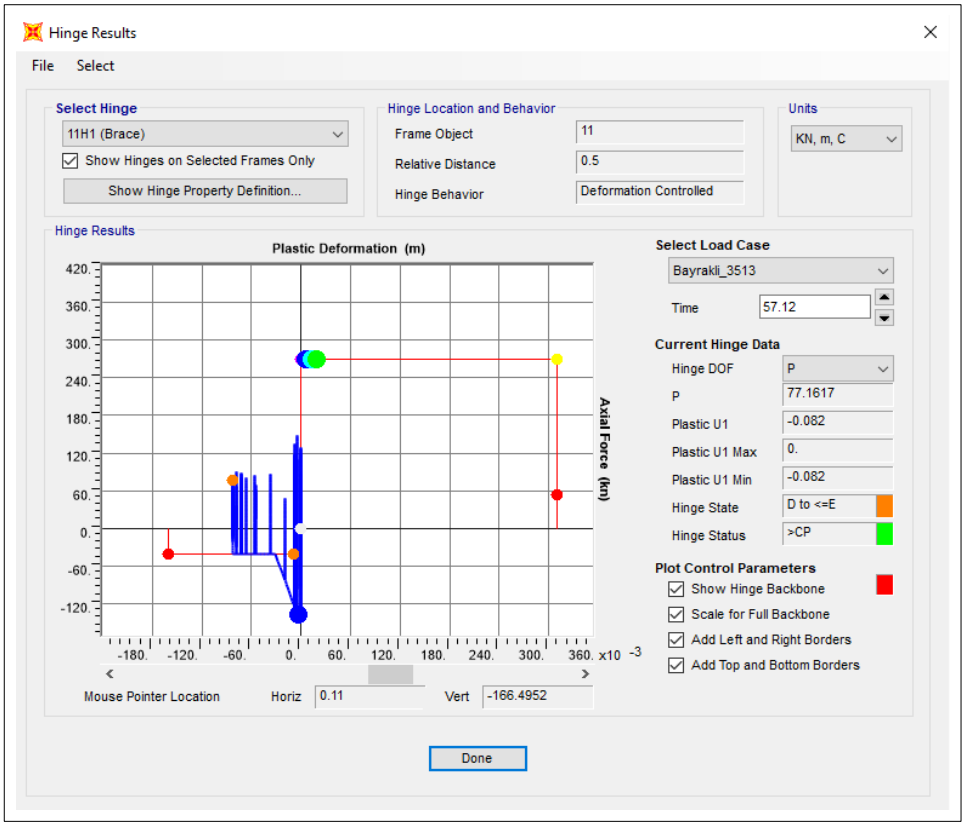

Figure 5.23: Hinge results of Silo-3 at 1.20 g (Bayraklı).

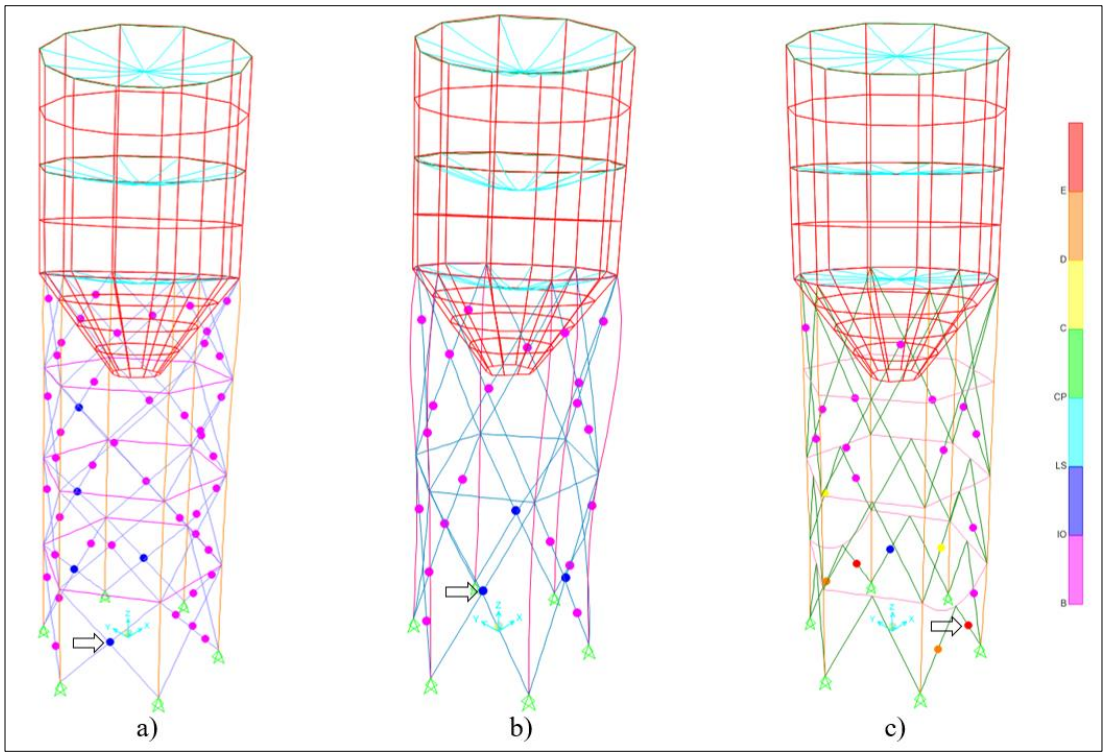

Figure 5.24: Deformed shapes of a) Silo-1, b) Silo-2, c) Silo-3 at 1.40 g (Bayraklı).

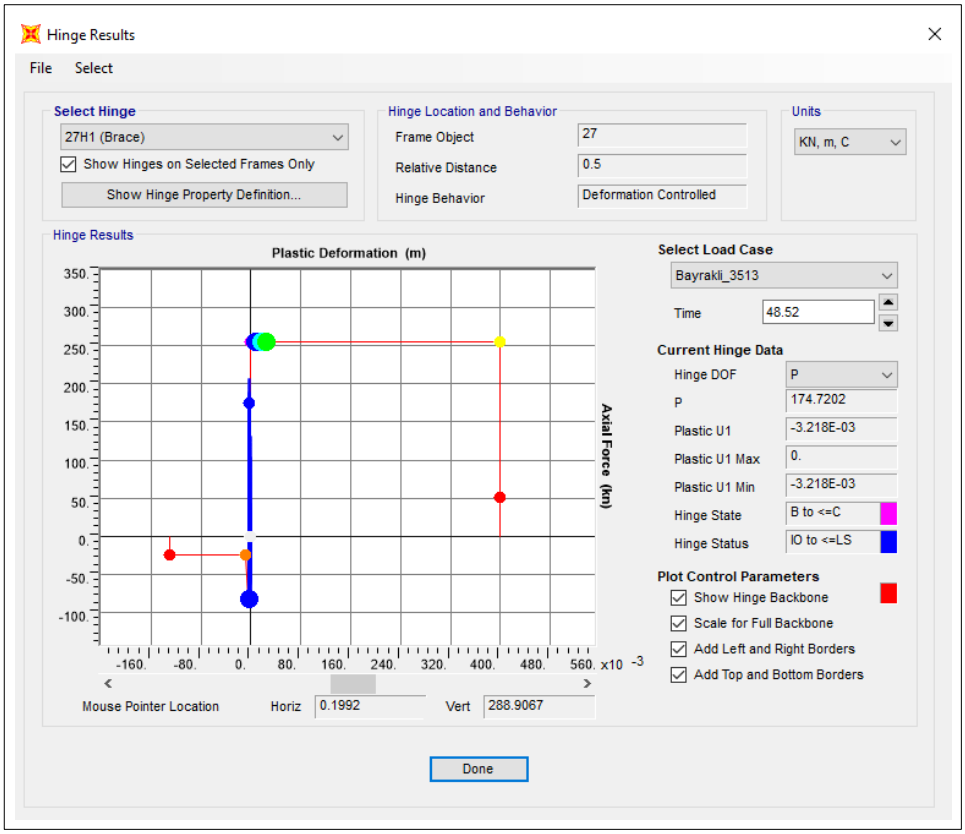

Figure 5.25: Hinge results of Silo-1 at 1.40 g (Bayraklı).

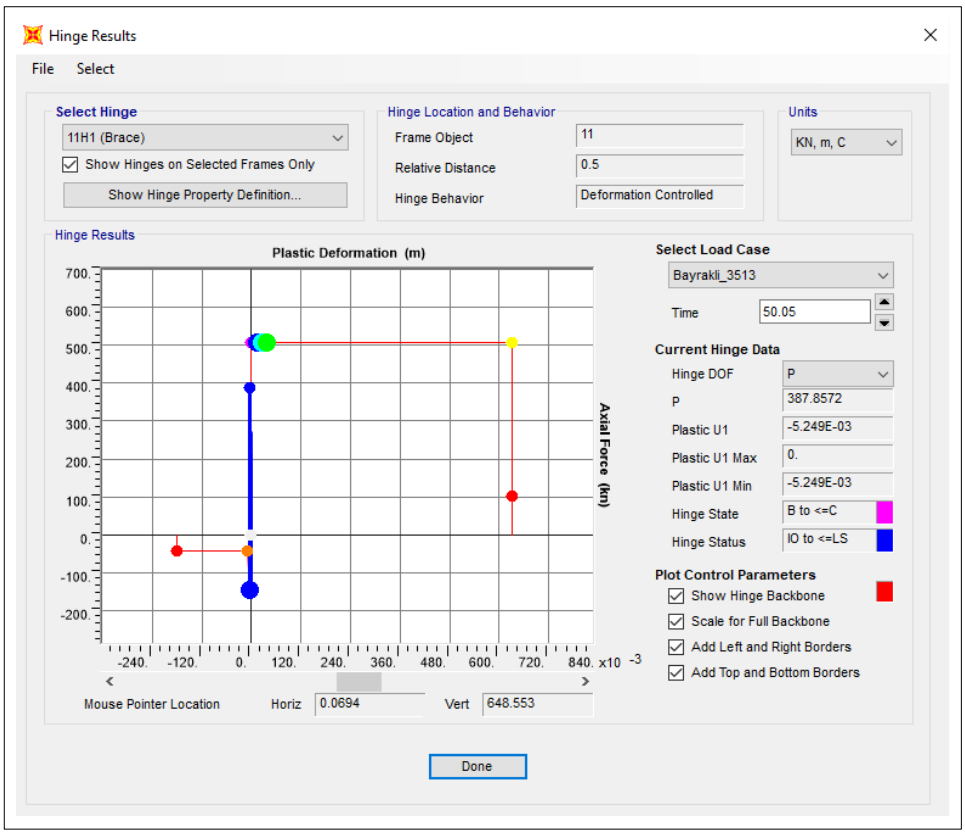

Figure 5.26: Hinge results of Silo-2 at 1.40 g (Bayraklı).

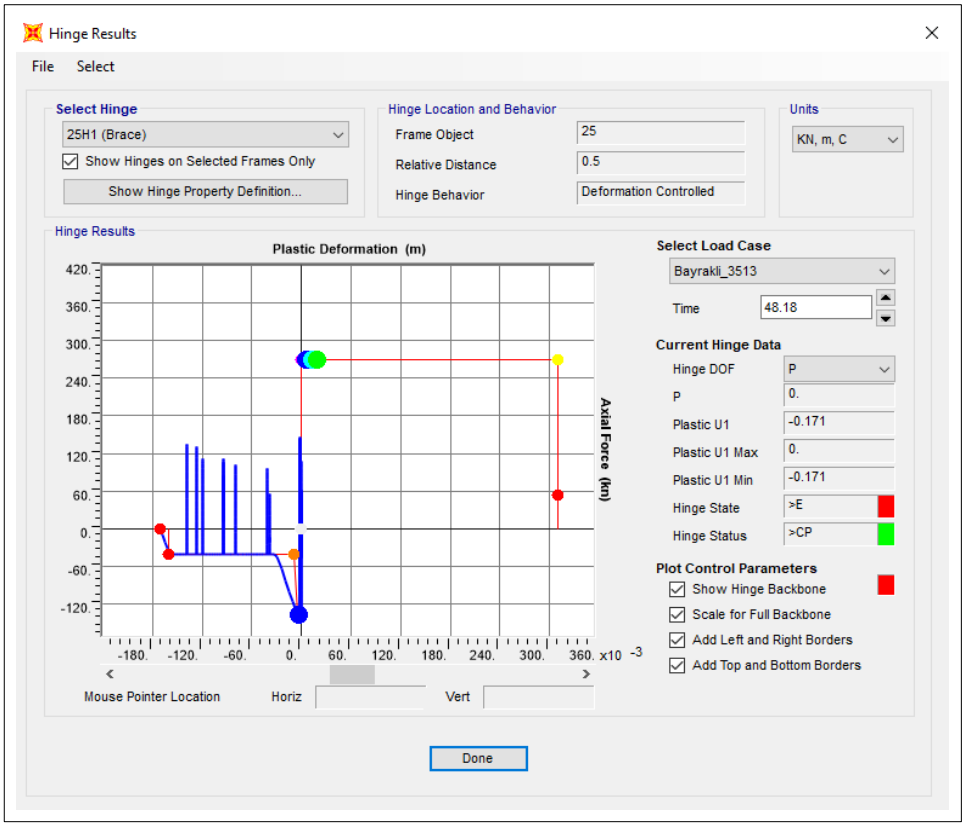

Figure 5.27: Hinge results of Silo-3 at 1.40 g (Bayraklı).

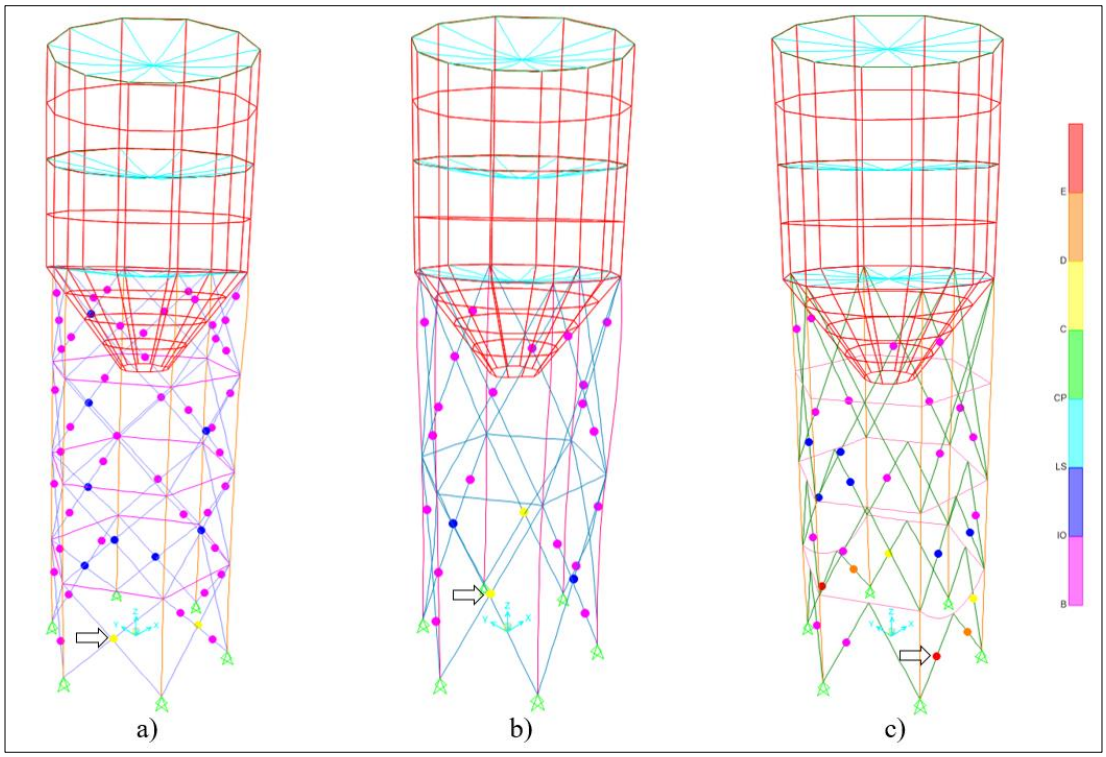

Figure 5.28: Deformed shapes of a) Silo-1, b) Silo-2, c) Silo-3 at 1.60 g (Bayraklı).

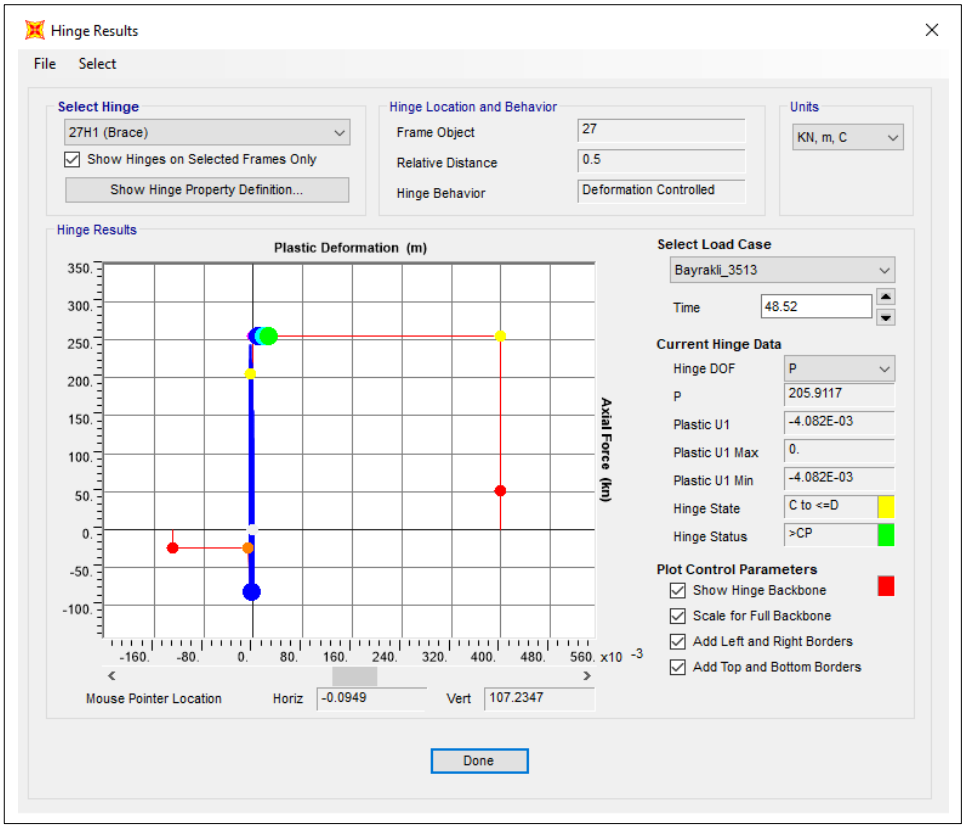

Figure 5.29: Hinge results of Silo-1 at 1.60 g (Bayraklı).

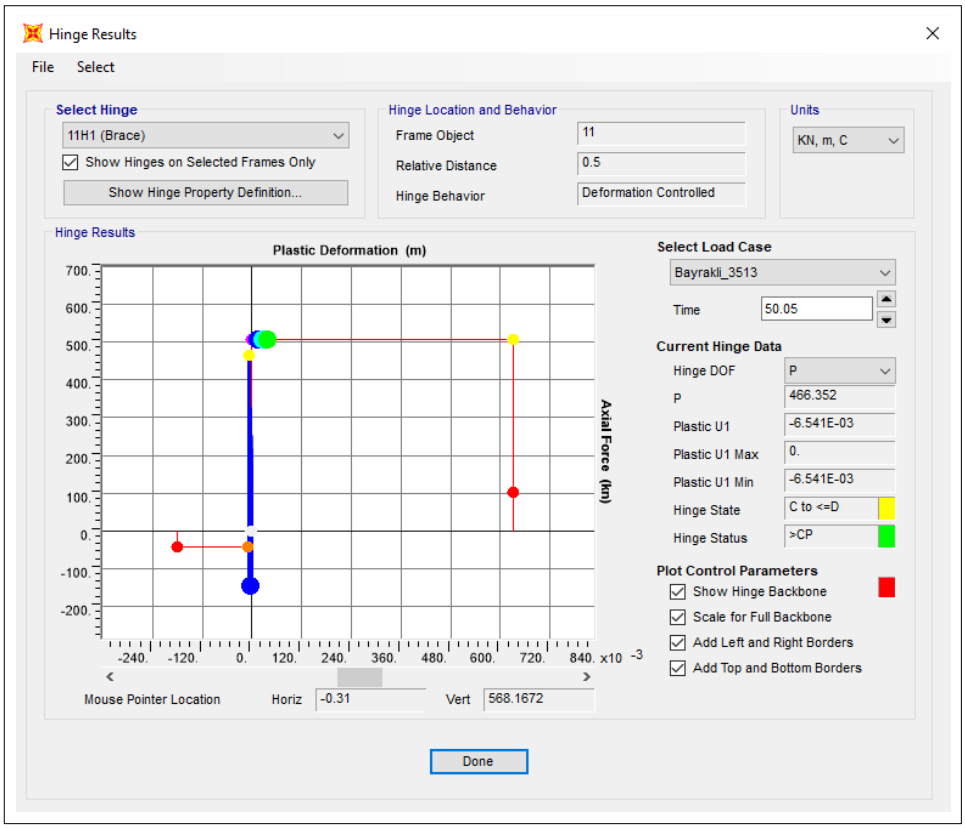

Figure 5.30: Hinge results of Silo-2 at 1.60 g (Bayraklı).

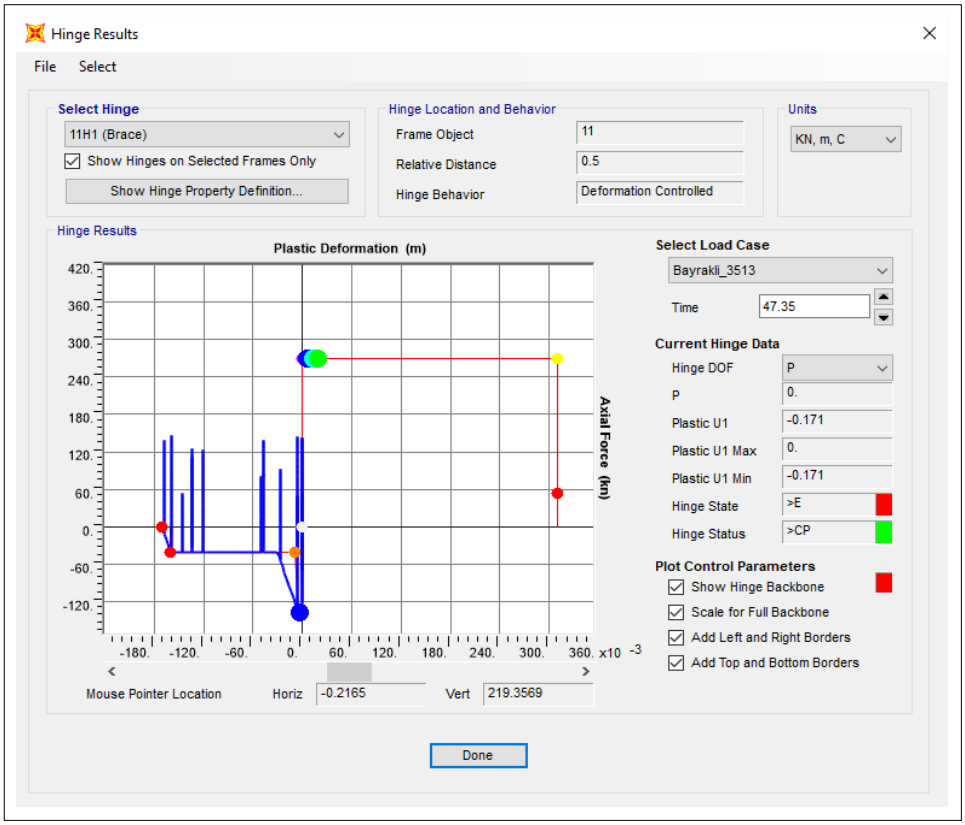

Figure 5.31: Hinge results of Silo-3 at 1.60 g (Bayraklı).

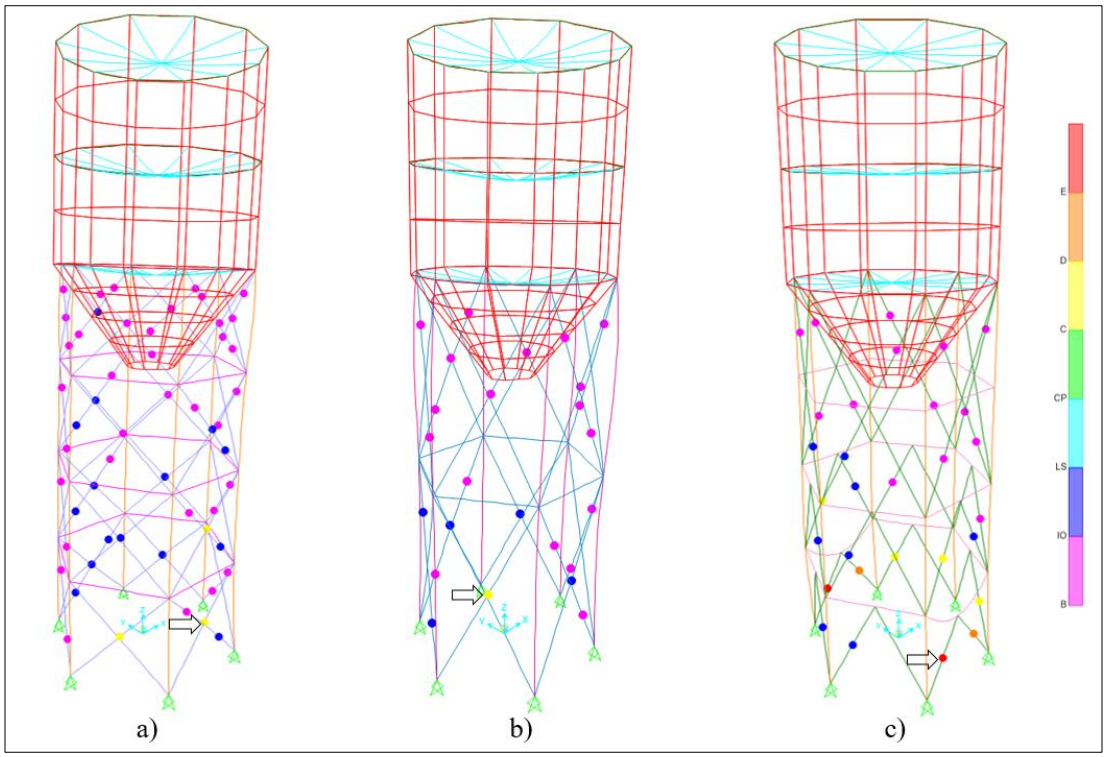

Figure 5.32: Deformed shapes of a) Silo-1, b) Silo-2, c) Silo-3 at 1.80 g (Bayraklı).

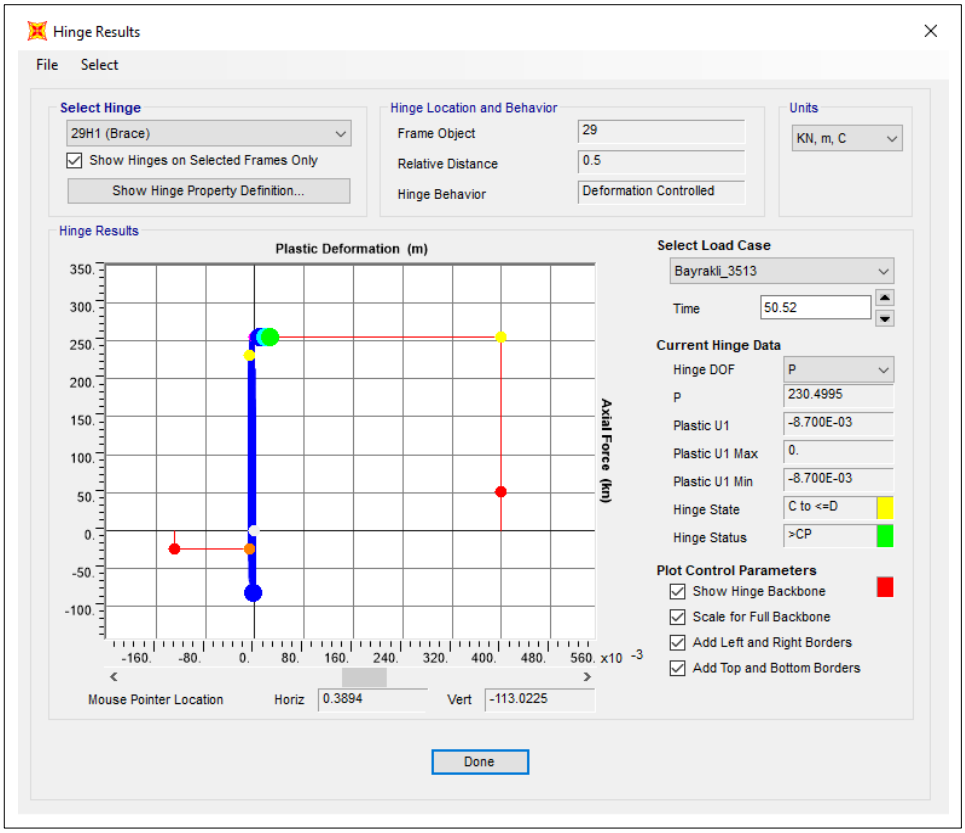

Figure 5.33: Hinge results of Silo-1 at 1.80 g (Bayraklı).

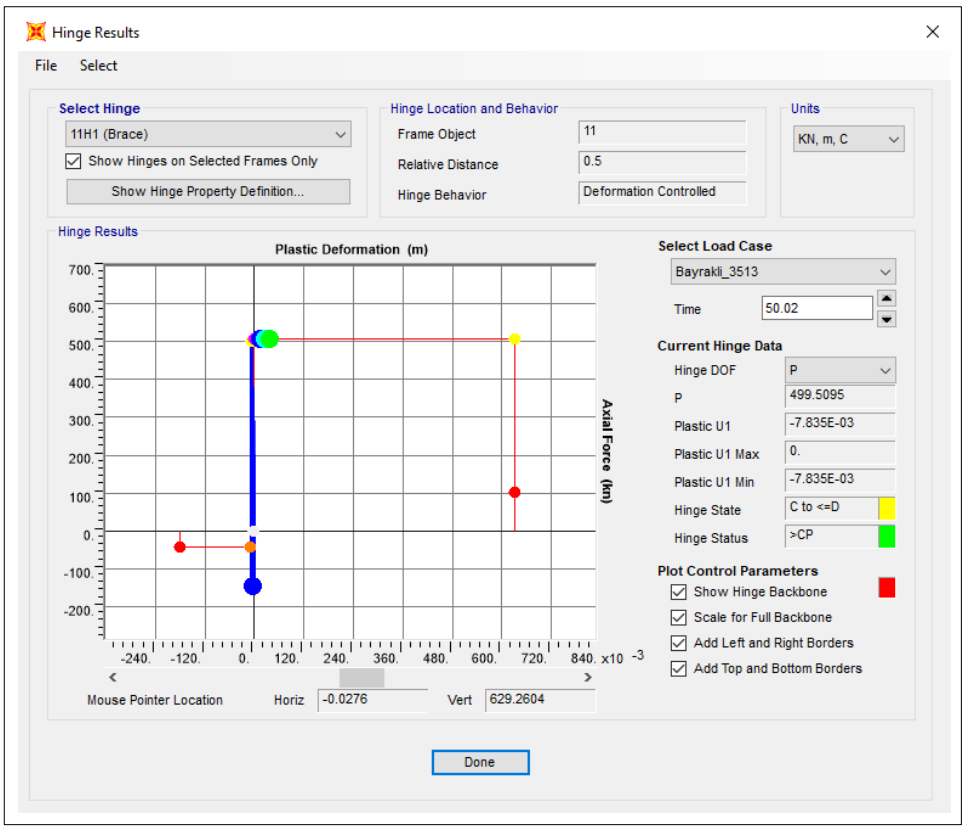

Figure 5.34: Hinge results of Silo-2 at 1.80 g (Bayraklı).

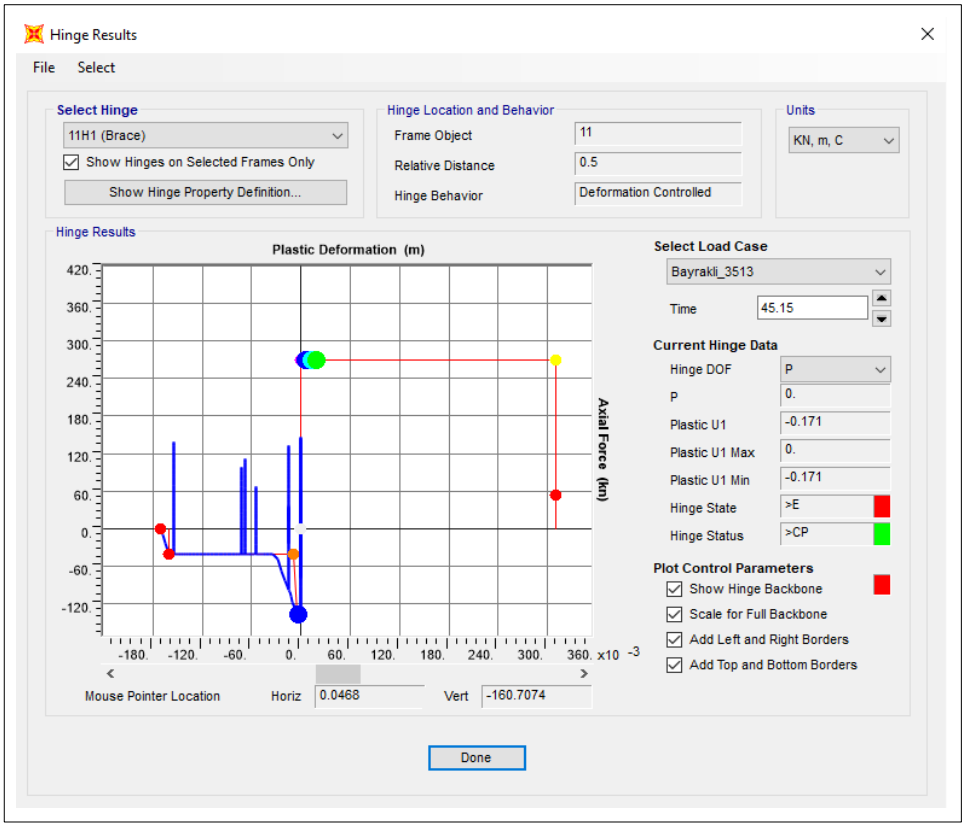

Figure 5.35: Hinge results of Silo-3 at 1.80 g (Bayraklı).

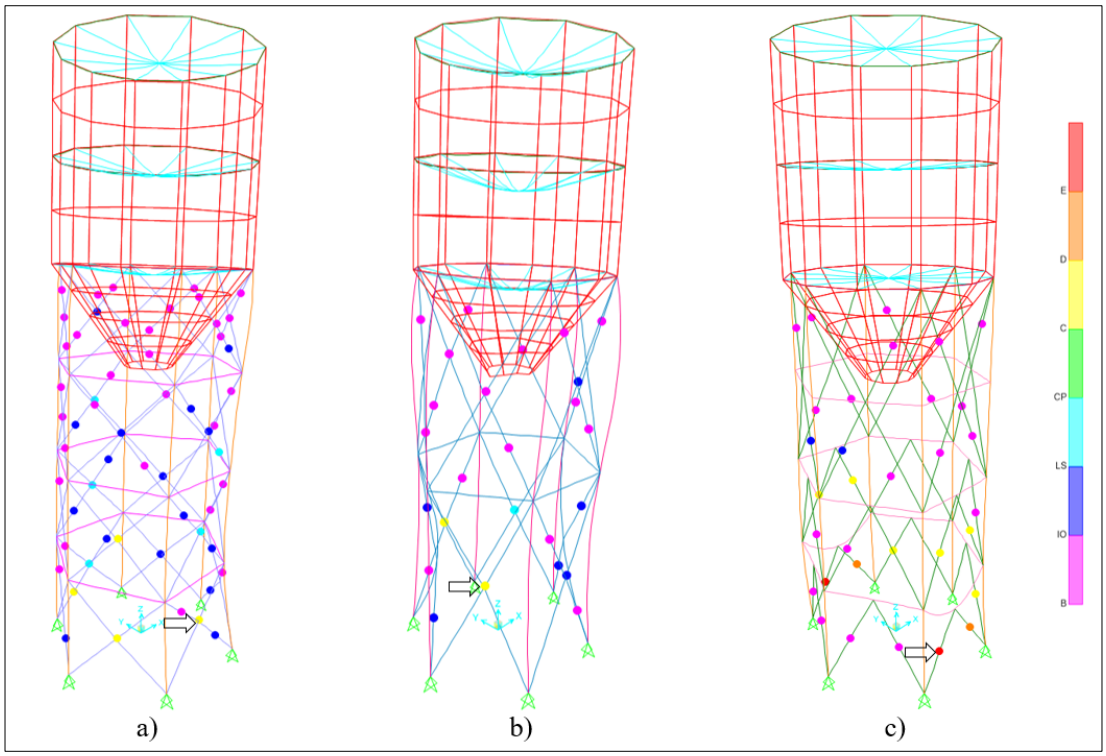

Figure 5.36: Deformed shapes of a) Silo-1, b) Silo-2, c) Silo-3 at 2.00 g (Bayraklı).

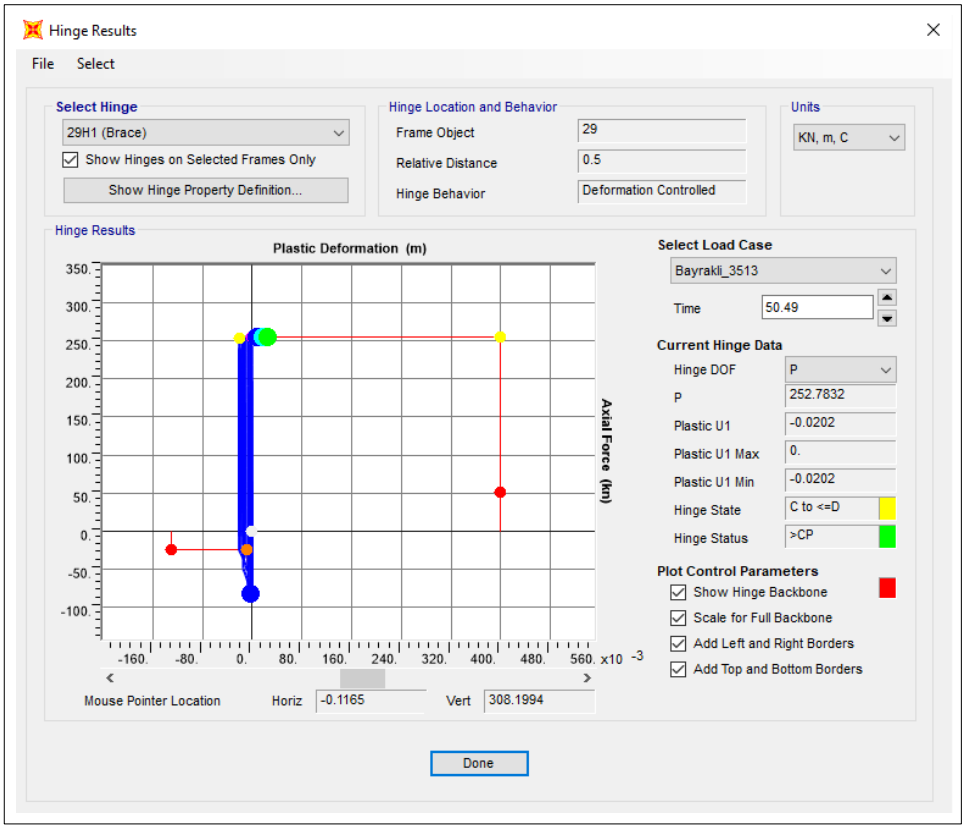

Figure 5.37: Hinge results of Silo-1 at 2.00 g (Bayraklı).

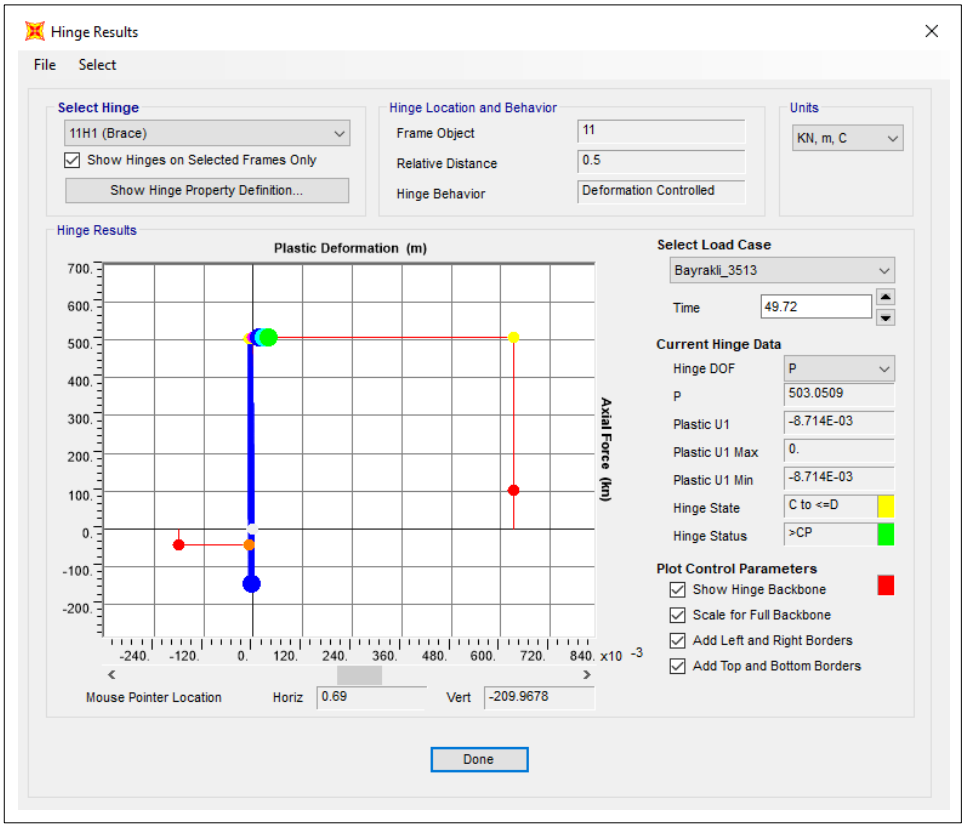

Figure 5.38: Hinge results of Silo-2 at 2.00 g (Bayraklı).

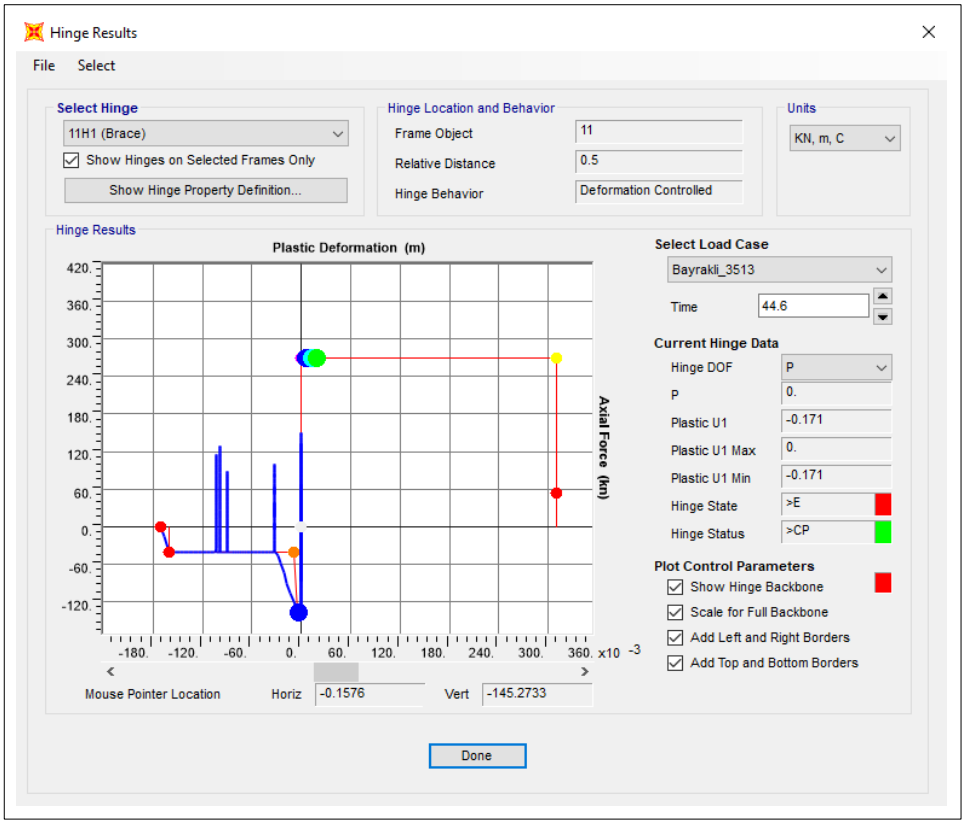

Figure 5.39: Hinge results of Silo-3 at 2.00 g (Bayraklı).

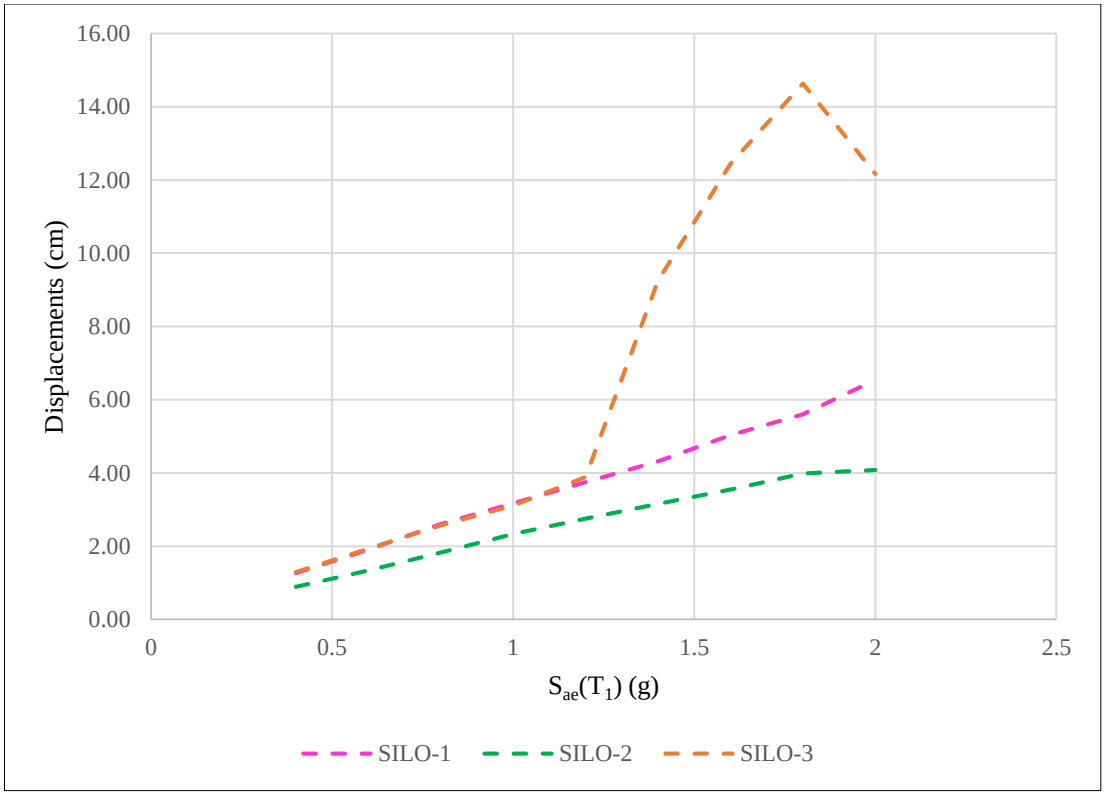

Figure 5.40: Top displacements in Bayraklı-3513 Earthquake.

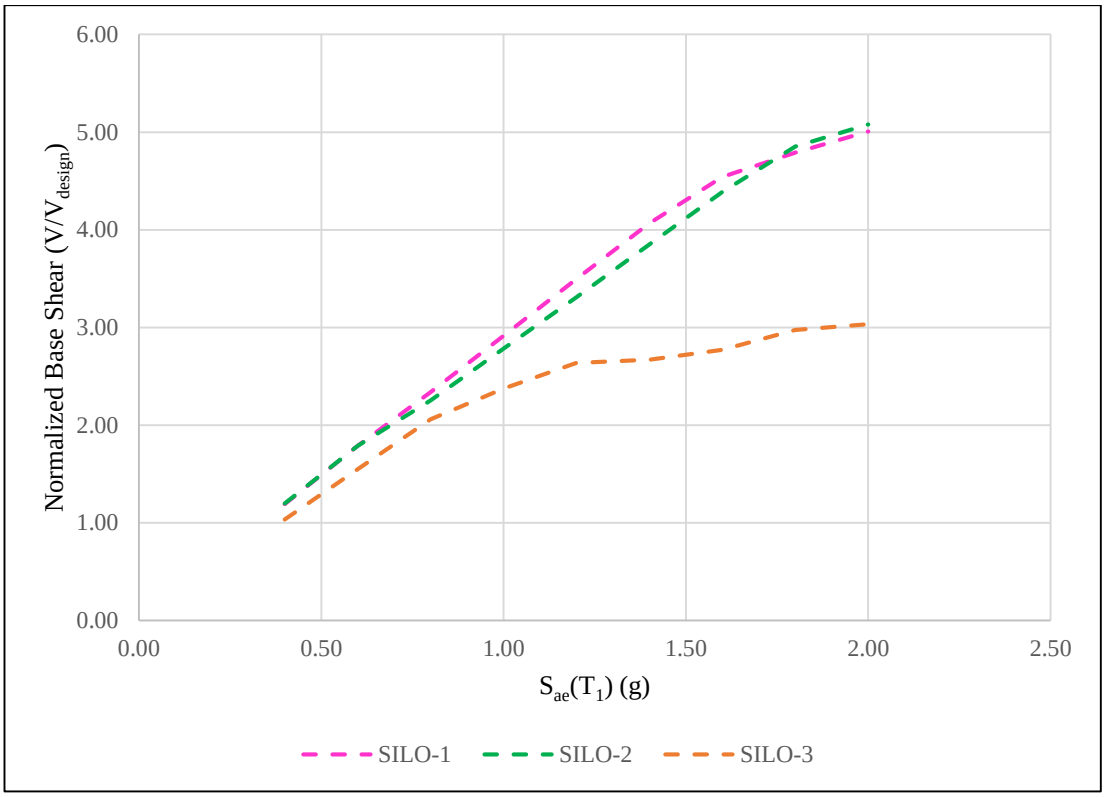

Figure 5.41: Normalized base shear forces in Bayraklı-3513 Earthquake.

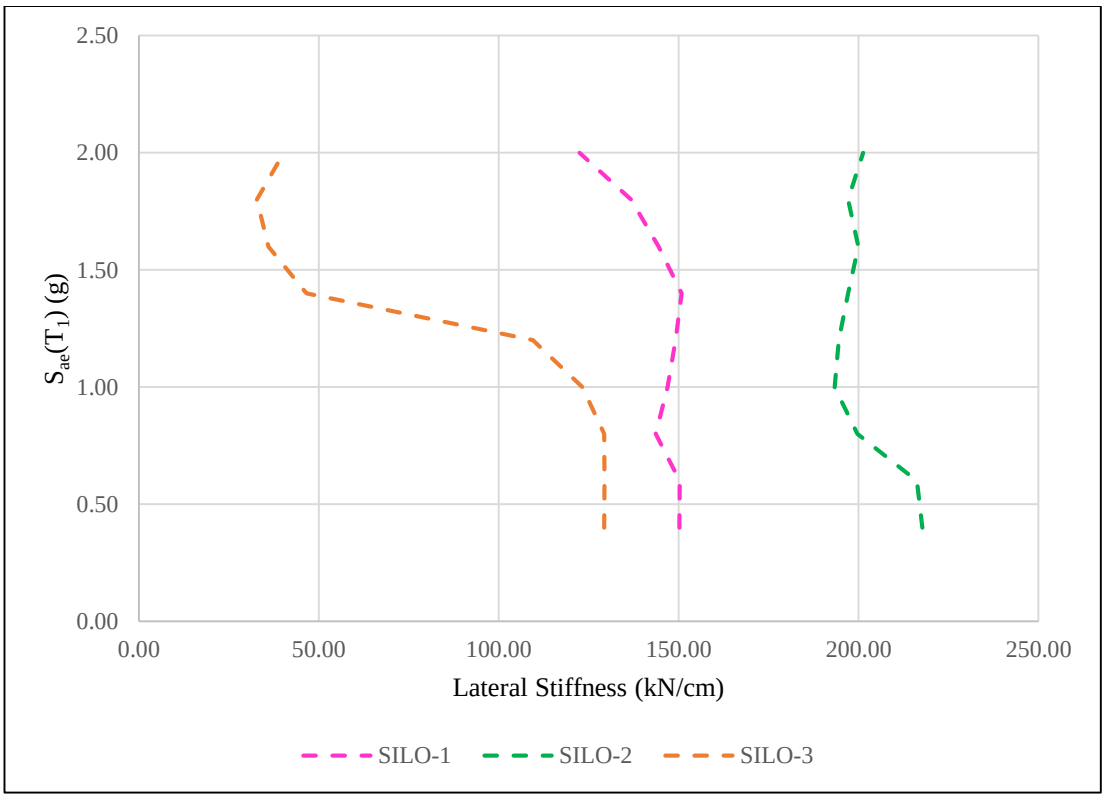

Figure 5.42: Lateral stiffness in Bayraklı-3513 Earthquake.

5.3.2. Hinge Results for Bornova-3522

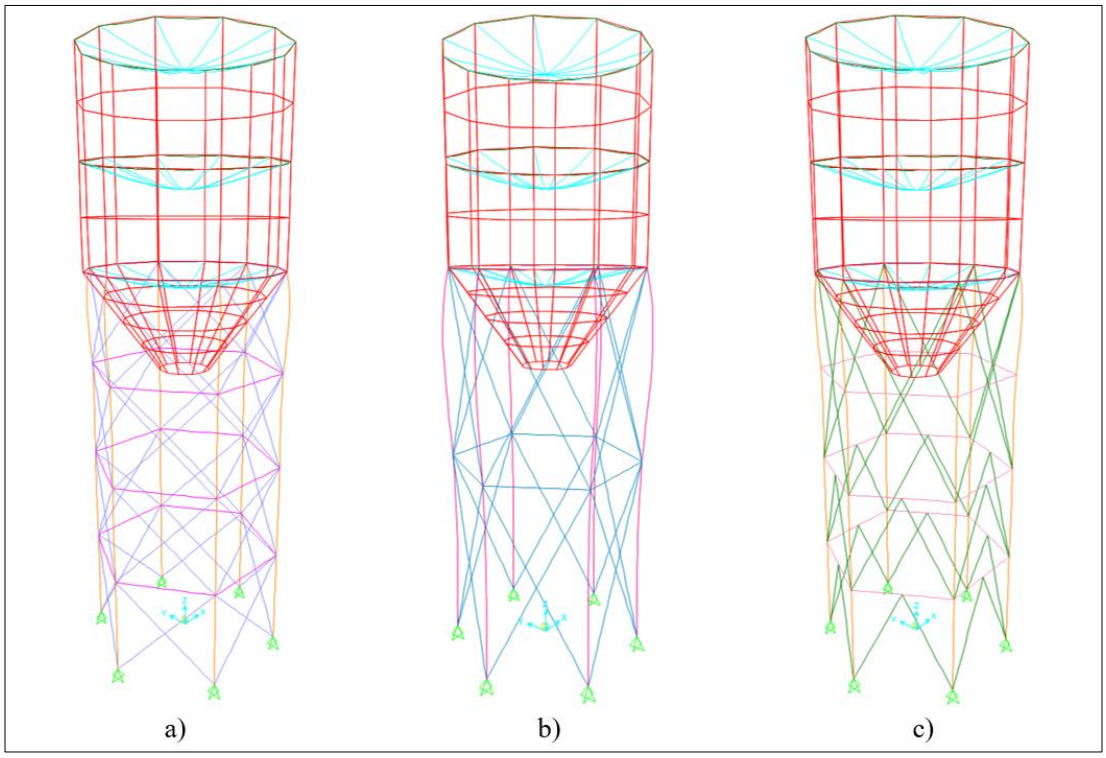

Figure 5.43: Deformed shapes of a) Silo-1, b) Silo-2, c) Silo-3 at 0.40 g (Bornova).

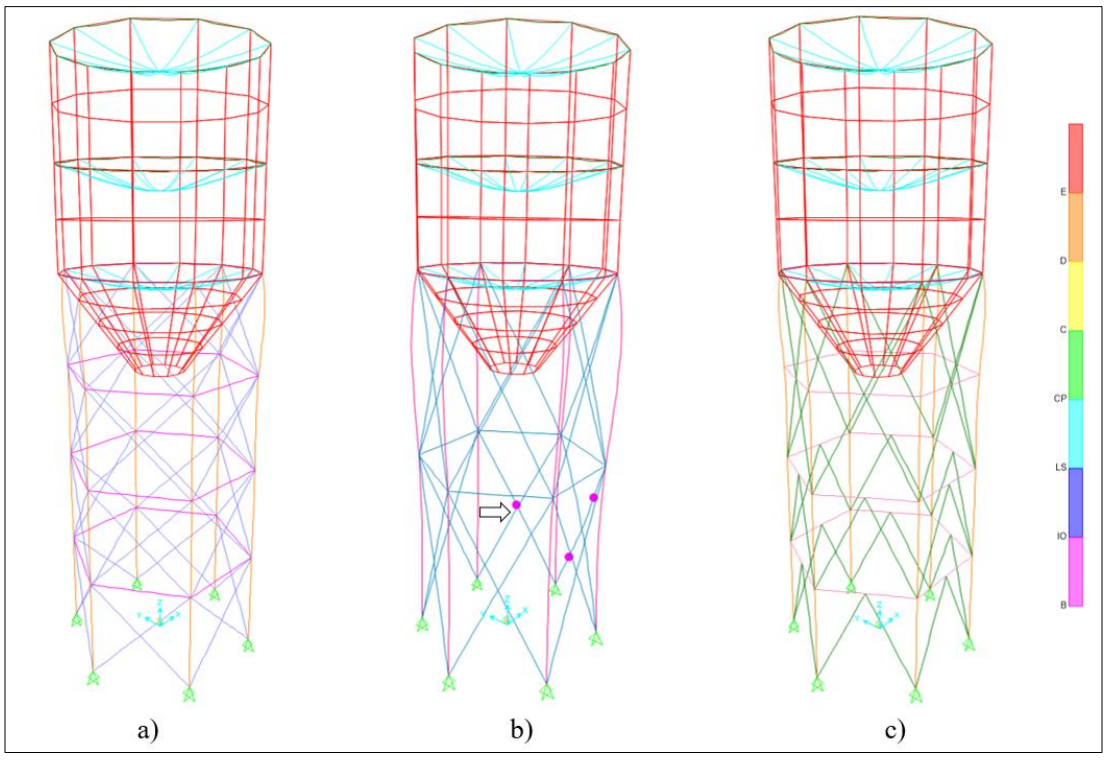

Figure 5.44: Deformed shapes of a) Silo-1, b) Silo-2, c) Silo-3 at 0.60 g (Bornova).

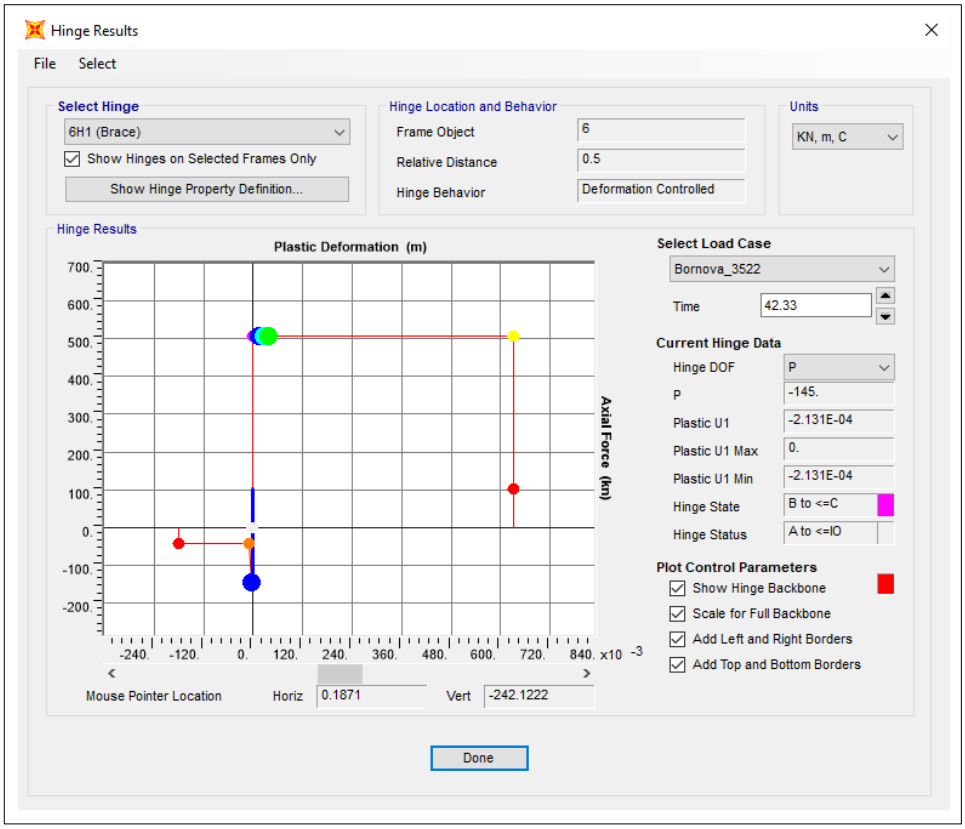

Figure 5.45: Hinge results of Silo-2 at 0.60 g (Bornova).

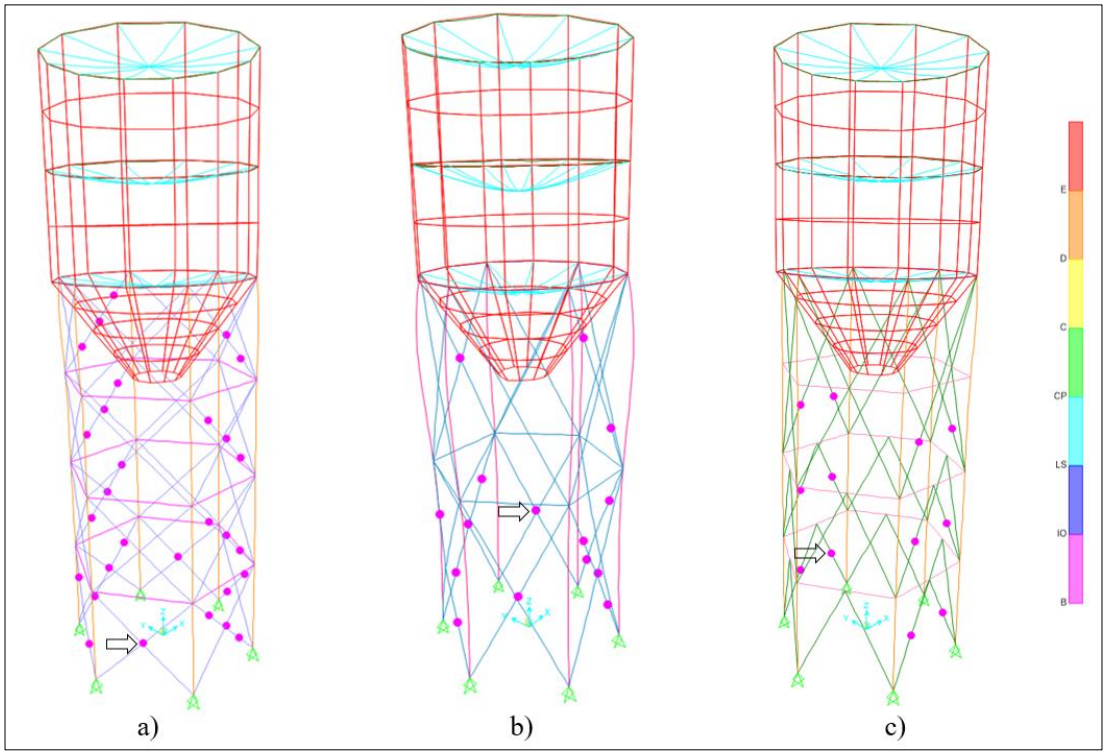

Figure 5.46: Deformed shapes of a) Silo-1, b) Silo-2, c) Silo-3 at 0.80 g (Bornova).

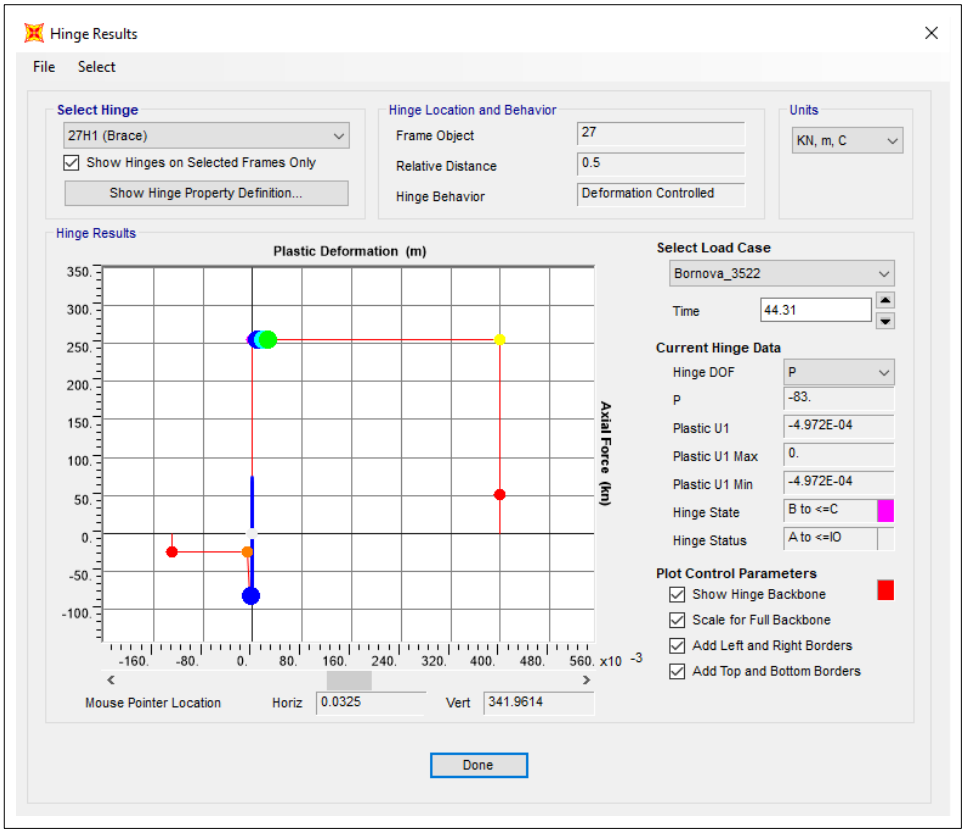

Figure 5.47: Hinge result of Silo-1 at 0.80 g (Bornova).

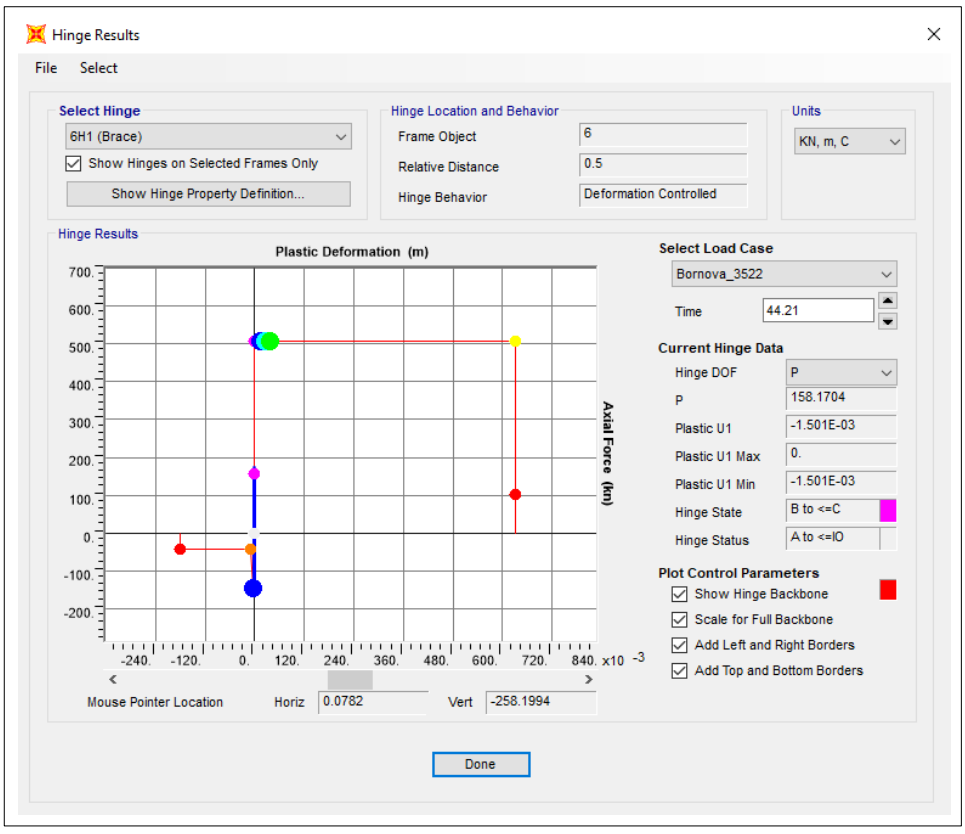

Figure 5.48: Hinge results of Silo-2 at 0.80 g (Bornova).

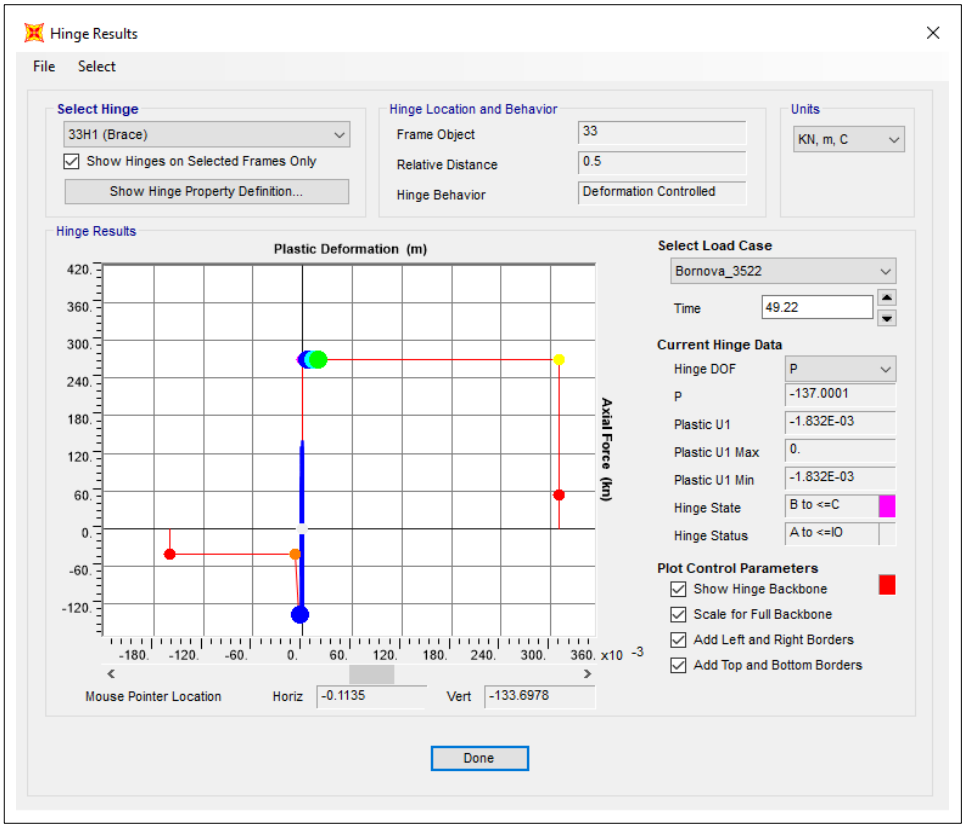

Figure 5.49: Hinge results of Silo-3 at 0.80 g (Bornova).

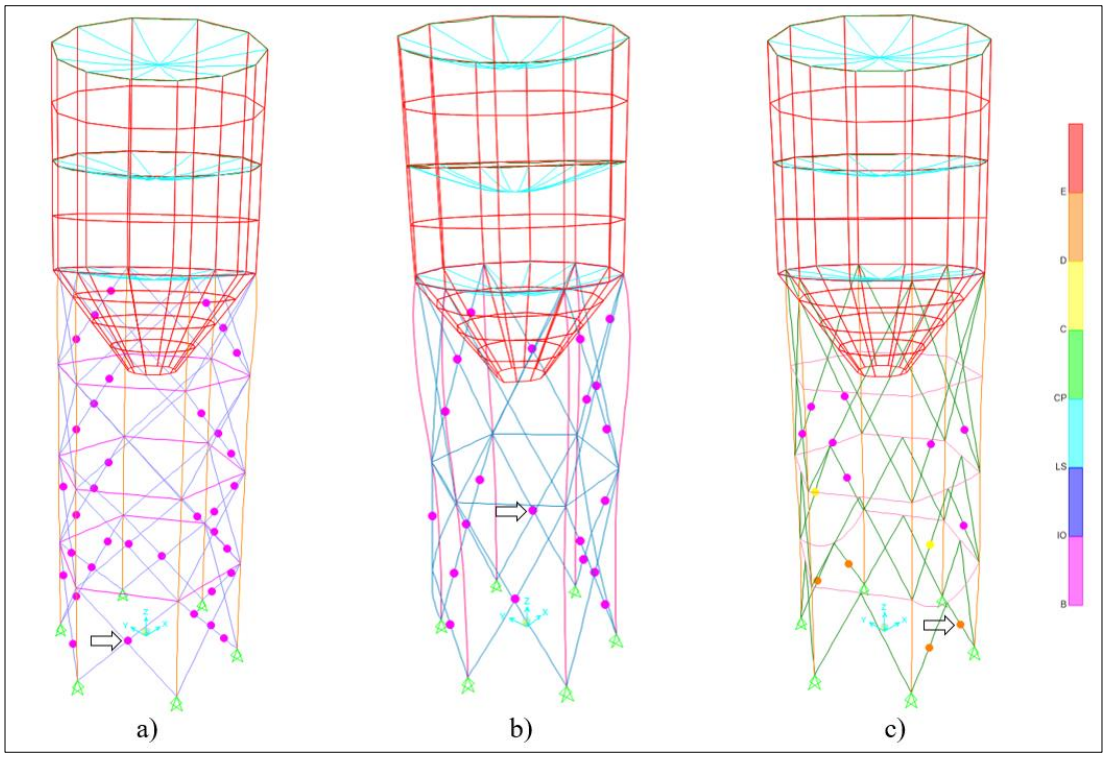

Figure 5.50: Deformed shapes of a) Silo-1, b) Silo-2, c) Silo-3 at 1.00 g (Bornova).

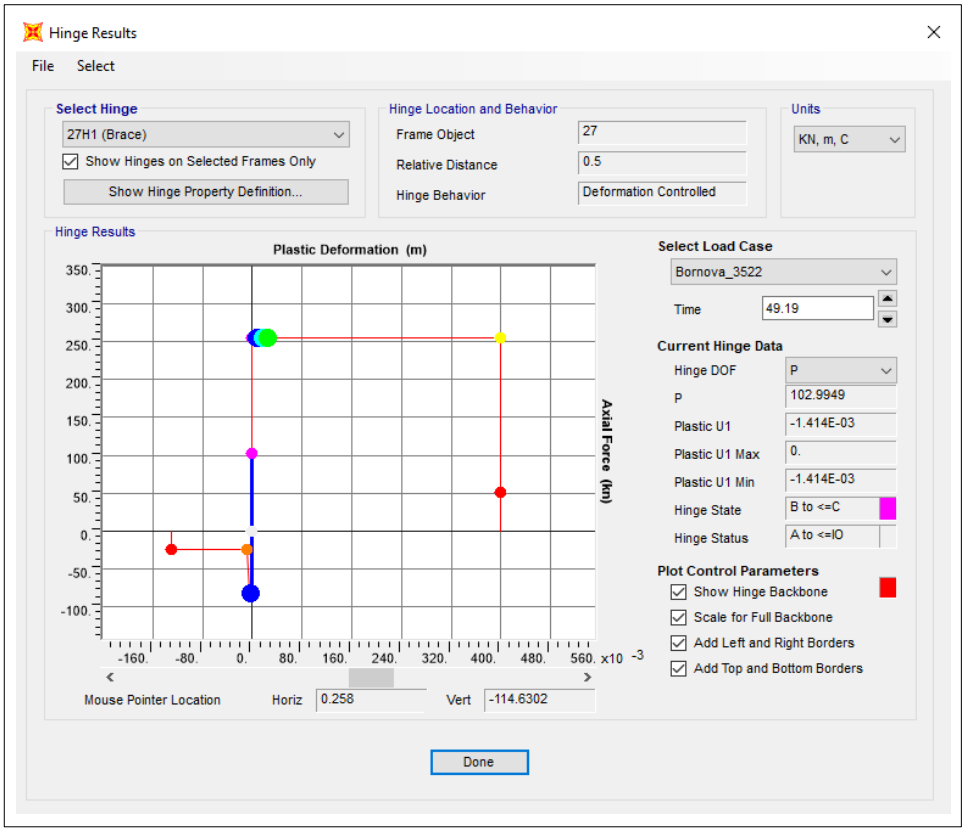

Figure 5.51: Hinge results of Silo-1 at 1.00 g (Bornova).

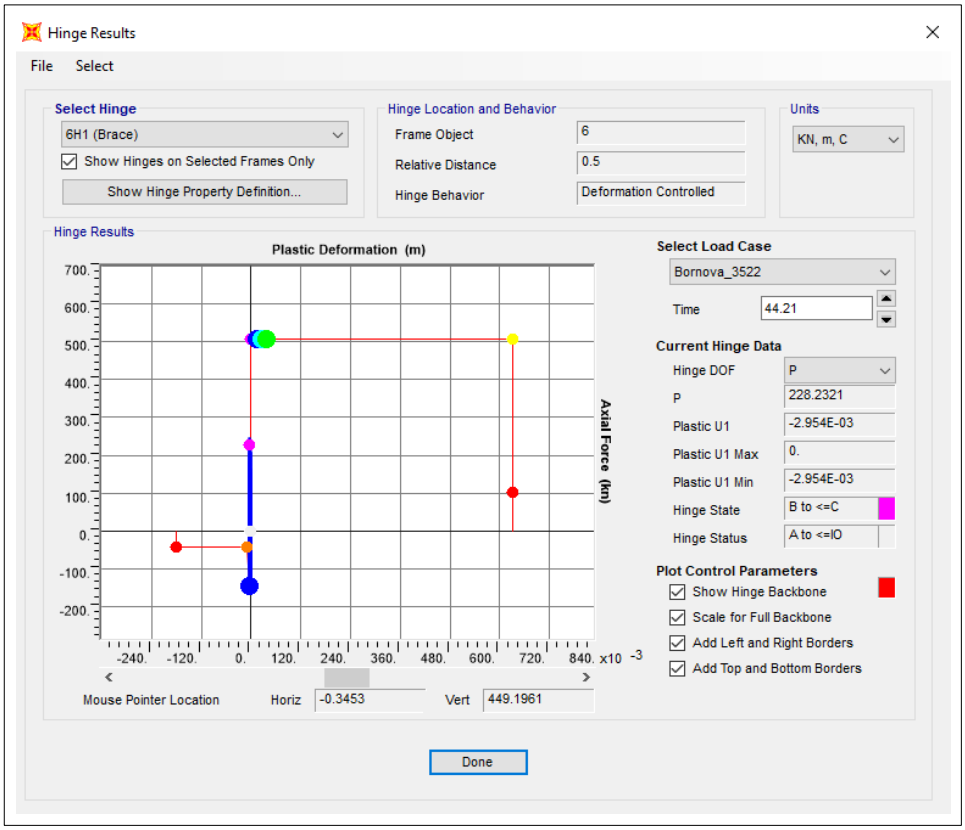

Figure 5.52: Hinge results of Silo-2 at 1.00 g (Bornova).

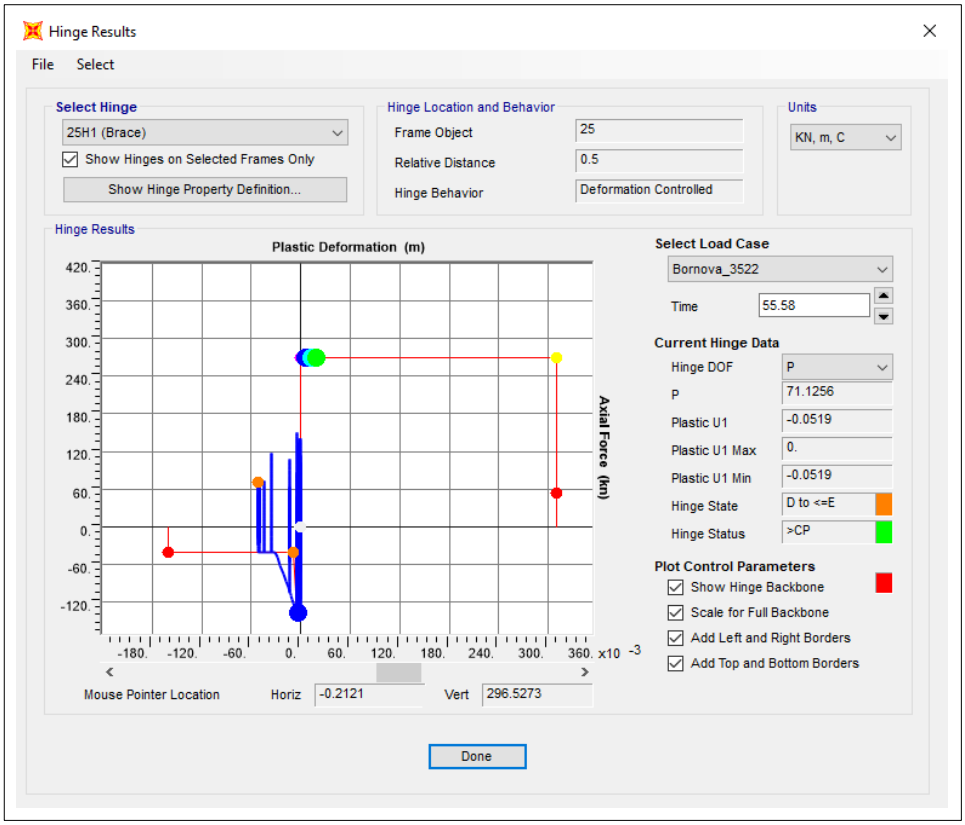

Figure 5.53: Hinge results of Silo-3 at 1.00 g (Bornova).

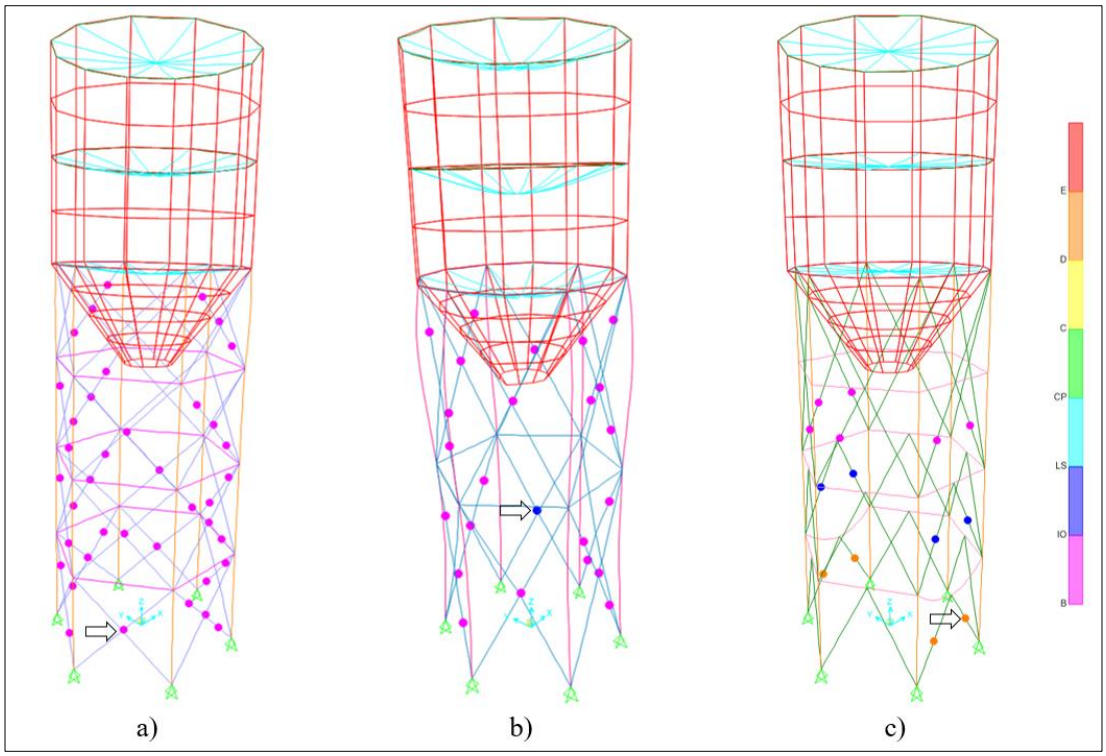

Figure 5.54: Deformed shapes of a) Silo-1, b) Silo-2, c) Silo-3 at 1.20 g (Bornova).

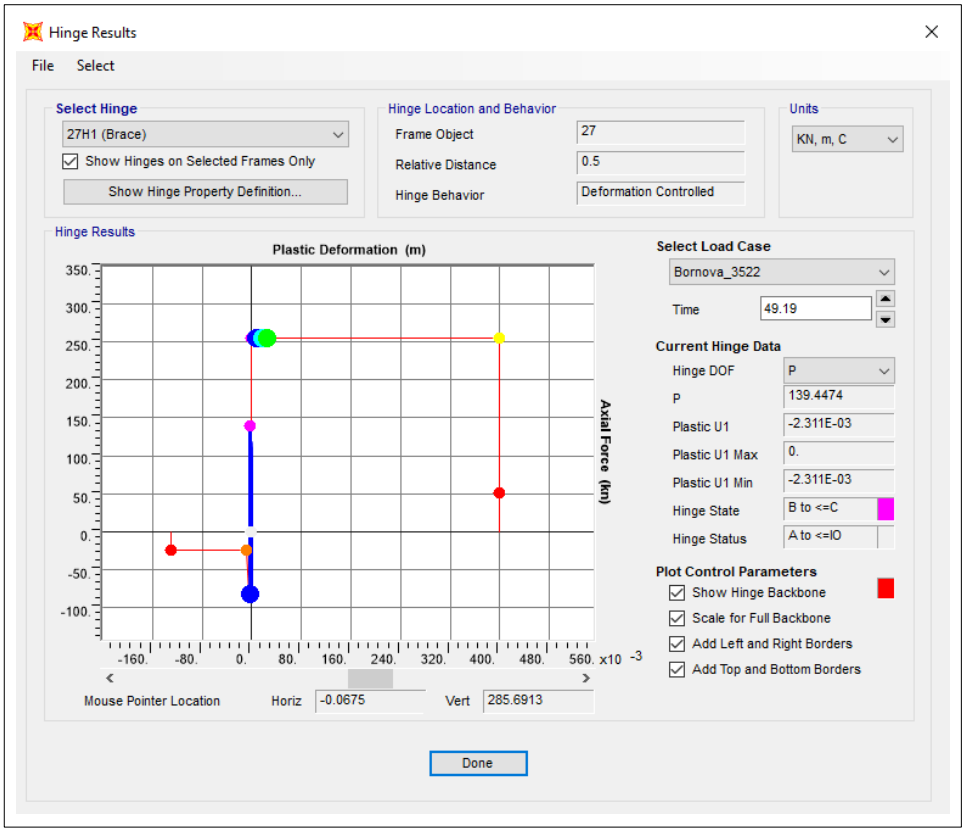

Figure 5.55: Hinge results of Silo-1 at 1.20 g (Bornova).

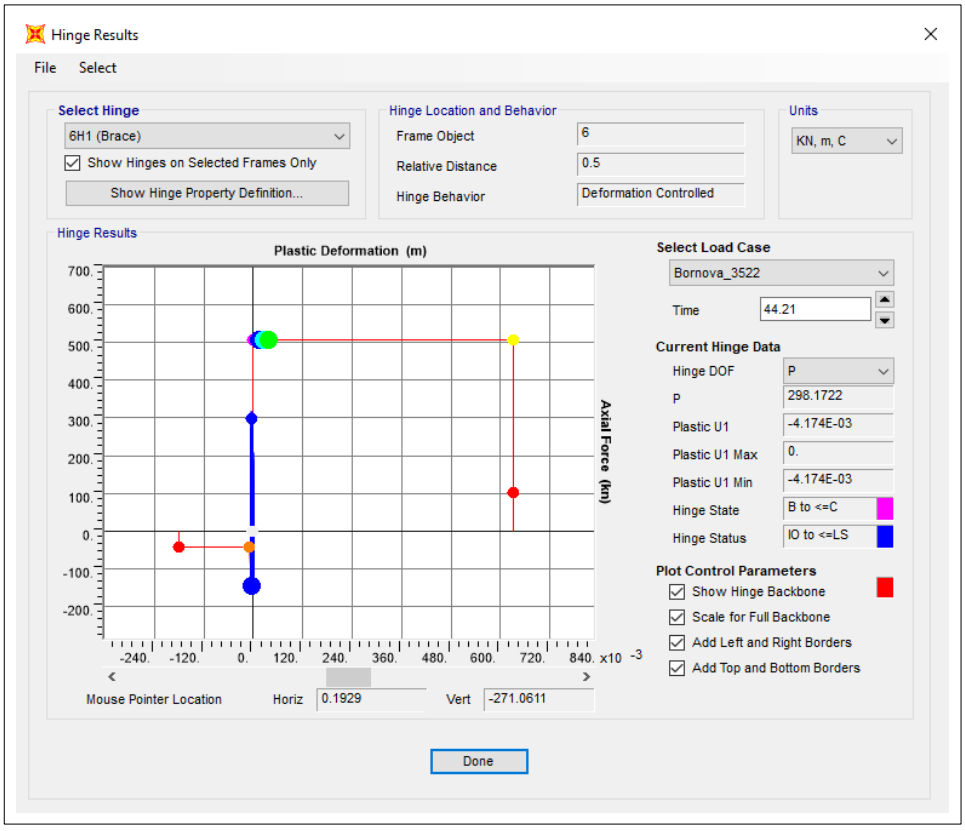

Figure 5.56: Hinge results of Silo-2 at 1.20 g (Bornova).

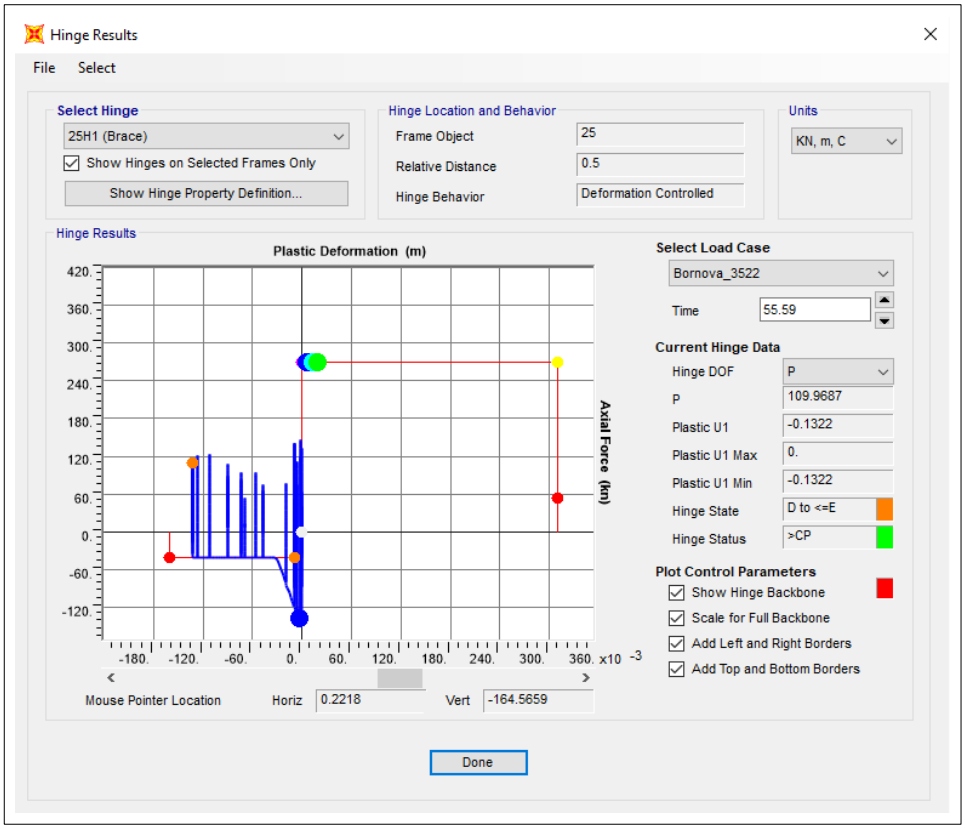

Figure 5.57: Hinge results of Silo-3 at 1.20 g (Bornova).

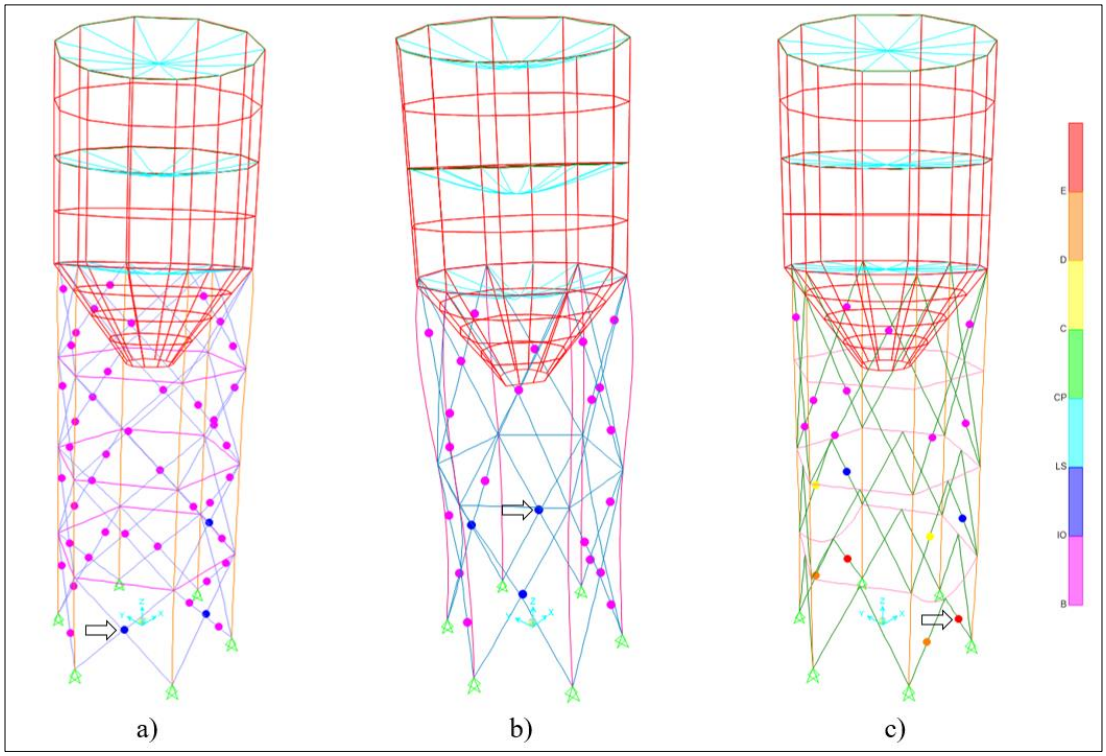

Figure 5.58: Deformed shapes of a) Silo-1, b) Silo-2, c) Silo-3 at 1.40 g (Bornova).

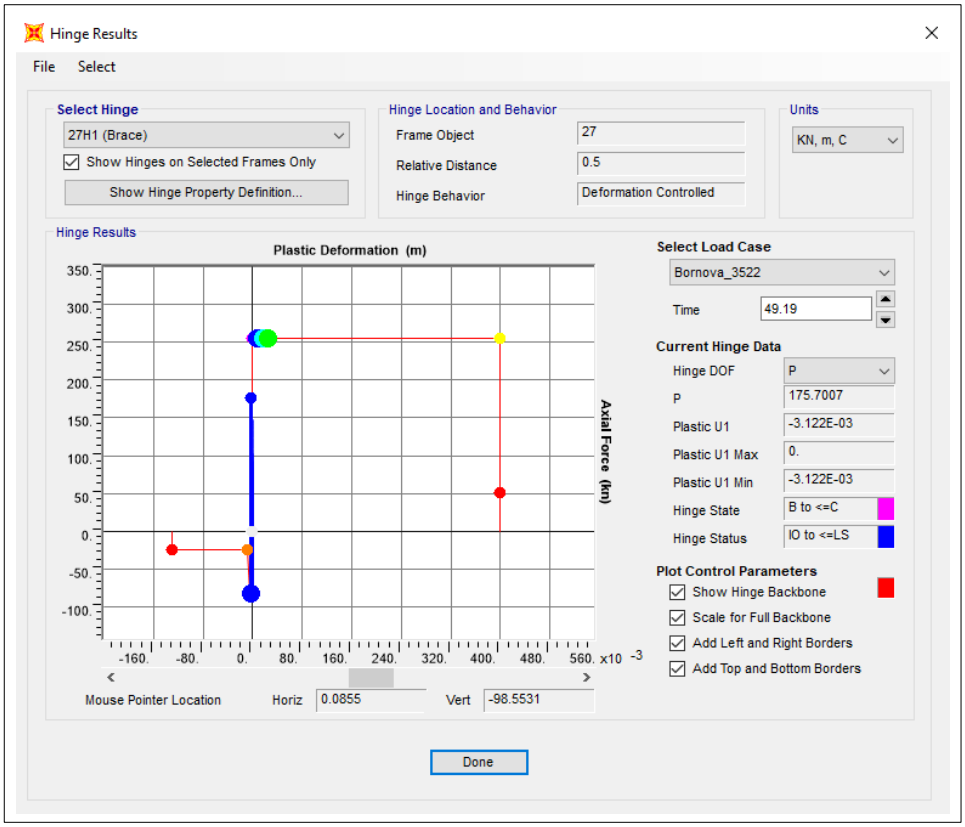

Figure 5.59: Hinge results of Silo-1 at 1.40 g (Bornova).

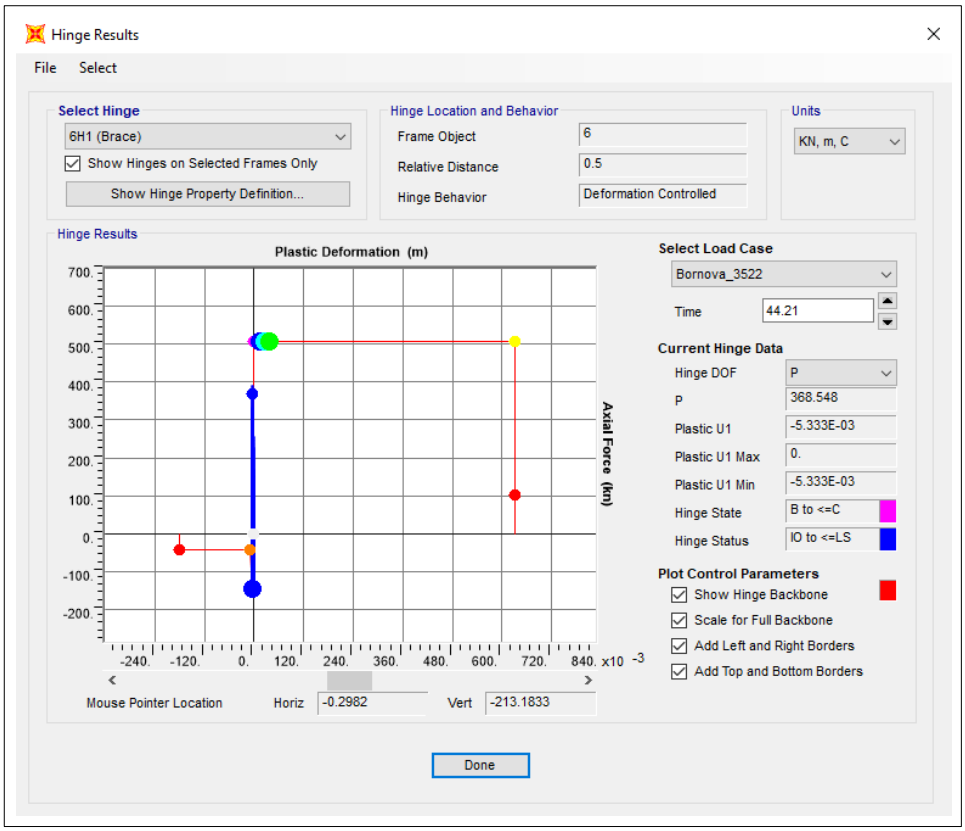

Figure 5.60: Hinge results of Silo-2 at 1.40 g (Bornova).

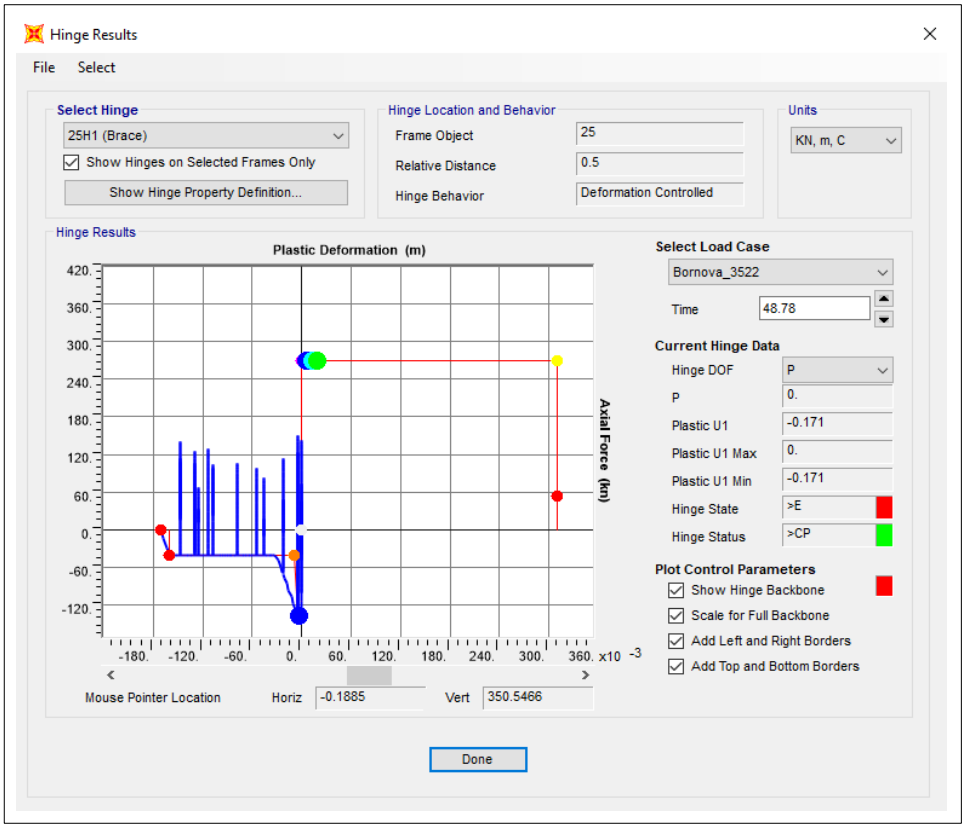

Figure 5.61: Hinge results of Silo-3 at 1.40 g (Bornova).

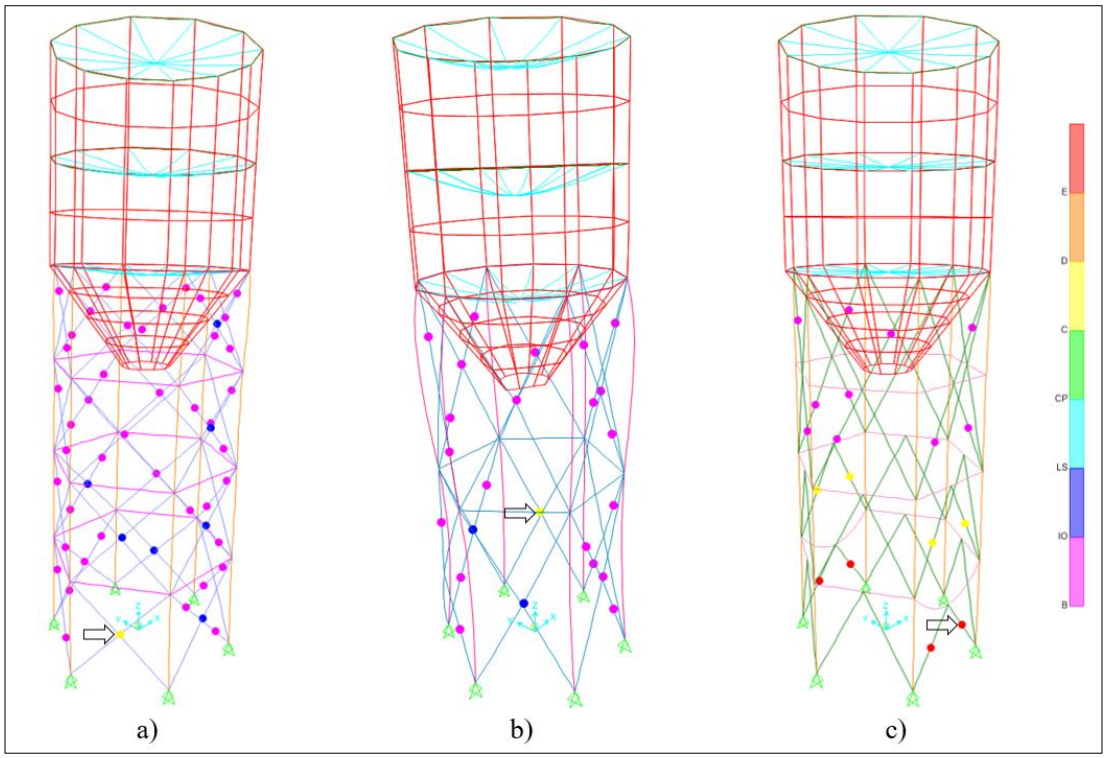

Figure 5.62: Deformed shapes of a) Silo-1, b) Silo-2, c) Silo-3 at 1.60 g (Bornova).

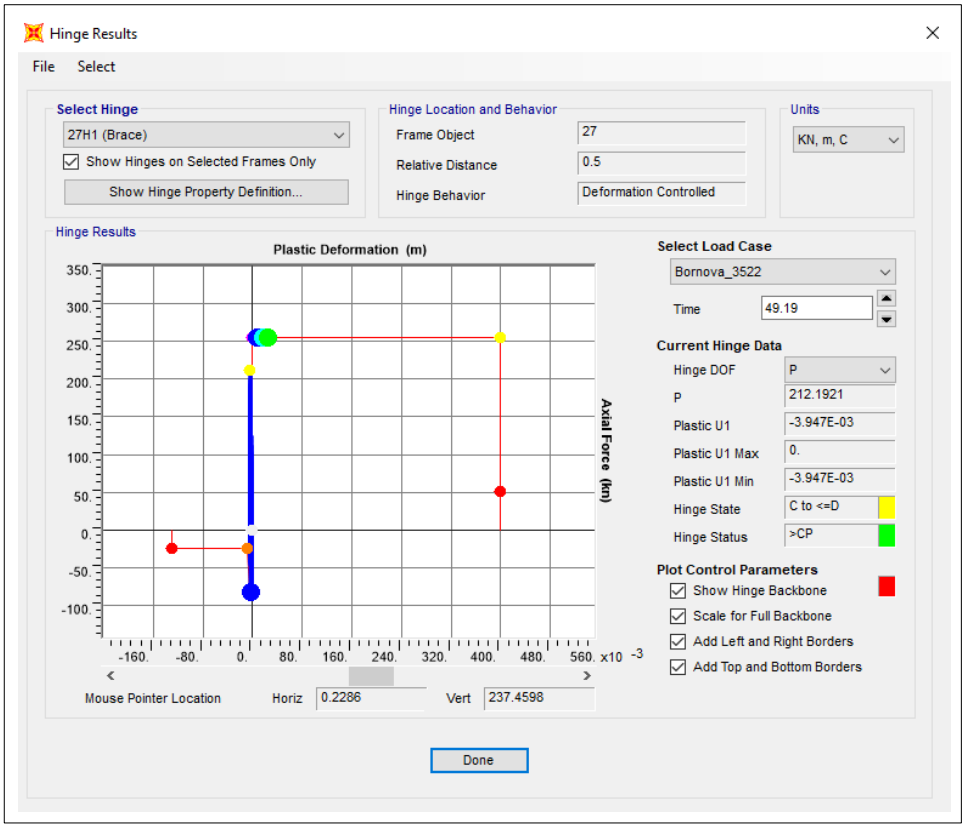

Figure 5.63: Hinge results of Silo-1 at 1.60 g (Bornova).

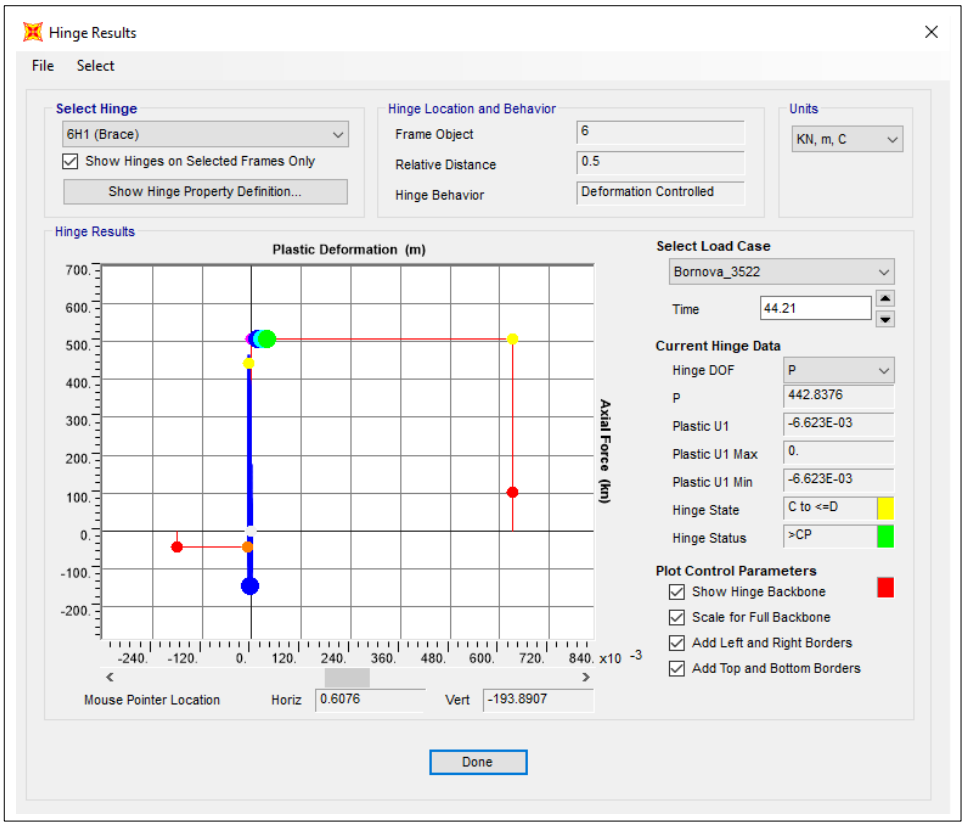

Figure 5.64: Hinge results of Silo-2 at 1.60 g (Bornova).

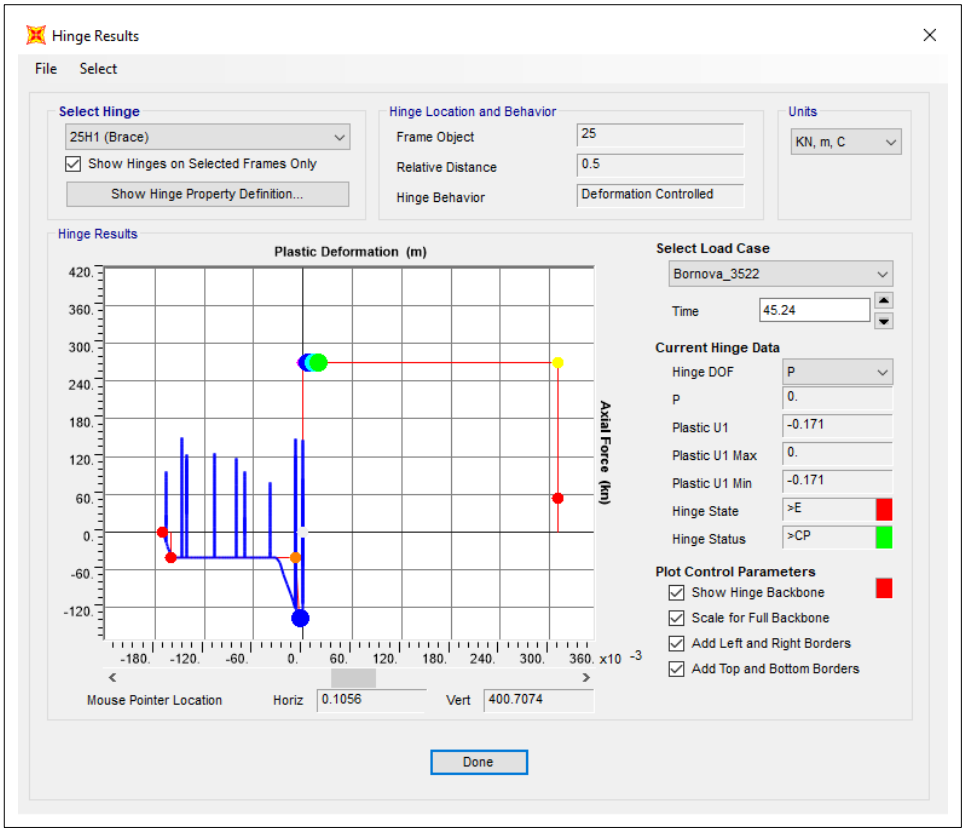

Figure 5.65: Hinge results of Silo-3 at 1.60 g (Bornova).

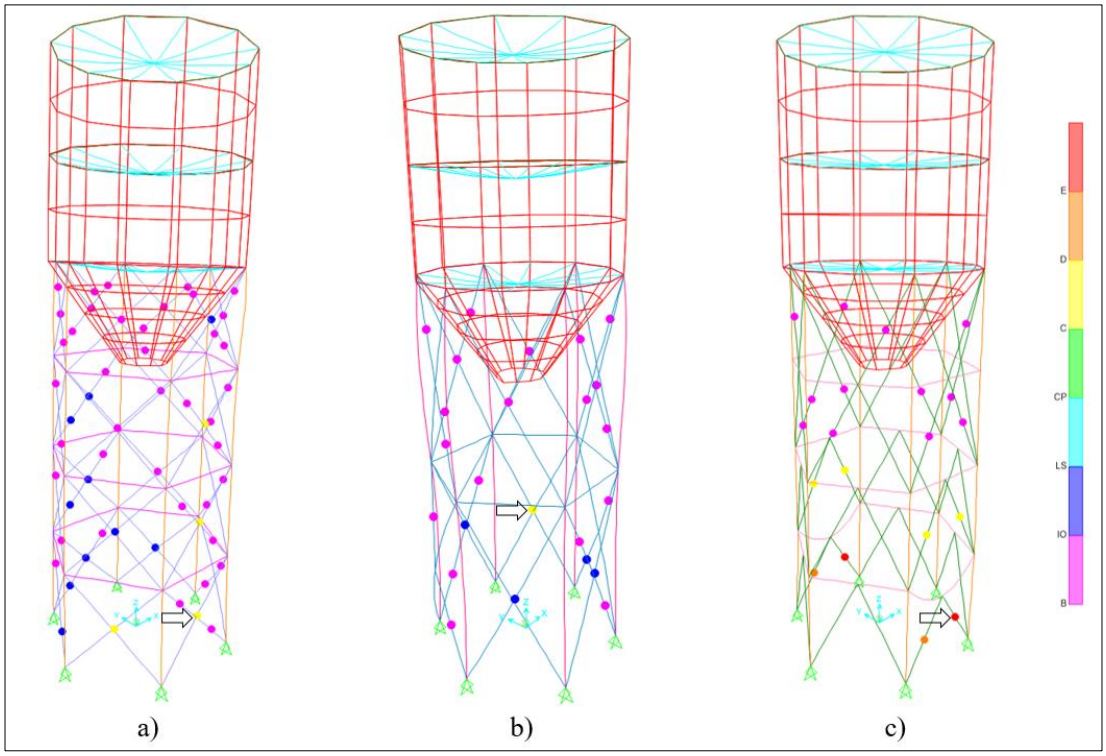

Figure 5.66: Deformed shapes of a) Silo-1, b) Silo-2, c) Silo-3 at 1.80 g (Bornova).

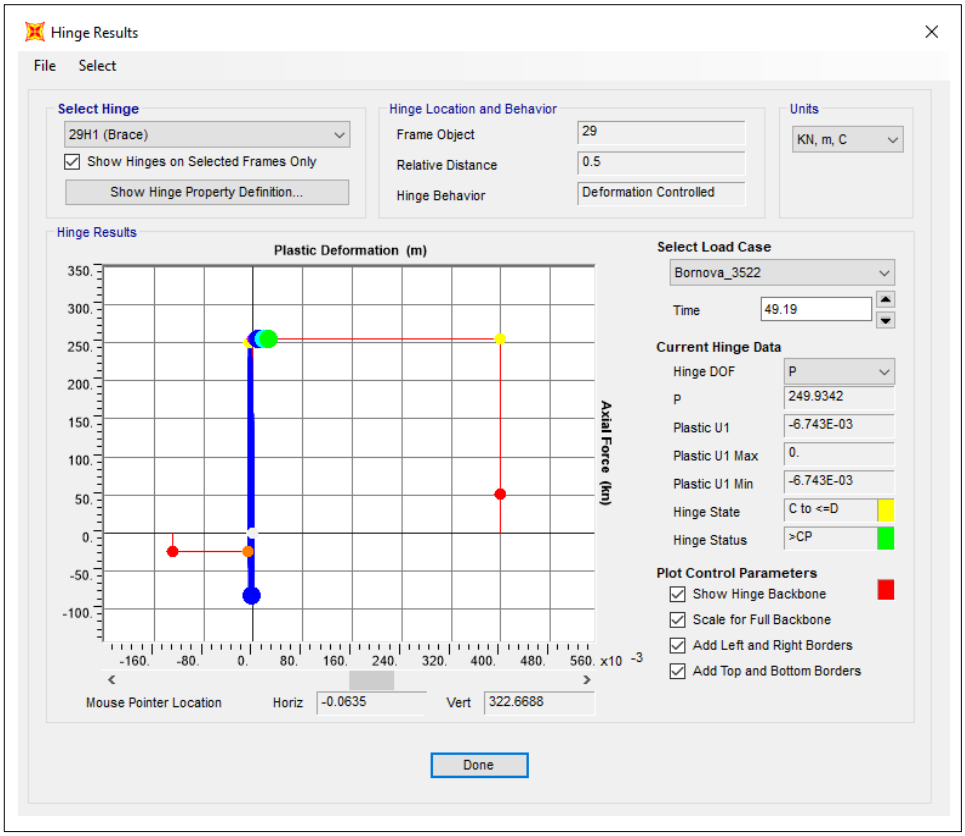

Figure 5.67: Hinge results of Silo-1 at 1.80 g (Bornova).

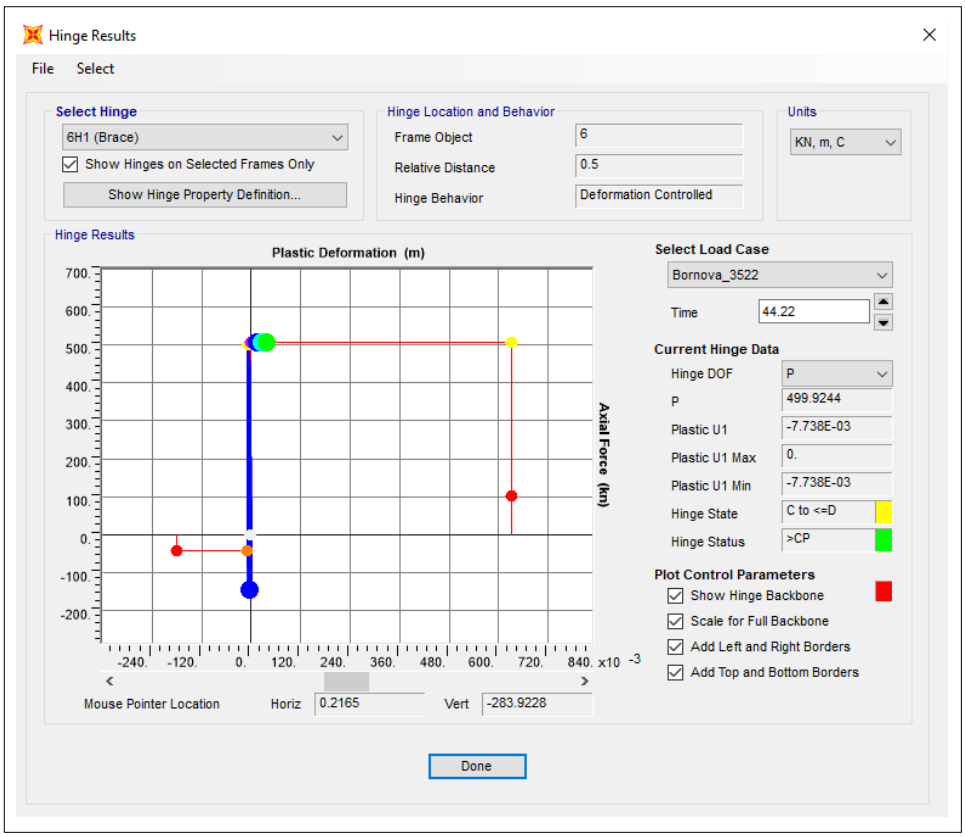

Figure 5.68: Hinge results of Silo-2 at 1.80 g (Bornova).

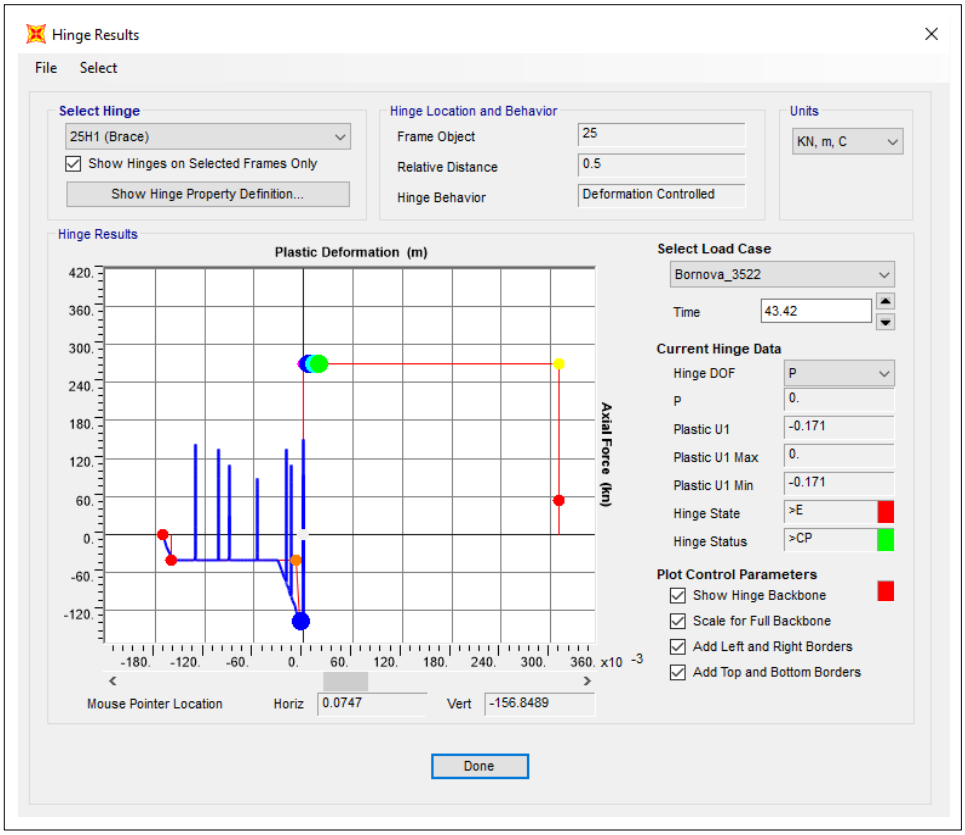

Figure 5.69: Hinge results of Silo-3 at 1.80 g (Bornova).

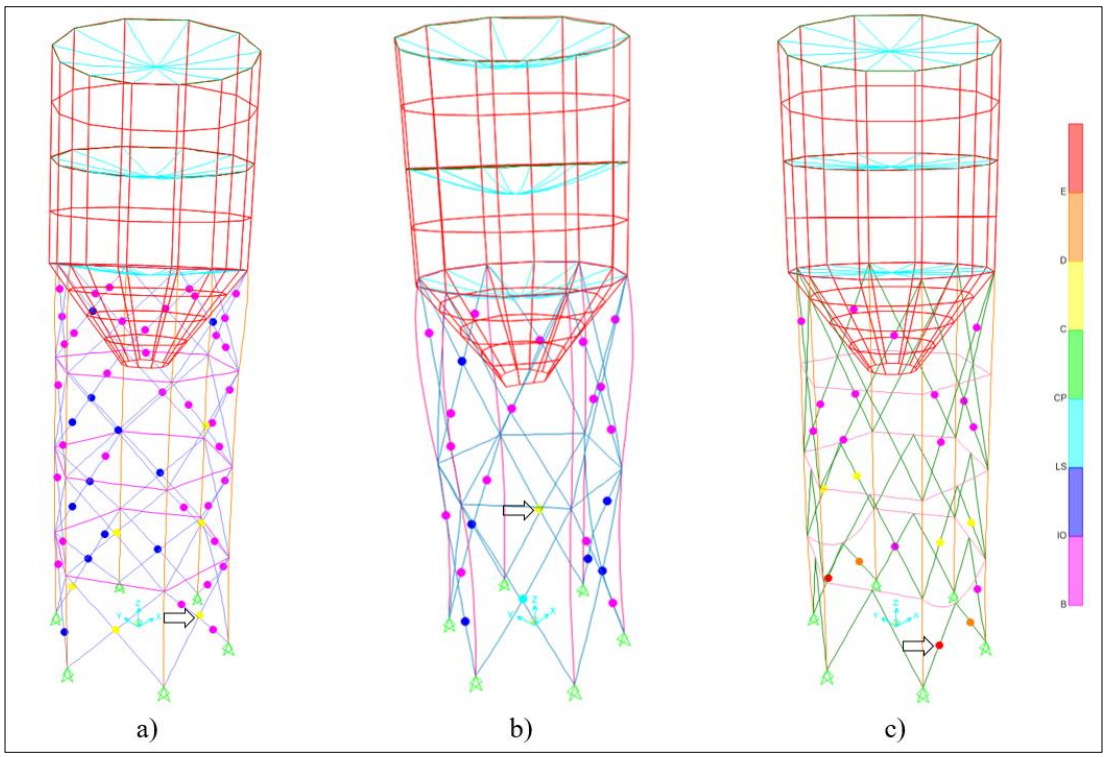

Figure 5.70: Deformed shapes of a) Silo-1, b) Silo-2, c) Silo-3 at 2.00 g (Bornova).

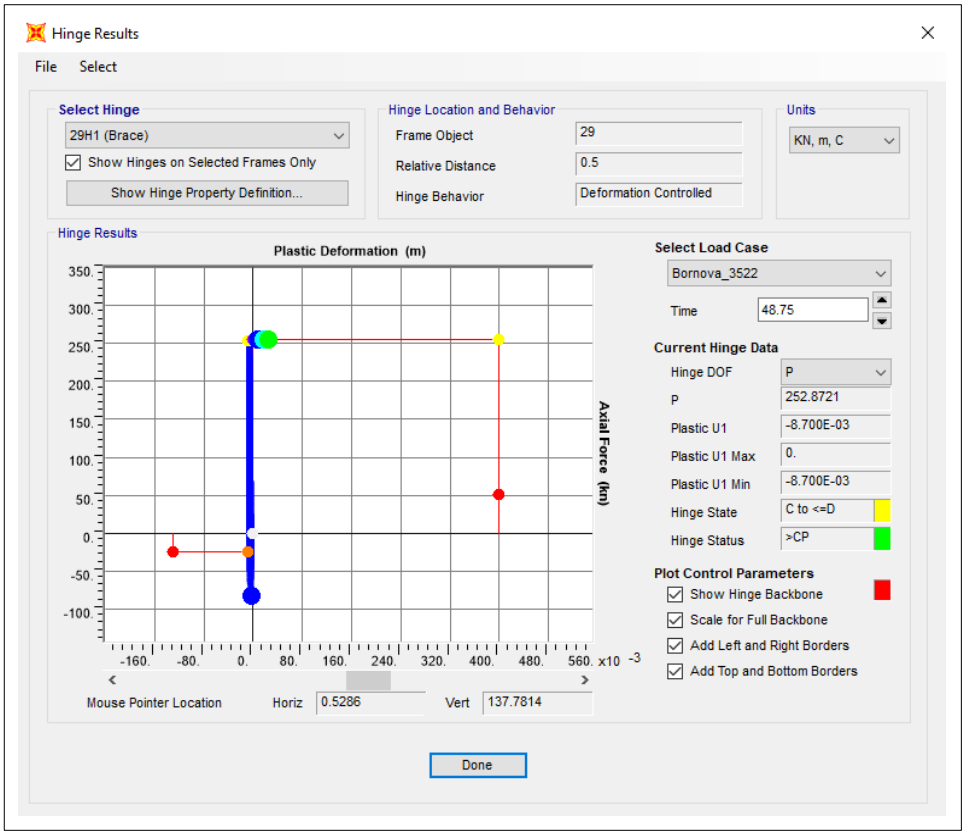

Figure 5.71: Hinge results of Silo-1 at 2.00 g (Bornova).

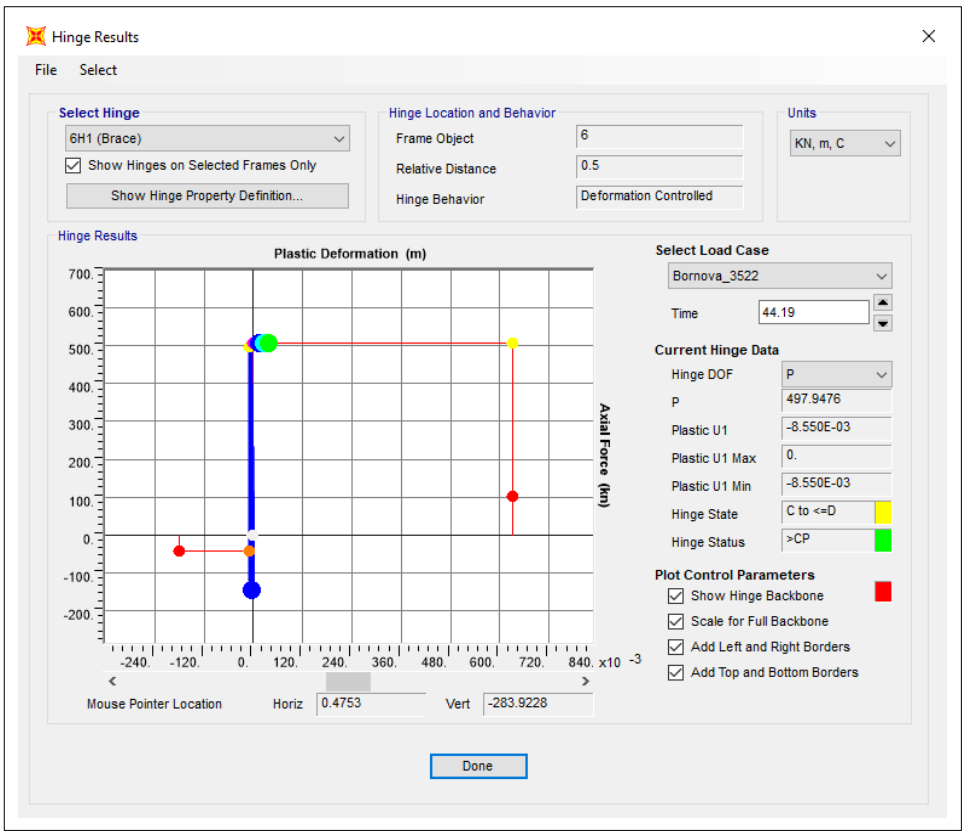

Figure 5. 72: Hinge results of Silo-2 at 2.00 g (Bornova).

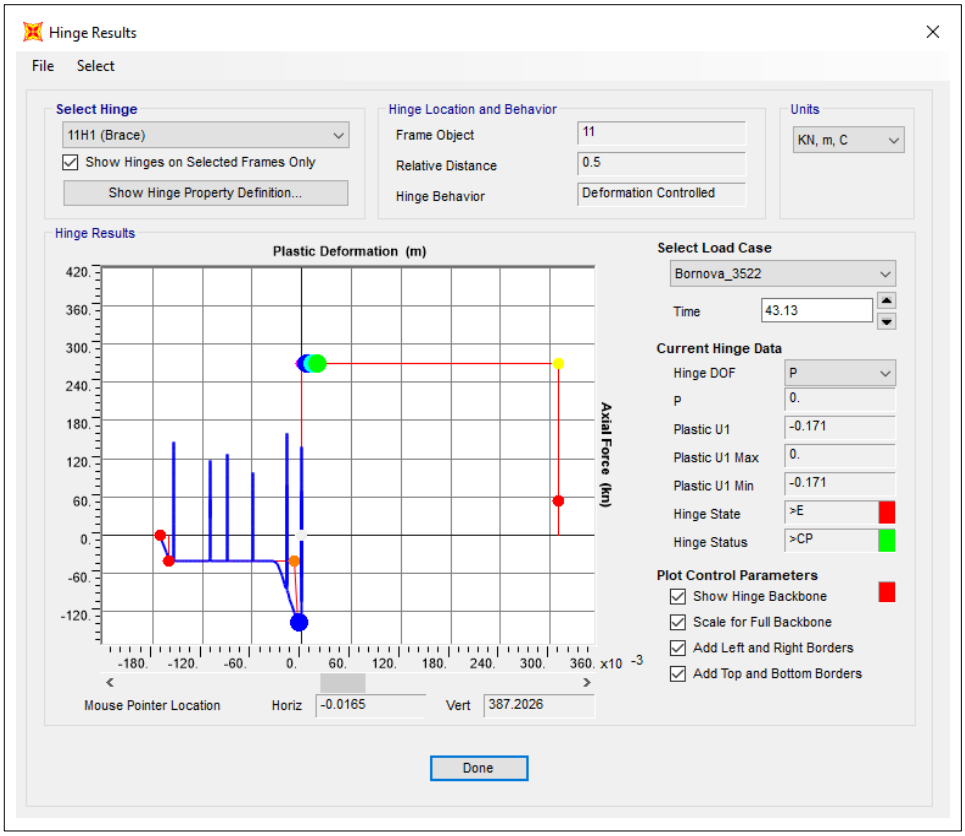

Figure 5.73: Hinge results of Silo-3 at 2.00 g (Bornova).

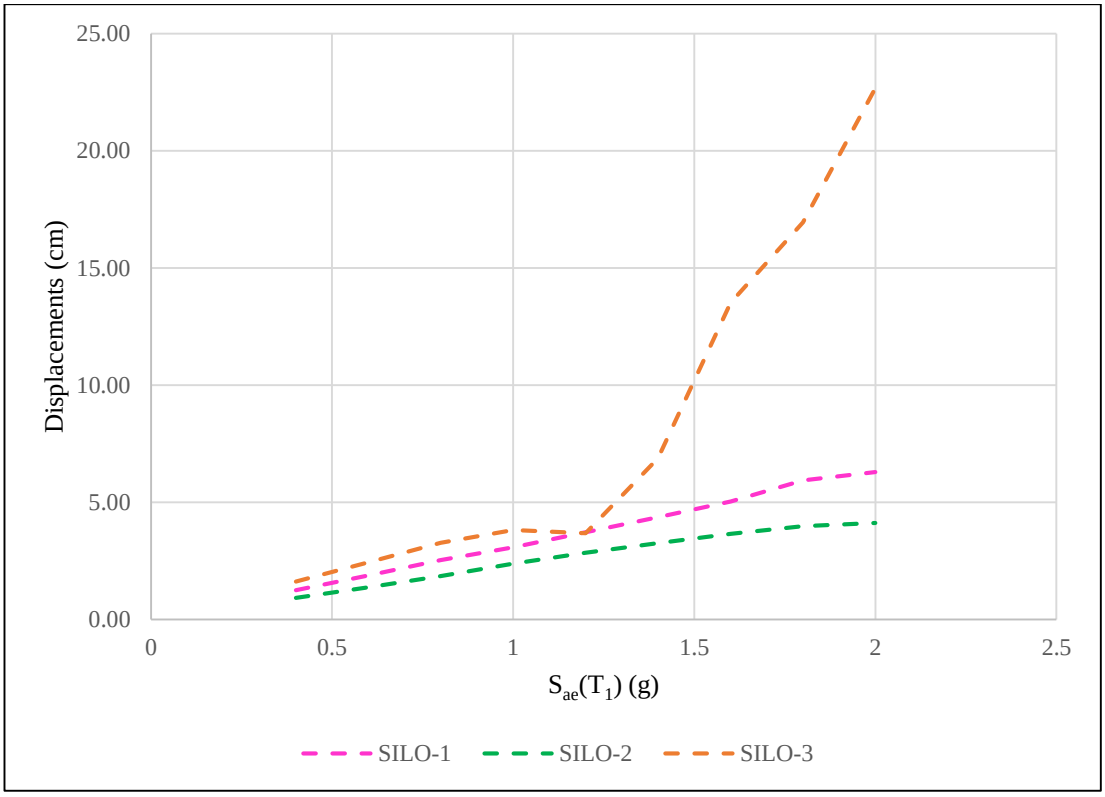

Figure 5.74: Top displacements in Bornova-3522 Earthquake.

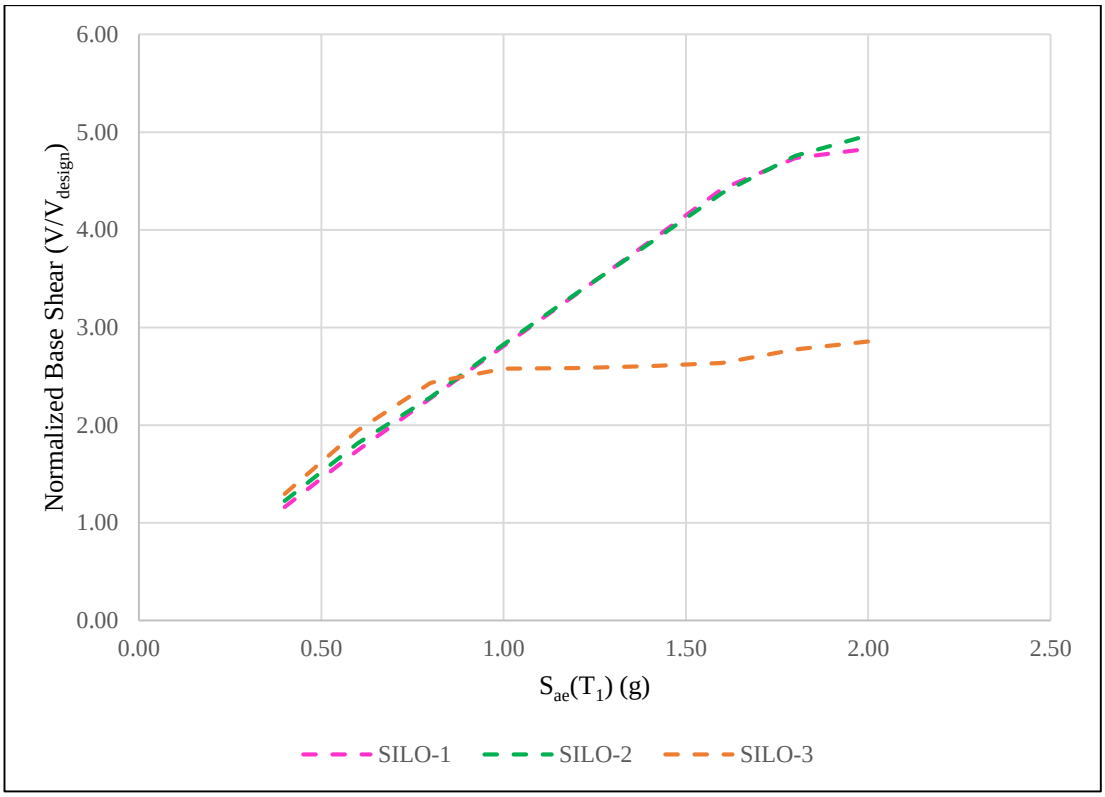

Figure 5.75: Normalized base shear forces in Bornova-3522 Earthquake.

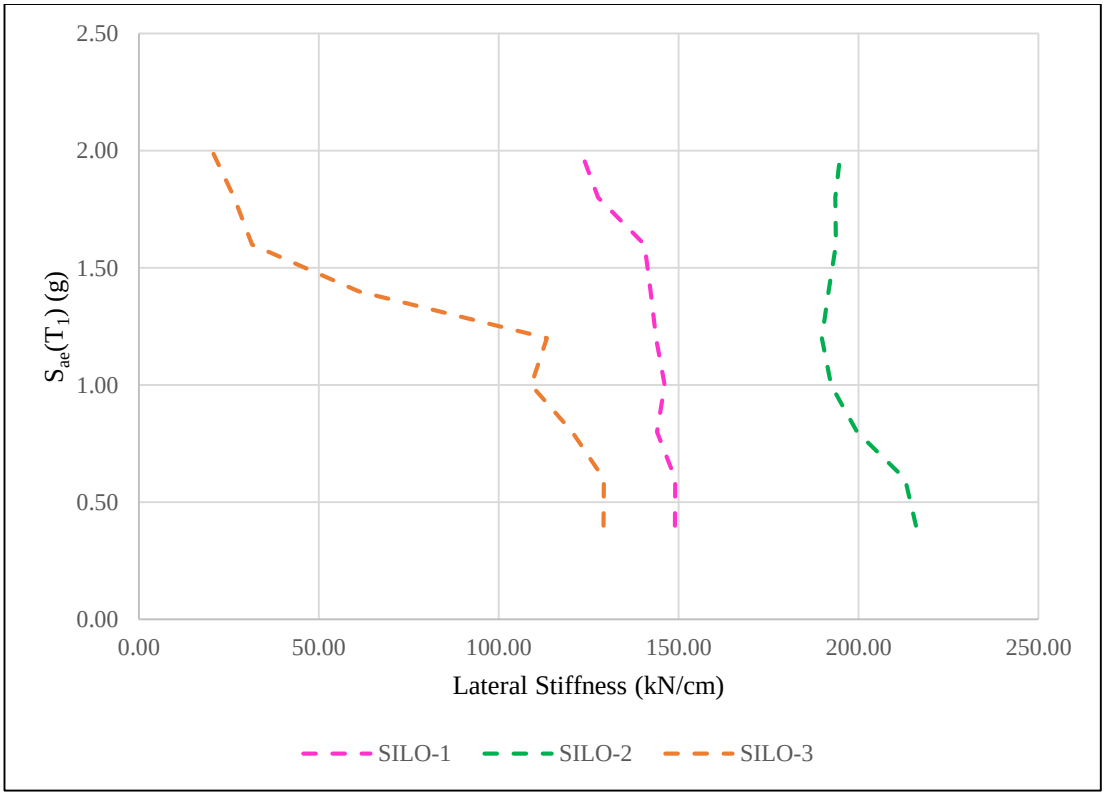

Figure 5.76: Lateral stiffness in Bornova-3522 Earthquake.

5.3.3. Hinge Results for Iwate-5774

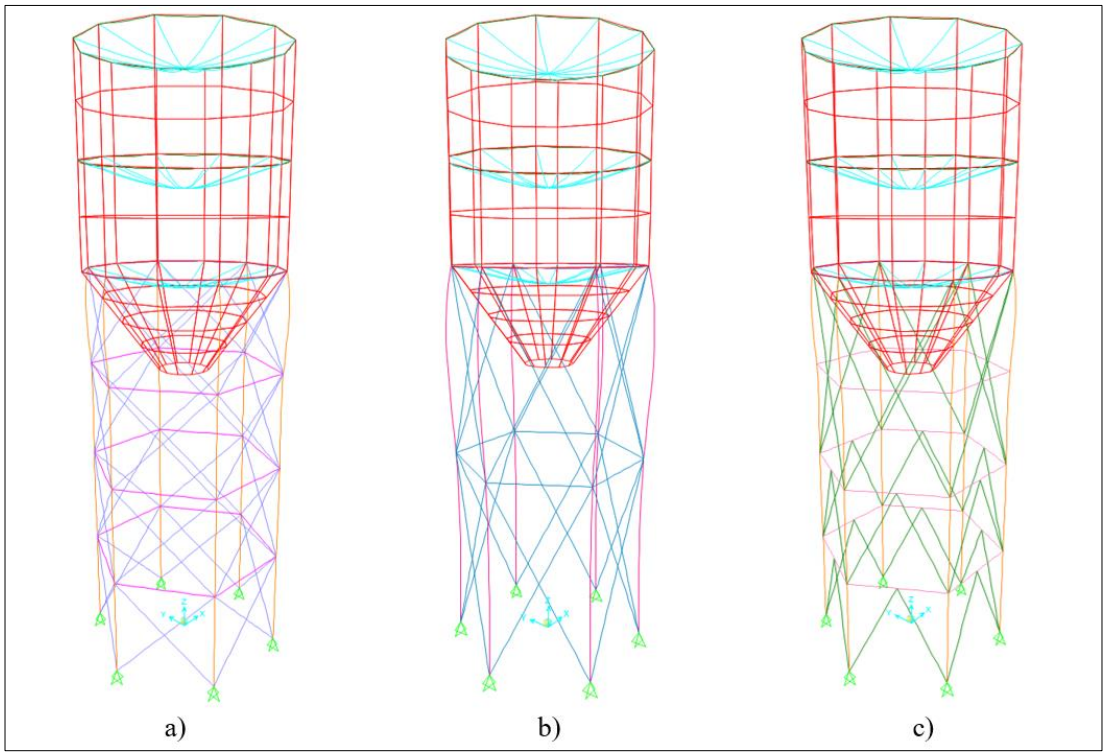

Figure 5.77: Deformed shapes of a) Silo-1, b) Silo-2, c) Silo-3 at 0.40 g (Iwate).

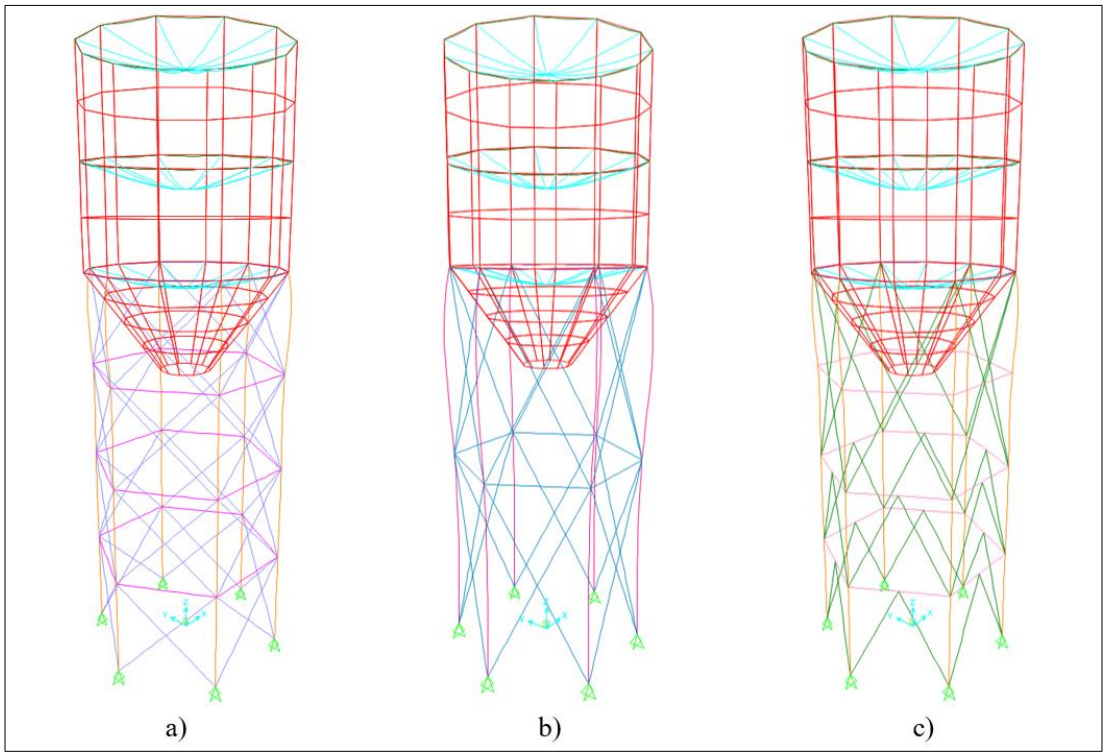

Figure 5.78: Deformed shapes of a) Silo-1, b) Silo-2, c) Silo-3 at 0.60 g (Iwate).

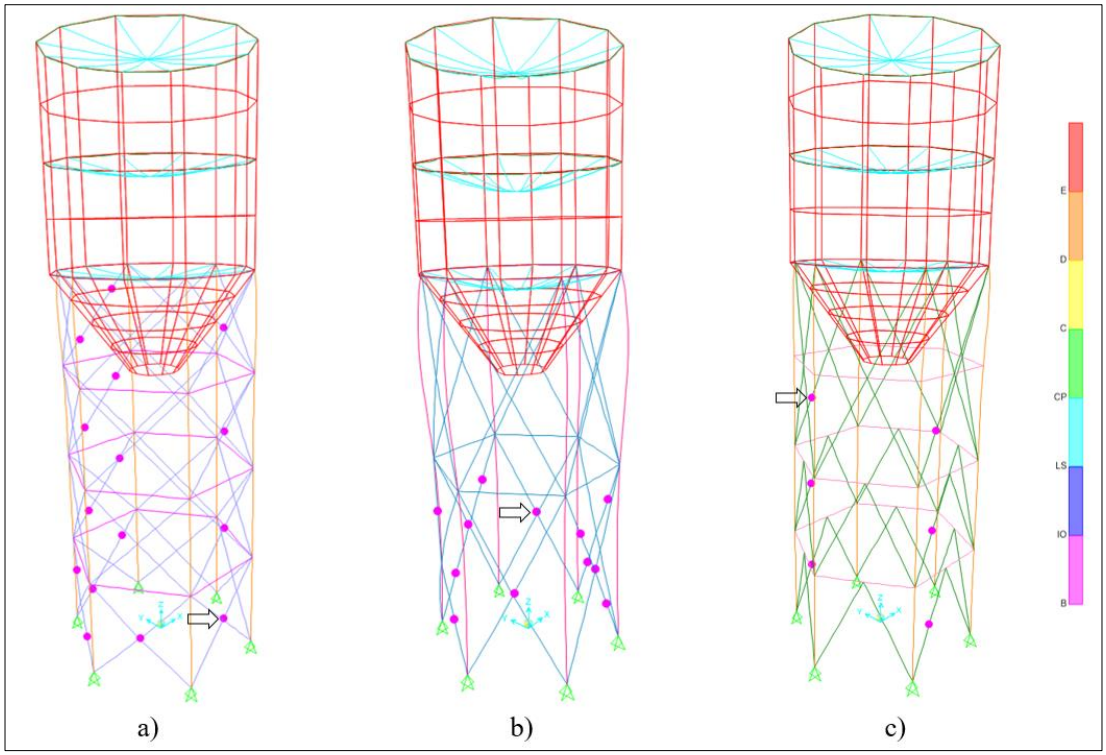

Figure 5.79: Deformed shapes of a) Silo-1, b) Silo-2, c) Silo-3 at 0.80 g (Iwate).

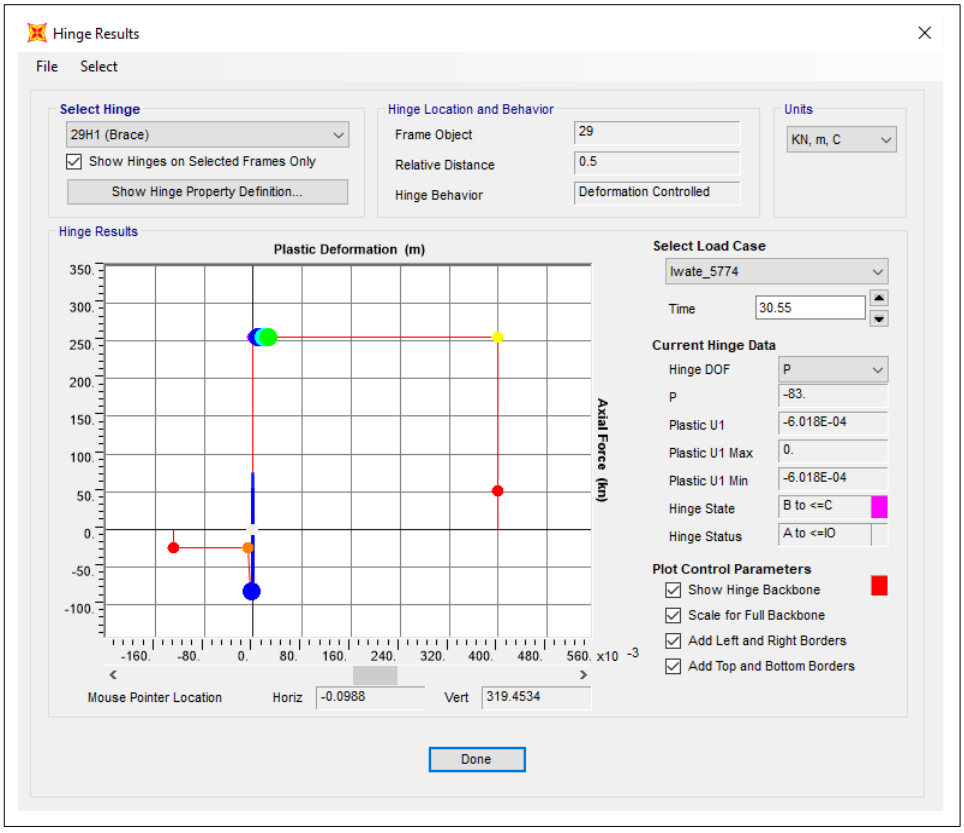

Figure 5.80: Hinge results of Silo-1 at 0.80 g (Iwate).

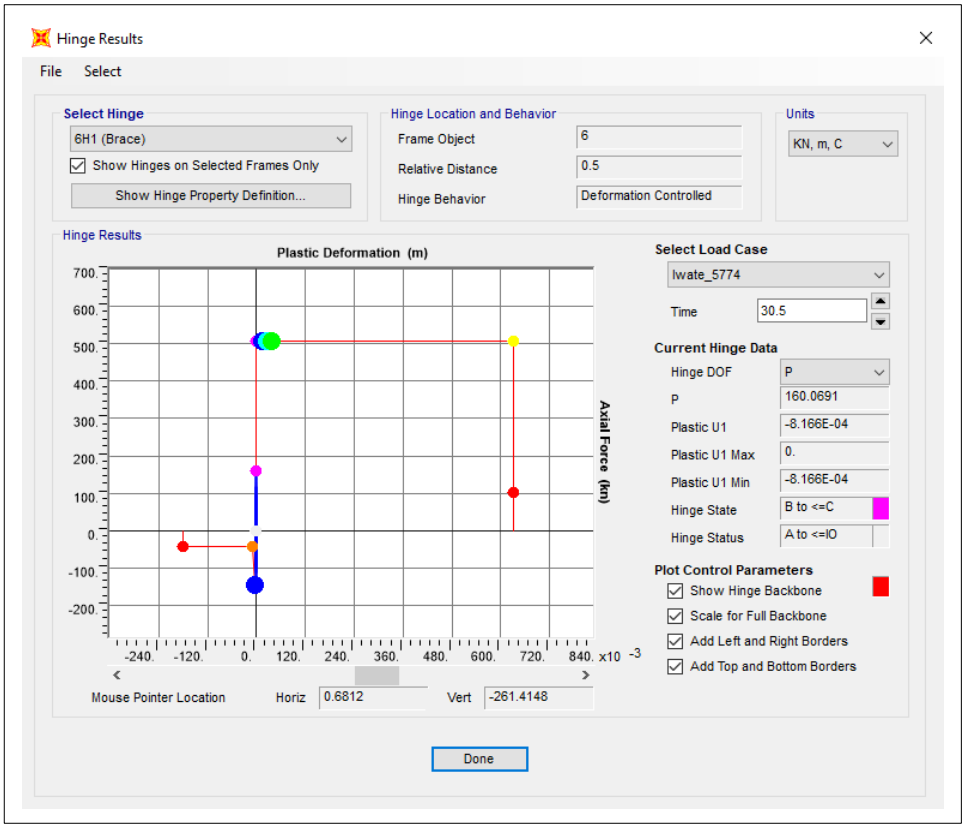

Figure 5.81: Hinge results of Silo-2 at 0.80 g (Iwate).

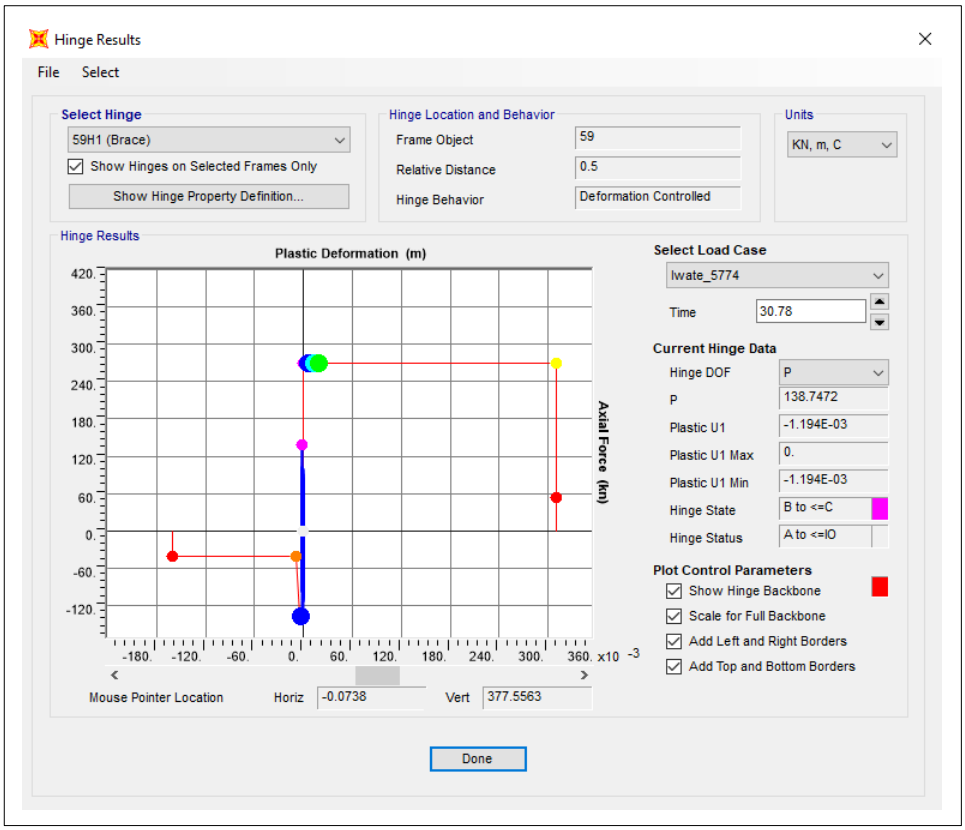

Figure 5.82: Hinge results of Silo-3 at 0.80 g (Iwate).

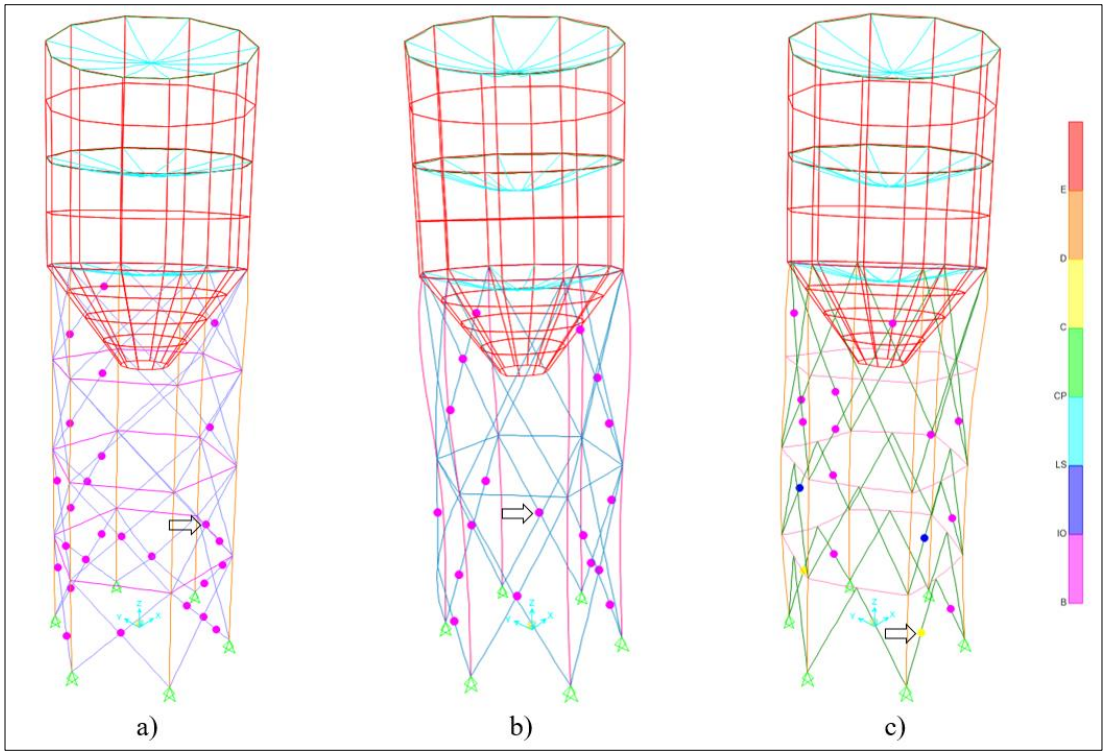

Figure 5.83: Deformed shapes of a) Silo-1, b) Silo-2, c) Silo-3 at 1.00 g (Iwate).

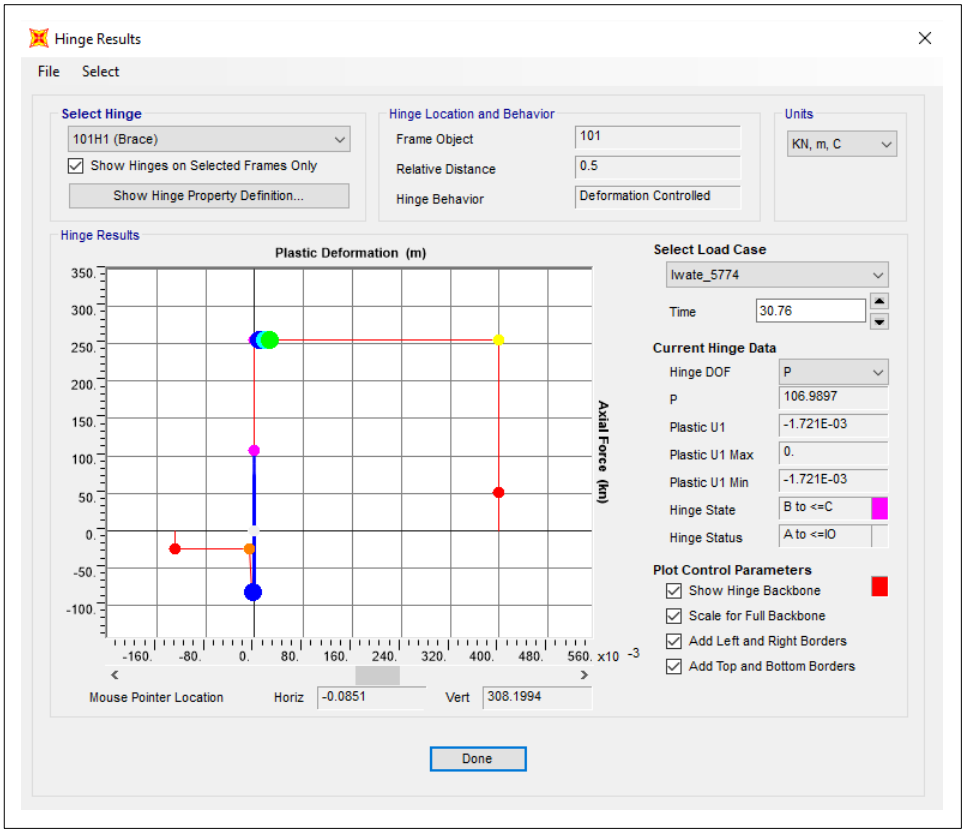

Figure 5.84: Hinge results of Silo-1 at 1.00 g (Iwate).

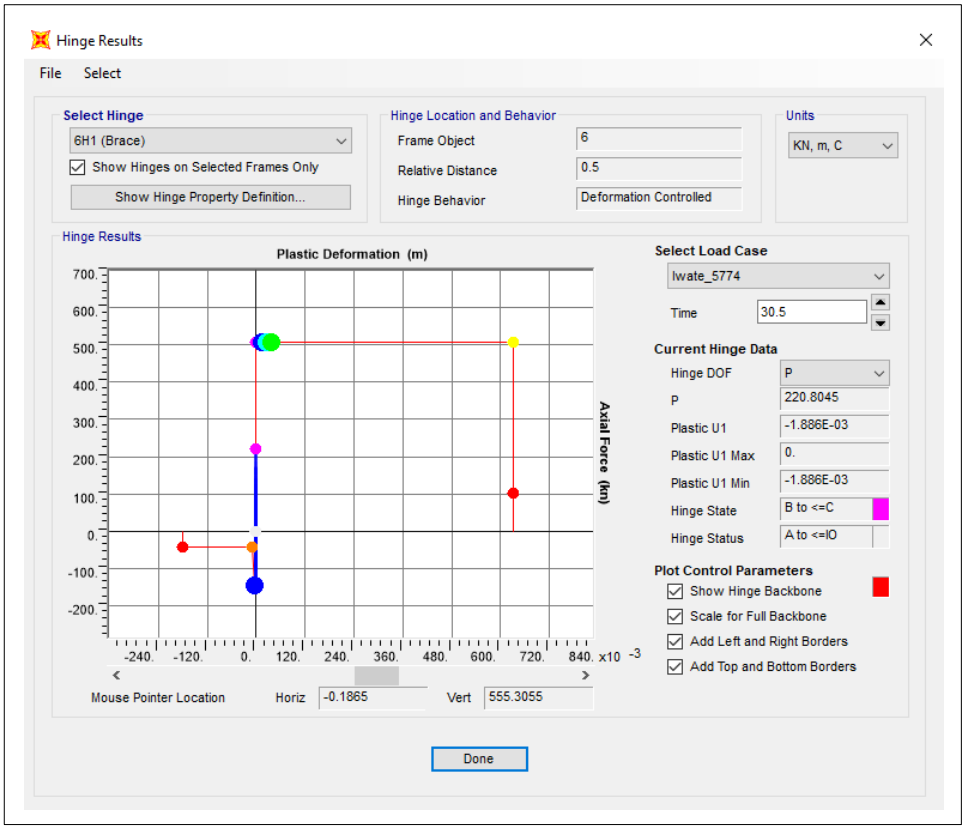

Figure 5.85: Hinge results of Silo-2 at 1.00 g (Iwate).

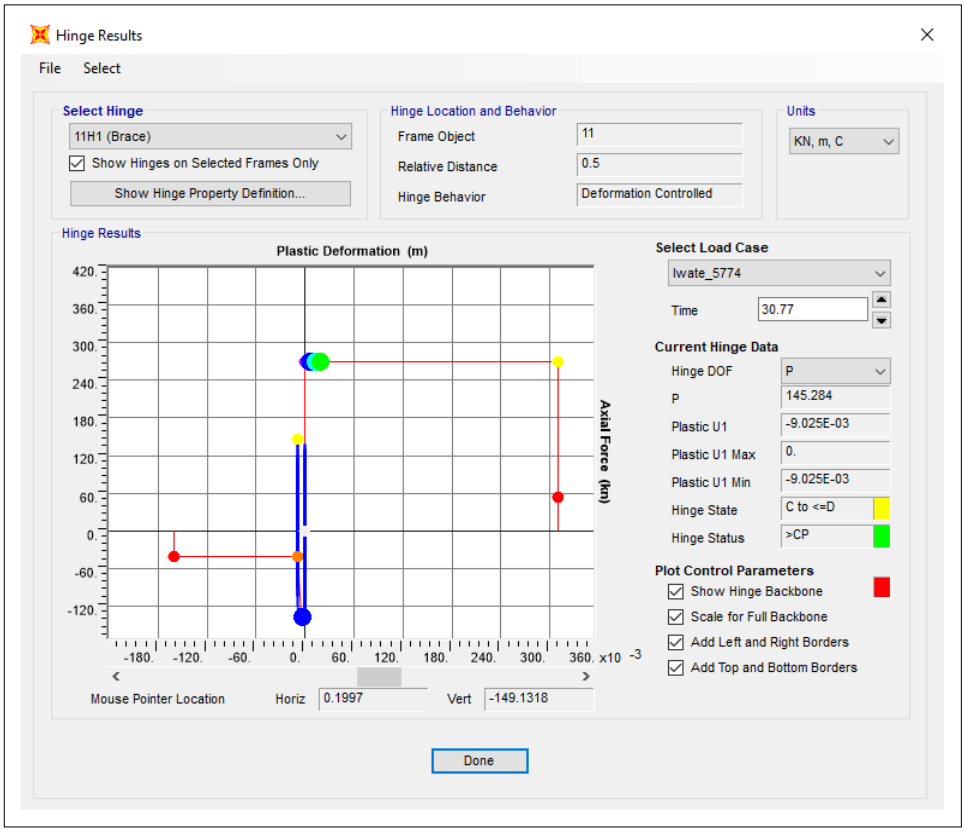

Figure 5.86: Hinge results of Silo-3 at 1.00 g (Iwate).

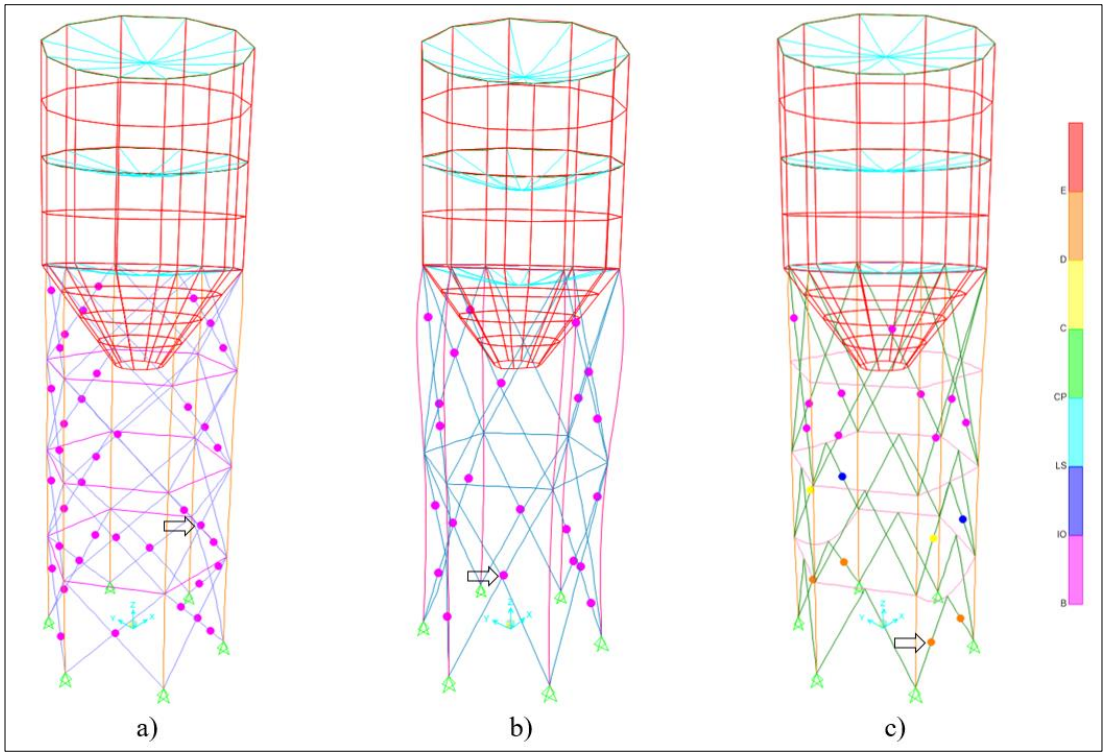

Figure 5.87: Deformed shapes of a) Silo-1, b) Silo-2, c) Silo-3 at 1.20 g (Iwate).

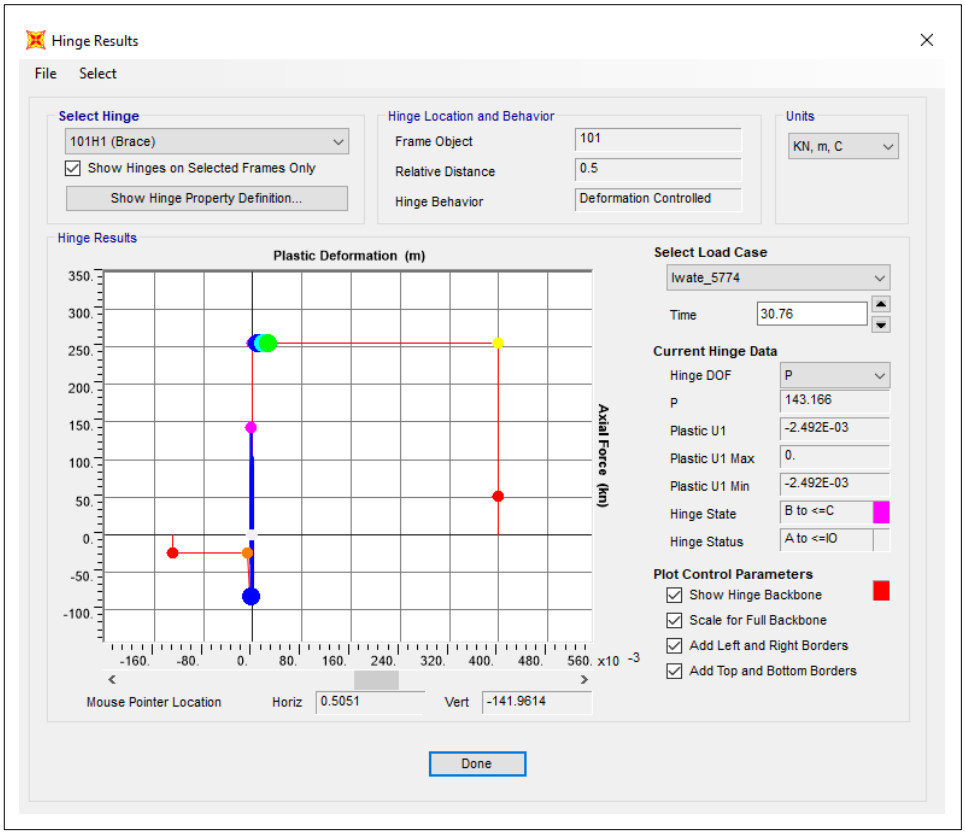

Figure 5.88: Hinge results of Silo-1 at 1.20 g (Iwate).

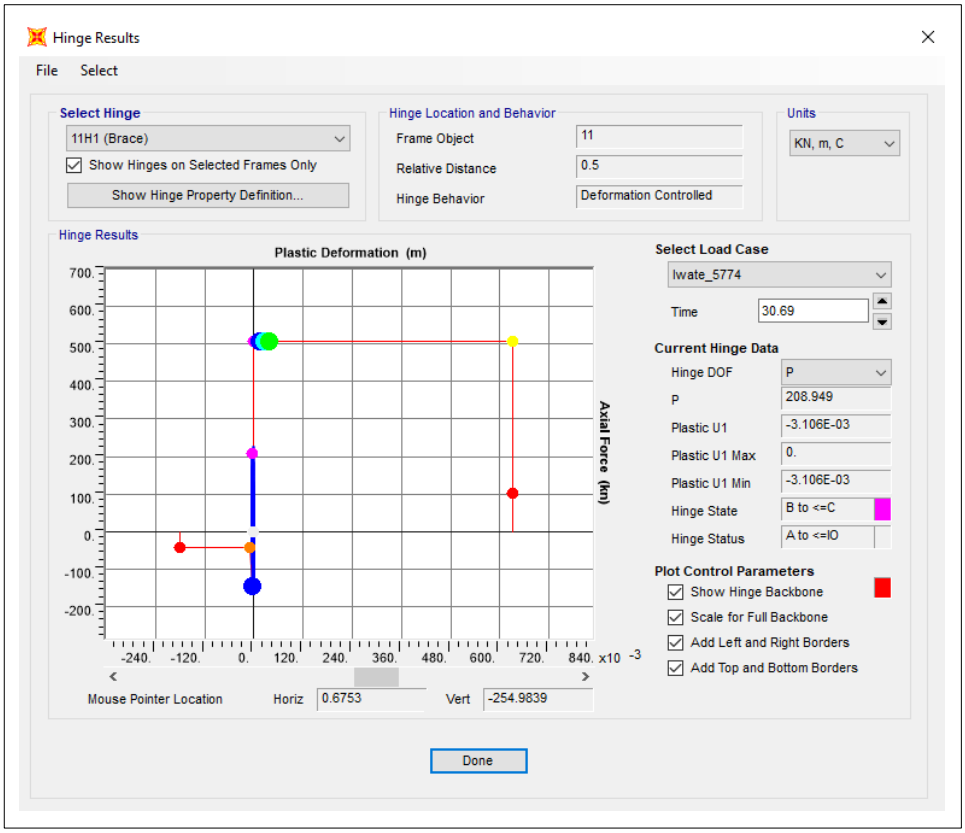

Figure 5.89: Hinge results of Silo-2 at 1.20 g (Iwate).

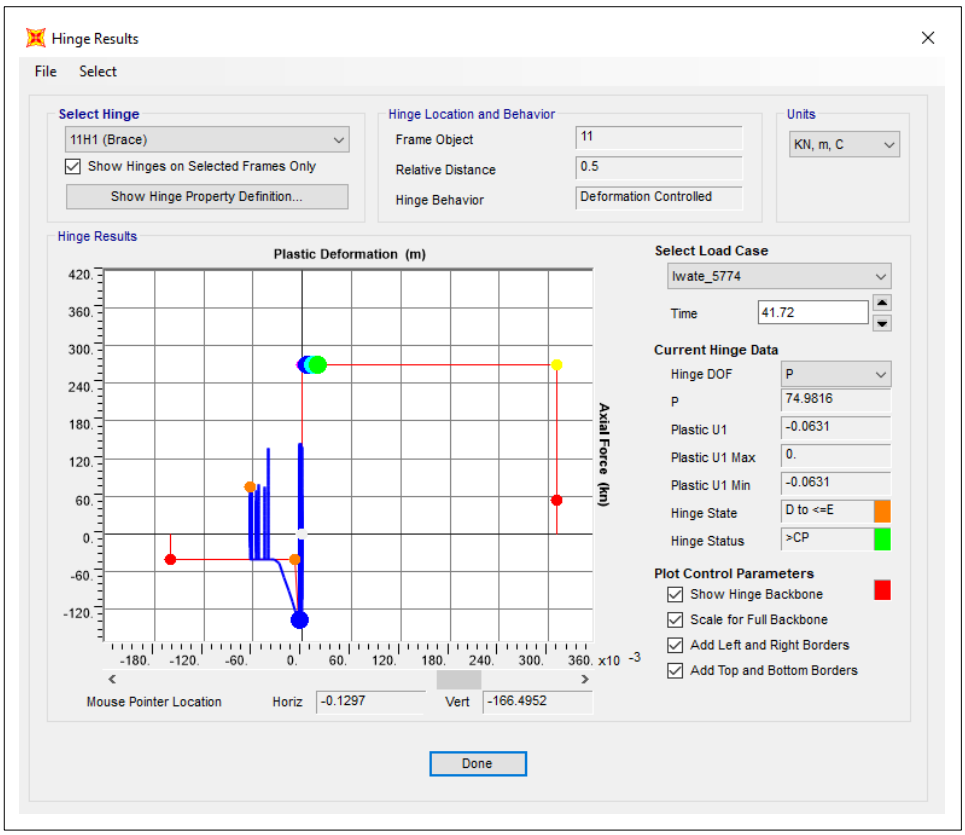

Figure 5.90: Hinge results of Silo-3 at 1.20 g (Iwate).

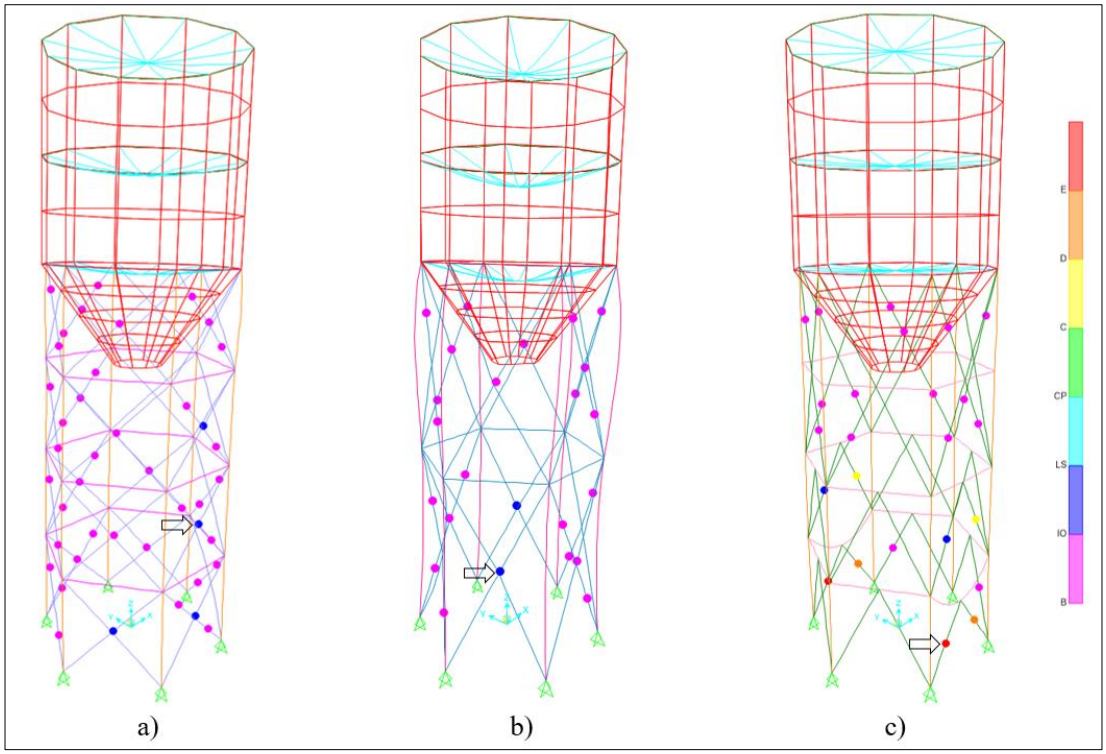

Figure 5.91: Deformed shapes of a) Silo-1, b) Silo-2, c) Silo-3 at 1.40 g (Iwate).

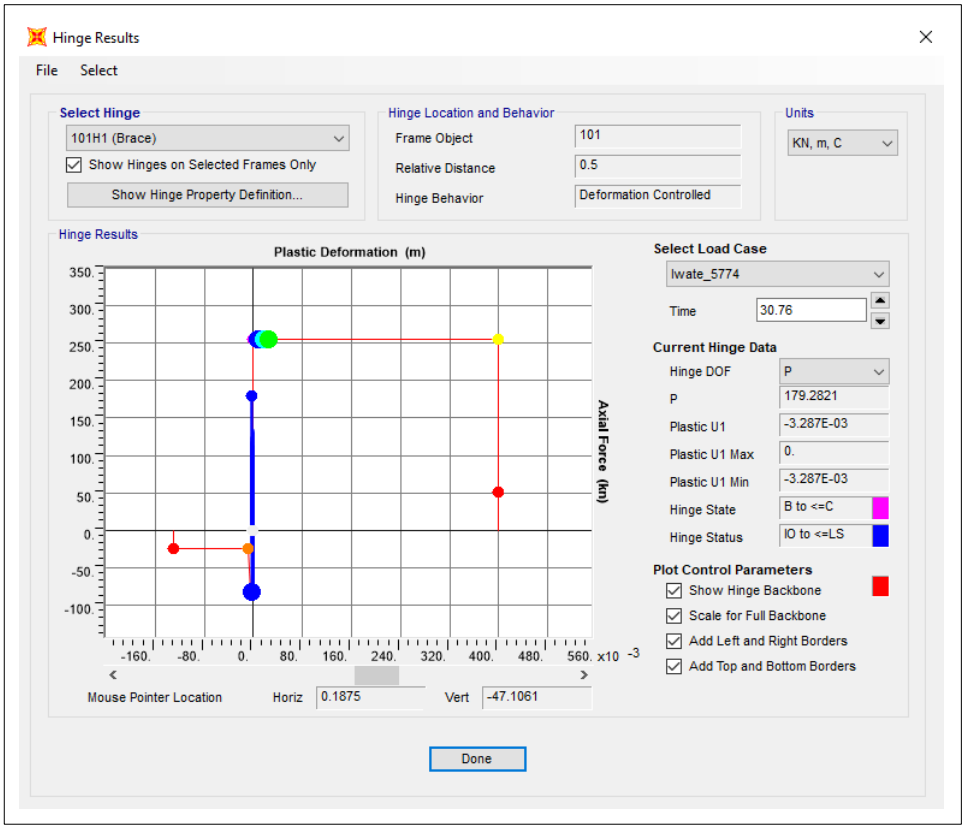

Figure 5.92: Hinge results of Silo-1 at 1.40 g (Iwate).

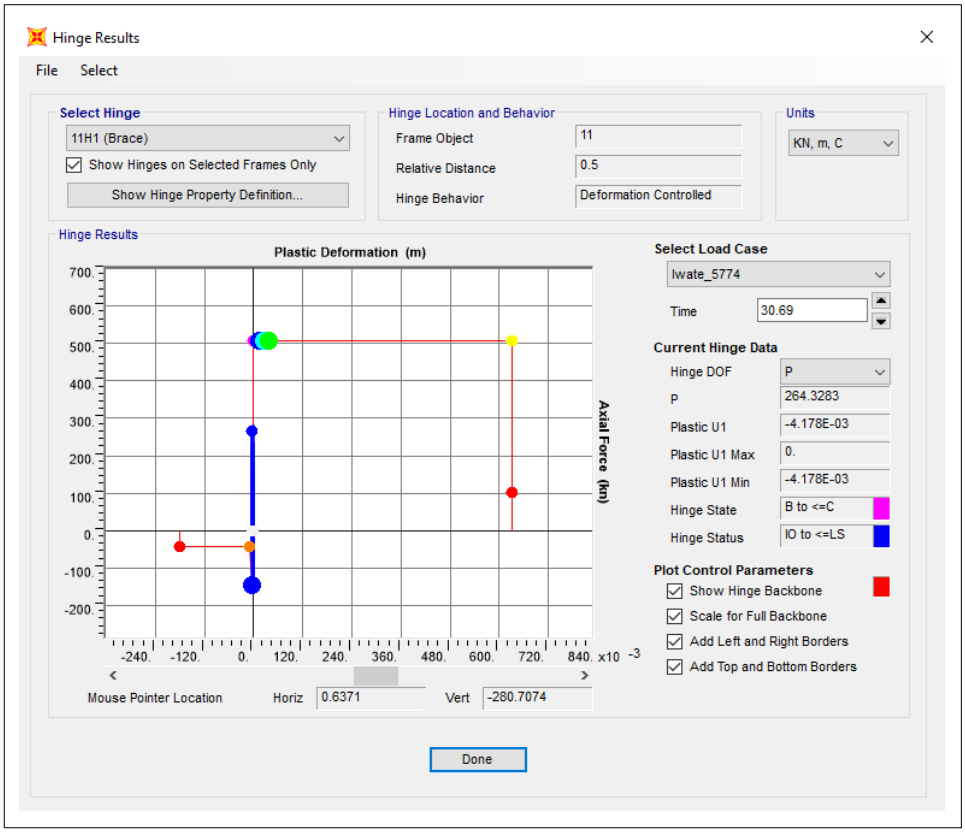

Figure 5.93: Hinge results of Silo-2 at 1.40 g (Iwate).

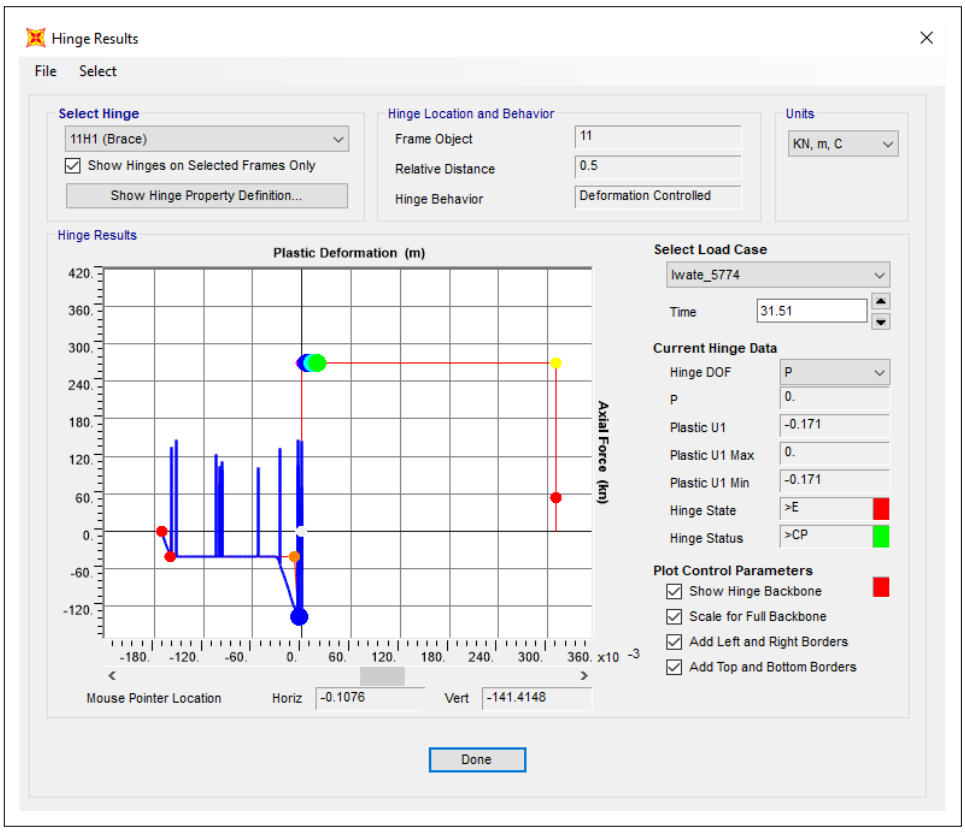

Figure 5.94: Hinge results of Silo-3 at 1.40 g (Iwate).

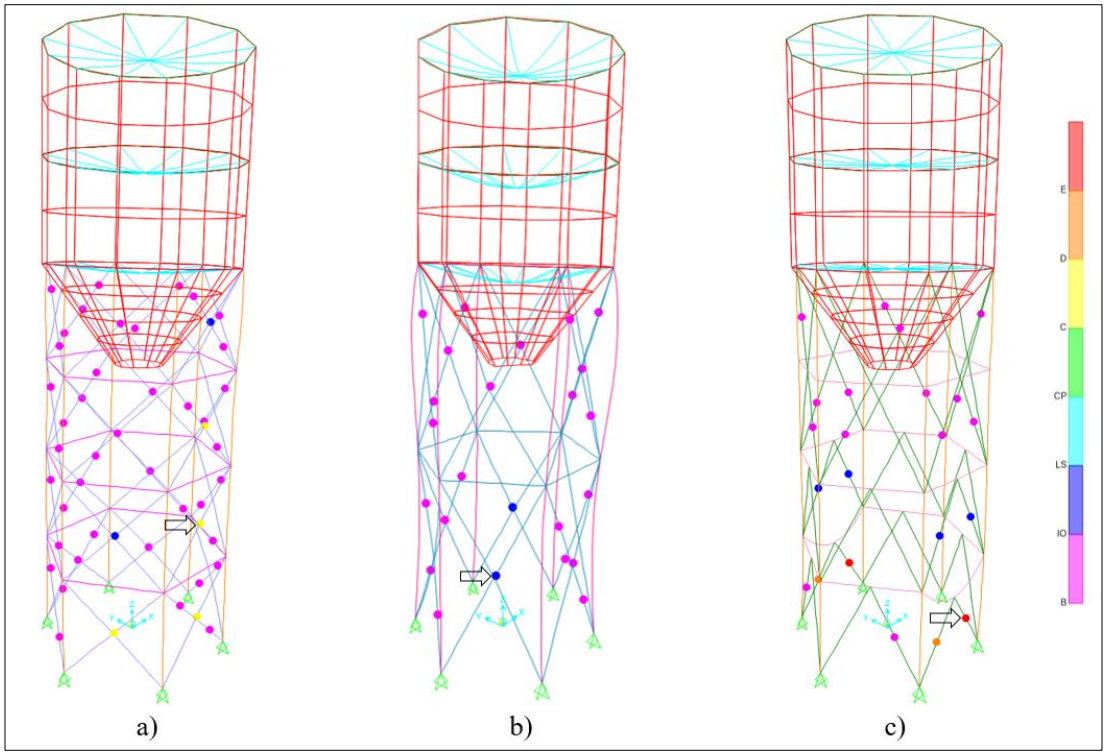

Figure 5.95: Deformed shapes of a) Silo-1, b) Silo-2, c) Silo-3 at 1.60 g (Iwate).

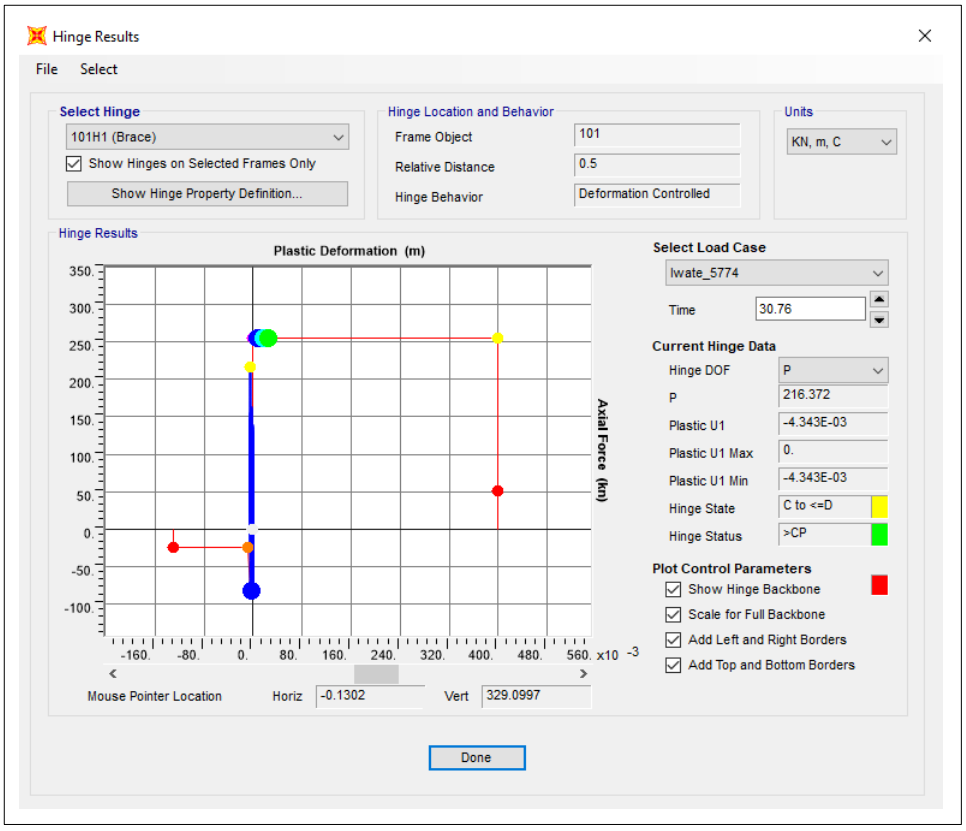

Figure 5.96: Hinge results of Silo-1 at 1.60 g (Iwate).

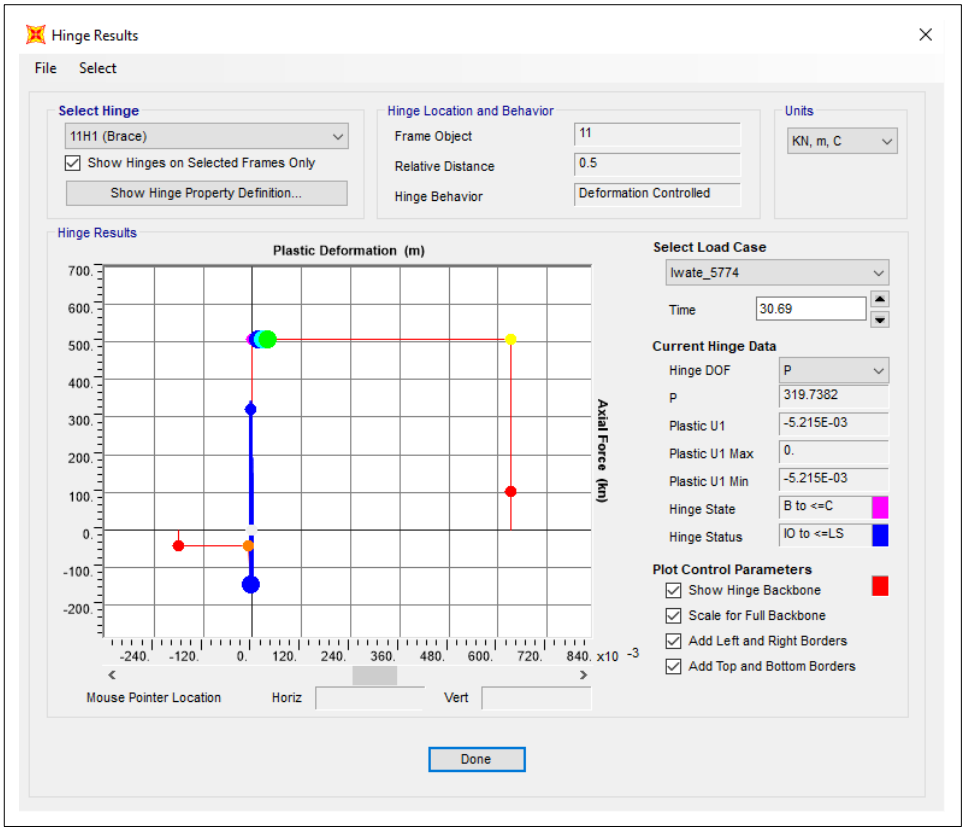

Figure 5.97: Hinge results of Silo-2 at 1.60 g (Iwate).

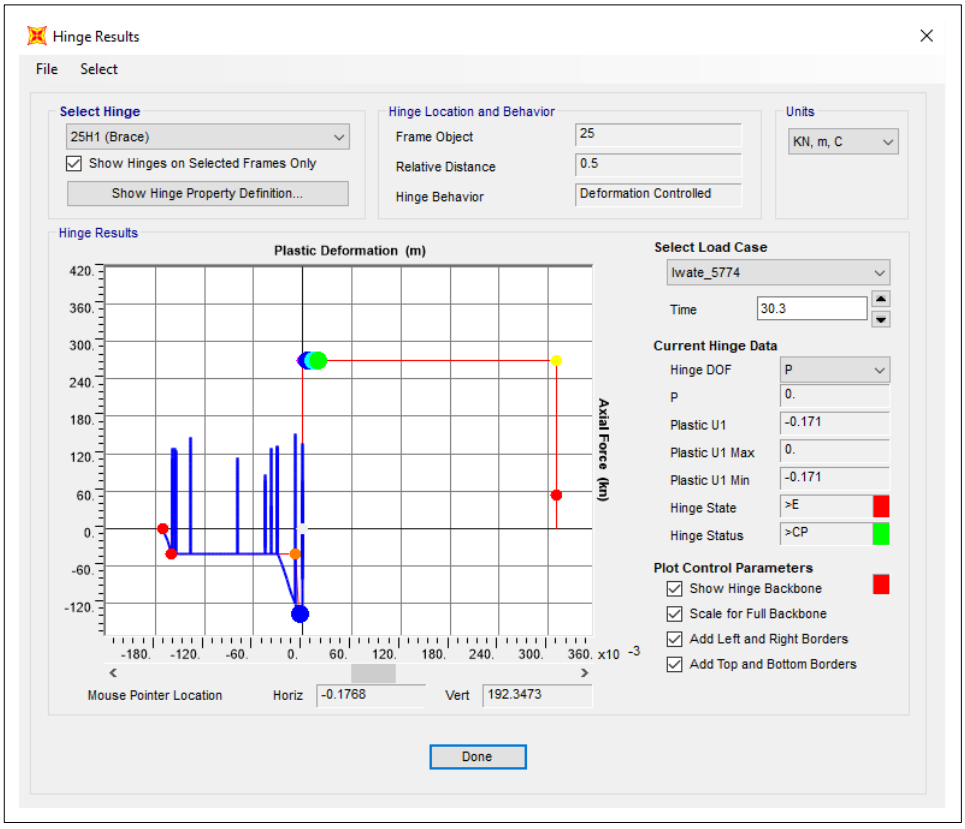

Figure 5.98: Hinge results of Silo-3 at 1.60 g (Iwate).

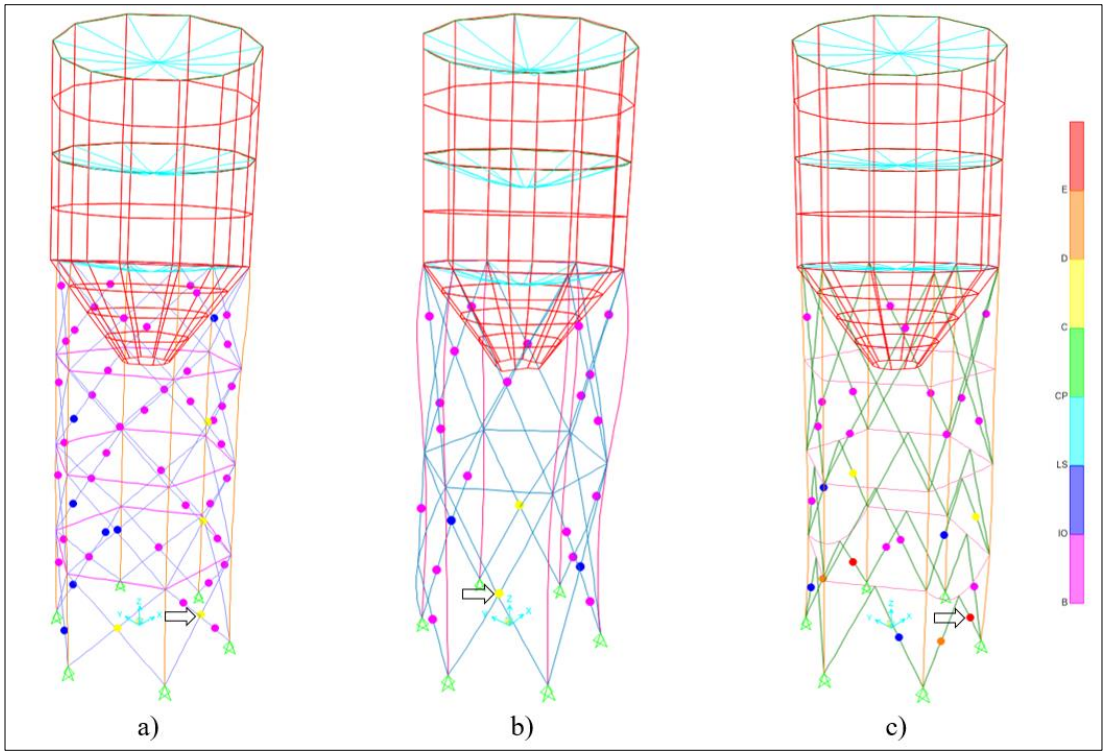

Figure 5.99: Deformed shapes of a) Silo-1, b) Silo-2, c) Silo-3 at 1.80 g (Iwate).

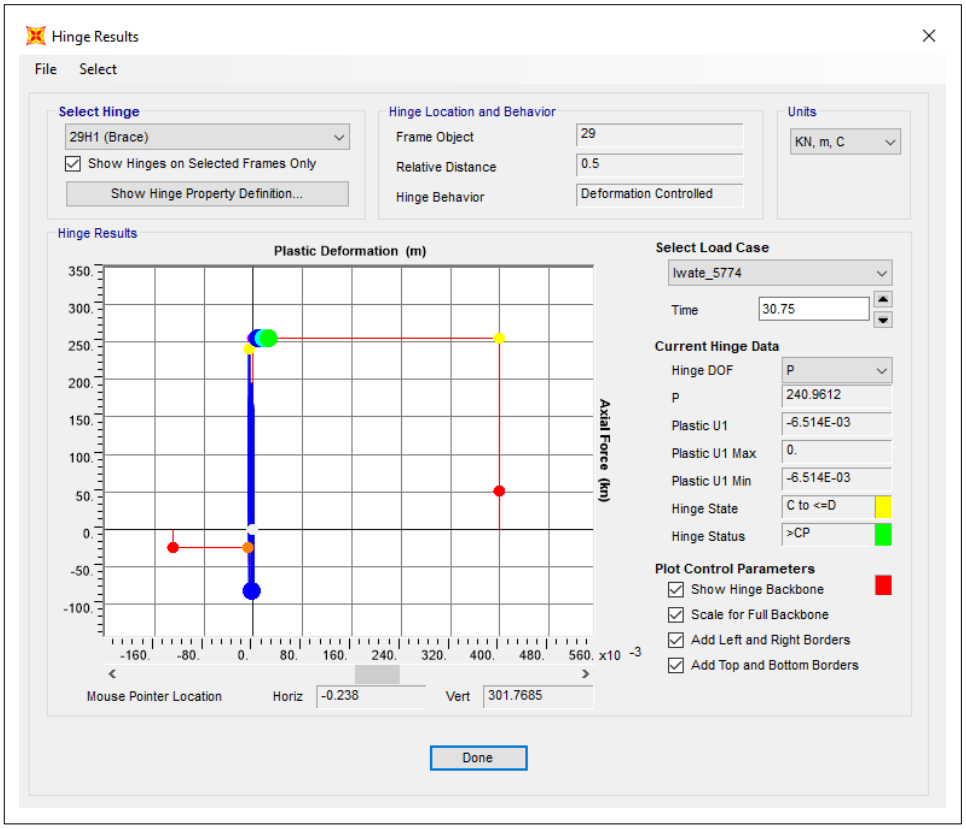

Figure 5.100: Hinge results of Silo-1 at 1.80 g (Iwate).

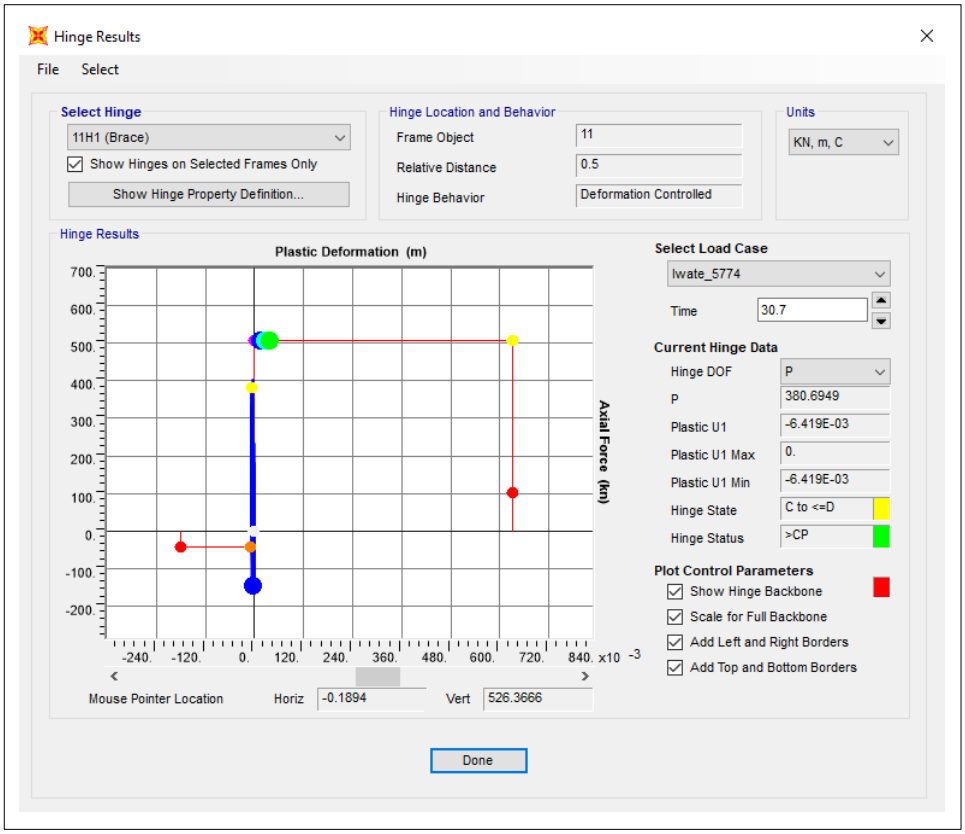

Figure 5.101: Hinge results of Silo-2 at 1.80 g (Iwate).

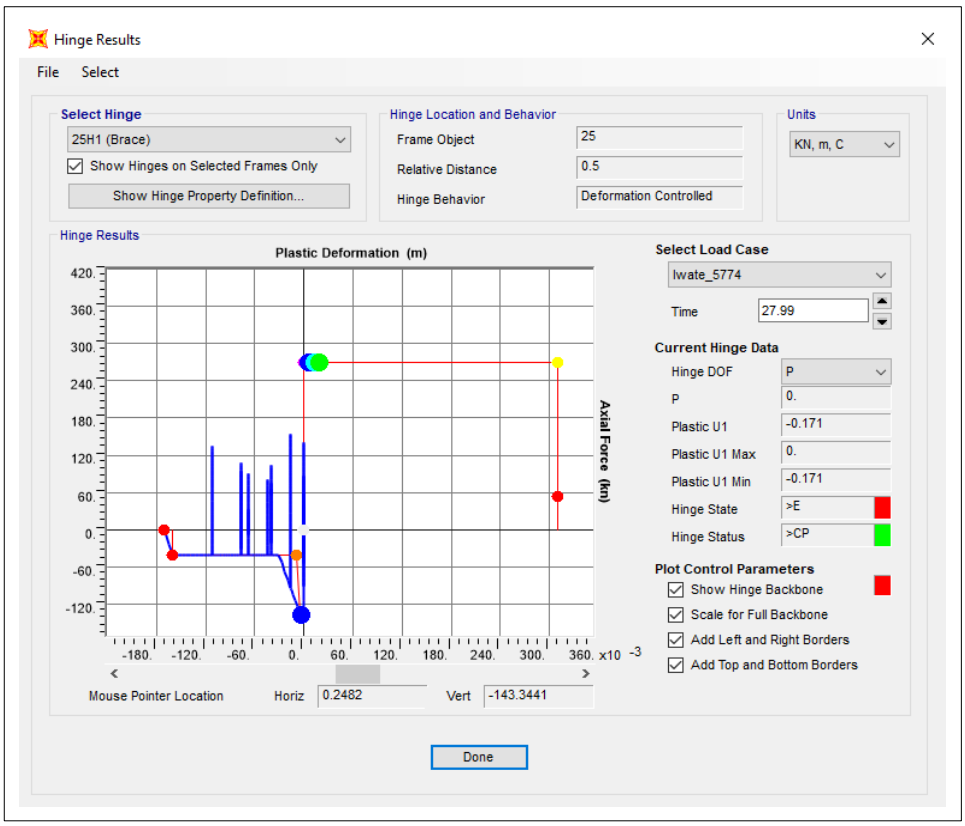

Figure 5.102: Hinge results of Silo-3 at 1.80 g (Iwate).

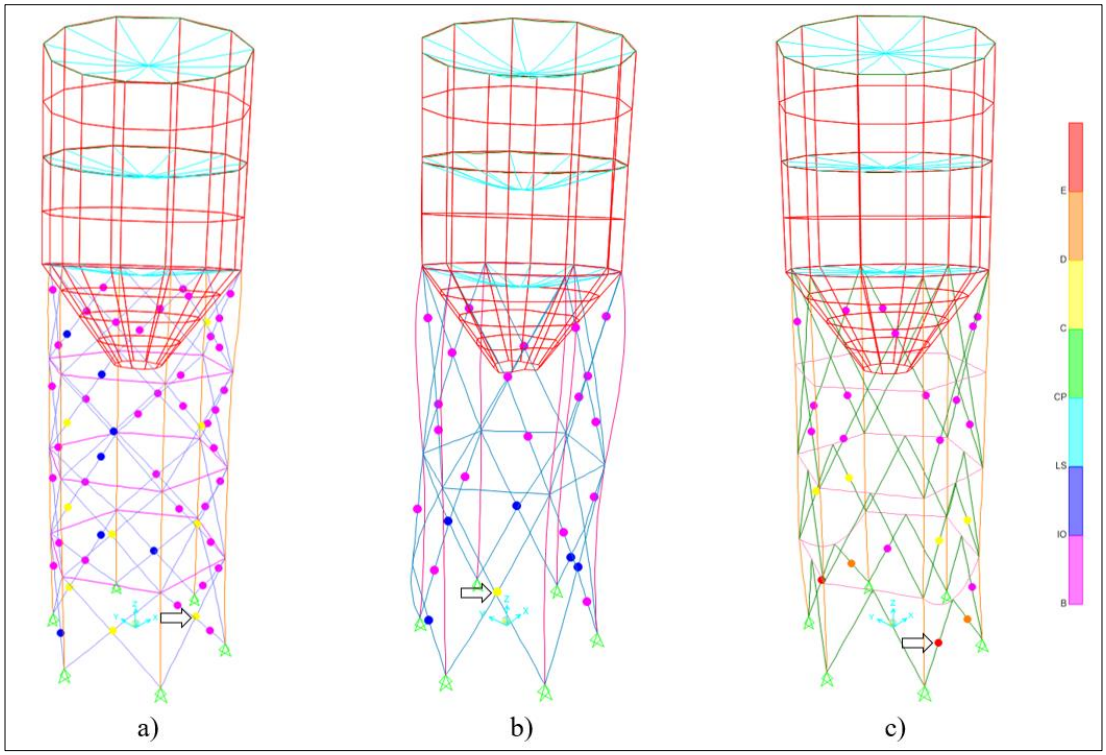

Figure 5.103: Deformed shapes of a) Silo-1, b) Silo-2, c) Silo-3 at 2.00 g (Iwate).

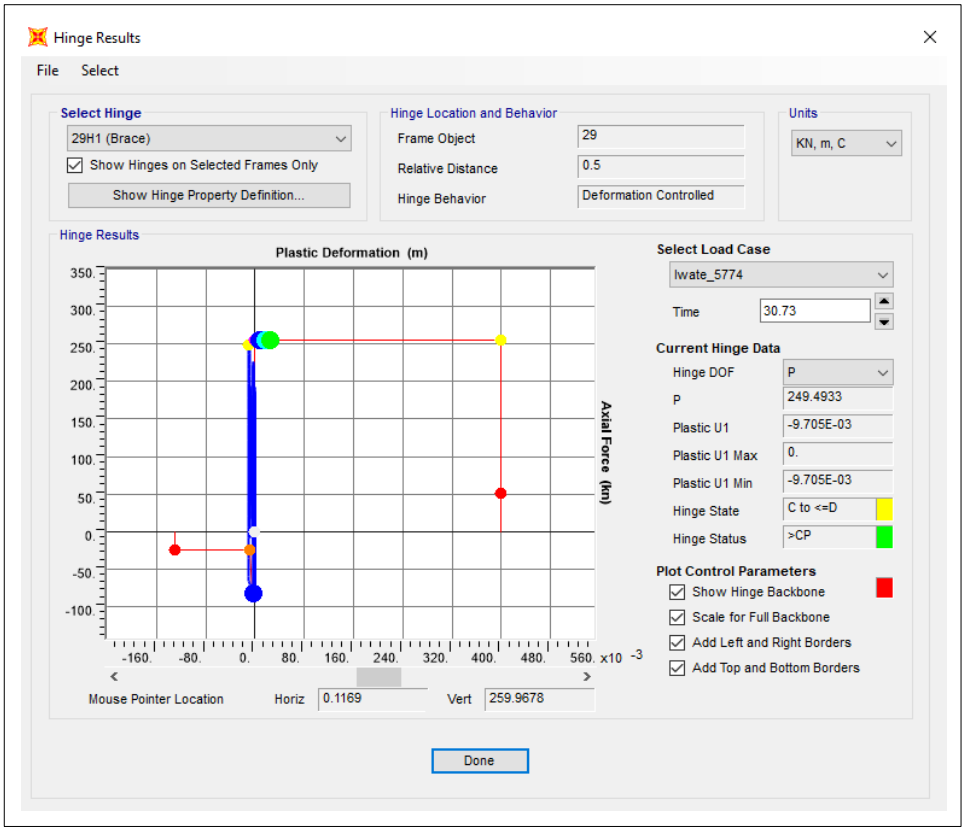

Figure 5.104: Hinge results of Silo-1 at 2.00 g (Iwate).

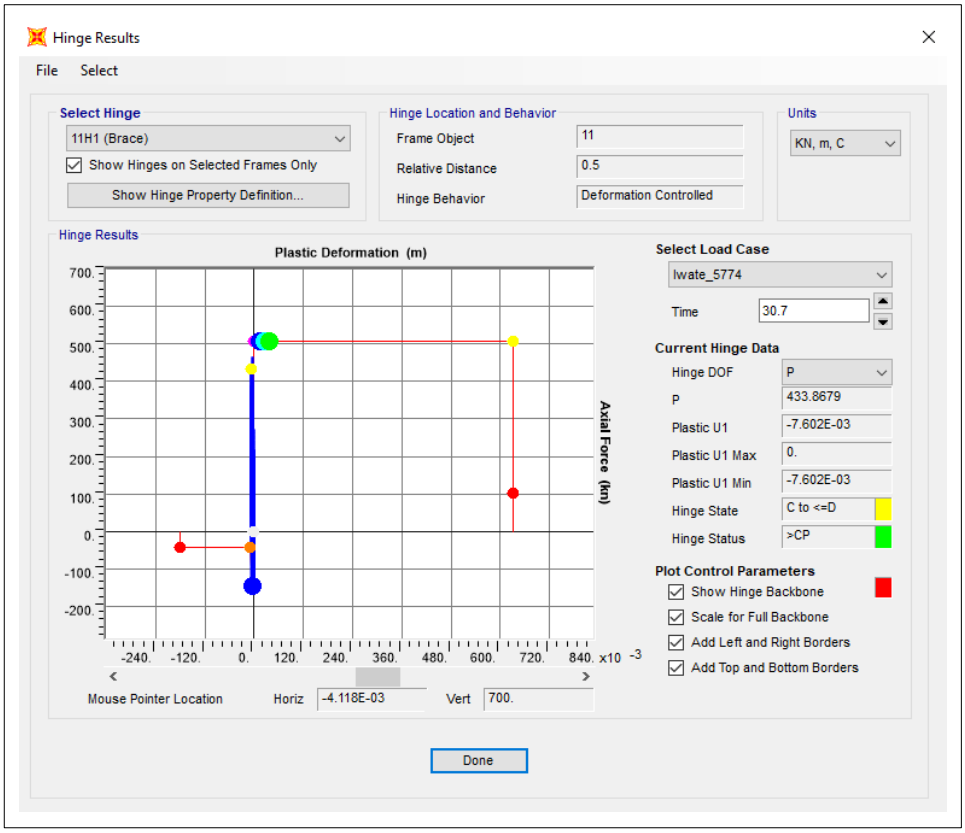

Figure 5.105: Hinge results of Silo-2 at 2.00 g (Iwate).

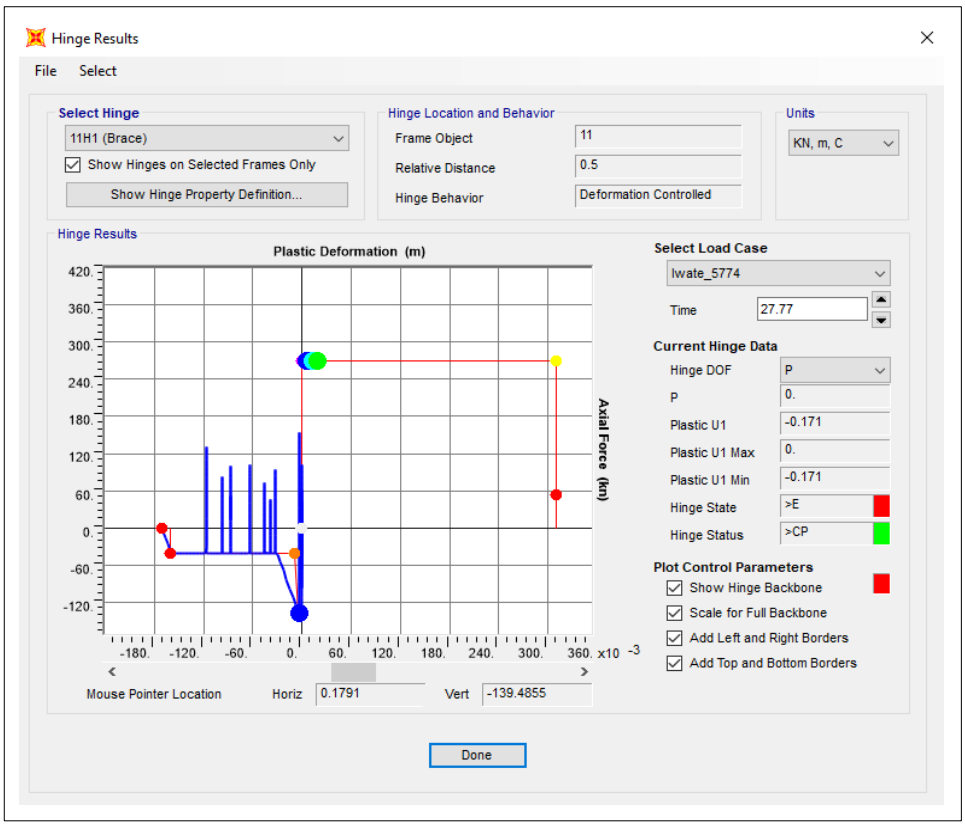

Figure 5.106: Hinge results of Silo-3 at 2.00 g (Iwate).

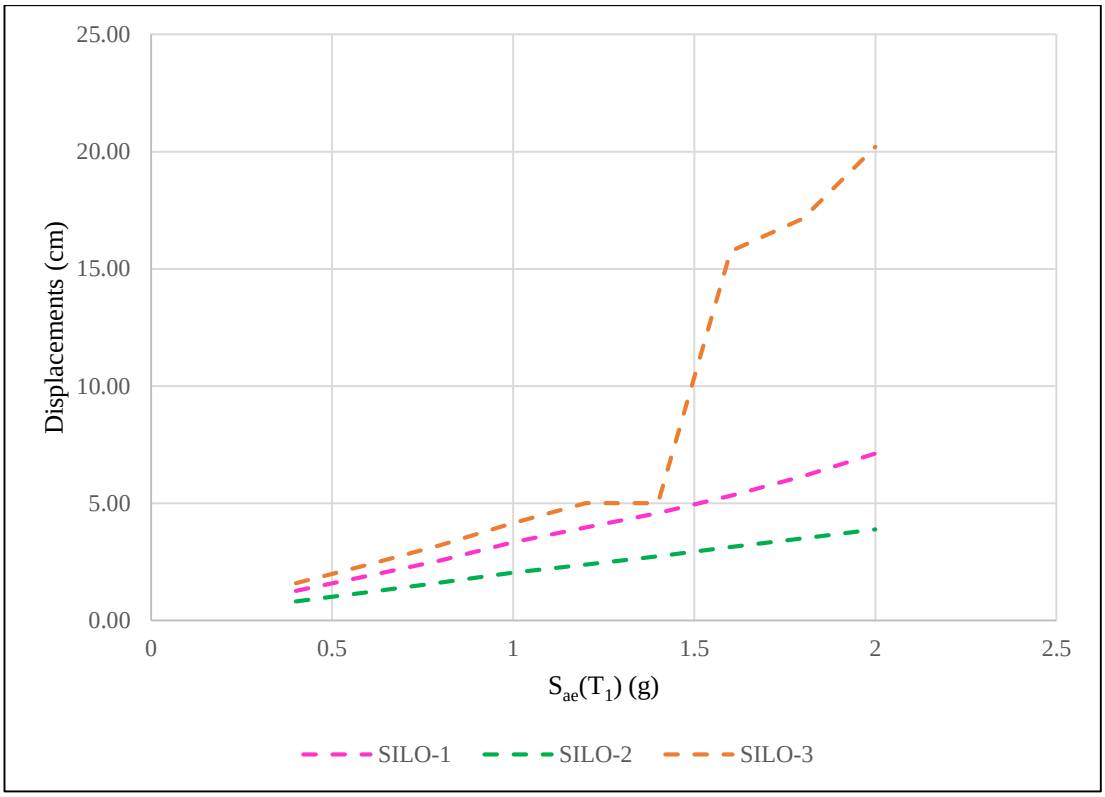

Figure 5.107: Top displacements in Iwate-5774 Earthquake.

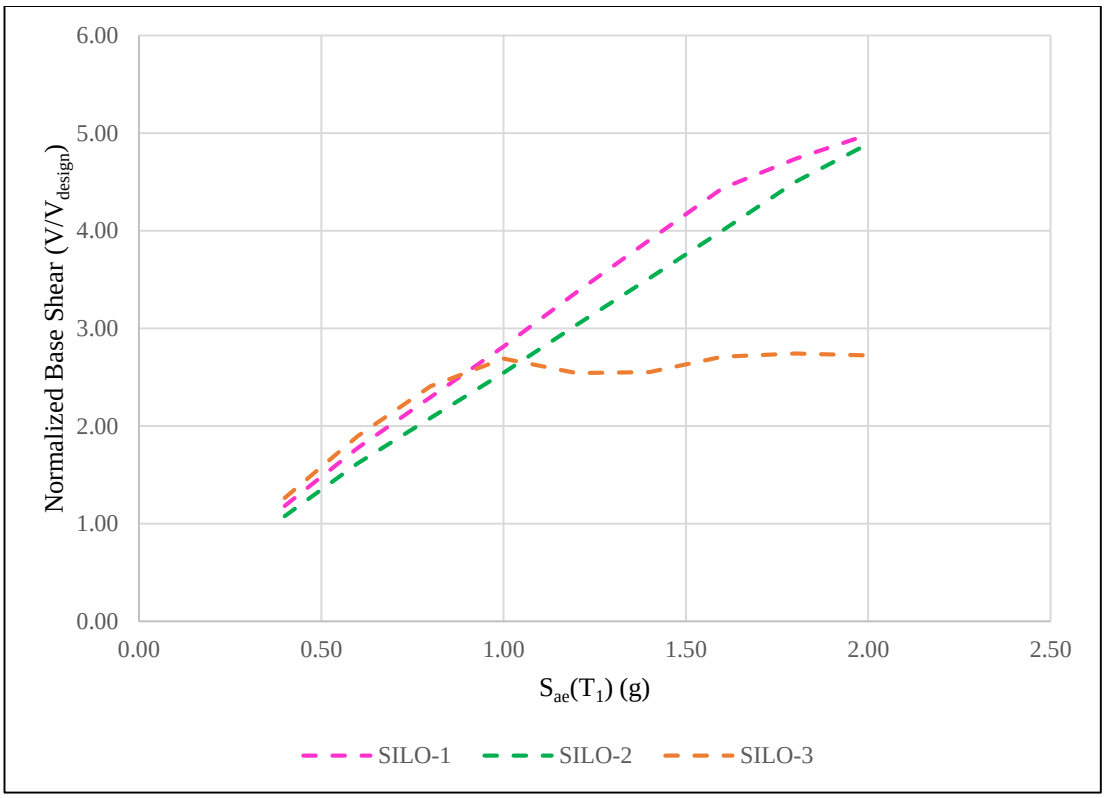

Figure 5.108: Normalized base shear forces in Iwate-5774 Earthquake.

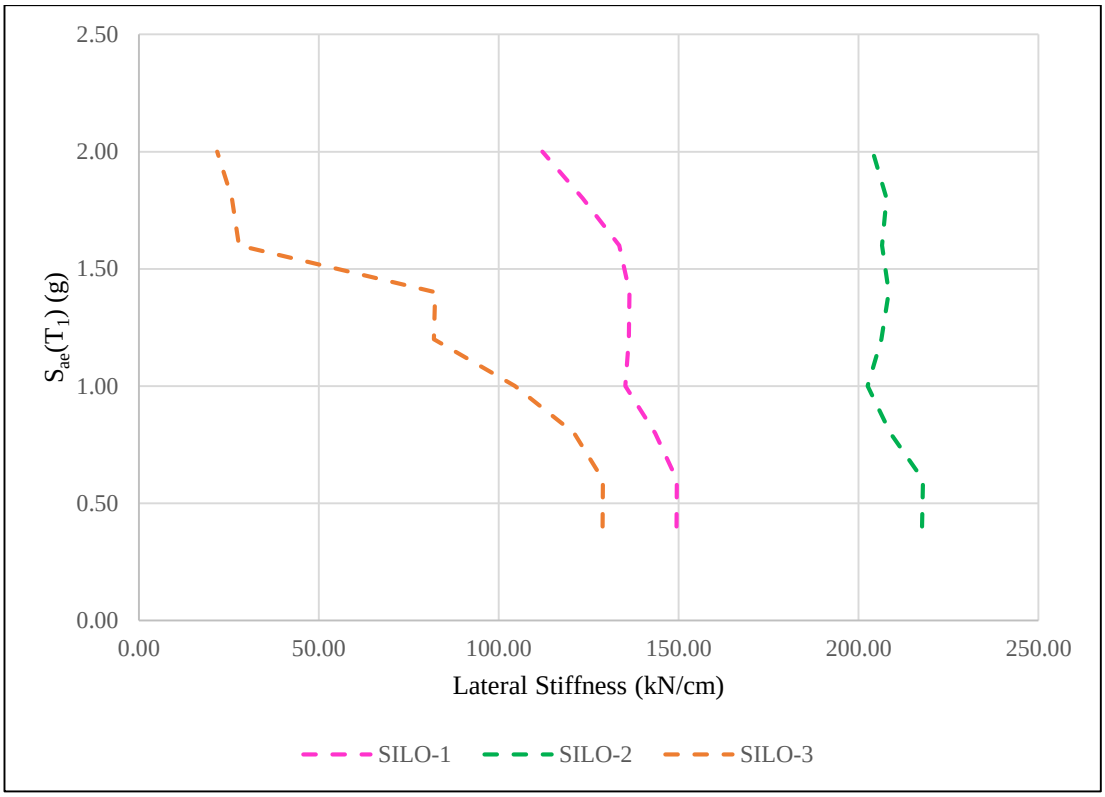

Figure 5.109: Lateral stiffness in Iwate-5774 Earthquake.

5.3.4. Hinge Results for Kobe-1121

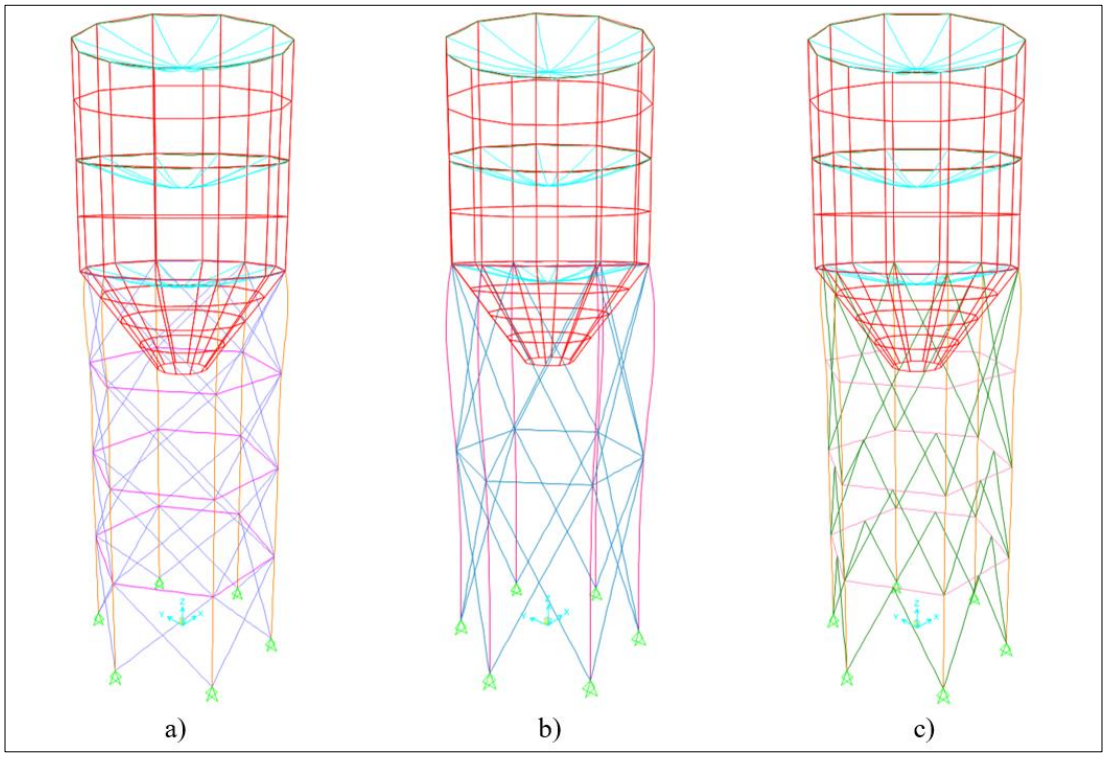

Figure 5.110: Deformed shapes of a) Silo-1, b) Silo-2, c) Silo-3 at 0.40 g (Kobe).

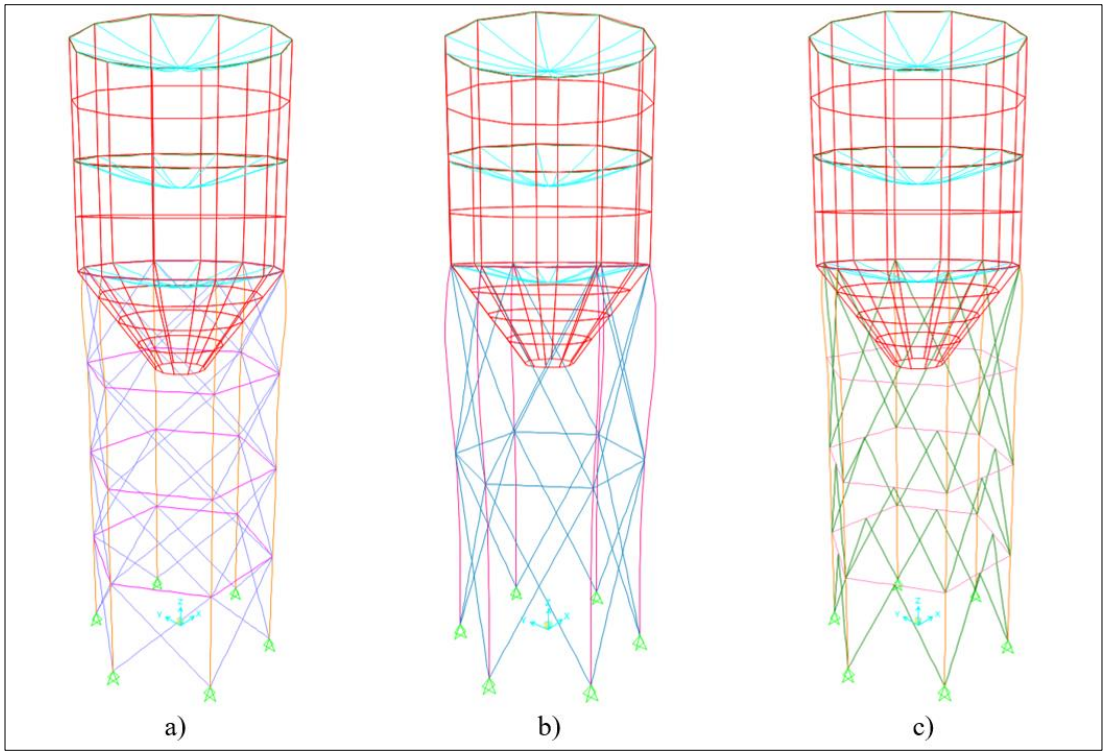

Figure 5.111: Deformed shapes of a) Silo-1, b) Silo-2, c) Silo-3 at 0.60 g (Kobe).

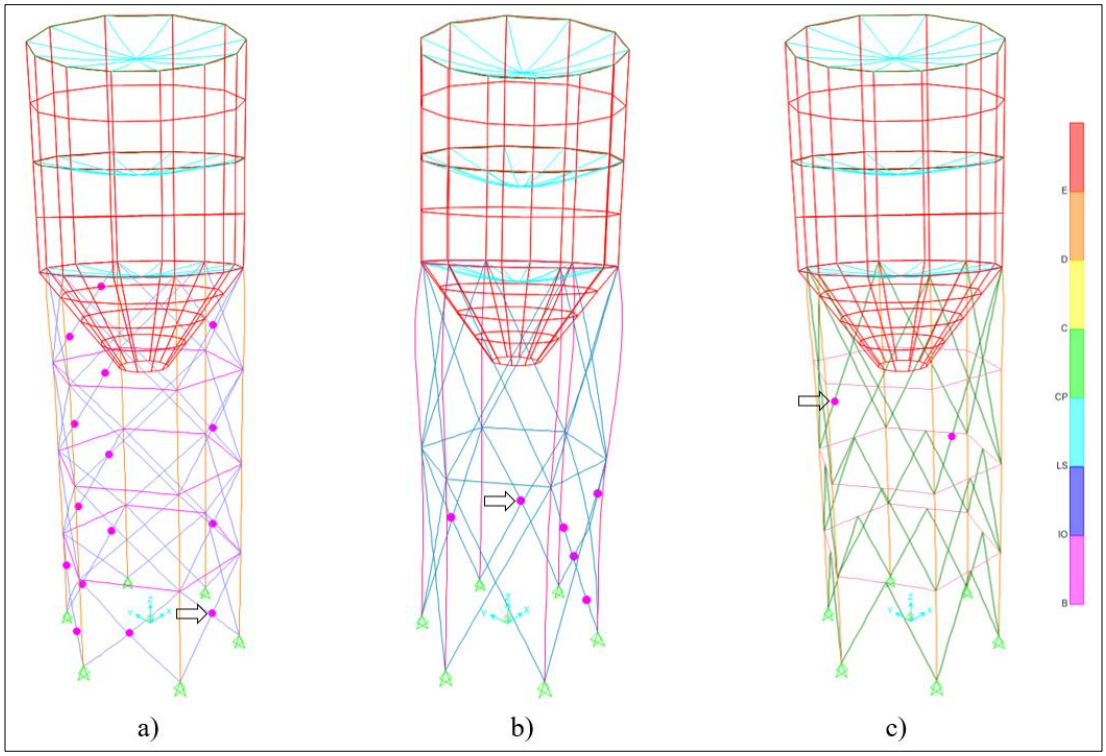

Figure 5.112: Deformed shapes of a) Silo-1, b) Silo-2, c) Silo-3 at 0.80 g (Kobe).

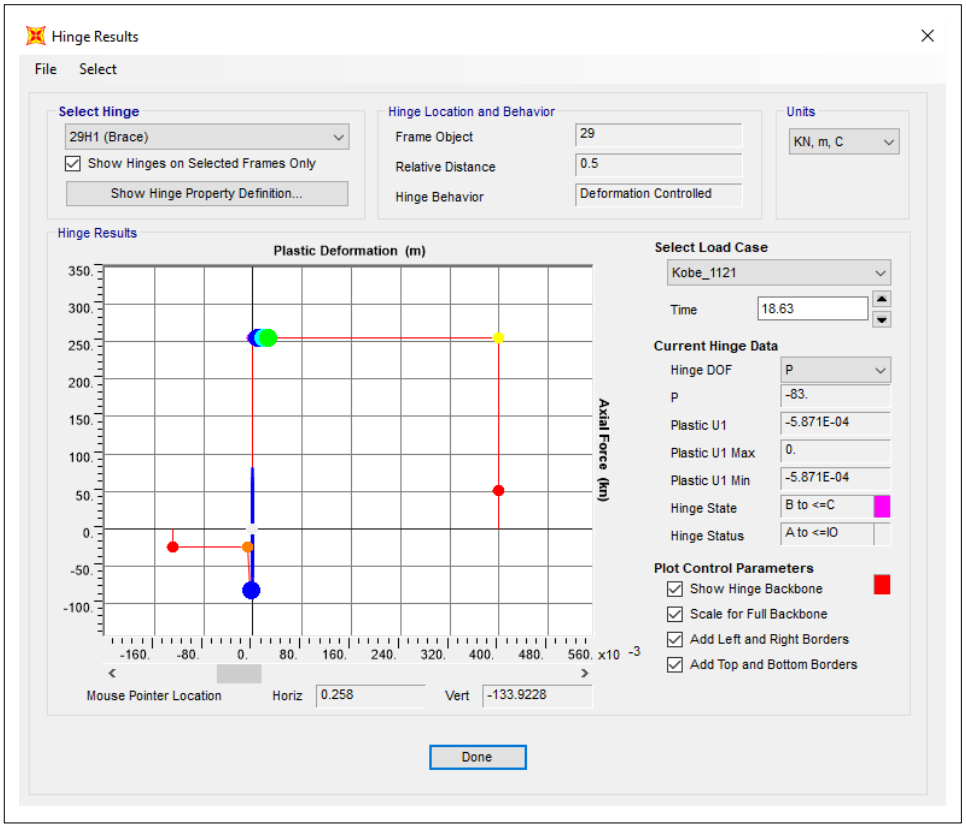

Figure 5.113: Hinge results of Silo-1 at 0.80 g (Kobe).

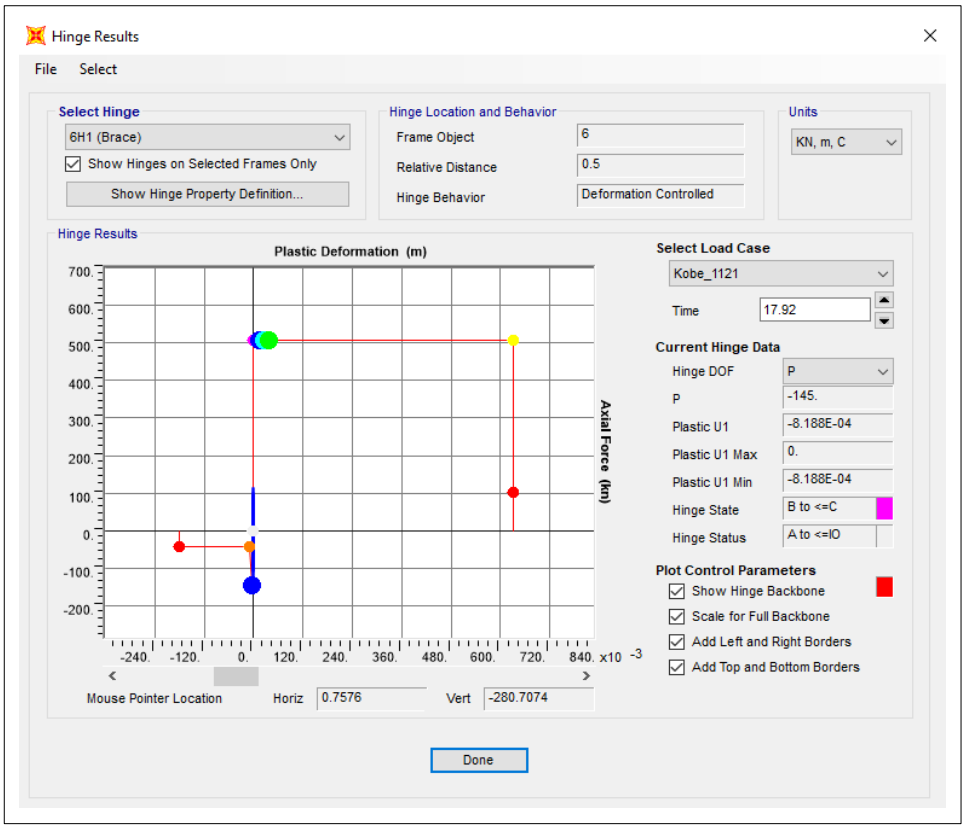

Figure 5.114: Hinge results of Silo-2 at 0.80 g (Kobe).

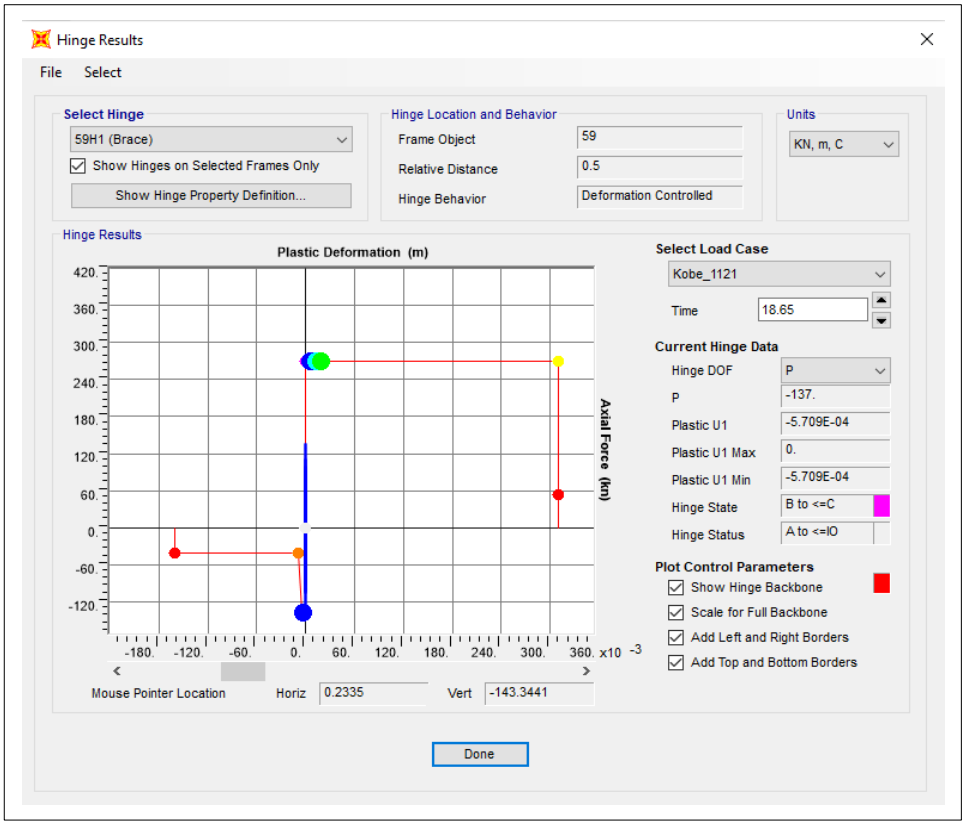

Figure 5.115: Hinge results of Silo-3 at 0.80 g (Kobe).

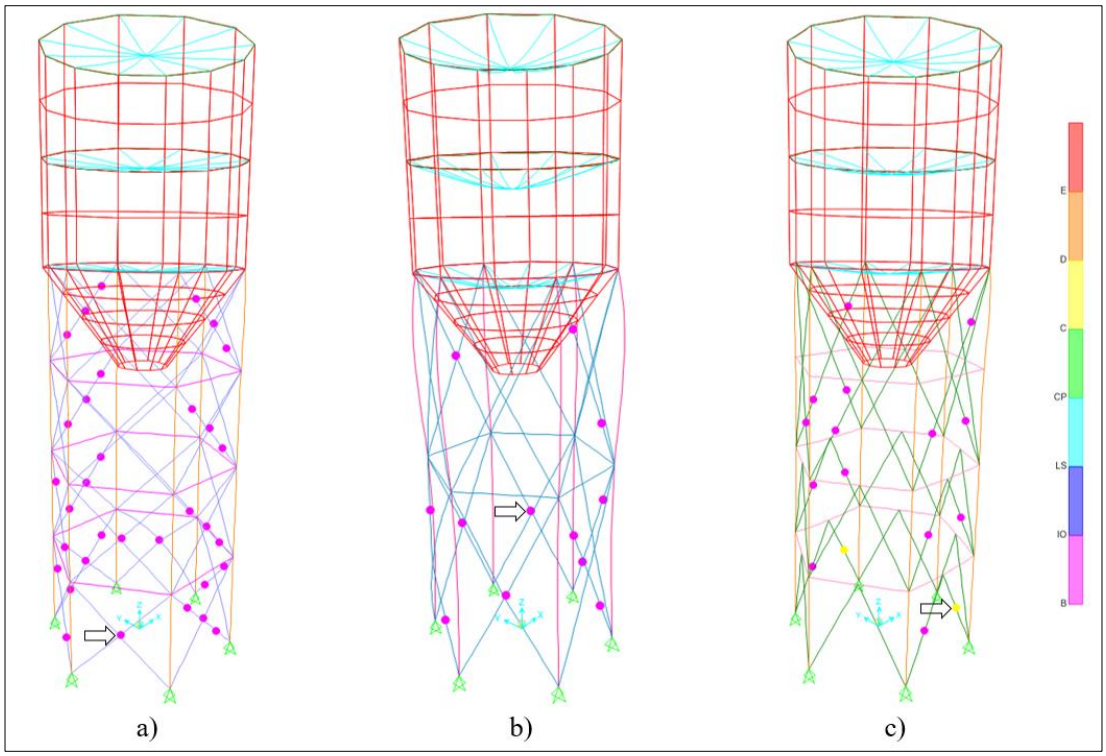

Figure 5.116: Deformed shapes of a) Silo-1, b) Silo-2, c) Silo-3 at 1.00 g (Kobe).

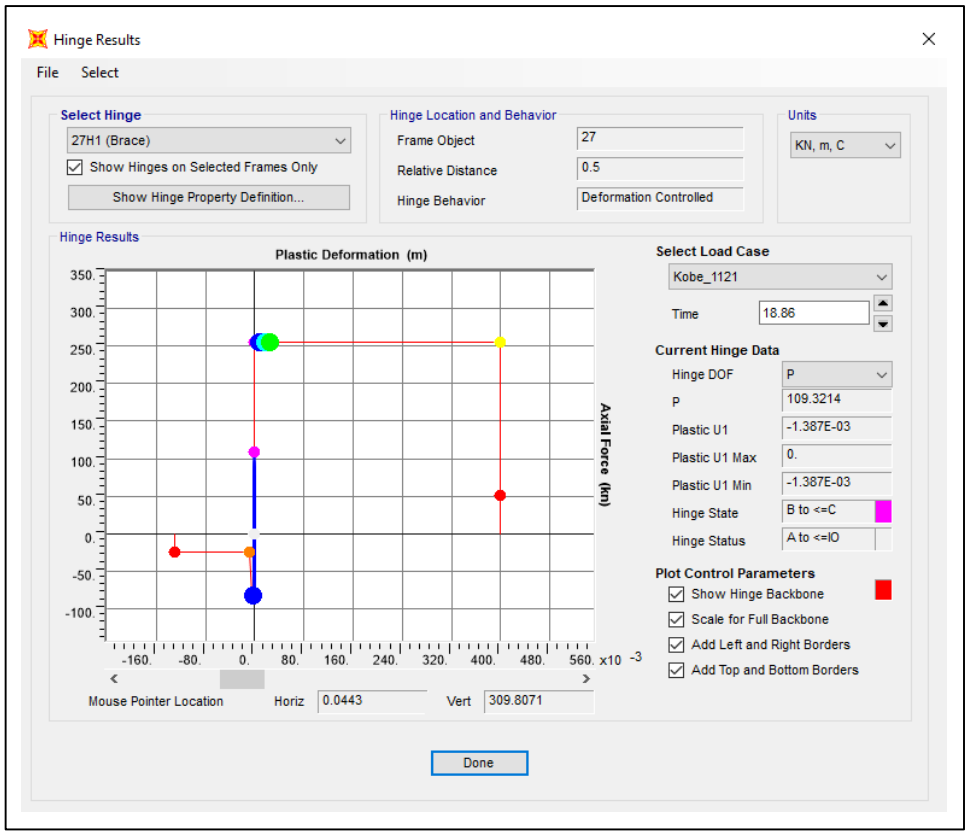

Figure 5.117: Hinge results of Silo-1 at 1.00 g (Kobe).

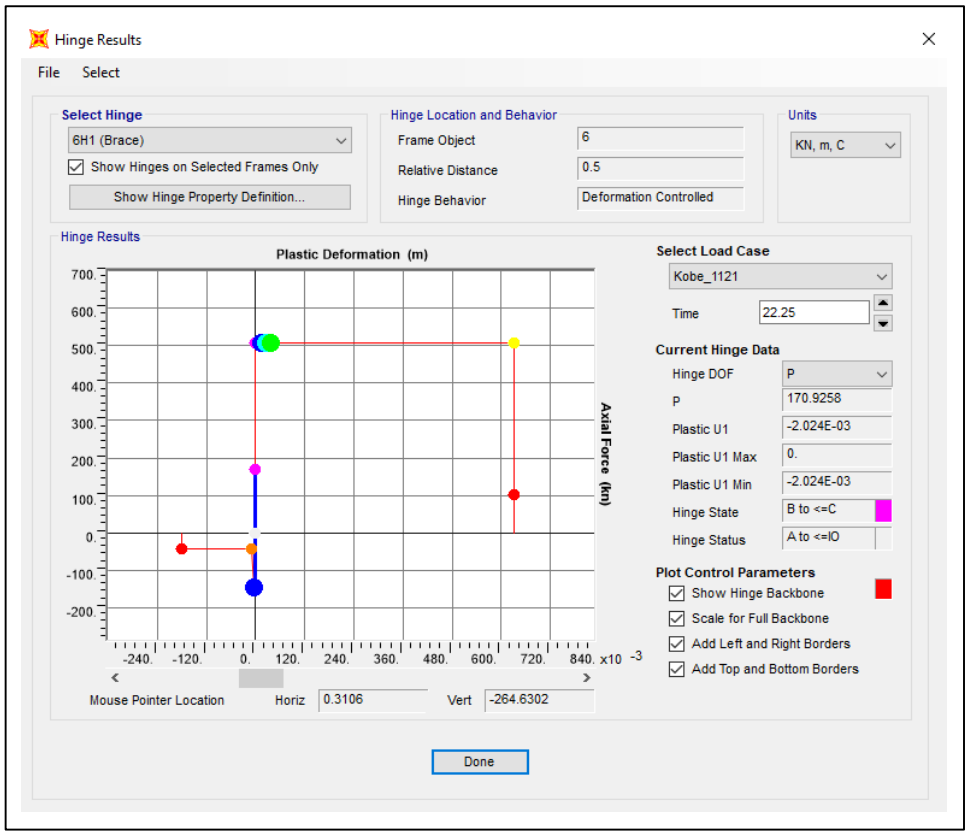

Figure 5.118: Hinge results of Silo-2 at 1.00 g (Kobe).

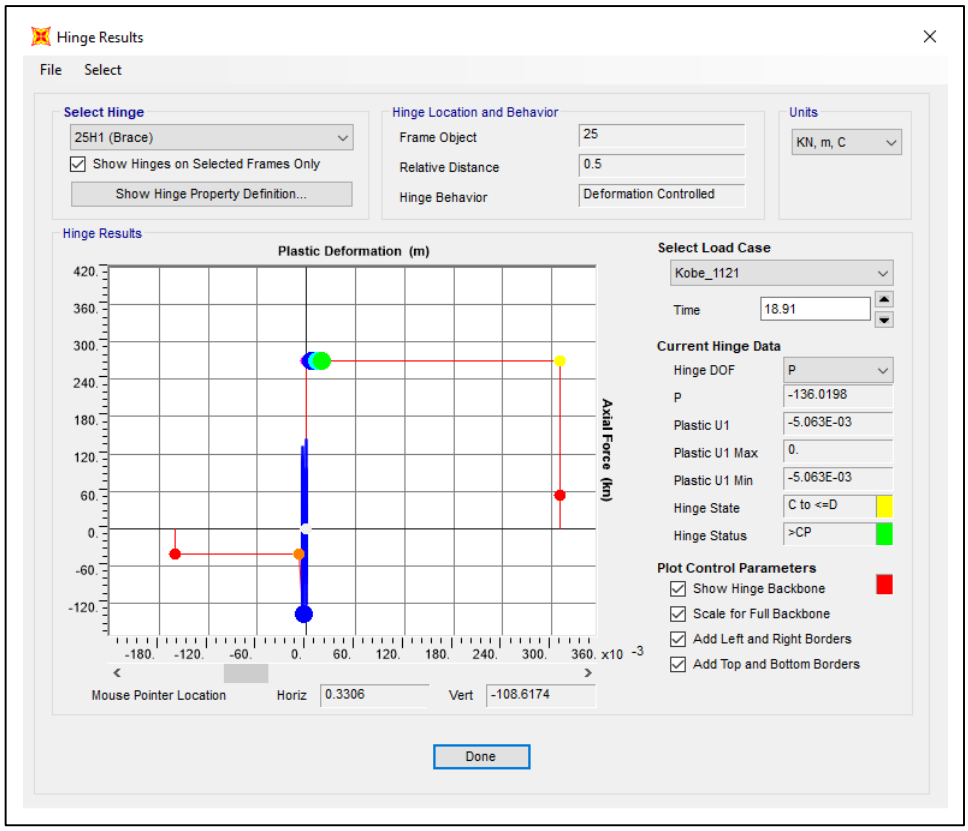

Figure 5.119: Hinge results of Silo-3 at 1.00 g (Kobe).

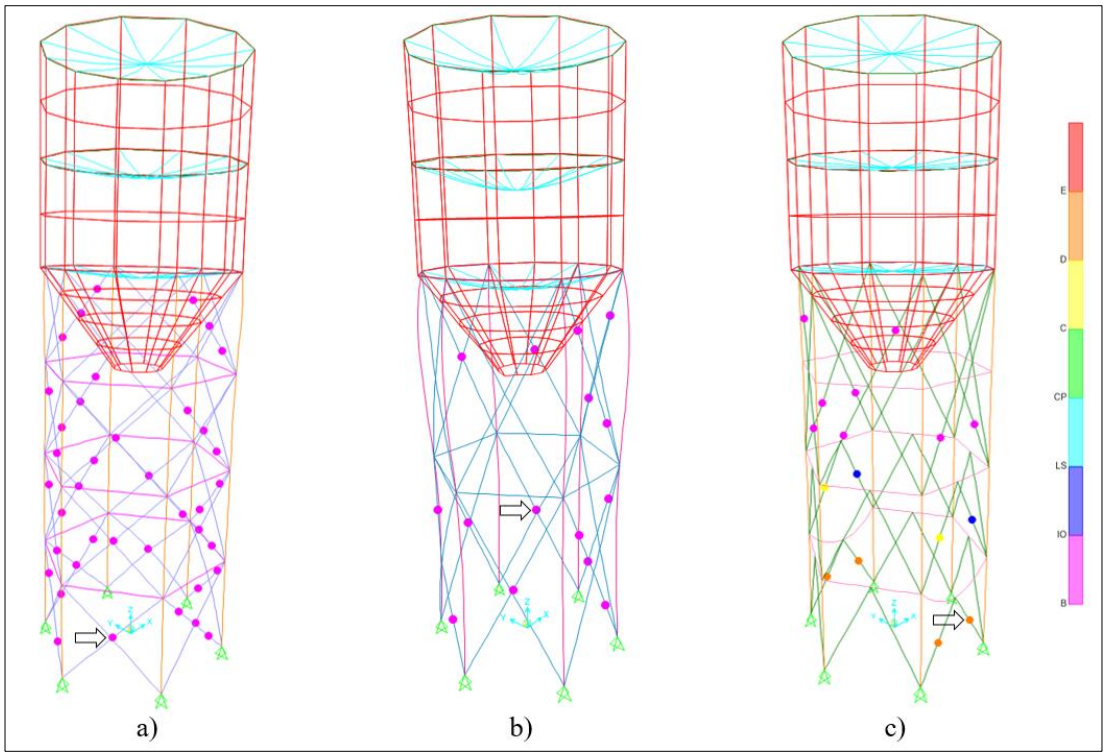

Figure 5.120: Deformed shapes of a) Silo-1, b) Silo-2, c) Silo-3 at 1.20 g (Kobe).

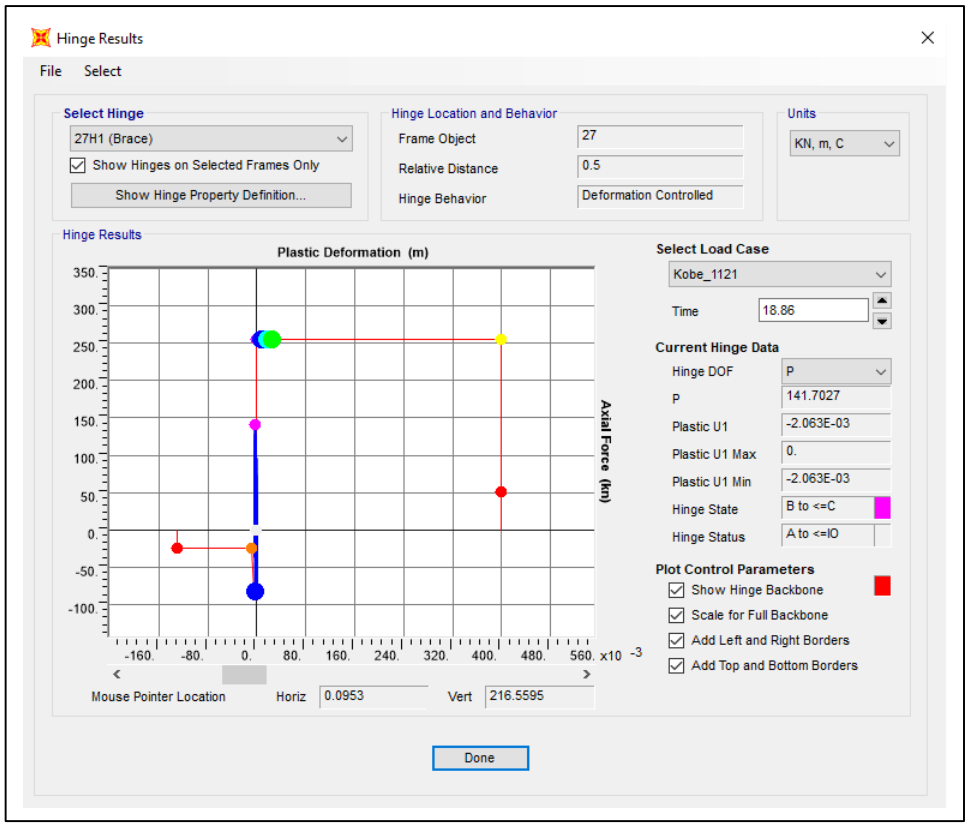

Figure 5.121: Hinge results of Silo-1 at 1.20 g (Kobe).

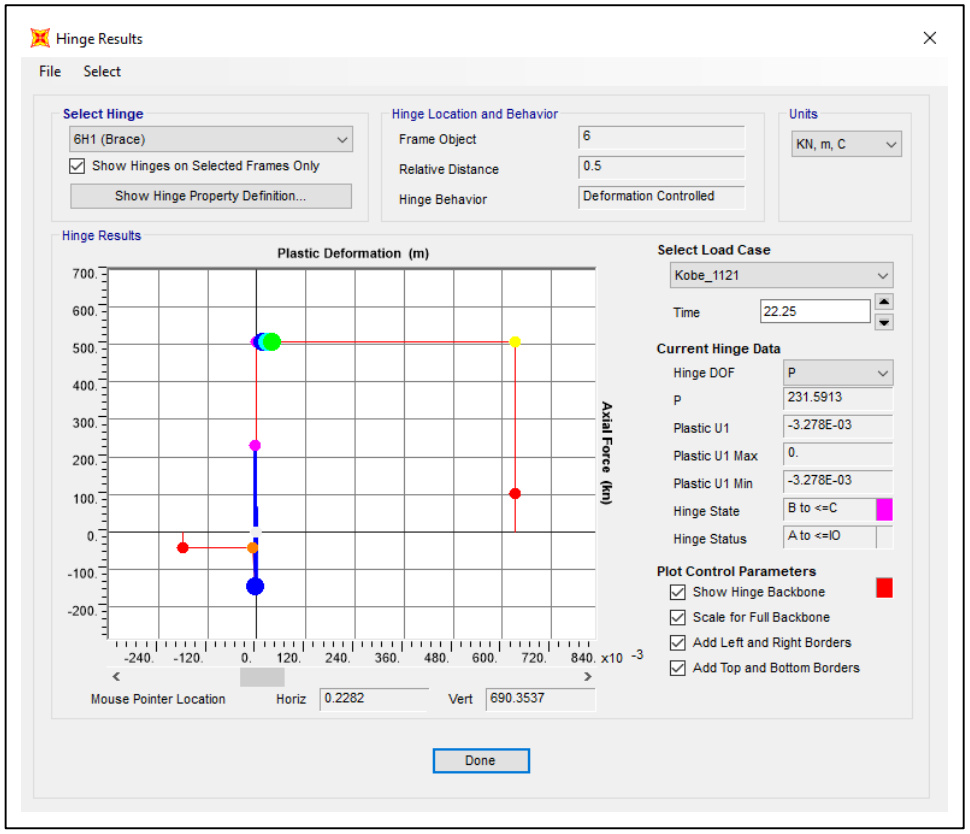

Figure 5.122: Hinge results of Silo-2 at 1.20 g (Kobe).

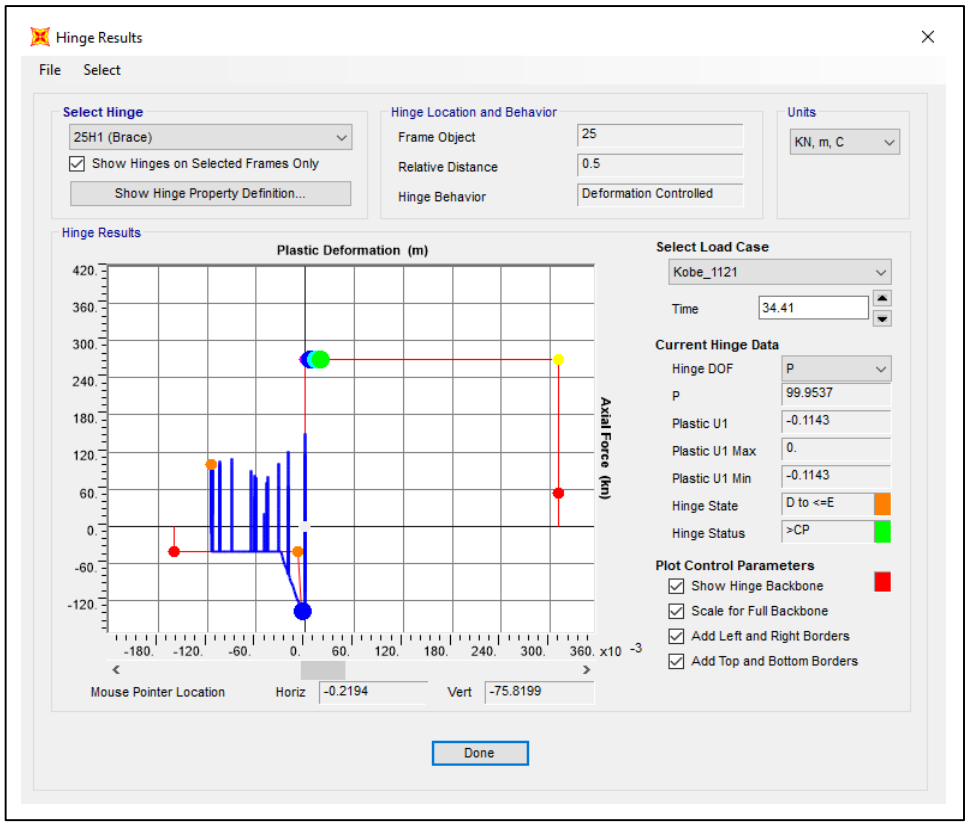

Figure 5.123: Hinge results of Silo-3 at 1.20 g (Kobe).

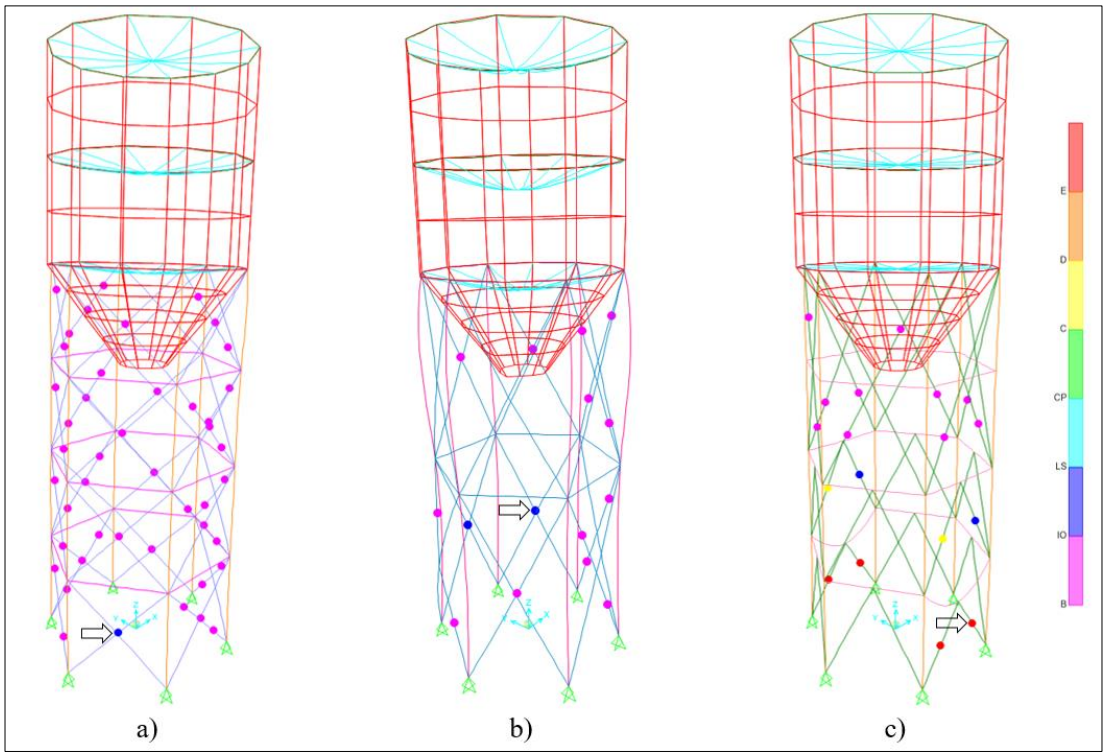

Figure 5.124: Deformed shapes of a) Silo-1, b) Silo-2, c) Silo-3 at 1.40 g (Kobe).

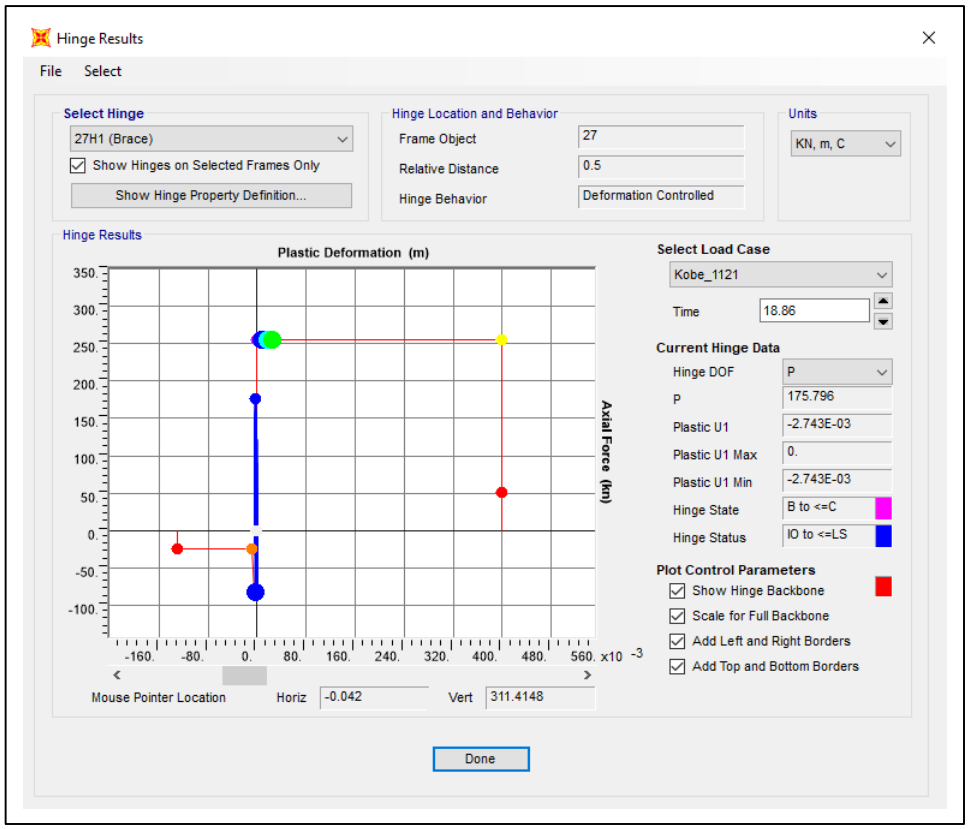

Figure 5.125: Hinge results of Silo-1 at 1.40 g (Kobe).

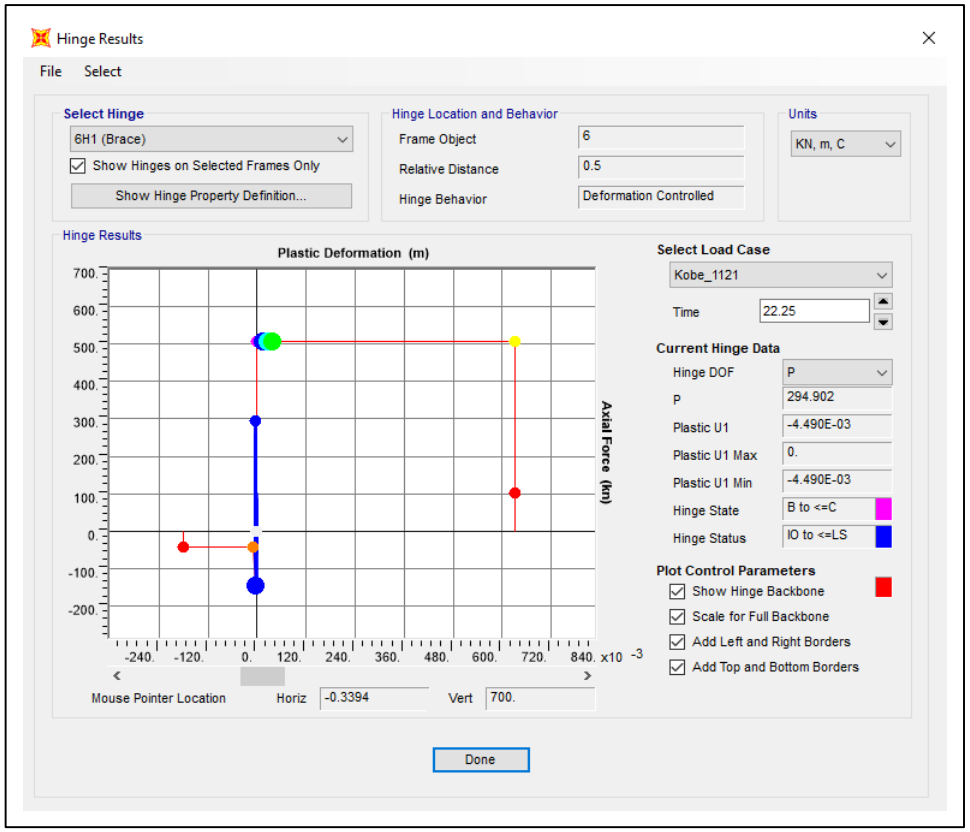

Figure 5.126: Hinge results of Silo-2 at 1.40 g (Kobe).

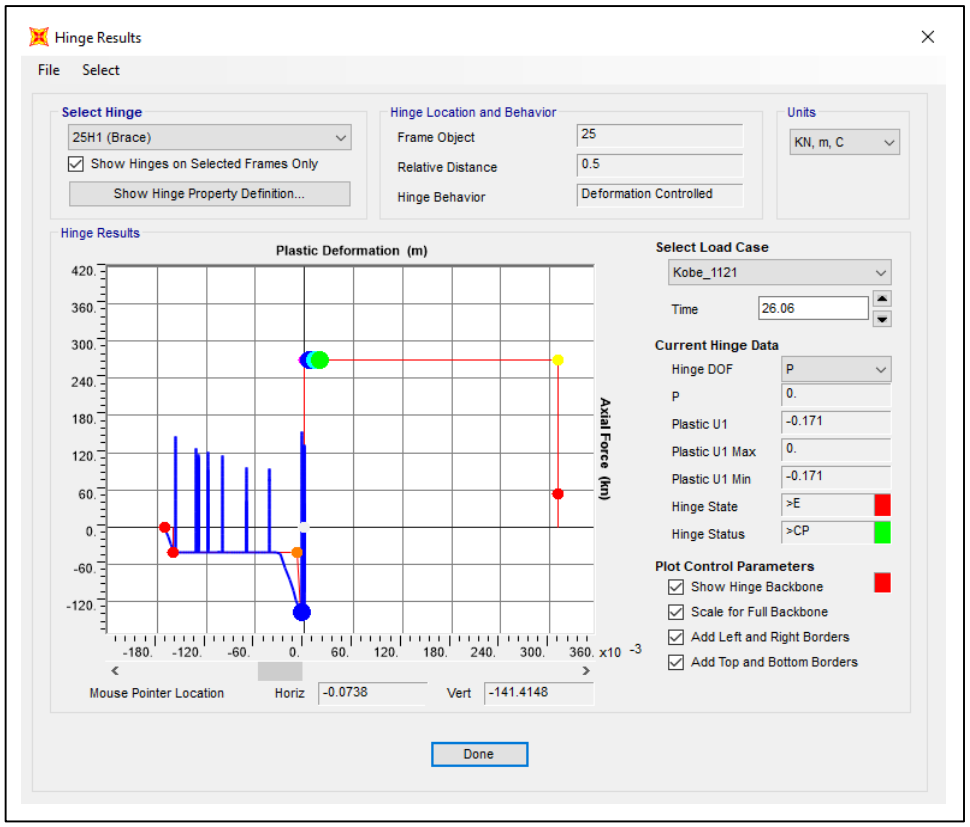

Figure 5.127: Hinge results of Silo-3 at 1.40 g (Kobe).

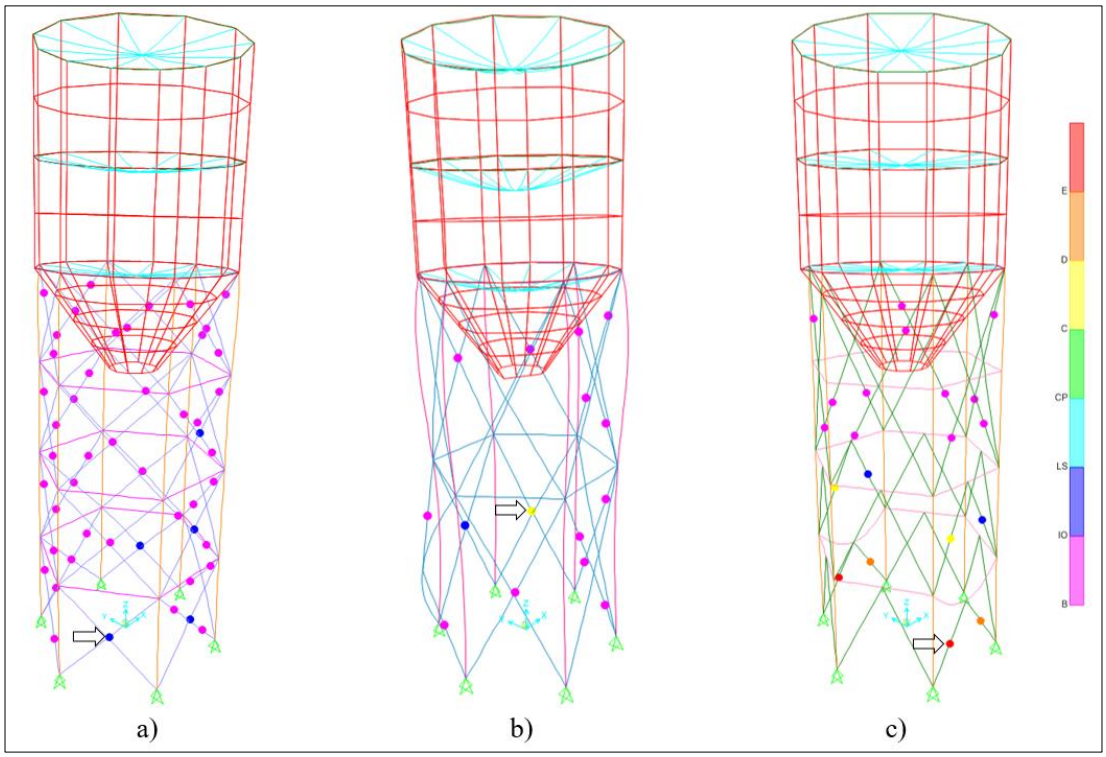

Figure 5.128: Deformed shapes of a) Silo-1, b) Silo-2, c) Silo-3 at 1.60 g (Kobe).

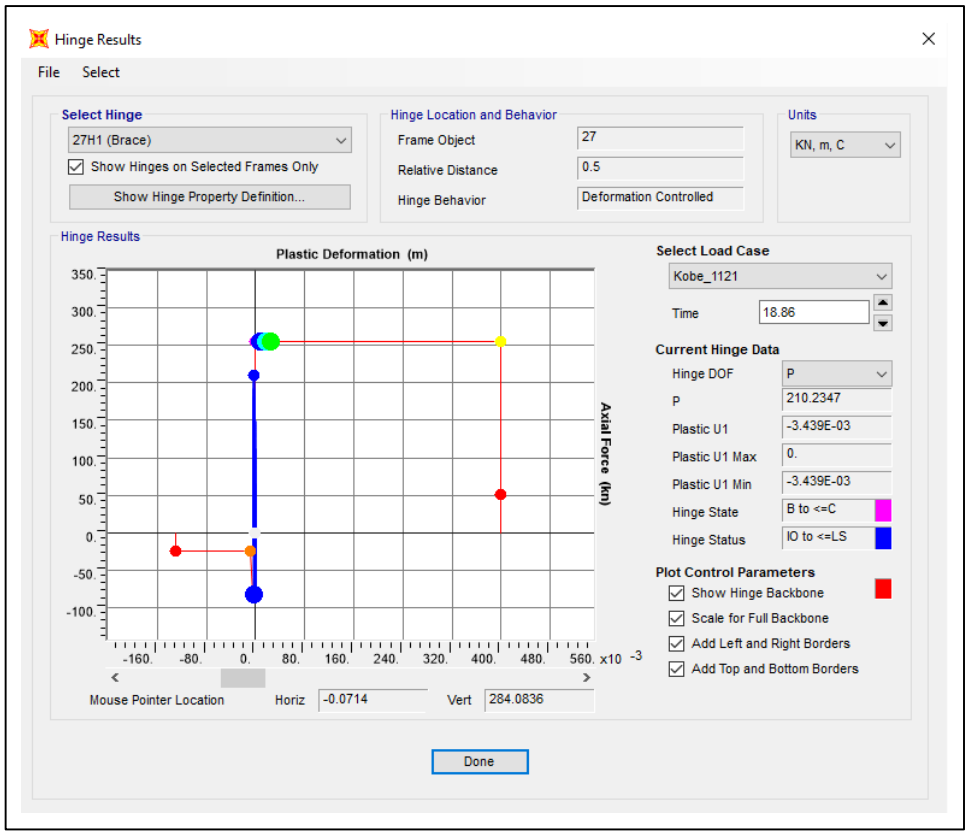

Figure 5.129: Hinge results of Silo-1 at 1.60 g (Kobe).

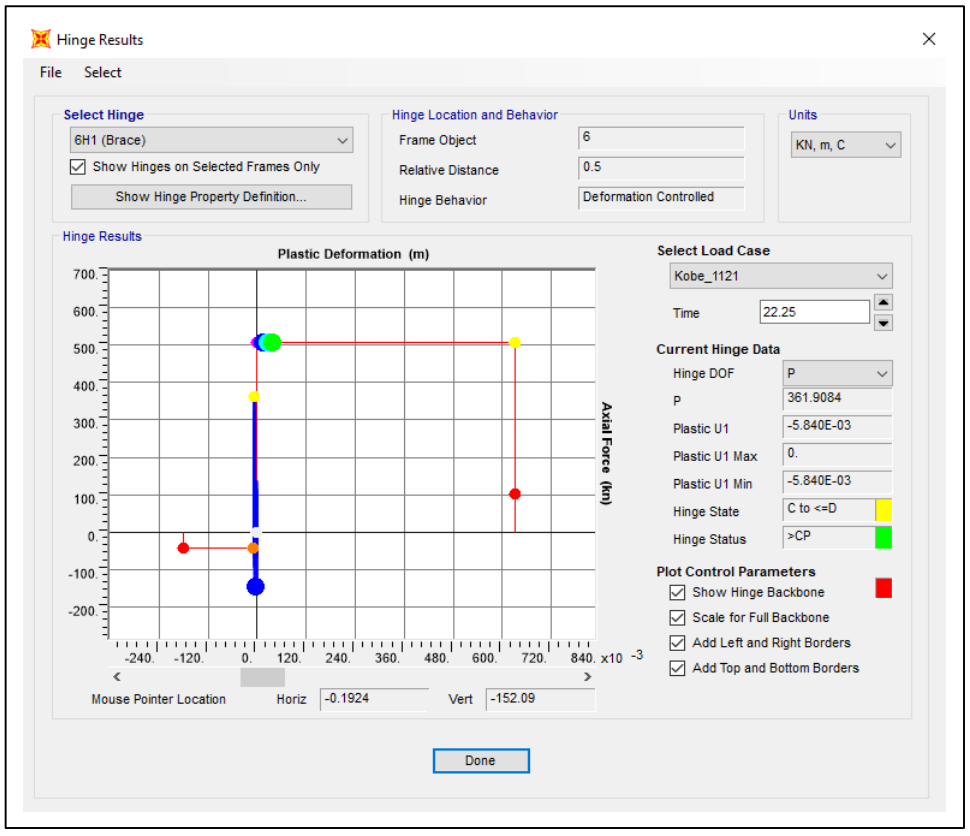

Figure 5.130: Hinge results of Silo-2 at 1.60 g (Kobe).

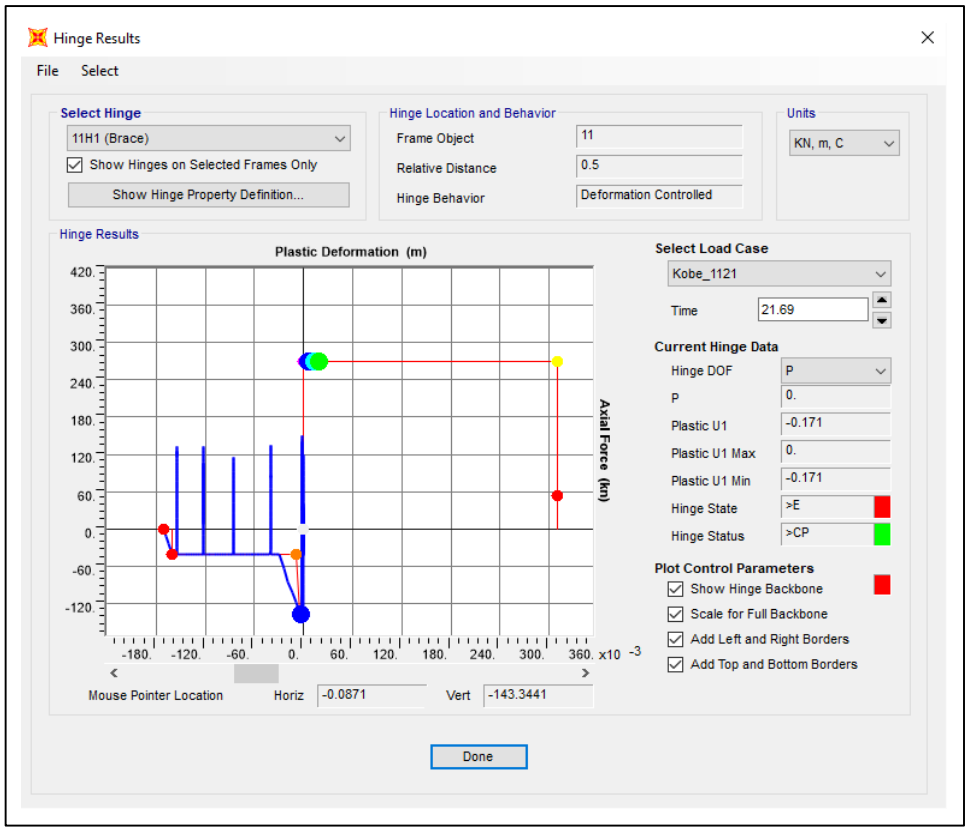

Figure 5.131: Hinge results of Silo-3 at 1.60 g (Kobe).

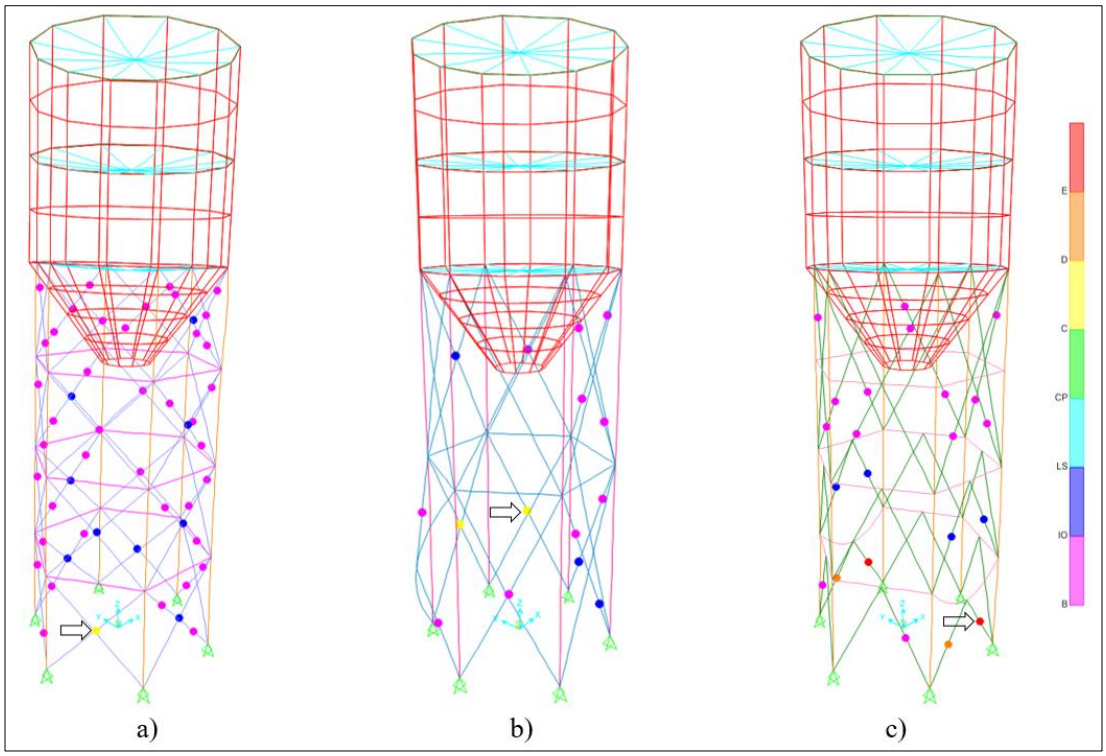

Figure 5.132: Deformed shapes of a) Silo-1, b) Silo-2, c) Silo-3 at 1.80 g (Kobe).

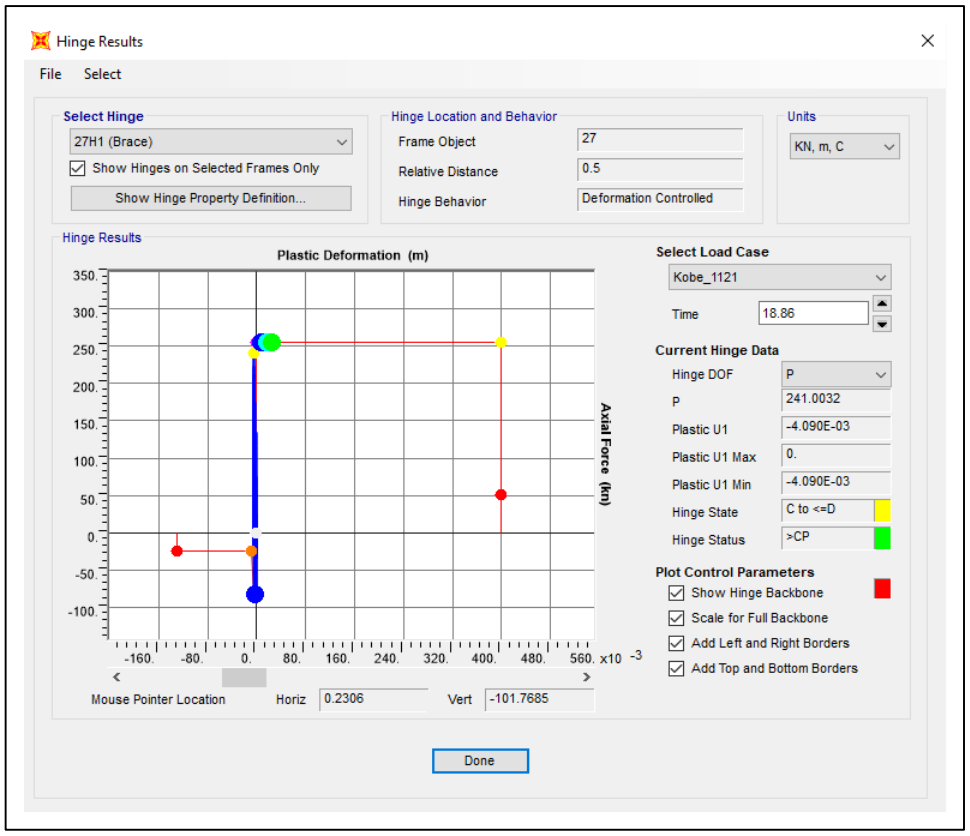

Figure 5.133: Hinge results of Silo-1 at 1.80 g (Kobe).

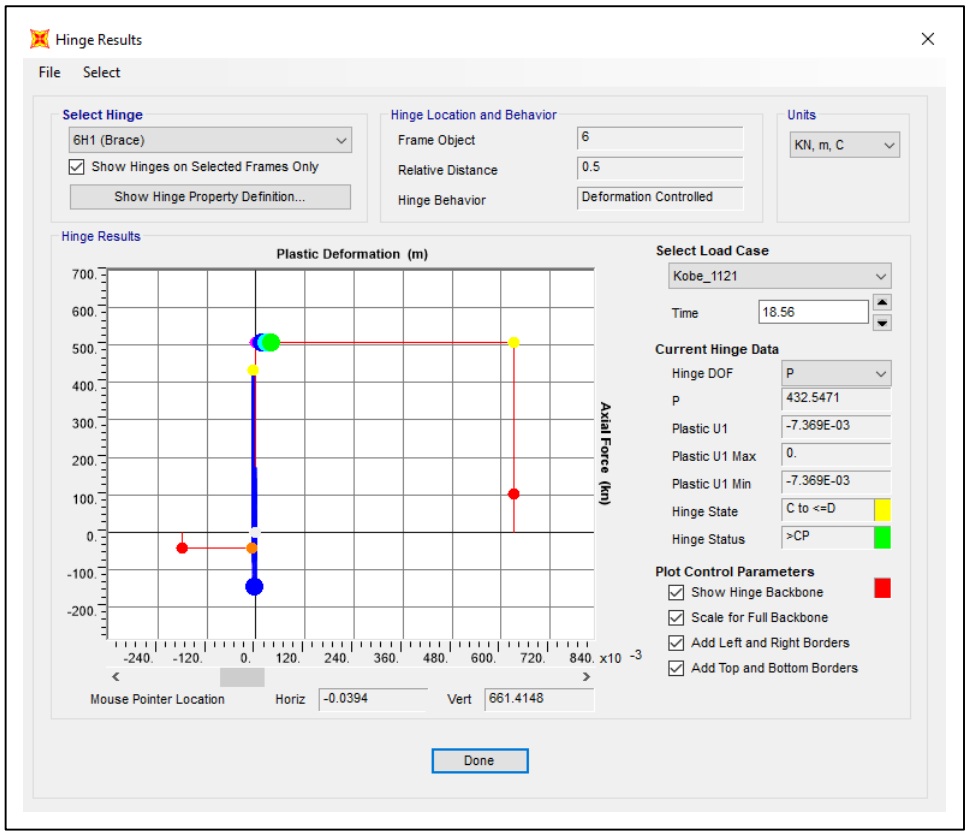

Figure 5.134: Hinge results of Silo-2 at 1.80 g (Kobe).

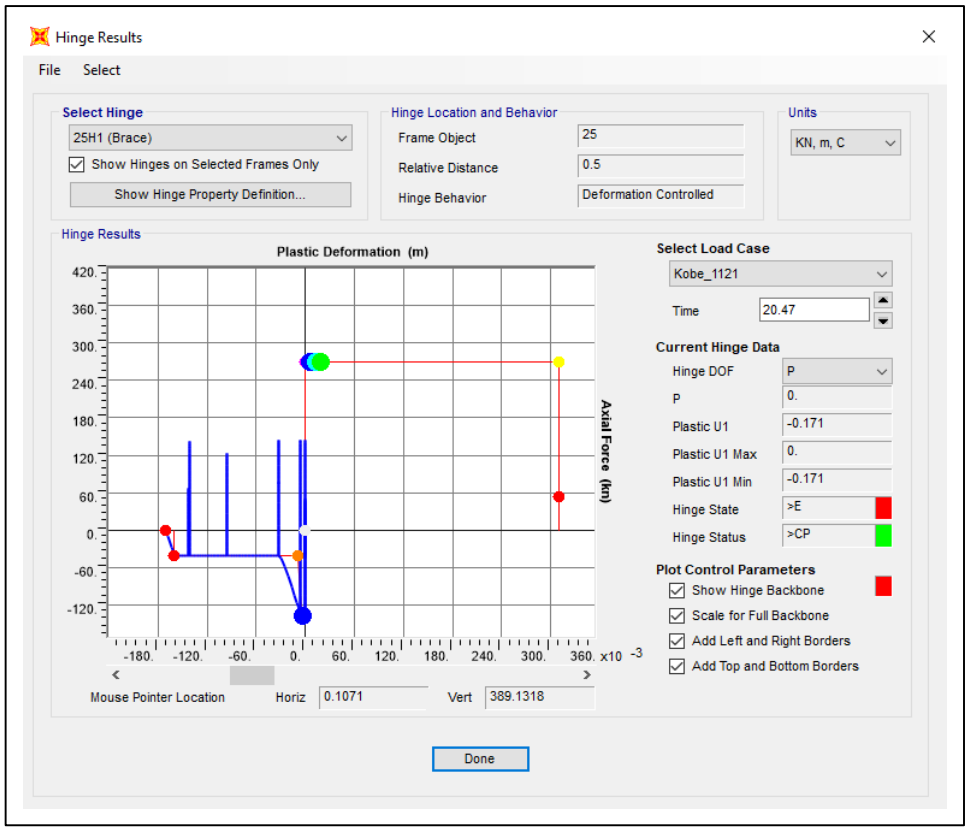

Figure 5.135: Hinge results of Silo-3 at 1.80 g (Kobe).

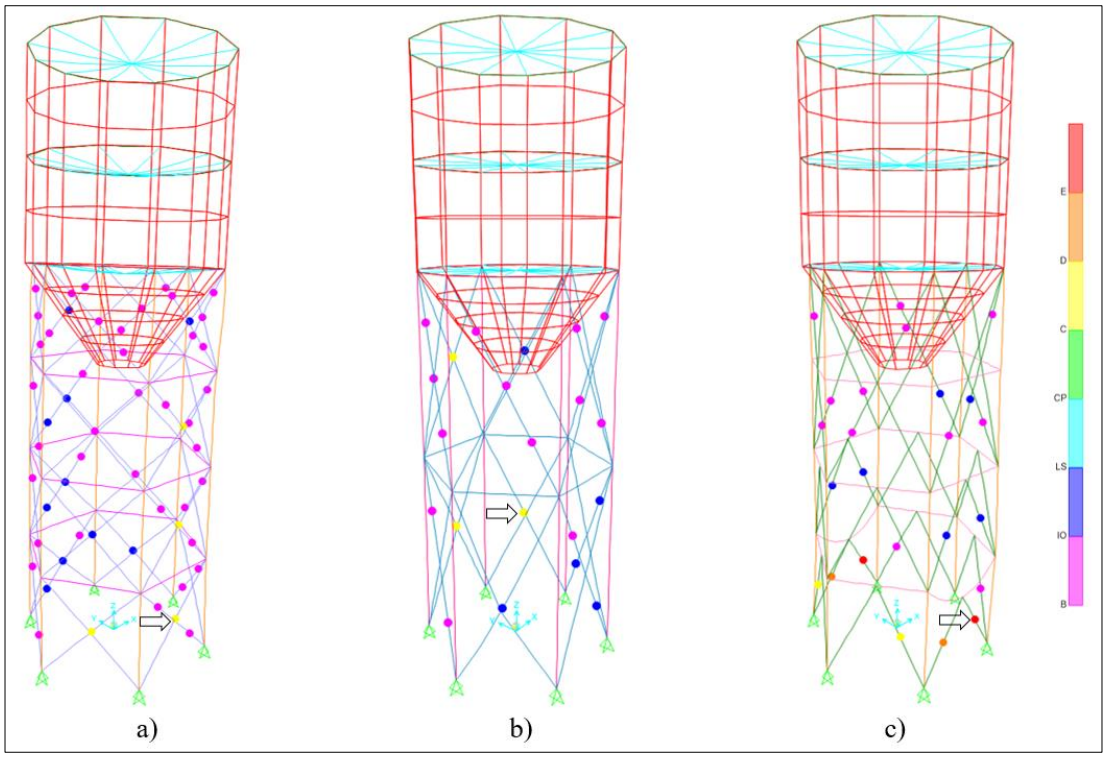

4

Figure 5.136: Deformed shapes of a) Silo-1, b) Silo-2, c) Silo-3 at 2.00 g (Kobe).

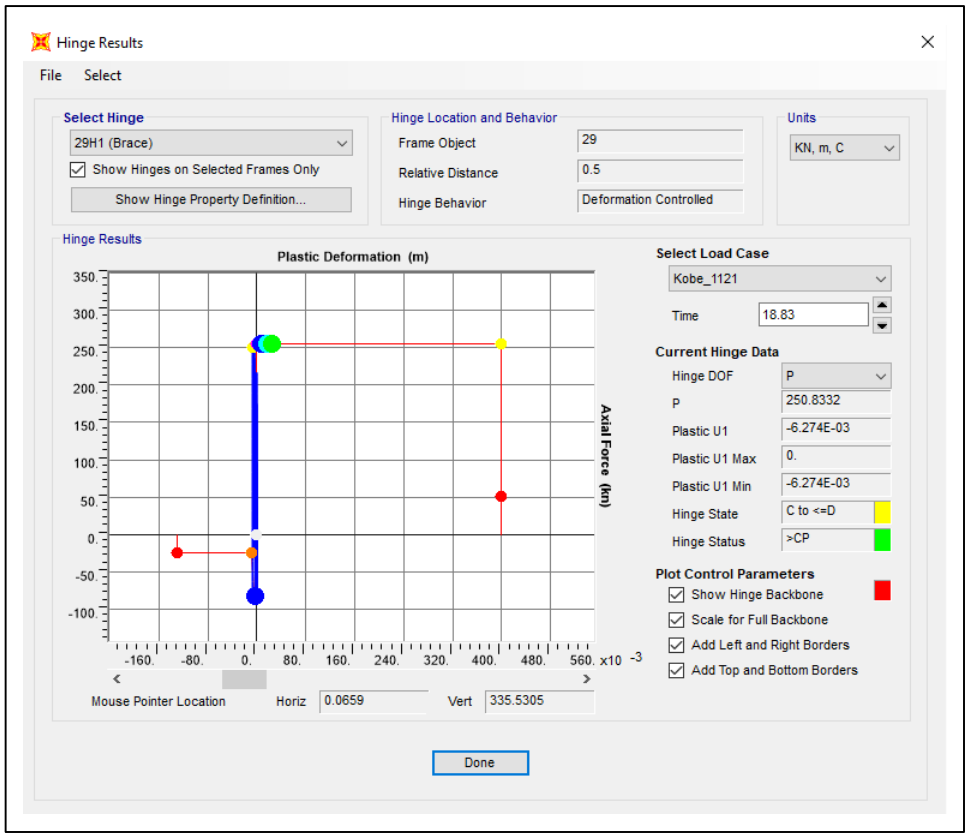

Figure 5.137: Hinge results of Silo-1 at 2.00 g (Kobe).

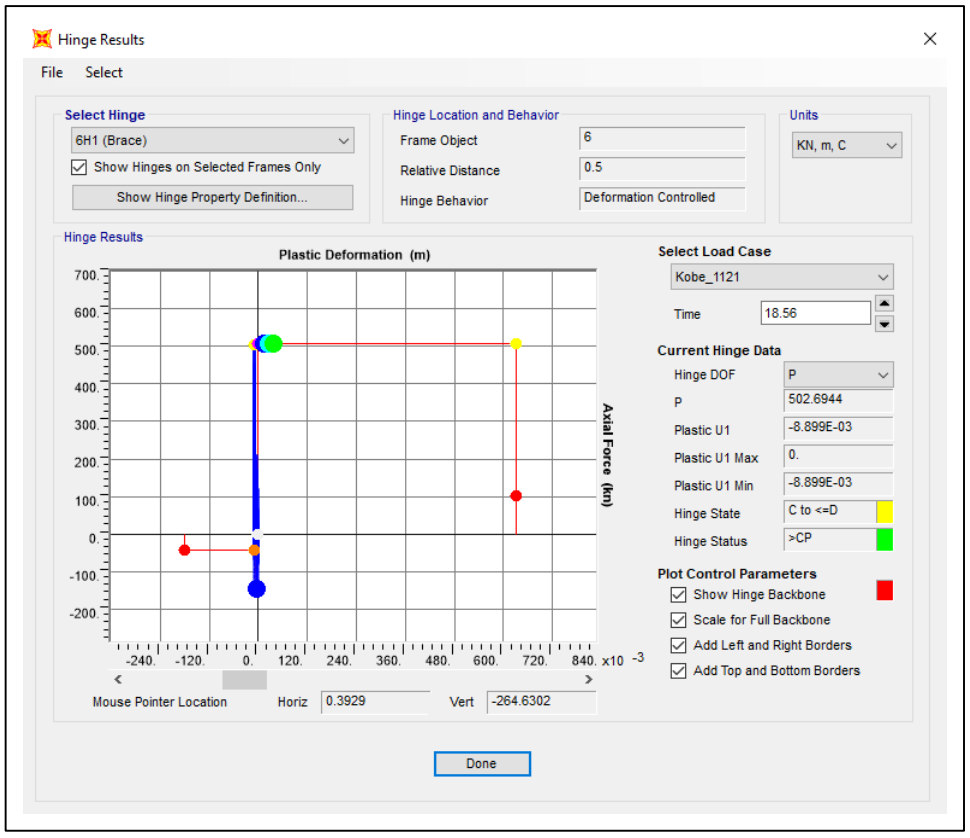

Figure 5.138: Hinge results of Silo-2 at 2.00 g (Kobe).

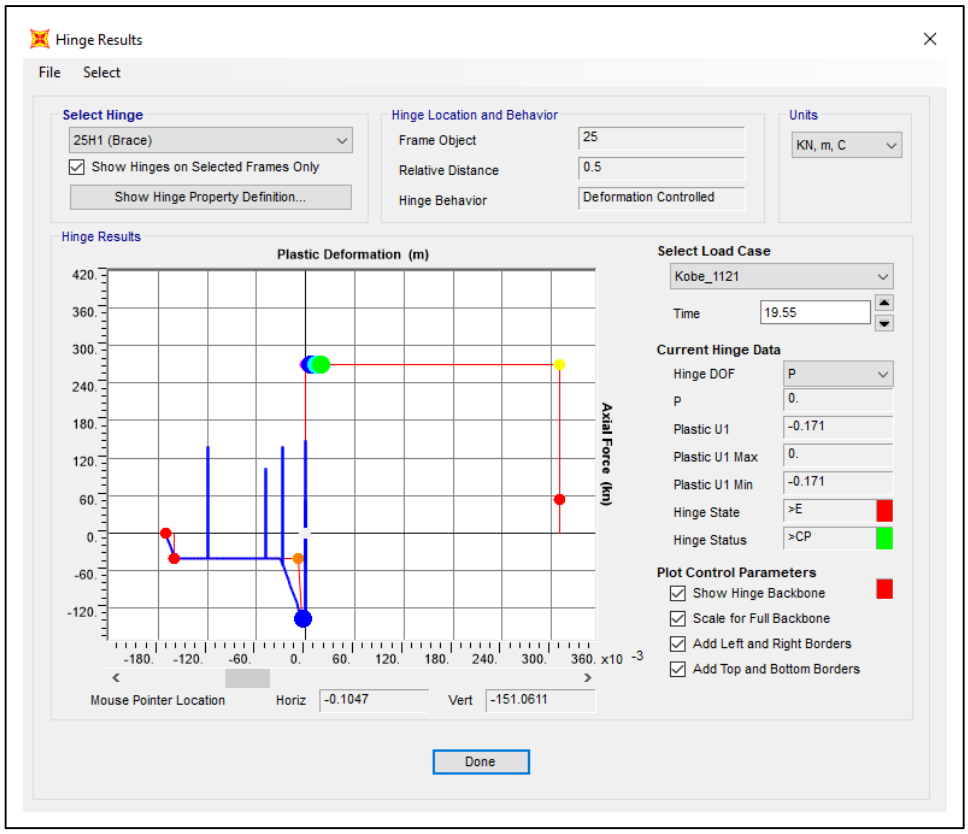

Figure 5.139: Hinge results of Silo-3 at 2.00 g (Kobe).

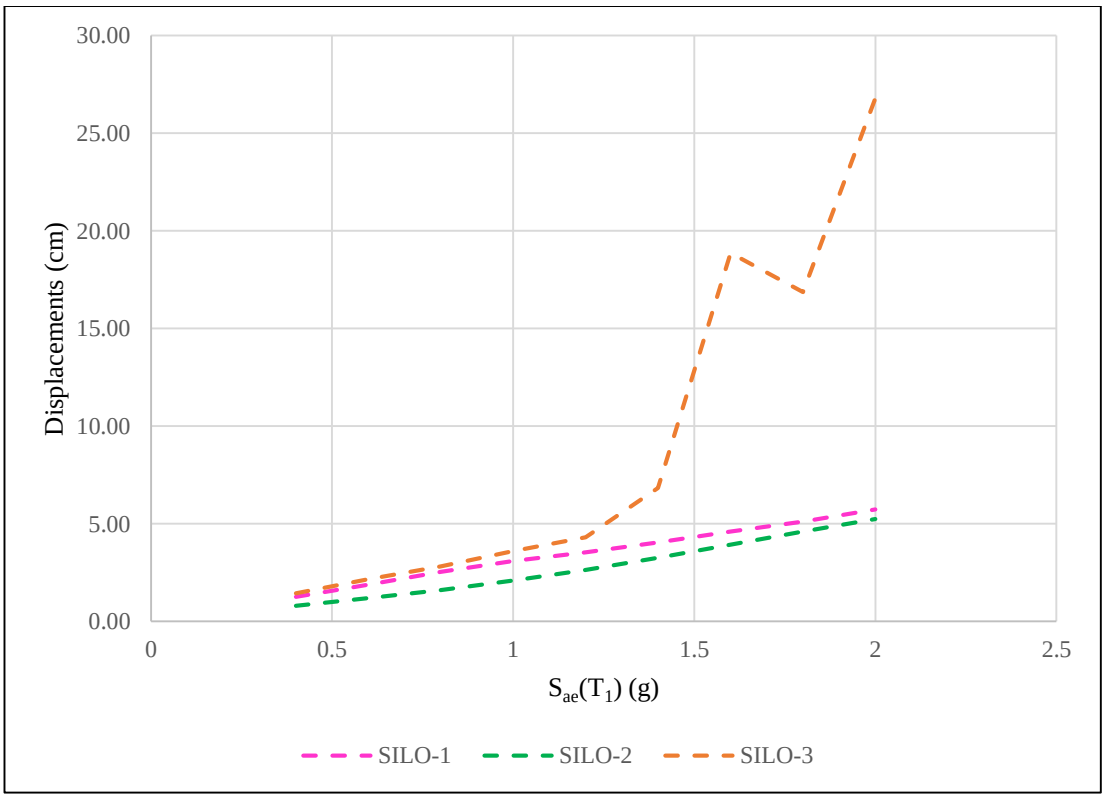

Figure 5.140: Top displacements in Kobe-1121 Earthquake.

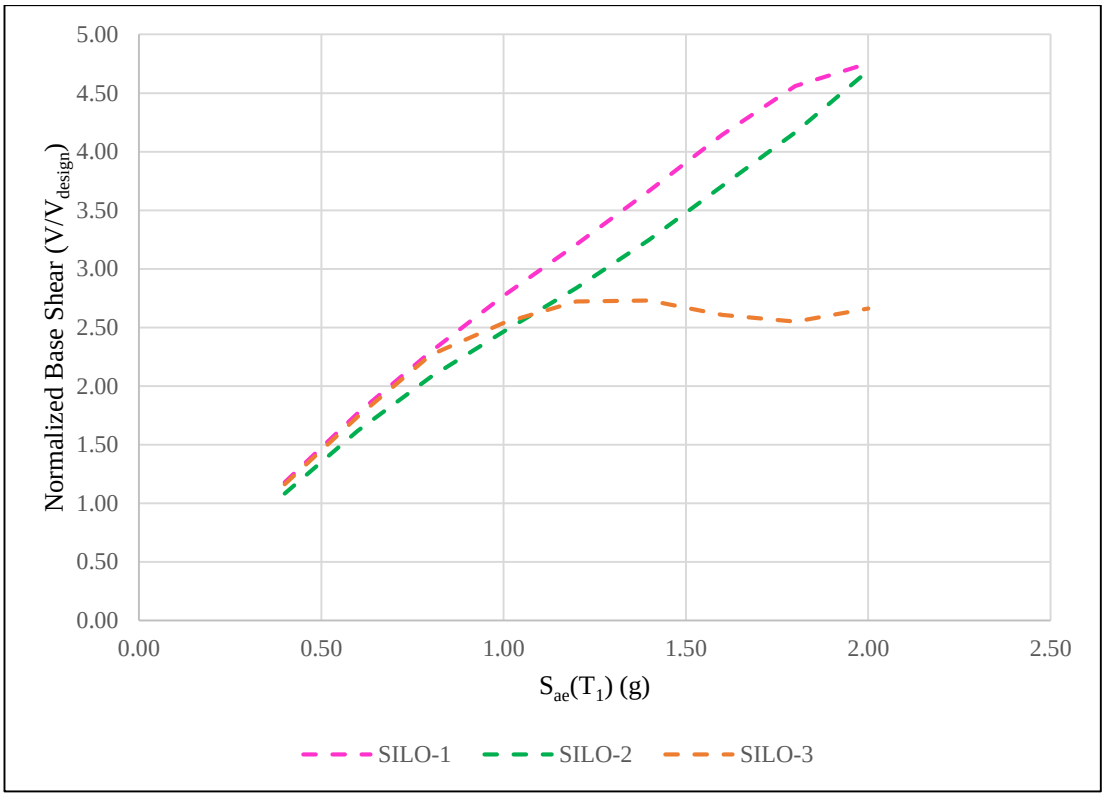

Figure 5.141: Normalized base shear forces in Kobe-1121 Earthquake.

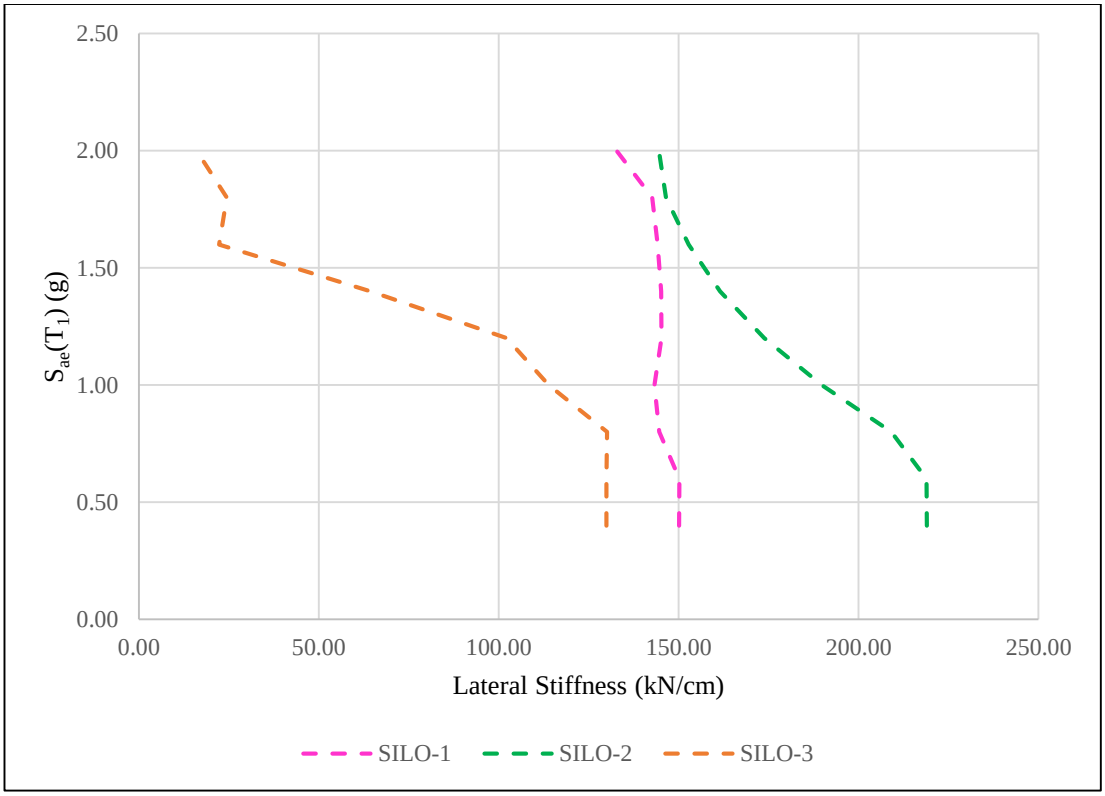

Figure 5.142: Lateral stiffness in Kobe-1121 Earthquake.

The global behavior parameter for braced frames is axial plastic elongation/shortening. The amounts of greatest axial plastic elongation/shortening in the braces during the earthquakes are given in Table 5.4.

Table 5.4: Axial Plastic Elongation/Shortening Values.

Earthquake	**$S_{ae}(T_1)$ (g)**	**Elongation/Shortening (m)**		
		Silo-1	**Silo-2**	**Silo-3**
Bayraklı-3513	0.40	No Hinge	No Hinge	No Hinge
	0.60	No Hinge	0.00013	No Hinge
	0.80	0.00060	0.00141	0.00005
	1.00	0.00157	0.00287	0.00234
	1.20	0.00243	0.00407	0.08200
	1.40	0.00322	0.00525	0.17100
	1.60	0.00408	0.00654	0.17100
	1.80	0.00870	0.00784	0.17100
	2.00	0.02020	0.00871	0.17100
Bornova-3522	0.40	No Hinge	No Hinge	No Hinge
	0.60	No Hinge	0.00021	No Hinge
	0.80	0.00050	0.00150	0.00183
	1.00	0.00141	0.00295	0.05190
	1.20	0.00231	0.00417	0.13220
	1.40	0.00312	0.00533	0.17100
	1.60	0.00395	0.00662	0.17100
	1.80	0.00674	0.00774	0.17100
	2.00	0.00870	0.00855	0.17100
Iwate-5774	0.40	No Hinge	No Hinge	No Hinge
	0.60	No Hinge	No Hinge	No Hinge
	0.80	0.00060	0.00082	0.00119
	1.00	0.00172	0.00189	0.00903
	1.20	0.00249	0.00311	0.06310
	1.40	0.00329	0.00418	0.17100
	1.60	0.00434	0.00522	0.17100
	1.80	0.00651	0.00642	0.17100
	2.00	0.00971	0.00760	0.17100
Kobe-1121	0.40	No Hinge	No Hinge	No Hinge
	0.60	No Hinge	No Hinge	No Hinge
	0.80	0.00059	0.00082	0.00057
	1.00	0.00139	0.00202	0.00506
	1.20	0.00206	0.00328	0.11430
	1.40	0.00274	0.00449	0.17100
	1.60	0.00344	0.00584	0.17100
	1.80	0.00409	0.00737	0.17100
	2.00	0.00627	0.00890	0.17100

In accordance with ASCE7-16, Table 1.5-1, risk category is selected as I and according to Table 12.12-1, allowable story drift is determined as 0.020 h_{sx}. Accordingly, the maximum drift of the three silos with a height of 8^{m} is identified as 16^{cm}. The results of top displacements for each silos in each earthquakes are given in Table 5.5.

Table 5.5: Top Displacements.

SILO NUMBER	$S_{ae}(T_1)$ (g)	Bayraklı_3513		Bornova_3522		Iwate_5774		Kobe_1121	
		SF	Δ_i (cm)	SF	Δ_i (cm)	SF	Δ_i (cm)	SF	Δ_i (cm)
1	0.40	1.717	1.269	1.419	1.246	0.671	1.266	0.904	1.255
	0.60	2.575	1.904	2.128	1.870	1.007	1.901	1.356	1.883
	0.80	3.434	2.606	2.838	2.531	1.342	2.563	1.808	2.537
	1.00	4.292	3.176	3.547	3.077	1.678	3.334	2.260	3.097
	1.20	5.151	3.749	4.257	3.720	2.013	3.960	2.712	3.533
	1.40	6.009	4.315	4.966	4.364	2.349	4.585	3.164	4.042
	1.60	6.867	5.033	5.675	5.033	2.684	5.316	3.615	4.601
	1.80	7.726	5.605	6.385	5.938	3.020	6.145	4.067	5.116
	2.00	8.584	6.541	7.094	6.293	3.355	7.113	4.519	5.729
2	0.40	1.331	0.890	1.563	0.917	0.869	0.802	1.144	0.799
	0.60	1.997	1.336	2.345	1.377	1.304	1.201	1.716	1.196
	0.80	2.662	1.826	3.127	1.852	1.739	1.614	2.287	1.607
	1.00	3.328	2.330	3.909	2.376	2.174	2.033	2.859	2.101
	1.20	3.994	2.751	4.690	2.852	2.608	2.379	3.431	2.640
	1.40	4.659	3.158	5.472	3.256	3.043	2.729	4.003	3.253
	1.60	5.325	3.548	6.254	3.654	3.478	3.134	4.575	3.925
	1.80	5.990	3.982	7.035	3.977	3.913	3.504	5.147	4.599
	2.00	6.656	4.081	7.817	4.119	4.347	3.880	5.719	5.250
3	0.40	1.425	1.290	1.678	1.619	0.748	1.585	0.849	1.442
	0.60	2.137	1.930	2.517	2.430	1.121	2.377	1.274	2.160
	0.80	2.849	2.570	3.357	3.263	1.495	3.213	1.698	2.811
	1.00	3.562	3.110	4.196	3.819	1.869	4.155	2.123	3.599
	1.20	4.274	3.885	5.035	3.679	2.243	5.007	2.547	4.301
	1.40	4.987	9.247	5.874	6.875	2.616	5.007	2.972	6.840
	1.60	5.699	12.450	6.713	13.520	2.990	15.750	3.396	18.870
	1.80	6.411	14.630	7.552	16.940	3.364	17.140	3.821	16.870
	2.00	7.124	12.170	8.391	22.670	3.738	20.210	4.245	26.780

The design base shear forces of three silos are 160.03^{kN}, 161.74^{kN} and 161.40^{kN}, respectively. The results of base shear forces for each silos in each earthquakes are shown in Table 5.6.

Table 5.6: Base Shear Forces.

SILO NUMBER	$S_{ae}(T_1)$ (g)	Bayraklı_3513		Bornova_3522		Iwate_5774		Kobe_1121	
		SF	V_{base} (kN)	SF	V_{base} (kN)	SF	V_{base} (kN)	SF	V_{base} (kN)
1	0.40	1.717	190.593	1.419	185.584	0.671	189.207	0.904	188.389
	0.60	2.575	286.198	2.128	278.652	1.007	284.272	1.356	282.912
	0.80	3.434	374.364	2.838	364.382	1.342	367.618	1.808	366.950
	1.00	4.292	466.494	3.547	449.557	1.678	450.685	2.260	443.610
	1.20	5.151	559.220	4.257	534.701	2.013	539.248	2.712	513.163
	1.40	6.009	650.707	4.966	620.429	2.349	625.008	3.164	586.788
	1.60	6.867	726.812	5.675	707.225	2.684	709.501	3.615	663.289
	1.80	7.726	766.708	6.385	757.528	3.020	757.902	4.067	729.869
	2.00	8.584	801.139	7.094	772.801	3.355	797.827	4.519	760.612
2	0.40	1.331	193.691	1.563	197.976	0.869	174.569	1.144	174.898
	0.60	1.997	288.900	2.345	293.184	1.304	261.673	1.716	261.844
	0.80	2.662	364.611	3.127	369.623	1.739	337.118	2.287	335.968
	1.00	3.328	450.496	3.909	457.050	2.174	411.668	2.859	398.713
	1.20	3.994	535.111	4.690	541.360	2.608	490.962	3.431	458.730
	1.40	4.659	622.358	5.472	624.108	3.043	568.603	4.003	525.421
	1.60	5.325	709.336	6.254	707.884	3.478	647.160	4.575	599.793
	1.80	5.990	784.935	7.035	769.593	3.913	727.922	5.147	673.709
	2.00	6.656	821.408	7.817	803.490	4.347	791.182	5.719	758.911
3	0.40	1.425	166.830	1.678	209.015	0.748	204.211	0.849	187.303
	0.60	2.137	249.799	2.517	313.914	1.121	306.437	1.274	280.671
	0.80	2.849	332.335	3.357	392.871	1.495	388.685	1.698	365.821
	1.00	3.562	383.452	4.196	416.227	1.869	434.142	2.123	409.841
	1.20	4.274	425.301	5.035	417.182	2.243	410.492	2.547	439.321
	1.40	4.987	431.020	5.874	420.125	2.616	412.178	2.972	440.503
	1.60	5.699	447.432	6.713	425.322	2.990	437.569	3.396	420.891
	1.80	6.411	479.942	7.552	447.959	3.364	442.971	3.821	411.652
	2.00	7.124	489.479	8.391	460.774	3.738	439.886	4.245	429.441

Lateral stiffness is the slope of the base shear force and roof displacement graph. By considering the slope, lateral stiffness values for each silos in each earthquakes are given in Table 5.7.

Table 5.7: Lateral Stiffness.

SILO NUMBER	$S_{ae}(T_1)$ (g)	Bayraklı_3513	Bornova_3522	Iwate_5774	Kobe_1121
		Stiffness (kN/cm)	Stiffness (kN/cm)	Stiffness (kN/cm)	Stiffness (kN/cm)
1	0.40	150.19	148.94	149.45	150.11
	0.60	150.31	149.01	149.54	150.25
	0.80	143.65	143.97	143.43	144.64
	1.00	146.88	146.10	135.18	143.24
	1.20	149.17	143.74	136.17	145.25
	1.40	150.80	142.17	136.32	145.17
	1.60	144.41	140.52	133.47	144.16
	1.80	136.79	127.57	123.34	142.66
	2.00	122.48	122.80	112.16	132.77
2	0.40	217.70	215.94	217.67	219.01
	0.60	216.24	212.92	217.88	218.93
	0.80	199.68	199.58	208.87	209.07
	1.00	193.35	192.36	202.49	189.77
	1.20	194.52	189.82	206.37	173.76
	1.40	197.07	191.68	208.36	161.52
	1.60	199.93	193.73	206.50	152.81
	1.80	197.12	193.51	207.74	146.49
	2.00	201.28	195.07	203.91	144.55
3	0.40	129.33	129.10	128.84	129.89
	0.60	129.43	129.18	128.92	129.94
	0.80	129.31	120.40	120.97	130.14
	1.00	123.30	108.99	104.49	113.88
	1.20	109.47	113.40	81.98	102.14
	1.40	46.61	61.11	82.32	64.40
	1.60	35.94	31.46	27.78	22.30
	1.80	32.81	26.44	25.84	24.40
	2.00	40.22	20.33	21.77	16.04

6. RESULTS AND DISCUSSIONS

6.1. Conclusions of Study

In this study, the seismic design and analysis of Multi-Tiered Ordinary Concentrically Steel Braced Frames are investigated. Linear and Nonlinear Analysis – Response Spectrum and Incremental Dynamic Analysis - are carried out.

SAP2000 Structural Analysis Software is used to perform analyses and design. The results obtained from the analyses are presented in the form of graphs and tables for comparison. The maximum elongation/shortening of the braces corresponding to the highest axial plastic hinging as well as top displacements and base shear forces of the silos are tabulated. After examining the results as discussed in the previous chapters, the following conclusions are drawn out of this study:

For Silo-1, which X-Bracing configuration is applied:

- No hinging is occurred at 0.40 g and 0.60 g in all four earthquakes. This means that the silo is in the elastic region.
- After 0.6 g, the silo exceeds the elastic limit and braces are exposed to plastic deformation in all earthquakes. In the Bayraklı-3513 Earthquake, buckling is observed in the compression braces from 0.80 g to 1.60 g, while it is observed from 0.80 g to 1.80 g in other three earthquakes. In Bayraklı-3513 Earthquake, at 1.60 g, 1.80 g and 2.00 g, compression braces buckle first and then tension braces yield whereas in other earthquakes this situation is observed at 1.80 g and 2.00 g.

For Silo-2, which 2-Tier X-Bracing configuration is applied:

- While hinging is happened after 0.60 g in Iwate-5774 and Kobe-1121 Earthquakes, it is happened after 0.40 g in Bayraklı-3513 and Bornova-3522 Earthquakes. Before these acceleration values, the silo is not experienced plastic deformation.
- Afterwards, braces cross the elastic region and reach the plastic zone. In Bayraklı-3513 and Bornova-3522 Earthquakes, buckling is occurred in the

compression braces from 0.60 g to 1.80 g, whereas this condition is occurred from 0.80 g to 2.00 g in other two earthquakes. In Iwate-5774 and Kobe-1121 Earthquakes, compression braces buckle first and then tension braces yield at 2.00 g, whereas in other earthquakes this situation is occurred at 1.80 g and 2.00 g.

For Silo-3, which Chevron Bracing configuration is applied:

- At 0.40 g and 0.6 g, the silo is remained in the elastic zone. In this case, no hinging is observed in all four earthquakes in this acceleration values.
- After the acceleration value is reached 0.8 g, silo takes place in the plastic zone and is exposed to plastic deformation. In four earthquakes, from 0.80 g to 1.40 g, only buckling is occurred in the compression braces. From 1.40 g onwards, as a result of the collapse which is occurred in buckled braces, no yielding is observed in the tensile braces.

The braces with the greatest axial plastic hinging are selected and it is deduced that the results from X-Bracing and 2-Tier X-Bracing configurations are close to each other while results of Chevron Bracing configuration are different and bigger than the X- and 2-Tier X-Bracing configurations.

Lateral stiffness is the slope of the base shear force vs. roof displacement graph. Although it is not necessary to check drift limitation, since the lateral stiffness (rigidity) of the braced frames is much more than the moment frames, it is concluded that the roof displacement results of X-Bracing and 2-Tier X-Bracing are similar but different from Chevron Bracing results. Besides, considering the slope of the base shear force vs. roof displacement, it is determined that X-Bracing and 2-Tier X-Bracing configurations are more rigid.

Incremental Dynamic Analysis is performed for the selected Bayraklı-3513, Bornova-3522, Iwate-5774 and Kobe-1121 Earthquakes between 0.40 g and 2.00 g. In general, according to the Time History Analysis, at 0.40 g and 0.60 g, silos, which have X-Bracing and 2-Tier X-Bracing configurations, are remained in the elastic region and do not experience plastic deformation. While buckling is observed in the compression braces between 0.80 g and 1.60 g, from 1.80 g onwards, first the compression braces buckle, after that tension braces yield. In Chevron Bracing configuration, there is not any hinging at 0.40 g and 0.60 g, similarly. However, by

performing the Incremental Dynamic Analysis from 0.80 g onwards, only buckling is occurred in the compression braces and from 1.40 g onwards, the buckled braces collapse and it could not allow to tension braces to yield.

The results of this study are demonstrated that the braces collapse only by buckling in Chevron Bracing configuration, whereas both buckling and yielding, without collapsing, are observed in the X-Bracing and 2-Tier X-Bracing configurations.

In consequences of this study, it is inferred that the greatest axial plastic hinging and the maximum elongation/shortening values are observed in Chevron Bracing configuration. Besides, the results show that the behavior of X-Bracing and 2-Tier X-Bracing configurations are similar. However, by considering the linear behavior for X-Bracing and 2-Tier X-Bracing configurations, it can be concluded that the X-Bracing configuration is more economical.

6.2. Future Studies and Recommendations

The results of this study can help the engineers with selecting the best steel bracing configuration type for Multi-Tiered Ordinary Concentrically Braced Frame to keep the axial plastic hinging to a minimum. The proposed results calculated in this study need to be verified by further case studies, for instance:

- The same research can be performed by changing the tier levels, heights and widths of the silos using other structural analysis software.
- Seismic responses with different locations and different earthquake data can be studied.
- Nonlinear links can be defined and assigned to braces to examine the inelastic behavior of braces in more accurate way.
- The seismic behavior of Multi-Tiered Concentrically Steel Braced Frames can be compared with Conventional Concentrically Steel Braced Frames.
- Future studies should look for the best Multi-Tiered Ordinary Concentrically Braced Frame structure which is able to tolerate any kind of deformation.

REFERENCES

[1] Imanpour, A, A.M.ASCE, Tremblay, R, Fahnestock, L, P.E., M.ASCE, Stoakes, C, "Analysis and Design of Two-Tiered Steel Braced Frames under In-Plane Seismic Demand", *Journal of Structural Engineering*, ASCE, ISSN 0733-9445, pp.1-13 (2016).

[2] Imanpour, A, A.M.ASCE, Tremblay, R, Davaran, A, Stoakes, C, Fahnestock, L, P.E., M.ASCE, "Seismic Performance Assessment of Multitiered Steel Concentrically Braced Frames Designed in Accordance with the 2010 AISC Seismic Provisions", *Journal of Structural Engineering*, ASCE, ISSN 0733-9445, pp.1-13 (2016).

[3] Karamanci, E, Lignos, D, "Collapse Assessment and Performance-Based Evaluation Techniques for Concentrically Braced Frames Designed in Seismic Regions", *Journal of Structural Engineering,* Volume 140, Issue 8, (August 2014).

[4] Web 1, (2019), "Steel Multi-Tiered Braced Frames (MT-BFs)", https://www.cisc-icca.ca/2019-g-l-kulak-award-recipient-explores-steel-multi-tiered-braced-frames/

[5] Web 2, "Steel Bracings" https://www.sefindia.org/forum/files/steel_bracings_146.pdf

[6] Web 3, (2020), Gannon, M, "A Story to Brace For", https://www.structuremag.org/?p=14720 (21/10/2020).

[7] Pieraccini, L, Silvestri, S, Trombetti, T, "Flat-Bottom Silos Filled with Grain-Like Material: Refinements of the Silvestri et al. (2012) Theory", *Second European Conference on Earthquake Engineering and Seismology*, Istanbul Aug. 25-29, pp.1-12 (2014).

[8] Uckan, E, Akbas, B, Shen, J, Wen, R, Turandar, K, Erdik, M, "Seismic Performance of Elevated Steel Silos during Van Earthquake, October 23, 2011", *Journal of Nat Hazards*, pp.1 (2015).

[9] Imanpour, A, Tremblay, R, "Seismic Performance Evaluation and Design of Multi-Tiered Steel Concentrically Braced Frames", *Proceedings of the 10th National Conference in Earthquake Engineering*, Earthquake Engineering Research Institute, Anchorage, AK, pp.1-11 (2014).

[10] Imanpour, A, Tremblay, R, "Seismic Design and Response of Steel Multi-Tiered Concentrically Braced Frames in Canada", *Canadian Journal of Civil Engineering*, pp.1-29 (2016).

[11] Imanpour, A, Tremblay, R, "Seismic Design Procedure for Steel Multi-Tiered Concentrically Braced Frames Beyond CSA S16 Limit", *Resilient Infrastructure London*, pp.1-9 (2016).

[12] Agarwal, A, Fahnestock, L, "Seismic Performance Assessment of Steel Multi-Tiered Ordinary Concentrically-Braced Frames", *Proceedings of the Annual Stability Conference,* Structural Stability Research Council, Baltimore, Maryland, pp.1-15 (2018).

[13] Web 4, "What is an earthquake and what causes them to happen?", https://www.usgs.gov/faqs/what-earthquake-and-what-causes-them-happen?qt-news_science_products=0#qt-news_science_products

[14] TBDY – 2018, Turkish Building Seismic Code – 2018

[15] Web 5, "AFAD", https://tadas.afad.gov.tr/map

[16] Azarbakht, A, Dolsek, M, "Progressive Incremental Dynamic Analysis for First-Mode Dominated Structures", *Journal of Structural Engineering,* Volume 137, Issue 3 (March 2011).

[17] ÇYTHYDE – 2016, Code on Design, Calculation and Construction Principles of Steel Structures

[18] ANSI/AISC 341 – 16, Seismic Provisions for Structural Steel Buildings

[19] ASCE7-16, Minimum Design Loads and Associated Criteria for Buildings and Other Structures

[20] ANSI/AISC 360-16, Specification for Structural Steel Buildings

[21] Web 6, (2019) "Modal Analysis", https://wiki.csiamerica.com/display/kb/Modal+analysis (27/03/2019)

[22] Lestuzzi, P, Charif, H, Rossier, S, Ferrière, M, Person, J, "Nonlinear Time-History Analysis for Validation of the Displacement-Based Seismic Assessment of the RC Upper Bridge of a Dam", *Advances in Civil Engineering,* pp.7 (2018).

[23] Web 7, "North Anatolian Fault, Turkey", https://www.geolsoc.org.uk/Policy-and-Media/Outreach/Plate-Tectonic-Stories/Great-Glen-Fault/North-Anatolian-Fault

[24] "İzmir'in Deprem Haritası", 27 January 2020 date and 16:24 time Manşet Türkiye Newspaper.

[25] Web 8, "İzmir İlinin İlçeleri", https://www.lafsozluk.com/2009/03/izmir-ilinin-ilceleri-ve-nufus-sayilari.html, (05/10/2020)

BIOGRAPHY

Yasemin Ezgi AKYILDIZ successfully completed the Civil Engineering Department of the Faculty of Engineering and Natural Sciences of Istanbul Bilgi University in 2017, which she started in 2013, and started her master's degree in Gebze Technical University Graduate School of Natural and Applied Sciences Department of Civil Engineering Earthquake and Structural Engineering Program in 2019. She worked as a civil engineer at FONTAS ENGINEERING between 2018 and 2019, and has been working as a structural engineer at ARUP ENGINEERING since 2020.